Author:
Needs, Hope Isobel I

Title:
Mitochondrial import failure and rescue
links to neurodegeneration

Mitochondrial Import Failure and Rescue:

Links to Neurodegeneration

Hope I. Needs

A dissertation submitted to the University of Bristol in accordance with the requirements for award of the degree of Doctor of Philosophy in the Faculty of Life Sciences

School of Biochemistry, University of Bristol, UK.

March 2022

Word Count: 53,393

Abstract

Protein import into mitochondria is an intricate and highly conserved process central to normal cellular function, especially given the fundamental interplay between mitochondrial protein import and respiratory complexes assembly and function. This is particularly important in cells with high energetic demands such as neurons. Consequently, it is not surprising that defects in mitochondrial import are often observed in models of neurodegeneration. However, relatively little is known about the precise mechanism(s) by which dysfunctional import contributes to neurodegeneration.

To facilitate better understanding of import processes in health and disease, I developed an assay system to monitor import in real-time in live mammalian cells, using NanoLuc technology. Intriguingly, whilst import efficiency was diminished following acute stalling of a precursor during translocation, there was no apparent change in import function in cells exposed to chronic precursor trapping, despite alterations in mitochondrial morphology and dynamics. Disease prone Tau^{P301L} variant appeared to associate with TOM40 and induced mitochondrial changes resembling those observed with precursor trapping, indicative of a common mechanism. Both insults correlate with reduced neuronal complexity and synapse abundance, resembling phenotypic changes characteristic of neurodegeneration.

Additionally, this thesis describes how a cellular rescue mechanism compensates for import perturbations in cells exposed to a stalled precursor or Tau^{P301L}-TOM40 association. Perturbing import induced the formation of tunnelling nanotubes (TNTs) which rescue import function by enabling intercellular mitochondrial transfer. TNT formation was also induced by a small molecule TIM17 inhibitor, MB20, demonstrating that this could represent a widespread response to import dysfunction.

Overall, the work presented in this thesis demonstrates how a novel assay system can be exploited to advance knowledge of the mechanisms linking mitochondrial import defects and neurodegeneration. Furthermore, it shows how a known stress response mechanism, mitochondrial transfer *via* TNTs, is activated in response to failed import, and proposes an intriguing link between Tau and mitochondrial import relevant to disease.

Acknowledgements

Finally, my PhD journey is coming to an end. It would not have been possible if it weren't for the help, support, and guidance of many people. I am immensely grateful to my supervisors, Ian and Jeremy, for the opportunity to complete my PhD in your labs. Thank you for all the support, encouragement, and freedom to try out my own ideas, as well as for showing me what a great boss looks like. I am also incredibly grateful to Gonçalo Pereira, for helping develop this project, as well as for the continued mentorship, advice, and chats even after you left our lab.

Thank you to all the other members of M and G floors, past and present, for all the help and support along the way. My PhD experience would not have been half as enjoyable were it not for my lab mates always being there to bounce ideas off, have a tea break with, or go for a beer at the Robin with. Special thanks go to the M floor mito crew for helping me understand the complicated world of mitochondria.

I am hugely grateful to everyone who has provided support and assistance over the years. Special thanks to Suko and Kev for all the neuron advice and for providing me with bucket loads of neurons while I frantically attempted some final experiments. Thanks to everyone in the Wolfson Bioimaging Facility for all the support with imaging experiments, particularly Dr Stephen Cross for exceptional macro writing, saving both my time and sanity. I appreciate support from the FACS facility for my Seahorse work, and the proteomics facility, principally Dr Phil Lewis, for proteomics support. Thanks to my progression panel members, Professor Jon Lane and Professor Jon Hanley, for guidance and great discussions. I am thankful for great collaborators in Bielefeld and Exeter, for enabling me to carry out exciting experiments and learn new techniques.

I am forever grateful to the Wellcome Trust for providing me with generous funding, but mostly for the opportunity to carry out my research alongside wonderful course mates. I couldn't imagine better PhD pals to go through this journey with.

Perhaps the biggest thank you of all goes to George, for all the encouragement and support, and for always believing in me even when I didn't believe in myself. You have been there through the highs and lows, and I couldn't have done it (nor would I be finishing my PhD with any remaining sanity) without you (and Frank, of course!). Finally, thank you boundlessly to my amazing family and friends, I would not be where I am today were it not for your continuous love, support, and belief in me.

Author's Declaration

I declare that the work in this dissertation was carried out in accordance with the requirements of the University's *Regulations and Code of Practice for Research Degree Programmes* and that it has not been submitted for any other academic award. Except where indicated by specific reference in the text, the work is the candidate's own work. Work done in collaboration with, or with the assistance of, others, is indicated as such. Any views expressed in the dissertation are those of the author.

SIGNED: ..... DATE: .....

Table of Contents

Chapter 1. General Introduction 1
1.1. Mitochondrial Morphology & Dynamics 2
1.1.1. Mitochondrial Fission and the Role of DRP1 5
1.1.2. Mitochondrial Fusion 6
1.2. Mitochondrial Bioenergetics 8
1.3. Protein Translocation 10
1.3.1. Crossing the Outer Membrane 10
1.3.2. Biogenesis of OMM proteins 15
1.3.2.1. Insertion of β-Barrel Proteins in the OMM 16
1.3.2.2. Incorporation of α-Helical Anchors in the OMM 16
1.3.3. Co- and Post-Translational Translocation 17
1.3.4. Staying in the Intermembrane Space: The Disulfide Relay System 18
1.3.5. Crossing or Insertion in the Inner Membrane 18
1.3.5.1. TIM23 Complex (Presequence Pathway) 18
1.3.5.2. TIM22 Complex (Carrier Pathway) 21
1.3.5.3. OXA1 Pathway 23
1.4. Neuronal Structure & Function 25
1.5. Mitochondrial Protein Import and Neurodegeneration 28
1.5.1. Alzheimer's Disease 32
1.5.1.1. Amyloid Precursor Protein 32
1.5.1.2. Tau Protein 32
1.5.2. Parkinson's Disease 35
1.5.3. Huntington's Disease 37
1.5.4. Amyotrophic Lateral Sclerosis 38
1.6. Stress Response Pathways 39
1.6.1. UPR^{mt} 39
1.6.2. UPR^{am} 41
1.6.3. mPOS 41
1.6.4. mitoCPR 42
1.6.5. mitoTAD 43
1.7. Tunnelling Nanotubes 44
1.8. Aims 46
1.9. Thesis Overview 47

Chapter 2. Materials & Methods 48
2.1. Molecular Biology/Cloning 49
2.2. Protein Purification 51
2.2.1. GST-tagged Recombinant Perfringolysin (rPFO) 51
2.2.2. GST-Dark Peptide 51

2.2.3. His-tagged Su9-EGFP-HiBit....52
2.2.4. His-SUMO--Su9-ACP1-D-ACP1-D-DHFR-Myc....52
2.3. Cell Culture....53
2.3.1. HeLa/HEK293T Cell Culture....53
2.3.2. Primary Neuronal Culture....53
2.4. Transfection of Cells....55
2.4.1. HeLa Cell Transfection....55
2.4.2. Neuron Transfection....55
2.5. Lentivirus Production & Transduction....55
2.5.1. Lentivirus Production....55
2.5.2. Lentiviral Transduction....55
2.6. SRB Assay....56
2.7. Total Protein Cell Lysis....56
2.8. Western Blotting Analysis....56
2.9. Fluorescence Microscopy....58
2.9.1. Fixed Cell Confocal Microscopy....58
2.9.2. Live Cell Confocal Microscopy....58
2.9.3. Live Cell Structured Illumination Microscopy....58
2.9.4. Long Term Live Cell Imaging (IncuCyte)....59
2.9.5. Light Microscopy Image Analysis....59
2.9.5.1. Mitochondrial Morphology Analysis....59
2.9.5.2. Membrane Potential Analysis....60
2.9.5.3. Aggregate Analysis....60
2.9.5.4. Neuronal Morphology Analysis....60
2.10. Cryo-Electron Tomography (cryo-ET)....61
2.10.1. Sample Preparation....61
2.10.2. Cryo-ET Imaging....61
2.11. NanoLuc Assay....62
2.11.1. Intact Cell Assay....62
2.11.2. Permeabilised Cell Assay....62
2.12. CUTE Assay....63
2.13. Mitochondrial Respiratory Function Analysis....64
2.13.1. Oroboros Oxygraph Assay....64
2.13.2. Seahorse Assay: Mitochondrial Stress Test....64
2.14. Mitochondrial Isolations....65
2.15. Immunoprecipitations....65
2.16. Tandem Mass Tagging Mass Spectrometry....65
2.17. Statistical Analysis....65

Chapter 3. The NanoLuc System to Monitor Mitochondrial Import....66
3.1. Introduction....67

3.2. Aims 69
3.3. Results: The Intact Cell NanoLuc System 70
3.3.1. Optimisation of NanoLuc Component Expression 70
3.3.2. The Intact System Quantifies Import but not Kinetics 75
3.4. Results: The Controlled Unmasking of Targeting Elements (CUTE) System 76
3.4.1. POI Localises to Mitochondria in Absence of Biotin 78
3.4.2. MTS Masking Depends on MTS and SBP: Streptavidin Ratio 80
3.4.3. SLC5A6 Improves Speed of Unmasking and Translocation 83
3.5. Results: The Permeabilised Cell NanoLuc System 87
3.5.1. Optimisation of Key Components of the Permeabilised Cell System 87
3.5.2. The Permeabilised Cell NanoLuc Assay Depends on ATP and PMF 93
3.6. Discussion 97
3.6.1. The Intact Cell NanoLuc System 97
3.6.2. The CUTE System 99
3.6.3. The Permeabilised Cell NanoLuc Assay System 101
3.6.4. Summary 103
Chapter 4. Exploring the Impact of Failed Import *via* Precursor Stalling 104
4.1. Introduction 105
4.2. Aims 108
4.3. Results 109
4.3.1. DHFR-MTX Trapping Captures the Precursor Protein in Transit 109
4.3.2. Acute but not Chronic Trapping Reduces Mitochondrial Import Function 116
4.3.3. Precursor Stalling Leads to Mitochondrial Fission and Alters Cristae 117
4.3.4. Enhancement of Proteins Associated with the Trapped Precursor 125
4.4. Discussion 129
4.4.1. Key Findings 129
4.4.2. DHFR-MTX Trapping to Model Failed Import 129
4.4.3. Failed Import Impact on Mitochondria 130
4.4.3.1. Mitochondrial Import 130
4.4.3.2. Mitochondrial Morphology 131
4.4.3.3. Mitochondrial Respiratory Function 131
4.4.4. Cellular Response to Import Stress: Hypotheses 132
4.4.4.1. Lateral Insertion of the Precursor into the OMM 132
4.4.4.2. Activation of a Stress Response Mechanism 132
4.4.4.3. Activation of a Compensatory Mechanism i.e., Mitochondrial Transfer 133
4.4.5. Summary 133
Chapter 5. Association of Tau^{P301L} with Mitochondrial Import Pathways 134
5.1. Introduction 135
5.2. Aims 136
5.3. Results 137

5.3.1. Disease Prone Tau Variant Tau^{P301L} Forms Aggregates in HeLaGAL Cells 137
5.3.2. Mitochondrial Tau^{P301L} is Increased Despite Fewer Translocases 139
5.3.3. Tau^{P301L} Associates with the TOM40 Channel in HeLaGAL Cells 141
5.3.4. Import Activity is Unchanged in HeLaGAL Cells Overexpressing Tau^{P301L} 144
5.3.5. Mitochondrial Network is Less Complex in Cells Expressing Tau^{P301L} 145
5.3.6. Respiratory Function is Unchanged in Tau^{P301L} Cells 148
5.4. Discussion 150
5.4.1. Key Findings 150
5.4.2. Tau^{P301L} Expression and Localisation in HeLaGAL Cells 150
5.4.3. Tau^{P301L} Impacts on Mitochondria 151
5.4.3.1. Mitochondrial Import 151
5.4.3.2. Mitochondrial Morphology 152
5.4.3.3. Mitochondrial Respiratory Function 152
5.4.4. Implications in Disease 153
5.4.5. Summary 153

Chapter 6. The Role of Mitochondrial Import in Neuronal Health & Disease 154
6.1. Introduction 155
6.2. Aims 156
6.3. Results 157
6.3.1. Neuronal Viability is Unaffected by Import Insults 157
6.3.2. Precursor Trapping Leads to Reduced Neuronal Complexity 158
6.3.3. Tau^{P301L} Overexpression Causes Reduced Neuronal Complexity 161
6.3.4. Cells Subjected to Precursor Trapping have Fewer Synapses 164
6.3.5. Cells Overexpressing Tau^{P301L} Display Altered Synaptic Protein Localisation 169
6.4. Discussion 172
6.4.1. Key Findings 172
6.4.2. Import Insults and Neuronal Viability 172
6.4.3. Import Insults and Neuronal Morphology: Hints at Neurodegeneration? 172
6.4.4. Perturbed Import and Neuronal Mitochondria 173
6.4.5. Summary 174

Chapter 7. Import Function Rescue *via* Intercellular Mitochondrial Transfer 175
7.1. Introduction 176
7.2. Aims 177
7.3. Results 178
7.3.1. Cells Subjected to Mitochondrial Precursor Trapping Form TNTs 178
7.3.2. TNTs Transfer Mitochondria Intercellularly in Response to Import Failure 186
7.3.3. Inhibiting TNT Formation Blocks Rescue of Import Function 190
7.3.4. Tau^{P301L} Overexpression Induces TNT Formation 192
7.3.5. TNTs may Represent a Widespread Response to Import Disruption 197
7.4. Discussion 199

7.4.1. TNTs as a Compensatory Mechanism to Precursor Trapping....201
7.4.1.1. Precursor Trapping Induces Type 2 TNT Formation....201
7.4.1.2. Mitochondria Transfer via TNTs....202
7.4.1.3. Import Recovery is Blocked by Inhibition of TNT Formation....203
7.4.2. TNTs as a Rescue Mechanism for Tau^{P301L} Induced Import Dysfunction....204
7.4.3. TNTs as a Widespread Response to Import Dysfunction: MB20....204
7.4.4. Therapeutic Relevance of Mitochondrial Transfer via TNTs....205
7.4.5. Summary....206

Chapter 8. Research Summary & Concluding Remarks....207
8.1. Summary of Research....208
8.1.1. The NanoLuc Assay System to Monitor Import in Live Mammalian Cells....209
8.1.2. Modelling Failed Import via an Engineered Stalled Precursor....210
8.1.3. Tau^{P301L} and Mitochondrial Import....210
8.1.4. The Implications of Import Failure on Primary Neurons....211
8.1.5. Mitochondrial Transfer via TNTs as an Import Rescue Mechanism....212
8.2. Outstanding Questions....213
8.3. Final Remarks....214

Bibliography....215
Appendix 1: Constructs and Cloning Methods....237
Appendix 2: Image Analysis Macros....243
Appendix 3: Proteomic Data....244

List of Figures

Figure 1.1: Mitochondrial Structure 3
Figure 1.2: Mitochondrial Dynamics 4
Figure 1.3: OPA1 Processing 7
Figure 1.4: Mitochondrial Respiratory Chain 9
Figure 1.5: Overview of Mammalian Mitochondrial Import Pathways 12
Figure 1.6: Neuronal Structure and Synaptic Transmission 26
Figure 1.7: Hallmarks of Neurodegeneration 29
Figure 1.8: Tau Pathogenesis 34
Figure 1.9: Tunnelling Nanotubes 45
Figure 3.1: NanoLuc System to Monitor Mitochondrial Import in Isolated Yeast Mitochondria 68
Figure 3.2: Intact Cell NanoLuc Assay System to Monitor Mitochondrial Protein Translocation 72
Figure 3.3: Optimisation of LgBit and HiBit Expression 74
Figure 3.4: Intact Cell NanoLuc System Quantifies Import but does not Report Kinetics 75
Figure 3.5: CUTE System as an add-on to the Intact NanoLuc Assay 77
Figure 3.6: CUTE Protein Localises to Mitochondria in the Presence and Absence of Biotin 79
Figure 3.7: Cox8a MTS and Increased Streptavidin Improve CUTE Cytosolic Trapping 82
Figure 3.8: SLC5A6 Speeds up CUTE Mitochondrial Import 85
Figure 3.9: Permeabilised Cell NanoLuc Assay System: Experimental Outline 89
Figure 3.10: Permeabilised Cell NanoLuc Assay Optimisation: rPFO, GST-Dark, and Fz 92
Figure 3.11: Permeabilised NanoLuc Assay Monitors Import *via* the Presequence Pathway 96
Figure 4.1: Modelling Failed Precursor Import using the DHFR-MTX Affinity System 107
Figure 4.2: DHFR-MTX Trapping System Captures Prevents DHFR-Precursor Import 110
Figure 4.3: Principle of SR 3D-SIM 112
Figure 4.4: The Stalled Precursor Accumulates around the OMM of ~43% of Mitochondria 115
Figure 4.5: Acute but not Chronic Trapping Reduces Import of a Chasing Precursor Protein 116
Figure 4.6: Mitochondrial Morphology is Altered Following Trapping 118
Figure 4.7: Mitochondria Subjected to Trapping are Circularised and Less Elongated 120
Figure 4.8: Phosphorylation of DRP1 at S616 is Increased Following Precursor Trapping 121
Figure 4.9: Precursor Trapping Alters Cristae Abundance but Respiration is Unchanged 124
Figure 4.10: Proteomic Analysis of Proteins Associated with Trapped Precursor: Setup 126
Figure 4.11: Enhancement of Proteins Associated with Trapped Precursor 127
Figure 5.1: Both Tau Variants Form Aggregates in HeLaGAL Cells 138
Figure 5.2: Tau^{P301L} Expression Alters Mitochondrial Import in HeLaGAL Cells 140
Figure 5.3: Tau^{P301L} Associates with TOM40 143
Figure 5.4: Import is Unchanged in HeLaGAL Cells Exposed to Tau^{P301L}-TOM40 Association 144
Figure 5.5: Mitochondrial Branching is Decreased in HeLaGAL Cells Expressing Tau^{P301L} 147
Figure 5.6: Tau Variants have no Impact on Mitochondrial Respiratory Function or $\Delta\Psi$ 149
Figure 6.1: Import Perturbations do not Impact Neuronal Viability 157
Figure 6.2: Neurons Subjected to Trapping have Fewer Processes and Shorter Axons 160

Figure 6.3: Neuronal Complexity is Reduced in Cells Expressing Tau^{P301L} 163
Figure 6.4: Synapse Abundance is Reduced in Cells Subjected to Trapping 165
Figure 6.5: Precursor Trapping has no Impact on Synaptic Protein Overall Abundance 168
Figure 6.6: Synapse Abundance is Reduced in Hippocampal Neurons Expressing Tau^{P301L} 170
Figure 6.7: Synaptic Marker Expression is Unchanged with Tau Variants 171
Figure 7.1: Precursor Trapping Induces Protrusion Formation in HeLaGAL Cells 180
Figure 7.2: Protrusions are Composed of Tubulin and Actin and Contain Cellular Structures 182
Figure 7.3: Protrusion Formation is Decreased by Cytochalasin D and Nocodazole 185
Figure 7.4: Mitochondria are Transferred *via* TNTs 189
Figure 7.5: Rescue of Import Function is Partially Reversed by Blocking TNT Formation 191
Figure 7.6: HeLaGAL Cells Expressing Tau^{P301L} Form TNTs that Contain Mitochondria 194
Figure 7.7: Tau^{P301L} Induced TNTs are Dependent on Microtubules and Actin 196
Figure 7.8: MB20 Induced Import Perturbation is Rescued by TNT Formation 198
Figure 7.9: Proposed Import Rescue Mechanism by Mitochondrial Transfer *via* TNTs 200

List of Tables

Table 1.1: Subunits of the Mitochondrial Translocase Complexes in Humans and Yeast 13
Table 1.2: Summary of Import Defects Associated with Neurodegeneration 30
Table 2.1: Compositions of Commonly Used Buffers 50
Table 2.2: Cell Culture Media Compositions 54
Table 2.3: Primary Antibodies 57
Table 2.4: Secondary Antibodies 57
Table 4.1: Proteins of Interest with Enhanced Association to Trapped Precursor 128

List of Abbreviations

Δψ, mitochondrial transmembrane potential; α-syn, alpha-synuclein; Aβ, amyloid-beta peptide; AD, Alzheimer's Disease; ADP, adenosine diphosphate; AGK, acylglycerol kinase; AIF, apoptosis inducing factor; ALS, Amyotrophic lateral sclerosis; AMPA, α-amino-3-hydroxy-5-methyl-4-isoxazolepropionic acid; AO, antimycin A and oligomycin; APP, amyloid precursor protein; ATP, adenosine triphosphate; BAM, β-barrel assembly machinery; BCA, bicinchoninic acid; BRET, bioluminescence resonance energy transfer; BSA, bovine serum albumin; CCCP, carbonyl cyanide-m-lorophenylhydrazone; CHCHD, coiled-coil-helix-coiled-coil-helix domain; CI-V, mitochondrial respiratory complexes one to five; CLZ, coelenterazine; COPI, coat protein complex I; cryo-EM, cryogenic electron microscopy; cryo-ET, cryogenic electron tomography; CDK1/5, cyclin dependent kinase 1 or 5; CLEM, correlative light and electron microscopy; CMT, Charcot-Marie-Tooth; CBD, corticobasal degeneration; CTE, chronic traumatic encephalopathy; Cox8a, cytochrome c oxidase subunit viii mitochondrial targeting sequence; CUTE, controlled unmasking of targeting elements; DAMPs, damage-associated molecular patterns; DAPI, 4′,6-diamidino-2-phenylindole; DIV, days *in vitro*; DHFR, dihydrofolate reductase; DMSO, dimethylsulfoxide; DRP1, dynamin-related protein 1; DTT, dithiothreitol; EGFP, enhanced green fluorescent protein; eIF2α, eukaryotic translation initiation factor 2 alpha; ER, endoplasmic reticulum; ETC, electron transport chain; $FADH_2$, flavin adenine dinucleotide; FBS, foetal bovine serum; FTLD, frontotemporal lobar degeneration; GDAP1, Ganglioside-induced differentiation-associated protein 1; GDN, glyco-diosgenin amphiphile; GST, Glutathione S-transferase; H_2O_2, hydrogen peroxide; HD, Huntington's disease; HeLaGAL, HeLa cells cultured in galactose medium; HeLaGLU, HeLa cells cultured in glucose medium; HBSS, Hanks' Balanced Salt Solution; HSR, heat shock response; Hsp, heat-shock protein; Htt, Huntingtin; IBM, inner boundary membrane; IMM, inner mitochondrial membrane; IMS, intermembrane space; iMTS, internal mitochondrial targeting sequence like signal sequence; IP, immunoprecipitation; IPTG, Isopropyl β-D-1-thiogalactopyranoside; IRES, internal ribosome entry site; ISR, integrated stress response; KA, kainate; KO, knock out; LHON, Leber hereditary optic neuropathy; MAPT, microtubule associated protein tau; MB1/6/10/20, MitoBloCK-1/6/10/20; MCIA, mitochondrial complex I intermediate assembly; MCSR, mitochondrial to cytosolic stress response; MDVs, mitochondrial-derived vesicles; MFF, mitochondrial fission factor; Mfn, mitofusin; Mgm1, mitochondrial genome maintenance 1; MIA, mitochondrial IMS assembly; MICOS, mitochondrial contact site and cristae organising system; MiD49/51, mitochondrial dynamics protein of 49/51 kDa; MIM, insertase of the outer mitochondrial membrane; MIP, mitochondrial intermediate peptidase; mitoCPR, mitochondrial compromised protein import response; mitoTAD, mitochondrial protein translocation-associated degeneration; MITRAC, Mitochondrial Translation Regulation Assembly

intermediate of Cytochrome c oxidase; mPOS, mitochondrial precursor over-accumulation stress; MPP, mitochondrial processing peptidase; mtDNA, mitochondrial DNA; MTS, mitochondrial targeting sequence; MTX, methotrexate; MV, microvesicle; NADH, nicotinamide adenine dinucleotide; NanoBiT, NanoLuc binary technology; NiRFP, near-infrared fluorescent protein; nDNA, nuclear DNA; NFTs, neurofibrillary tangles; NLS, nuclear localisation sequence; NMDA, N-methyl-D-aspartate; OCR, oxygen consumption rate; OMM, outer mitochondrial membrane; OPA1, optic dominant atrophy 1; OXA1, mitochondrial oxidase assembly protein 1; OXPHOS, oxidative phosphorylation; PAM, presequence translocase-associated motor; PARL, presenilin-associated rhomboid-like; PD, Parkinson's disease; PEST domain, polypeptide sequence rich in proline, glutamic acid, serine, and threonine; PKA, protein kinase A; PMF, proton motive force; PMSF, phenylmethylsulfonyl fluoride; PLL, poly-L-lysine; PSD95, post synaptic density protein 95; PSP, progressive supranuclear palsy; POI, protein of interest; PTM, post-translational modification; RAMP, reversible association with motor proteins; ROI, region of interest; ROS, reactive oxygen species; rPFO, recombinant perfringolysin; RUSH, retention using selective hooks; SAM, sorting and assembly machinery; SBP, streptavidin binding protein; SC, supercomplexes; SD, standard deviation; SN, Substantia Nigra; SR-3D SIM, super resolution 3-dimension structured illumination microscopy; SRB, sulforhodamine B; Su9, subunit 9 mitochondrial targeting sequence; TBS-T, tris buffered saline with tween; TIM22, translocase of the inner membrane 23; TIM23, translocase of the inner membrane 23; TK, tris-KCl; TMRM, tetramethylrhodamine; TMT-MS, tandem mass tagging mass spectrometry; TNT, tunnelling nanotube; TOM, translocase of the outer membrane; TOM-CC, translocase of the outer membrane core complex; UQCC1 and UQCC2, ubiquinol-cytochrome c reductase com-plex assembly factors 1 and 2; UPR^{am}, UPR activated by the mistargeting of proteins; UPR^{mt}, mitochondrial unfolded protein response; UTR, untranslated region.

Chapter 1. General Introduction

The following section is adapted from a published, peer reviewed review article (full citation below) on which I am first author [1].

***Needs, H.I.**; Protasoni, M.; Henley, J.M.; Prudent, J.; Collinson, I.; Pereira, G.C. Interplay between Mitochondrial Protein Import and Respiratory Complexes Assembly in Neuronal Health and Degeneration. Life 2021, 11, 432. https://doi.org/10.3390/life11050432.*

1.1. Mitochondrial Morphology & Dynamics

Mitochondria, often known as 'the powerhouse of the cell', provide the main source of cellular energy in the form of ATP. This is particularly important in high energy consuming cells such as neurons, as well as in cardiac and muscle cells. On top of this vital role in ATP synthesis, mitochondria have a plethora of other roles, including regulation of cellular metabolism, calcium storage and signalling, reactive oxygen species (ROS) signalling, damage-associated molecular patterns (DAMPs) production in inflammation and immunity, and programmed cell death [2].

Mitochondria are double membrane bound organelles (Figure 1.1), the outer of which (outer mitochondrial membrane; OMM) houses translocation machinery, required for protein import into mitochondria, among several other proteins such as those required for ion and molecule permeability, organelle tethering and morphology [3]. The inner mitochondrial membrane (IMM) also houses translocation machinery and solute carriers, among other proteins, and is organised into folds termed cristae. The cristae extend into the mitochondrial matrix and house the respiratory chain complexes required for their function in proton motive force (PMF) generation for ATP synthesis [3]. Between these two membranes is an area termed the intermembrane space (IMS), where several important proteins, including small TIM chaperones required for translocation and various proteins required for respiratory function are present, all of which are nuclear encoded [4, 5]. The 'text book' image of mitochondria, as singular, unconnected, oval shaped organelles, inferred by early electron micrographs which showed the very first mitochondrial structures in fixed cell slices [6], has proven to be misrepresentative, having not taken into account the dynamic behaviour of mitochondria in live cells.

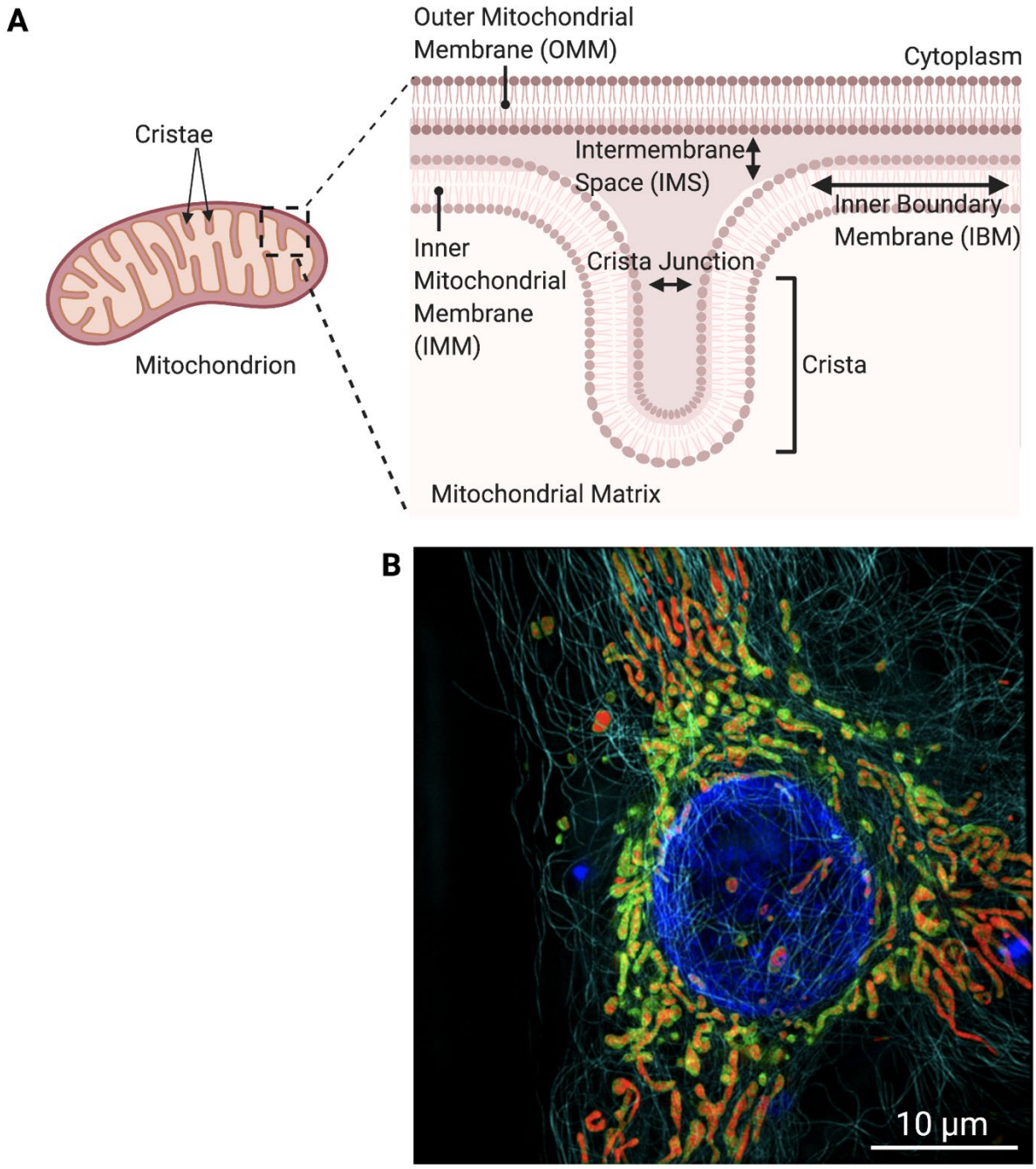

Figure 1.1: Mitochondrial Structure
(A) Mitochondria have two membranes, the OMM and the IMM. These are separated by the IMS, and within the IMM is the mitochondrial matrix. The IMM folds to form cristae, and the space between the folded IMM is known as the crista junction, where respiratory complexes are housed. The sections of IMM between cristae are known as the inner boundary membrane (IBM). *Schematic created in BioRender*
(B) Image showing the mitochondrial network in a live HeLa cell, captured by super resolution 3-dimension structured illumination microscopy (SR-3D SIM). HeLa cell was cultured in galactose medium (HeLaGAL), and fluorescence highlights the mitochondrial matrix (red, mitochondrial targeted mScarlet), mitochondrial outlines including cristae (green, stained with MitoTracker Green), nucleus (blue, stained with DAPI), and cytoskeleton (cyan, microtubules stained with Tubulin Tracker Deep Red). Scale bar is 10 µm. *SR-3D SIM image taken with assistance from Dr Wolfgang Hübner, using an OMX v4 microscope (GE Healthcare) at the University of Bielefeld.*

Owing to the huge span of the mitochondrion's function within the cell, mitochondria are not simply static, unchanging organelles, but dynamic and highly regulated, with the capacity to change their function, form, number, and position, in keeping with the needs of the cell [7]. Whilst records of such dynamic nature of mitochondria date back to early light microscopy studies from over 100 years ago [8], recent advances in live, high-resolution imaging techniques have allowed the scientific community to pinpoint the exact mechanisms by which such dynamic behaviour occurs: owing to two main processes responsible for altering mitochondrial morphology – fusion and fission (Figure 1.2) [9-12].

Mitochondrial fusion and fission, collectively known as mitochondrial dynamics, allow mitochondria to respond to the needs of the fluctuating physiological conditions of the cells in which they reside [4]. This is achieved by fusion and fission, which allow transfer and mixing of mitochondrial proteins, DNA, and lipids, as well as altering mitochondrial shape, size, and number [13].

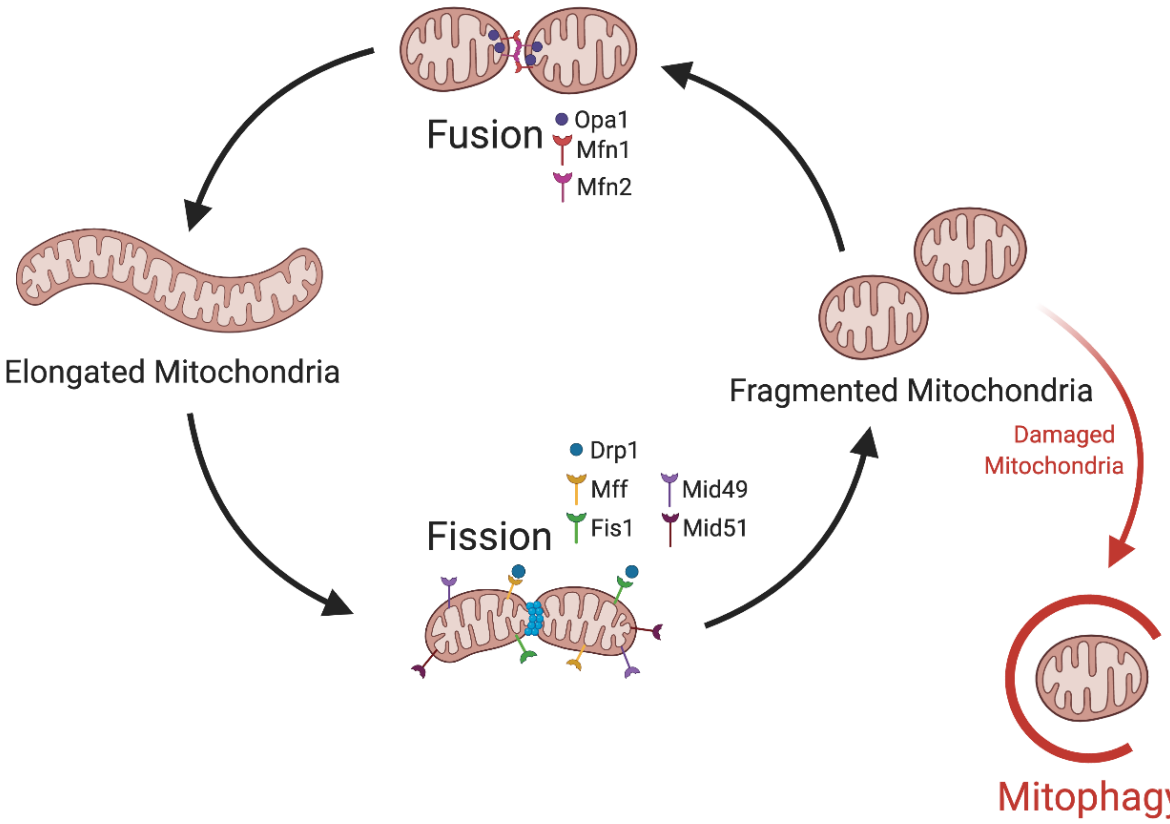

Figure 1.2: Mitochondrial Dynamics
Elongated mitochondria undergo fission, aided by DRP1 as well as receptor proteins MFF, FIS1, MiD49 and MiD51. This leads to formation of fragmented mitochondria. These, if damaged, can undergo mitophagy, or they continue in the fission: fusion cycle, where they fuse aided by MFN1, MFN2 and OPA1 in the inner membrane, to become elongated mitochondria. *Schematic created using BioRender.*

1.1.1. Mitochondrial Fission and the Role of DRP1

Mitochondrial fission is primarily mediated by a soluble, cytosolic GTPase which is conserved across species, known as dynamin-related protein 1 (DRP1 in mammals; Dnmp1 in yeast) [14-16]. DRP1 is recruited to the OMM where it polymerises into high-order oligomers, which assemble into spiral-like filaments, wrap around mitochondrial tubules and rely on GTPase activity to stimulate the constriction of mitochondria, inducing conformational changes required for mitochondrial division (Figure 1.2) [17-19]. It is likely that there are conformational changes prior to DRP1 assembly, for example it has been suggested that endoplasmic reticulum (ER) tubules wrap around and constrict mitochondria, in order to facilitate DRP1-mediated fission, since mitochondrial tubules are much larger than DRP1 spirals in diameter [9, 20]. Assembly of DRP1 on mitochondrial membranes is mediated by its numerous receptor proteins; mitochondrial fission factor (MFF), mitochondrial fission 1 protein (FIS1), and mitochondrial dynamics proteins of 49 and 51 kDa (MiD49 and MiD51) [21-23]. The interactions of DRP1 with mitochondria are highly regulated by various post-translational modifications (PTMs), including phosphorylation, ubiquitination, S-nitrosylation, and SUMOylation [24, 25].

The need for regulation of DRP1 activity by PTMs can be put down to its multiple steps in the process of mediating fission: translocation from the cytoplasm to the OMM, assembly into high-order spirals, GTP hydrolysis, and disassembly. Recent insights have shown that these modifications can occur both individually as well as in conjunction with one another to modify the various steps of mitochondrial fission, ensuring the fusion-fission balance remains in line with the requirements of the mitochondria and cell [25]. An example of mitochondrial dynamics regulation by PTM is phosphorylation of DRP1. It has been shown that phosphorylation of DRP1 at different sites has vastly differing effects on cells. Specifically, phosphorylation at Serine 616 (S616) by cyclin dependent kinase 1 or 5 (CDK1/5) promotes mitochondrial translocation and thus fission [26, 27], whilst, conversely, phosphorylation of DRP1 at Serine 637 (S637) by protein kinase A (PKA) leads to DRP1 detachment from mitochondria, inhibiting mitochondrial fission or promoting fusion [28, 29].

Such highly controlled regulation of DRP1 activity is important, as it has been shown that defective fission, as a result of either dysregulation of critical steps, or mutation of DRP1, has huge impacts on cell health and viability, and can lead to devastating diseases. One such example of a single heterozygous dominant-negative missense mutation DRP1 (A395D) was shown by genetic analysis in a patient born with a plethora of life-threatening problems which ultimately led to lethality within a matter of days [30]. The lethality as well as the broad spanning list of associated defects highlights the importance of functional mitochondrial fission in not only mitochondrial function and viability but that of the entire organism.

1.1.2. Mitochondrial Fusion

Mitochondrial fusion is also mediated by dynamin-like GTPases, optic dominant atrophy 1 (OPA1) and mitofusin (Mfn), which are highly conserved and known as mitochondrial genome maintenance 1 (Mgm1) and Fzo1 in yeast [12]. However, in contrast to fission, where a bundle of proteins can act on the OMM surface to slit both mitochondrial membranes, fusion involves protein machineries on the outer and inner membranes which must operate in synchrony for efficient merging of mitochondria (Figure 1.2). OPA1 is localised either in the IMS or associated with the IMM (see below), and controls IMM fusion [31, 32]. It is proposed that OPA1 interacts with Mfn proteins to form complexes responsible for coupling of the outer and inner membranes, allowing fusion of mitochondria to occur (Figure 1.2) [33, 34]. Mfn exists as two isoforms, Mfn1 and Mfn2, both of which are located in the OMM and act to fuse the outer membranes of adjacent mitochondria in a highly coordinated manner, *via* homotypic and heterotypic interactions [35, 36].

Fusion is a highly regulated process, owing to its many vital roles in the cell. Firstly, OPA1 exists as eight variants, produced by alternative splicing of one single gene, and, once they reach the mitochondria, these eight polypeptides are subjected to further proteolytic processing to form various long (embedded in IMM) and short (soluble in IMS) isoforms (Figure 1.3) [37]. This processing is thought to be mediated by several proteins including the rhomboid protease presenilin-associated rhomboid-like (PARL), IMS AAA-metalloprotease YME1L, and IMM AAA-protease paraplegin [38-42]. Additionally, the mitochondrial membrane potential (also known as delta-psi; $\Delta\Psi$) is important for stabilisation of longer isoforms and for inner membrane fusion, and destabilisation of the $\Delta\Psi$ can lead to a reduction in mitochondrial fusion. This leads to hyperfragmentation of mitochondria, which can induce mitophagy and subsequent cell death [42, 43].

Mutations in OPA1 are responsible for the onset of a hereditary, autosomal disease of progressive vision loss, known as autosomal dominant optic atrophy [37]. Mutations in Mfn2 or Ganglioside-induced differentiation-associated protein 1 (GDAP1), an OMM protein whose expression in neurons induces mitochondrial fragmentation, lead to Charcot-Marie-Tooth (CMT) Type 2A or 4A, respectively [44, 45]. Type 4A is a clinically similar but much more severe form of CMT compared to Type 2A [44]. CMT disease is the most common inherited neuropathy, affecting approximately one in 2500 people, and is characterised by sensory loss and weakness or atrophy of muscles, mainly effecting the lower extremities [27, 45]

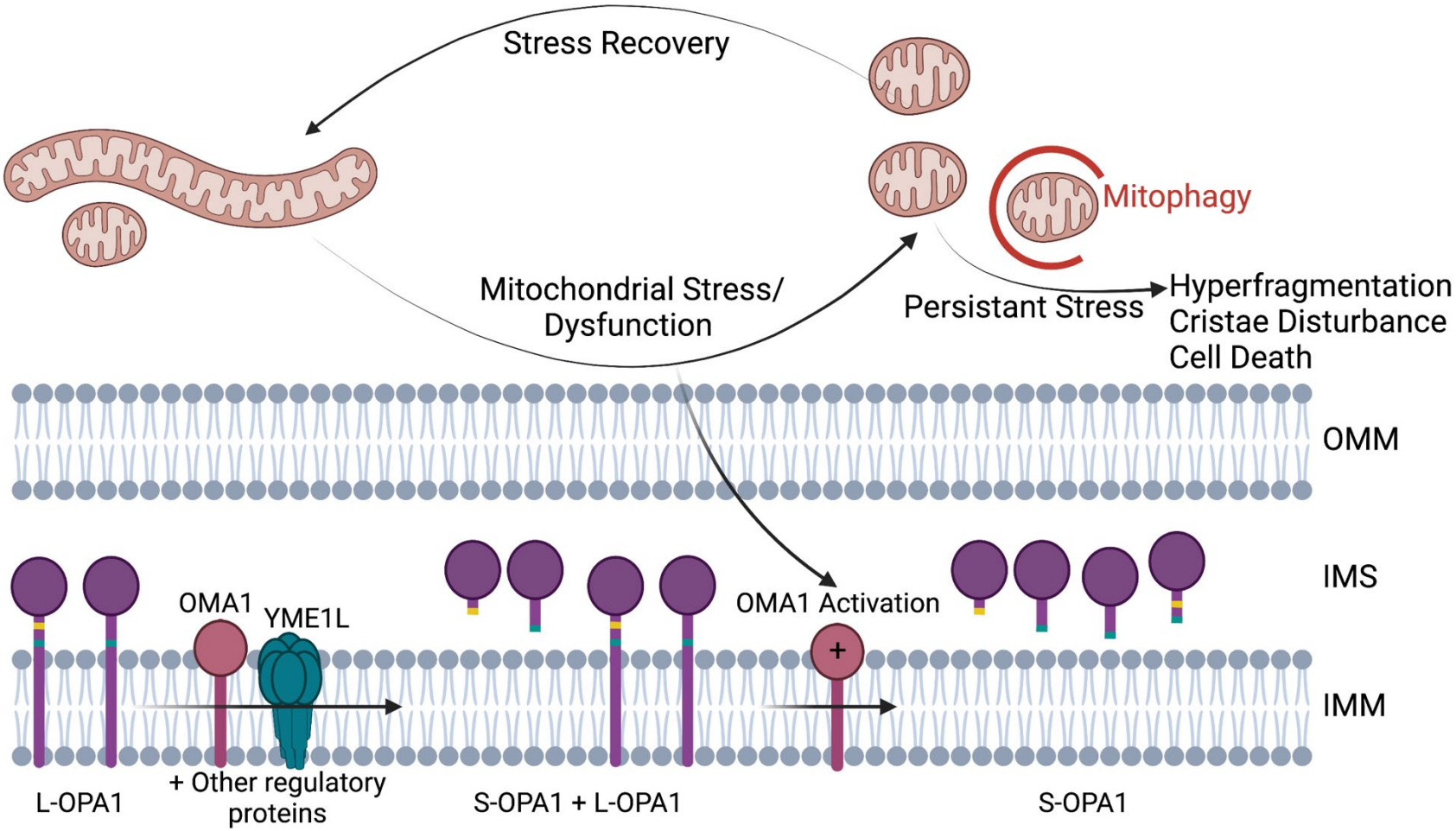

Figure 1.3: OPA1 Processing
L-OPA1 (uncleaved) mediates fusion of the IMM and preserves cristae structure. L-OPA1 is processed by OMA1, YME1L, and other regulatory proteins, to retain a balance between L-OPA1 and S-OPA1 (cleaved). However, in the presence of mitochondrial stress, such as oxidative stress or a reduction in $\Delta\Psi$, OMA1 becomes activated and increases cleavage of L-OPA1, resulting in an increase in IMS soluble S-OPA1, and loss of L-OPA1. This reduces mitochondrial fusion and enhances fission. Persistent stress leads to mitochondrial hyperfragmentation, cristae disturbances, mitophagy, and ultimately, cell death.

1.2. Mitochondrial Bioenergetics

The most vital role carried out by mitochondria is the production of cellular energy by the generation of ATP. This is carried out by the respiratory complexes of the respiratory chain. The respiratory chain is organised into four complexes, Complexes I-IV (CI-IV), which are each made up of various subunits, and have the ability to form supercomplexes (SCs) [46].

The respiratory chain functions to generate ATP as the major energy source of the cell, and this is achieved by oxidative phosphorylation (OXPHOS), which was first described as the chemiosmotic theory by Peter Mitchell in the 1960s [47]. OXPHOS involves four respiratory complexes working as individual units or associated into SCs which facilitates electron transfer [48] . The electron transfer from reducing equivalents, *i.e.,* Nicotinamide adenine dinucleotide (NADH) and flavin adenine dinucleotide ($FADH_2$), to molecular oxygen occurs down their electrochemical potential with entry points at the CI level (NAD-ubiquinone oxidoreductase) and CII (Succinate dehydrogenase), following to CIII (Ubiquitinol cytochrome c oxidoreductase) and then CIV (Cytochrome c Oxidase) [48, 49] (Figure 1.4). The flow of electrons through the electron transfer chain (ETC) is coupled to the pumping of protons from the matrix to the IMS via CI, CIII, and CIV. This electro-proton gradient or PMF is used to power the production of ATP from ADP and Pi *via* Complex V (ATP synthase; Figure 1.4) [48].

As shown in Figure 1.4, the OXPHOS complexes are composed of both nuclear and mitochondrial-encoded subunits, requiring the synchronisation of a series of pathways and cellular machineries. Firstly, nuclear and mitochondrial gene expression must be coordinated. This process has been observed in yeast [50], but the underlying mechanisms are still poorly understood. It is believed that the translation of mtDNA-encoded mRNAs is regulated by a series of translational activators acting on the 5'-untranslated region (UTR), while other translational activators could interact with ribosomes or play a role in transcript stabilisation [51-54]. Moreover, feedback regulation mechanisms linking respiratory complex subunits expression with the state of complexes assembly have been described for CIII [55, 56], CIV [57-60], and CV [61, 62]. Furthermore, mitochondrial import is heavily reliant on the activity of the ETC, since many of the import pathways require both ATP and the $\Delta\Psi$ to function correctly. This will be discussed in more detail for each pathway in the following section, which will cover how cytoplasmic translated proteins are imported into mitochondria.

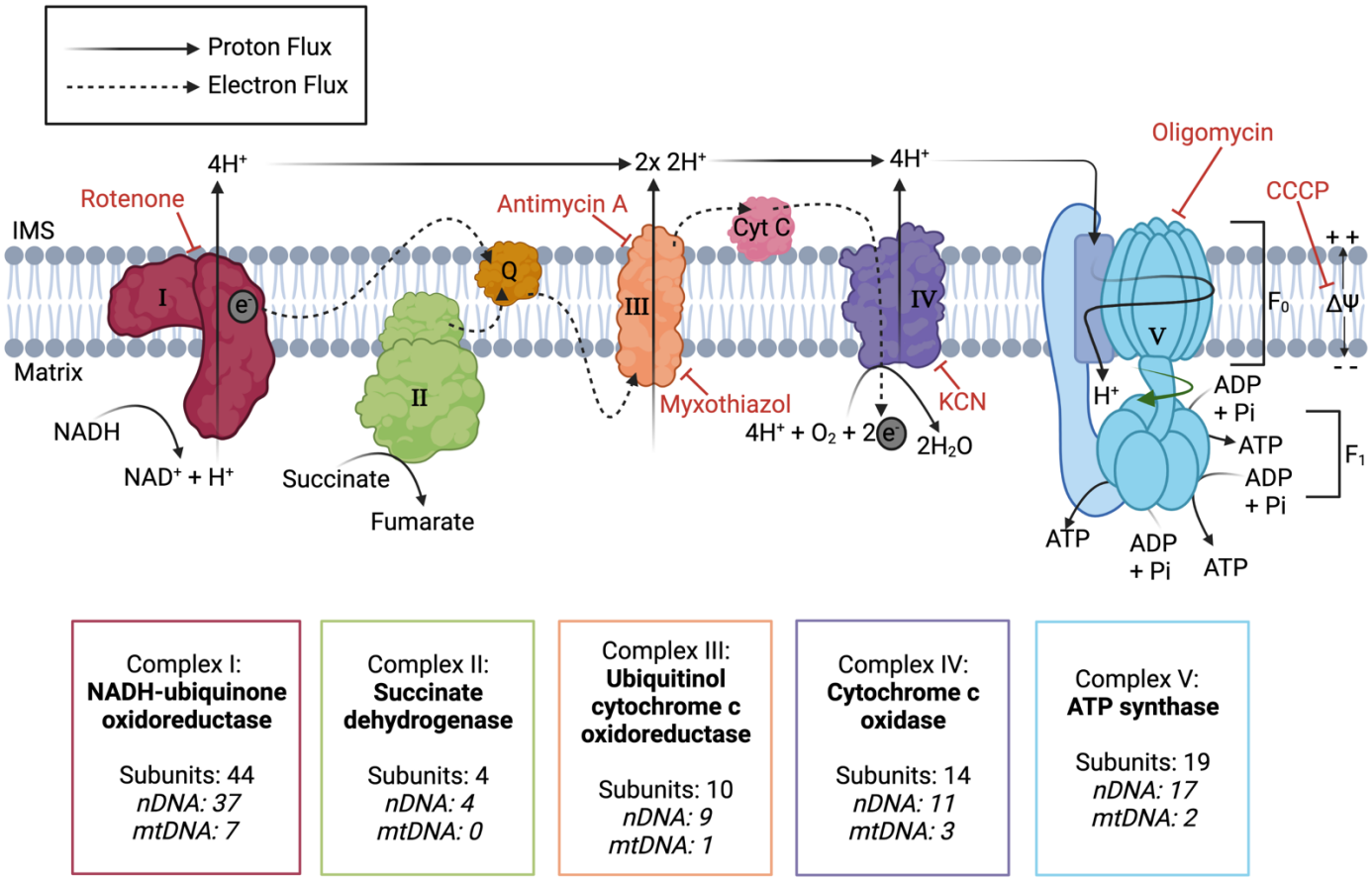

Figure 1.4: Mitochondrial Respiratory Chain
The respiratory chain consists of four complexes (Complexes I-IV) and two intermediary substrates (coenzyme Q; Q, and Cytochrome c; Cyt c). NADH and $FADH_2$ (a prosthetic group in succinate dehydrogenase) are oxidised to produce protons which form a proton gradient across the inner membrane. Electrons (e^-) are shuttled through the RC via a series of electron transporters. Finally, ATP synthase (Complex V) uses the protons (H^+) produced by the respiratory chain to produce ATP, powered by the PMF. The number of subunits required for formation of the respiratory chain complexes encoded by nuclear DNA (nDNA) and mitochondrial DNA (mtDNA) are shown below each complex. Standard inhibitors of each component are highlighted in red. *Schematic created using BioRender.*

1.3. Protein Translocation

All but 13 of the estimated >1000 human mitochondrial proteins [63] required to perform key mitochondrial functions are encoded by the nucleus and synthesised by cytoplasmic ribosomes, and consequently must be imported into mitochondria through highly conserved protein translocation pathways (Figure 1.5). Owing to the double membrane bound structure of mitochondria, these multistep protein translocation pathways involve numerous protein complexes (Figure 1.5 and Table 1.1). Moreover, their proteome consists of soluble, membrane-bound, and transmembrane proteins with different mitochondrial sub-localisations. Therefore, specialised import machinery has evolved to import all classes of proteins [64].

1.3.1. Crossing the Outer Membrane

All proteins destined for the mitochondria must first cross the OMM, which they gain access to *via* the translocase of the outer membrane (TOM) complex (Figure 1.5). The TOM core complex (TOM-CC) consists of five components: TOM40, TOM22, TOM7, TOM6, and TOM5. The TOM holo-complex is formed following weak association of the TOM-CC with an additional two subunits: TOM20 and TOM70 [65, 66]. These subunits are highly conserved between humans and yeast, as described in detail in Table 1.1.

Precursor proteins are recognised by the receptor proteins TOM20, which recognises proteins with a mitochondrial targeting sequence (MTS) *i.e.,* presequence proteins [67, 68], and TOM70, which specifically recognises precursors with internal targeting signals, such as those belonging to the solute carrier family (SLC25) [69, 70]. Proteins are then passed to the TOM40 pore *via* another receptor component, TOM22, which has also been shown to assist in the assembly of the TOM complex [65, 71, 72]. TOM22 physically interacts with TOM40 via its transmembrane segment, whilst its cytosolic domain has been suggested to act as a docking site for the other receptor proteins, TOM70 and TOM20. Recently, the OMM porin metabolite channel (also known as Voltage-dependent anion channel; VDAC) has been reported to regulate Tom22 integration into the TOM complex in yeast, thus regulating the assembly and stability of the TOM complex [73, 74]. Por1, the major yeast isoform of Porin, binds newly imported Tom22 and integrates it into the TOM complex, promoting formation of the mature trimeric form of the TOM complex required for import of precursor proteins [73]. Por1 also sequesters dissociated Tom22, stabilising the dimeric TOM complex under situations where this is preferable, *i.e.,* for the import of proteins destined for the mitochondrial IMS assembly (MIA) pathway [73]. Porin is also thought to cooperate with TOM6 in regulating trimeric TOM assembly and stability and thereby modulating protein import during the cell cycle [73, 75].

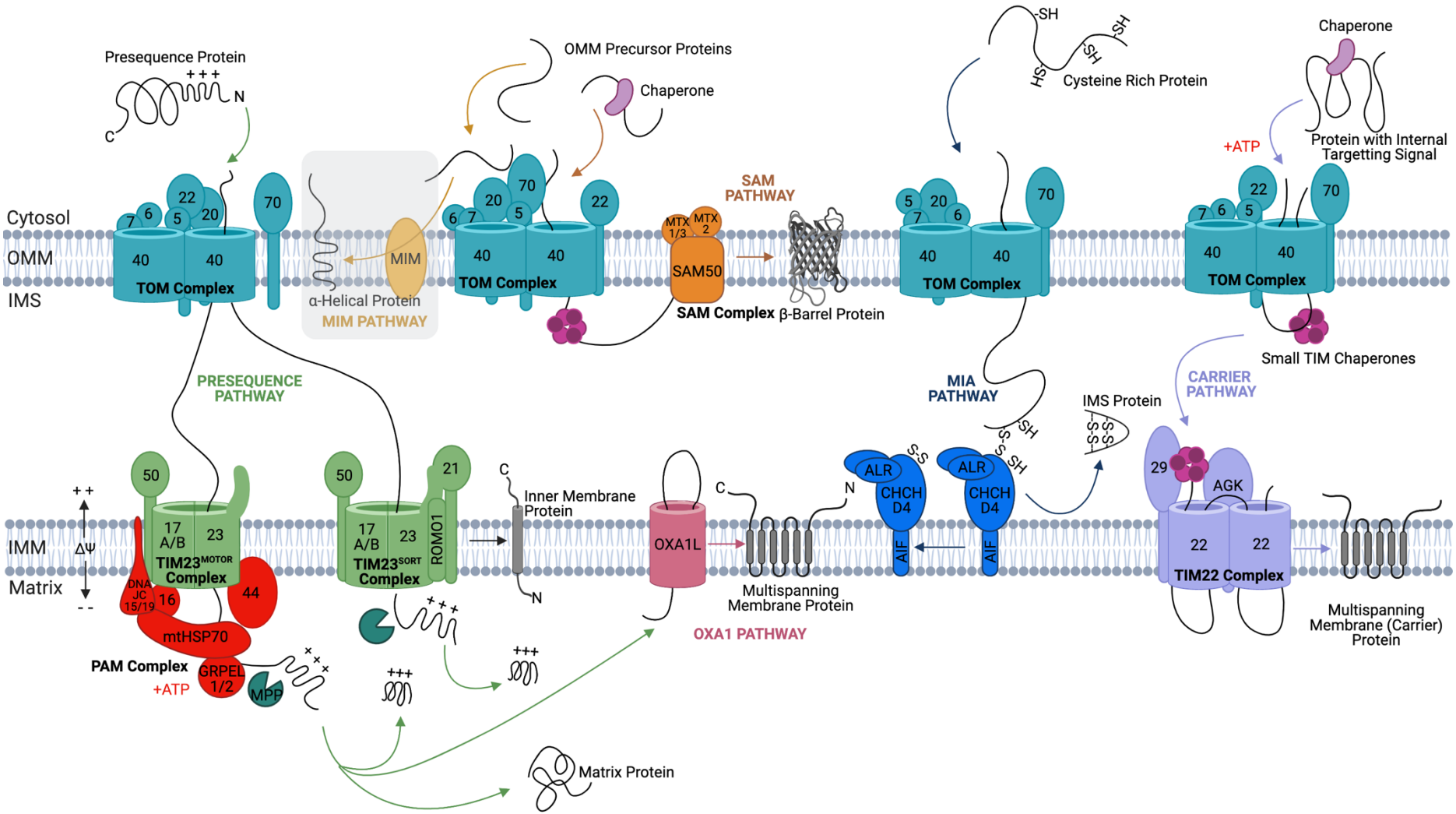
Presequence Protein
OMM Precursor Proteins
Chaperone
Cysteine Rich Protein
Chaperone
+ATP
Protein with Internal Targetting Signal
Cytosol
OMM
IMS
TOM Complex
MIM
α-Helical Protein
MIM PATHWAY
SAM PATHWAY
SAM50
SAM Complex
β-Barrel Protein
Small TIM Chaperones
PRESEQUENCE PATHWAY
MIA PATHWAY
CARRIER PATHWAY
IMS Protein
IMM
Matrix
ΔΨ
TIM23 MOTOR Complex
TIM23 SORT Complex
ROMO1
Inner Membrane Protein
OXA1L
Multispanning Membrane Protein
OXA1 PATHWAY
ALR
CHCH D4
AIF
AGK
TIM22 Complex
Multispanning Membrane (Carrier) Protein
PAM Complex
+ATP
mtHSP70
GRPEL 1/2
MPP
DNA JC 15/19
Matrix Protein

Figure 1.5: Overview of Mammalian Mitochondrial Import Pathways
The TOM complex acts as the central entry gate for precursor proteins to enter the IMS, where they are diverted into one of five pathways, depending on their structure, function, and target destination. The **MIM PATHWAY** (only currently understood in yeast) is an exception in that proteins usually do not cross the Tom40 channel. Instead, OMM α-helical proteins are recognised by Tom70 and transferred through MIM to be inserted into the OMM. The five major pathways proteins take after crossing the TOM channel are: **PRESEQUENCE PATHWAY**. Presequence containing precursor proteins are transported via the presequence pathway. Of these proteins, proteins with a hydrophobic sorting sequence are inserted into the IMM by the $TIM23^{SORT}$ complex, whereas hydrophilic matrix proteins are pulled through the $TIM23^{MOTOR}$ complex, with the help of the PAM complex and ATP hydrolysis cycles. The presequences of both these groups of proteins are cleaved by mitochondrial processing peptidase (MPP) on the matrix side. **OXA1 PATHWAY**. N-terminally inserted multispanning membrane proteins, once passed through $TIM23^{MOTOR}$ and cleaved by MPP, are passed to OXA1L which inserts them into the IMM in the N-terminal formation. OXA1L is also responsible for the insertion of mtDNA encoded proteins into the IMM. **SAM PATHWAY**. β-barrel proteins are transported to the TOM complex by cytoplasmic chaperones. They are then passed through the TOM complex and received by small TIM chaperones on the other side for insertion into the OMM by the SAM complex. **MIA PATHWAY**. Cysteine-rich proteins in an unfolded, reduced state are passed *via* the TOM complex to the MIA complex which inserts disulphide bonds in them, allowing them to reside in a folded, oxidised state in the IMS. **CARRIER PATHWAY**. Proteins with internal targeting signals are protected in the cytosol by cytosolic chaperones (Stage I) which pass them to the TOM complex (Stage II). They are received on the IMS side by small TIM chaperones (Stage III) which transfer them through the IMS to the TIM22 complex (Stage IV) for insertion into the IMM (Stage IV). *Schematic created using BioRender [1].*

Table 1.1: Subunits of the Mitochondrial Translocase Complexes in Humans and Yeast

Pathway	Complex		Subunit (Mammalian)	Yeast Homolog	Main Function	Topology
TOM	TOM-Holo Complex	Core Complex	TOM40 and TOM40L	Tom40	Channel protein	β-barrel (19 β strands) and one N-terminal α-helical segment located inside pore
			TOM22	Tom22	Receptor protein Located at the dimer interface between TOM40 pores	α-helical (single TMD); C_{in}-N_{out}
			TOM5	Tom5	Complex assembly/stability	α-helical (single TMD); C_{in}-N_{out}
			TOM6	Tom6	Complex assembly/stability	α-helical (single TMD); C_{in}-N_{out}
			TOM7	Tom7	Complex assembly/stability	α-helical (single TMD); C_{in}-N_{out}
		Receptors	TOM70	Tom70	Receptor for carrier precursors	α-helical (single TMD); N-terminally inserted
			TOM20	Tom20	Receptor for presequence precursors	α-helical (single TMD); N-terminally inserted
SAM	SAM Complex		SAM50	Sam50	Core subunit responsible for β-barrel protein insertion	β-barrel (16 β-strands)
			MTX1 and MTX3	Sam37	Accessory subunit	N/A
			MTX2	Sam35	Accessory subunit	N/A
MIM	MIM Complex		Unknown	Mim1	Biogenesis of α-helical OMM proteins	--
			Unknown	Mim2	Biogenesis of α-helical OMM proteins	--
MIA	MIA Complex		CHCHD4	Mia40	Oxidoreductase	Helix-loop-helix attached to a flexible helical arm
			ALR (GFER)	Erv1	Reoxidises Mia40	α-helical (a1-5) bundle
			Cytochrome C/ETC	Cytochrome C/ETC	Final electron acceptor	Class I of the c type cytochrome
			AIF	-	Anchors CHCHD4 to the IMM	One C-terminal TMD; N_{in}, C_{out}
TIM23/ Presequ-ence	$TIM23^{SORT}$ Complex		TIM21	Tim21	Recognition/direction of precursor proteins to TIM23	α-helical (single TMD) with a large IMS domain; N_{in}-C_{out}
			ROMO1	Mgr2	Lateral release of proteins into the IMM	Two α-helical TMDs, joined by a basic loop
		$TIM23^{M-OTOR}$ Complex	TIM17A/B	Tim17	Channel forming	4 TMDs and a small IMS domain
			TIM23	Tim23	Channel forming	Multiple TMDs, and IMS exposed hydrophilic domain

			TIM50	Tim50	Receptor Protein	Single TMD, large IMS exposed C-terminal domain
	PAM Complex		TIM44	Tim44	Scaffold for complex & binding emerging precursor	Peripheral membrane protein on matrix side
			mtHSP70 (Mortalin)	SSC1 (mtHsp70)	ATPase	β-sheet and α-helical domains
			DNAJC15 and DNAJC19	Pam18 (Tim14)	Stimulates ATPase activity of mHsp70	Single α-helical TMD, with large C-terminal matrix domain and small N-terminal IMS domain
			TIM16	Pam16 (Tim16)	Inhibits Pam18 stimulatory effect on ATPase activity of mHsp70	Three α-helices forming an antiparallel hairpin
			GrpEL1/2	Mge1	Regeneration of mtHSP70	Long N-terminal α-helical region, small helical bundle region, and a C-terminal β-sheet domain
			Unknown	Pam17	Binds precursor: chaperone complex in matrix	--
TIM22/ Carrier	TIM22 Complex		TIM22	Tim22	Channel	4 TMs that form a curved surface IMS-facing N-helix
			TIM29	-	Scaffold	Matrix-facing N-helix, single TM, and an IMS domain
			AGK	-	Assembly and function	N-terminally inserted with an IMS α/β motif
			TIM9	Tim9	Chaperone	Donut-shaped hexamer structure
			TIM10A	Tim10	Chaperone	
			TIM10B	Tim12	Chaperone	
			-	Tim54	Holds chaperone ring in tilted conformation	N-terminally inserted with an IMS α/β motif
			-	Tim18	Docking platform for chaperones	3 TMs and an amphipathic helix on the IMS side
			-	Sdh3	Docking platform for chaperones	3 TMs and an amphipathic helix on the IMS side
OXA	OXA		OXA1L	OXA1	Insertion of mtDNA encoded proteins and N-terminal insertion of nuclear encoded proteins into the IMM	5 TM helices and a large internal C-terminal domain; N_{out}-C_{in}

The different oligomeric states of the TOM complex and the nature of these different states remains unclear. Whilst it had generally been accepted that the mature form of TOM complex exists as a trimer [76-79], a cryogenic electron microscopy (cryo-EM) study in *Neurospora crassa* showed the TOM complex in a dimeric form [80]. More recently, high-resolution cryo-EM studies in *Saccharomyces cerevisiae* showed that the TOM-CC exists as dimers and tetramers. The latter is essentially a dimer of the dimeric form of TOM-CC, achieved by lateral stacking of the dimeric TOM complex [66]. Due to the dynamic properties of the TOM complex, it may be proposed that the trimeric complex is formed by dissociation of a monomer from the tetrameric form.

Of note, the only protein of the TOM complex with a significant IMS domain is TOM22, which is important for its role in directing emerging precursor proteins to the TIM50 receptor of the translocase of the inner membrane 23 (TIM23) complex for further translocation [81]. Structural analysis of the interactions between these differing structural subunits showed that association is mainly mediated by hydrophobic interactions, along with high surface complementarity between the transmembrane domains [66].

1.3.2. Biogenesis of OMM proteins

Evidence has also shown that, in yeast, Tom40 may simultaneously act as an insertase, assisting in the lateral release and insertion of proteins destined for the OMM. However, this is highly dependent on specific determining factors within the precursor sequence and is not yet fully understood [82]. Although this initial observation was monitored using an artificial import substrate, it has since been suggested that a similar process might be responsible for the accumulation of high-Mw PINK1 in the OMM in a TOM7-dependent manner [83, 84].

Recently, it has been proposed that in addition to their role in quality control, PINK1/Parkin also regulate protein import under physiological conditions where mitochondrial function remains normal [85]. It is proposed that ‘local dysfunction’, as in mitochondrial $\Delta\Psi$ depolarisation or reduced import efficiency, is sensed by the PINK1/Parkin pair which phosphorylates several subunits of the TOM complex, namely TOM20, TOM70 and TOM22, facilitating the import of precursor proteins [85]. Importantly, the ubiquitination pattern under this condition is significantly different from the PINK1/Parkin activation experienced from global mitochondrial dysfunction. Conversely, the mitochondrial deubiquitinase USP30 antagonises these effects [85-87]. Additionally, USP30 was shown to work in a reciprocal manner to MARCH5, an E3 ubiquitin-protein ligase of the OMM, under basal conditions, for deubiquitinating presequence substrates during translocation, facilitating their import. For other regulatory mechanisms of protein import please see [88].

1.3.2.1. Insertion of β-Barrel Proteins in the OMM

Precursors of β-barrel proteins destined to be inserted into the OMM are passed via small TIM chaperone proteins to the sorting and assembly machinery (SAM) complex, for insertion into the OMM [89-91]. The human SAM complex consists of accessory subunits MTX2 (yeast Sam35), MTX1 and MTX3 (yeast Sam37), and OMM associated β-barrel core subunit SAM50 (yeast Sam50; Table 1.1) [92]. In yeast, there are only four known families of β-barrel OMM proteins, and computational analysis predicts that there are no new ones to be discovered [93, 94]. Yeast β-barrel precursor proteins are translocated through the TOM complex where they are bound by small TIM chaperones and transferred through the IMS to the SAM complex (Figure 1.5). Substrate proteins are recognised by Sam35, which interacts with the β-signal located in the last strand of the substrate protein. This initiates insertion into Sam50, which is responsible for folding and inserting substrates into the OMM [90]. Sam37 is required for substrate release and has also recently been proposed to assist in the formation of a SAM-TOM SC, mediated by physical interaction of Sam37 and Tom22 on the cytosolic side of the OMM [95]. This SAM-TOM interaction has been shown to be essential for coupling of the two OMM complexes and promoting efficient precursor transfer [95]. Though not a part of the core SAM complex, Mdm10 is thought to associate with the SAM complex and have an important role in Tom40 assembly into the TOM complex [96]. This pathway is very similar to that observed for β-barrel proteins of the outer membrane in bacteria, which are folded and inserted into the outer membrane by the β-barrel assembly machinery (BAM) complex, the *E. coli* homolog of SAM [92].

1.3.2.2. Incorporation of α-Helical Anchors in the OMM

Over 90% of integral OMM proteins contain α-helical membrane anchors, yet the import pathway undertaken by these proteins is still relatively poorly understood, particularly in humans [97]. In yeast, the majority of these proteins are recognised by the Tom70 receptor of the TOM complex and passed on to the insertase of the outer mitochondrial membrane (MIM) complex which aids in their insertion into the OMM, completely bypassing the Tom40 channel (Figure 1.5 and Table 1.1) [98, 99]. Multiple copies of Mim1 arrange themselves in such a way that, when reconstituted into the lipid bilayer, a channel is formed, and along with a couple of copies of Mim2, this establishes the MIM complex [100, 101].

There are, however, known exceptions to this rule, whereby these α-helical proteins are passed through the Tom40 channel into the IMS prior to insertion into the OMM, aided by the MIM complex [102, 103]. Interestingly, one of these proteins, yeast Om45, has been shown to require the TOM, TIM23 and MIM complexes for insertion into the OMM, where it is

anchored by its N-terminal signal sequence with the bulk of the protein exposed to the IMS [102]. The final topology of Om45 is thus opposite to the N_{in}-C_{out} topology typical of MIM pathway proteins. The other known exception, yeast Mcp3, is also directed *via* TOM and TIM23, but is then processed by the inner mitochondrial membrane protease (IMP) before being transferred *via* MIM and inserted into the OMM with a final topology of N_{out}-C_{out} [103]. Notably, whilst both proteins interact with components of the TIM23 complex, and are dependent on Δψ, they do not cross or interact with the IMM [102, 103].

1.3.3. Co- and Post-Translational Translocation

Importantly, preproteins must be unfolded in the cytosol and subsequently stabilised, in an ATP dependent process, by molecular chaperones of the heat shock protein (hsp) families Hsp70 and Hsp90, to then be efficiently imported [104, 105]. Conversely, the subsequent translocation of these unfolded preproteins through the TOM channel occurs independently of ATP and Δψ, and instead relies on an indirect driving force. That is the increased affinity of the presequences for the *trans* over *cis* side of the TOM channel, allowing transport of the preproteins across the channel where the presequence is bound by TIM50 [106]. This transport is also thought to rely on the sequential binding of the presequence to acidic domains of receptor proteins in what is known as the ‘acid chain’ hypothesis [107]. A recent kinetic study from our lab, carried out in mitochondria isolated from yeast cells, showed that there are two rate limiting steps during import via the presequence pathway [108]. That is, precursor passage across the OMM, and presequence dependent initiation of transport across the IMM. It highlights these as two distinct steps, rather than one continuous import event, as was previously understood. Furthermore, this work describes the rapid rate of protein passage through the TIM23 channel and suggests this could be important in preventing import failure as a mechanism of maintaining mitochondrial fitness. Finally, this study suggests that transport across the TOM complex is reversible, and that proteins can indeed be retro-translocated back into the cytosol [108].

Interestingly, whilst the majority of preproteins are synthesised in the cytosol and must be unfolded prior to insertion into the TOM complex, others are unable to be imported into mitochondria post-translationally, and instead must undergo co-translational translocation whereby cytosolic ribosomes associate with mitochondria [109]. For this subgroup of proteins, it is thought that signals within the 3’-UTR and coding regions of their mRNAs mediate their targeting to the cytosolic side of the OMM [110-112], where cytosolic ribosomes have also been observed [113, 114].

1.3.4. Staying in the Intermembrane Space: The Disulfide Relay System

Proteins destined for the IMS take the route of the MIA pathway (Figure 1.5 and Table 1.1), which has been reviewed in great detail previously [115]. This class of proteins lack an MTS, are generally small and share a conserved coiled coil-helix 1-coiled coil-helix 2 domain (CHCHD). These cysteine-rich proteins contain two pairs of cysteines separated by three or nine amino acid residues (Cx_3C or Cx_9C) in the helices [115]. The small TIM chaperones of the IMS, important for translocase of the inner mitochondrial membrane 22 (TIM22)-dependent translocation (described below), and assembly factors of IMM proteins, such as the respiratory complexes, are some examples of MIA substrates. The substrates are also relatively unstable and prone to degradation prior to their reduction by the relay system [116]. These cysteine-rich proteins undergo oxidation driven import whereby, upon passing through the TOM complex in an unfolded, reduced state, they form transient disulphide bonds with Mia40 [117, 118]. CHCHD4 is the human ortholog of yeast Mia40 and shows high conservation despite the smaller size (16 vs 40 kDa, respectively), lack of MTS and no transmembrane anchor domain [119]. Instead, the human CHCHD4 interacts with the apoptosis inducing factor (AIF) and its cofactor NADH for association with the IMM [119].

The second player in the MIA pathway is ALR (also known as GFER; Erv1 in yeast), a FAD-linked sulfhydryl oxidase, that enables new rounds of precursor import and oxidation by re-oxidising reduced CHCHD4 after it has carried out its role as an oxidoreductase, thus allowing the cycle to continue [120]. Similarly, reduced ALR can relay its electrons to cytochrome *c* and, afterwards, to CIV of the respiratory chain [121]. Therefore, despite not requiring ATP or $\Delta\Psi$ to operate, the MIA pathway still depends on a functional ETC to successfully oxidise its substrates.

1.3.5. Crossing or Insertion in the Inner Membrane

Proteins that are destined elsewhere, namely the matrix or its membrane, must subsequently pass through or into the IMM (Figure 1.5). This membrane crossing (or insertion) import event is facilitated by one of two translocase complexes, the TIM23 complex or the TIM22 complex.

1.3.5.1. TIM23 Complex (Presequence Pathway)

Precursor proteins destined for the mitochondrial matrix, along with some IMM sorted proteins, containing an N-terminal presequence (*i.e.,* MTS), are passed directly from the TOM complex to the TIM23 complex [65, 88]. The MTS is a cleavable region of 15 to 50 amino acids that precedes the mature protein and which is rich in hydrophobic, hydroxylated, and basic residues, with an overrepresentation of arginine residues and a near absence of acidic

residues, forming a positively charged, amphipathic α-helix [64]. Interestingly, it has recently been suggested that preproteins may also contain additional internal MTS-like signal sequences (iMTS), located in the mature region of the preprotein, which act similarly to presequences and mediate the binding of the preprotein to TOM70, increasing the efficiency of protein import *via* the presequence pathway [122].

The TIM23 complex is anchored to the IMM and exists as a hetero-oligomeric complex, composed of various subunits (Table 1.1). It consists of an integral membrane embedded core complex as well as an import motor [123]. The core complex contains three essential subunits: TIM17A/B, TIM23, and TIM50 (Tim17, Tim23, and Tim50 in yeast) [106, 124-126]. Additionally, the membrane-embedded part has two non-essential subunits: TIM21 and ROMO1 (Tim21 and Mgr2 in yeast) [127, 128]. The import motor, also known as the presequence translocase-associated motor (PAM) complex, drives translocation across the IMM, aided by ATP hydrolysis, and consists of TIM44, mtHSP70, DNAJC15/19, TIM16, and GRPEL1/2. In yeast the homologs are Tim44, SSC1 (also known as mtHsp70), Tim16 (also known as Pam16), Tim14 (also known as Pam18), and Mge1, as well as Pam17 which is not known to have a human homolog [129-134].

In yeast, precursor proteins released from the TOM complex and destined for the presequence pathway are recognised by Tim50 and the IMS region of Tim23, which act as receptor proteins for the incoming precursors [123]. This is achieved by binding of the hydrophilic, IMS exposed part of the Tim23 subunit and the IMS-extending part of the Tim50 subunit, in the IMS [106, 125, 126, 135]. The Tim23 pore acts as a voltage gated channel and is ~13 Å wide, thus wide enough for only one α-helix to pass through at a time [136, 137]. The pore is formed by the hydrophobic, C-terminal membrane domain of Tim23, and Tim17, which has been shown in the yeast model to be important for formation of the twin-pore structure, since it is unable to form in Tim17-depleted mitochondria [138]. In the handover of proteins from the TOM complex to the TIM23 complex, Tim50 also interacts with various partner proteins, including Tom22 and Tom21, which are necessary for the correct recognition and direction of precursor proteins across the IMS to the Tim23 channel [135, 139-141]. Notably, it has recently been shown that phosphorylation/dephosphorylation of mammalian TIM50 is required for regulation of import activity, that is, phosphorylation of TIM50 reduces mitochondrial import, whilst its dephosphorylation by human phosphatase PPTC7 enhances it [142]. TIM50/Tim50 is phosphorylated on its matrix-facing segment in both mice and yeast (T33 and S103, respectively) [142], but the identity of the kinase(s) responsible for this effect is still unknown. Furthermore, various matrix proteins were found to have phosphorylation sites around their MTS, the dephosphorylation of which is also thought to be important for enhancing their import

and processing within the matrix [142]. This study highlights the importance of further work to dissect the currently unclear mechanisms regulating translocation.

The transport of precursor proteins across the import channel of the IMM is driven by a number of forces: the PMF, *i.e.,* ΔΨ and ΔpH, the affinity of the presequence for the *cis* side over the *trans* side of the membrane, and ATP hydrolysis [123, 143]. As mentioned above, the higher affinity of presequences towards Tim50 initiates the handover from TOM to TIM23. Additionally, the positively charged MTS means that the ΔΨ across the IMM exerts an electrophoretic effect on the proteins, facilitating the threading through TIM23.

As soon as the precursor emerges from the channel it immediately interacts with Tim44. Importantly, it was shown that the affinity of presequences is higher for Tim44 compared to Tim50 [139], strengthening the directionality of presequence movement across the IMM. Additionally, Tim44 is known to act as a scaffold and to recruit the PAM complex (Table 1.1) [144]. In this model, one arm of Tim44 is anchored to Tim23 while another arm is dynamic and interacts with mtHsp70, Tim16 and, indirectly, Tim14, controlling the active: inactive state of the motor [137]. A typical cycle would involve the recruitment of ATP-bound mtHsp70 followed by a loose binding to the emerging precursor. Then, Tim14 would stimulate the ATPase activity of mtHsp70, trapping the bound polypeptide and consequently releasing the chaperone from Tim44, allowing the sliding of the precursor: chaperone complex into the matrix. The binding of Mge1 to this complex in the matrix allows the release of ADP and subsequent binding of a new ATP molecule coupled with the release of bound precursor [145]. The presequences are cleaved off by MPP, allowing for protein folding and maturation [128].

Nonetheless, not all precursors that are passed to the TIM23 complex are destined for the matrix. In fact, TIM23 is also responsible for the sorting and lateral insertion of membrane proteins into the IMM. These proteins contain a stop transfer signal, a region adjacent to the presequence of ~20 amino acids which is rich in hydrophobic residues flanked by charged residues, also known as a sorting signal sequence, which targets them for this pathway of insertion [146]. The assembled TIM23 complex responsible for protein insertion into the IMM differs from the motor associated TIM23 in that it contains TIM21 (Tim21) and ROMO1 (Mgr2) and lacks the PAM complex [128], since it does not require the motor activity but is instead thought to be driven solely by Δψ [146, 147]. For these reasons the motor associated TIM23 complex is known as $TIM23^{MOTOR}$ complex, whilst the lateral release TIM23 complex is known as the $TIM23^{SORT}$ complex. Tim21 is important in regulating the lateral release of IMM proteins [148, 149]. Furthermore, Mgr2 is important in aiding the binding of Tim21 to the $TIM23^{SORT}$ complex, as well as in the lateral release of proteins into the IMM [150]. The ability of Mgr2 to be crosslinked to precursors in transit suggests that it may make up part of the channel [127].

1.3.5.2. TIM22 Complex (Carrier Pathway)

The previous section highlighted how proteins resident in the IMM, containing a single transmembrane domain and an MTS, use the TIM23 complex for insertion. However, some hydrophobic proteins destined for the IMM are synthesised without a presequence and comprise multiple transmembrane domains and consequently, require a different import pathway, namely the TIM22 or carrier pathway (Figure 1.5) [151-153]. Most of these proteins belong to the solute carrier family, typically containing six α-helical domains with multiple internal targeting sequences within the mature protein [151, 154]. However, the exact mechanism by which these internal targeting sequences target carrier proteins to the IMM remains to be fully elucidated. The carrier pathway is particularly important for mitochondrial protein translocation, since some of its substrates include translocase subunits TIM17, TIM22, and TIM23 [155].

Recent cryo-EM studies have determined the structure of the human TIM22 complex at 3.7 Å from overexpression in HEK293T cells [156]; and yeast TIM22 at 3.8 Å resolution from endogenous protein levels [157]. The obtained models revealed notable structural differences between the two. Human TIM22 is a complex of ~440 kDa and the cryo-EM structure (approximately 100 Å height and 160 Å width) revealed six subunits: TIM22, TIM29, acylglycerol kinase (AGK), TIM9, TIM10A, and TIM10B (Table 1) [156]. This structure shows the complex mainly extending into the IMS, along with a transmembrane region consisting of four transmembranes of TIM22 and one transmembrane of TIM29 and AGK. TIM29 acts as a scaffold, holding both TIM9-TIM10A-TIM10B and AGK in proximity to the TIM22 channel. The human TIM22 structure showed the chaperone ring to be tilted at a 45° angle [156]. It is also thought that TIM29 links the TIM22 and TOM complexes, mediating transfer of the carrier protein, a link that has not yet been shown in yeast [158, 159]. Recent studies have revealed that AGK, which is involved in lipid biosynthesis, is important for TIM22 assembly and function [160, 161].

In yeast, the TIM22 complex is ~300 kDa and is composed of seven subunits: Tim22, Tim18, Tim54, Sdh3, Tim9, Tim10, and Tim12 (Table 1.1) [157]. The yeast structure showed that the small TIM subunits (Tim9-Tim10-Tim12) sit on the membrane in a hexameric ring formation and are anchored to the rest of the TIM22 complex *via* a docking platform consisting of Tim18-Sdh3 and Tim22. Tim54 is also required to hold Tim9-Tim10-Tim12 in a tilted conformation, like in humans, at around 45°, allowing them to receive substrates and pass them to the Tim22 channel [157]. Interestingly, Sdh3 is also a component of respiratory Complex II [162]. However, there is no evidence to suggest that the human Sdh3 homolog SDHC associates with the TIM22 complex.

Overall, the TIM22 carrier import pathway can be divided into five distinct and consecutive stages (Figure 1.5) with different energy requirements, producing perceivable transport intermediates to be monitored *in vitro* [163]. The stages are described in yeast below but are thought to be very similar in humans. First, in *Stage I,* the recently translated precursor is found in a soluble chaperone-bound form (with chaperones of the Hsp70/Hsp90 families) not associated with mitochondria.

Then, during *Stage II*, the precursor-chaperone complex is passed on to the Tom70 receptor in an energy-independent manner, driven solely by the affinity of the receptor towards the precursor and the tetratricopeptide repeats in the chaperone. The Tom70 molecules contain two binding sites: one for the precursor and one for the chaperones [164], and aid in the transfer of the protein to Tom22 for insertion into the Tom40 channel [165, 166]. More recently, the biological function of Tom70 has been challenged and it was suggested that the receptor acts as a general interface between cytosolic chaperones and the mitochondrial import machinery, and not as a specific receptor for carrier precursors [167]. In this regard, Tom70 would play a key role in reducing precursor-induced proteotoxic stress. Next, ATP binding to the cytosolic chaperone triggers the release of the precursor and progression through the Tom40 channel. Importantly, the precursor can be arrested in *Stage II* by ATP depletion [163]. Interestingly, it is thought that carrier proteins are inserted into the Tom40 channel with both termini remaining in the cytosol, in a loop-like formation [168].

During *Stage III*, the precursor emerges from the IMS-facing side of the Tom40 channel, binding the small TIM chaperones (Tim9-Tim10), which tend to exist as hetero-hexameric complexes, for handover to the TIM22 complex. However, experimental data where $\Delta\Psi$ was dissipated showed the accumulation of two distinct populations, suggesting that the following stages, namely insertion, are $\Delta\Psi$-dependent, and that *Stage III* is further divided in two sub-stages. *Stage IIIa* represents the precursor deeply inserted in the TOM complex and protected from exogenous proteases [163]. *Stage IIIb* represents a fully translocated precursor across the OMM, tethered to the TIM22-bound TIM chaperone complex (Tim9-Tim10-Tim12) *via* hydrophobic interactions [163]. Tim12 is bound to the TIM22 complex and aids in passing chaperoned carrier proteins to the Tim22 channel *via* the Tim54 docking site. Recently, it has been shown in yeast that Porins can assist in translocation by recruiting and interacting with the TIM22 complex, forming contact sites between OMM/IMM, to spatially coordinate inner and outer membrane transport steps [169]. However, others have identified that these juxtapositions are maintained by the interaction of TIM22 with the mitochondrial contact site and cristae organising system (MICOS) complex in humans [170]. Conversely, MICOS is found in association with the TIM23 complex in yeast [170].

Interestingly, the last two stages of the translocation of carrier precursors show differential dependence on ΔΨ, confirmed experimentally using ionophores [153]. *Stage IV* (*docking)* can occur in a partially depolarised membrane (-120 to -60 mV) whereby the precursor is in full association with the TIM22 complex and one of its loops is inserted in the Tim22 channel [153]. Despite the low ΔΨ, the electrophoretic effect experienced by the positive charges on the matrix loops of the carrier precursor is sufficient to drive its partial translocation into the complex. Finally, *Stage V* requires a fully energised membrane (>-120 mV) to successfully insert the precursor into the IMM after lateral opening of TIM22 [153, 163].

Recently, the canonical even-numbered paired transmembrane helices with N_{out}- and C_{out}-terminal rule for TIM22 substrates has been challenged [171]. In this report, the authors observed that the yeast mitochondrial pyruvate carrier, which has an odd number of transmembrane segments and a matrix-facing N-terminus, was imported specifically *via* the TIM22 complex. Similarly, it has been reported that human sideroflexins, a class of IMM proteins that contain five transmembrane domains and that do not belong to the SLC25 family, are imported *via* TIM22 [172]. Therefore, one can assume that the TIM22 substrate spectrum is less intransigent and contains proteins with paired and non-paired transmembrane domains.

1.3.5.3. OXA1 Pathway

Despite the endosymbiotic character of mitochondria, the organelle lacks a SecY-like translocon and possesses instead an import machinery that more closely relates to the bacterial membrane insertase YidC [173]. The so called IMM protein Oxidase assembly protein 1 (OXA1L, OXA1 in yeast; Figure 1.5 and Table 1.1), is highly conserved from bacteria to mammals and plants [174]. OXA1 is nuclear-encoded, translated in the cytosol and imported by the TOM/TIM23 pathway *via* its N-terminal MTS, in an mtHsp70- and ATP-dependent manner [175]. Interestingly, recently imported OXA1 is first observed in the matrix and then uses endogenous OXA1 to successfully insert itself into the IMM [175]. Mature OXA1 (36 kDa) is known to form oligomers, although its behaviour is still controversial. For example, in *Neurospora crassa* it exists as a homo-tetramer [176] while human OXA1L has an apparent mass of 600-700 kDa, suggesting a hetero-oligomeric complex of unknown identity [177].

Since most mtDNA-encoded proteins are highly hydrophobic it is predictable that OXA1L interacts with mito-ribosomes for a co-translation process, whereby nascent chains associate with the insertase to suppress possible aggregation of the polypeptide in the matrix. This interaction occurs *via* the long C-terminus of OXA1L/OXA1 in both humans and yeast [178]. Recently, a cryo-EM structure showed an association between human OXA1L and

mitochondrial ribosomes in a native state, coupling protein synthesis and membrane delivery [179].

In addition to its role in the insertion of mtDNA-encoded proteins, OXA1 is also responsible for N-terminal insertion of some nuclear-encoded proteins [180]. In these cases, proteins with an N-terminal MTS are not arrested during import *via* $TIM23^{SORT}$ but are fully imported into the matrix *via* $TIM23^{MOTOR}$ and thereafter sorted for export from the matrix *via* OXA1, after cleavage of the MTS [180]. Similarly, multispanning proteins such as the ABC transporter Mdl1 can cooperatively make use of the stop-transfer (TIM23) and conservative (OXA1) sorting for integration into the IMM [181]. Regarding yeast Mdl1, the insertion topology occurs as follows: transmembranes 1 and 2 are imported *via* stop-transfer; subsequent transmembranes 3 and 4 are imported into the matrix in an mtHSP60/ATP-dependent manner and exported into the IMM *via* OXA1; transmembranes 5 and 6 are OXA1-independent and probably use the stop-transfer mechanism. Interestingly, the middle two TM helices 2 and 3 (of Mdl1), dependent on Oxa1 for their insertion, are not particularly hydrophobic. This ties in well with the noted evolutionary conservation and striking structural similarity of the Oxa1/YidC family with EMC3 of the ER membrane complex (EMC) [182-184]. Given their common mechanism for membrane protein insertion, it is perhaps significant that the EMC is also recruited for the incorporation of TM helices with reduced hydrophobicity [185]. Therefore, the possibility that OXA1 assists more widely in the insertion of less hydrophobic TM helices, such as those possessed by transporters, proton translocators and carriers, is worthy of further investigation.

Regarding energy dependence, OXA1 does not require ATP for protein insertion, similarly to TIM22; however, its dependence on $\Delta\Psi$ is not as clear. For example, export of the N-terminus of nuclear-encoded proteins requires an energised membrane [186], as is the case for the mtDNA-encoded Cox2 yeast protein [187], but not for yeast Cox1, Cox3 or cytochrome *b* [187]. Interestingly, this same correlation is observed in regard to negative charges, *i.e.,* substrates with a negatively charged N-terminus and/or IMS loops are $\Delta\Psi$-dependent, while those with less negative or neutral character are not [188]. This suggests that the content of charged residues in an IMM protein determines its dependence on the OXA1 translocase.

Due to the fundamental importance of mitochondrial homeostasis for the regulation of multiple central processes and pathways, it is not surprising that mitochondrial import defects have been implicated in several diseases [189]. These include neurodegenerative diseases [190], as well as mitochondrial diseases associated with respiratory complex deficiencies due to mutations affecting import machinery [191]. The impact of dysfunctional import on neuronal health and homeostasis, and indeed the links between defective import and progression of neurodegeneration will be discussed in the following sections.

1.4. Neuronal Structure & Function

Neurons, the basic functional units of the nervous system, are responsible for transmitting information encoding signals over long distances, which they do by generating electrical signals and passing these signals from cell to cell, in a manner reliant on their highly compartmentalised structural features. Neurons are made up of specialised regions, each of which is responsible for carrying out specific functions: the soma (also known as the cell body), the dendrites, the axon, and the axon terminals (Figure 1.6) [192].

The soma contains the nucleus and acts as the major site of protein synthesis for many neuronal proteins. Although there is accumulating evidence for the importance of local translation within both dendrites and axons in neuronal homeostasis [193], it is still understood that many proteins are synthesised in the soma. Axonal proteins synthesised in the cell body are assembled into vesicles or particles prior to anterograde transport along microtubules down the axon to their destination [194]. Conversely, damaged proteins and organelles are transported in a similar manner back up the axon, by retrograde transport, for degradation in the cell body, the predominant region in the neuron where lysosomes are present [194].

The pre-synapse, located in axons, acts as the primary signal transmitter of the neuron and the axonal membrane is responsible for conducting an action potential from the cell body to the axon terminus. An action potential is a transient, rapid depolarisation and subsequent repolarisation of the membrane from the resting state (non-stimulated, ~-60 mV) to the excited state (stimulated, up to ~+50 mV), and back to the resting state [195]. Action potentials are initiated by activation of excitatory postsynaptic receptors in the dendrite. If the frequency and net depolarisation of summated dendritic depolarisation is sufficient, action potentials are then propagated by the coordinated channel opening and closing Na^+ and K^+ in the outgoing axon. The action potential travels from the axon hillock close to the soma to the axon terminals at the synapses, where it is converted into chemical signals that are received by the dendrites of neighbouring neurons (Figure 1.6) [195]. Since a single axon can have synapses connecting to multiple other neurons, a single action potential can induce simultaneous responses in many other neurons. The pre-synapse of the signal transmitting neuron will transmit the signal to the dendritic synapse of the post-synaptic cell by the release of chemical signals known as neurotransmitters from vesicles in the pre-synapse, across the synaptic cleft, which bind to receptors on the post-synapse [195].

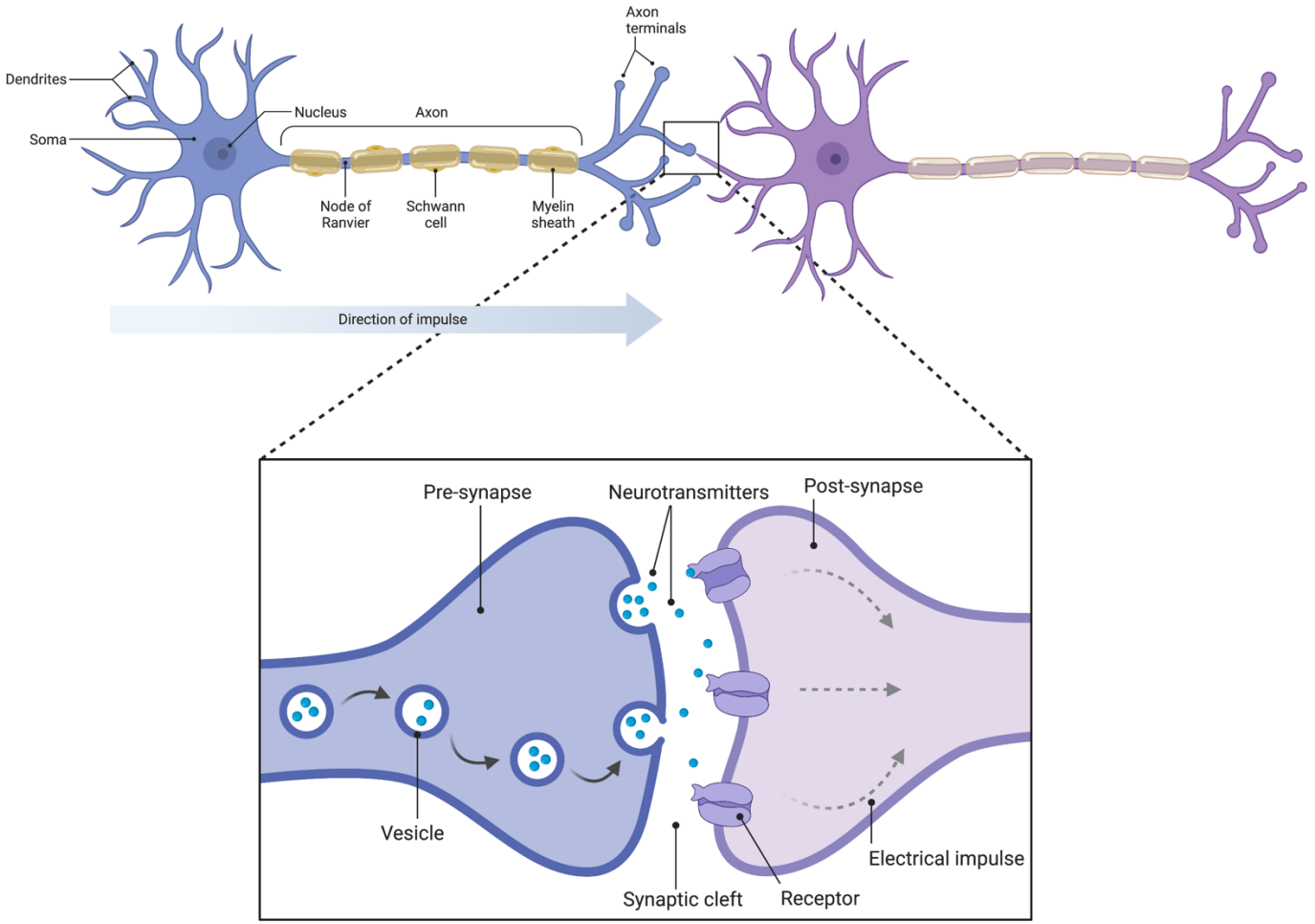

Figure 1.6: Neuronal Structure and Synaptic Transmission
Neurons have various specialised regions important for their role in signal transmission. Neurotransmitters, contained in vesicles in the pre-synapses (at axon terminals), are released at the pre-synapse, where they travel across the synaptic cleft, to receptors of the dendritic post-synapses. There, they are converted into electrical impulses that travel through the soma and down the axon of the neighbouring cell. The soma also contains the nucleus, and the axon is protected by the myelin sheath, made up of surrounding Schwann cells. Regions of unmyelinated axon are known as Nodes of Ranvier. *Created using BioRender.*

Once this chemical signal is received by dendrites in neighbouring neurons, it is converted back to electrical impulses which are transmitted towards the cell body and to the axon hillock, where, if the electric disturbance permits, a further action potential will be generated and the cycle continues, conducting the signal to more and more neurons [195].

This synaptic transmission in the central nervous system is energetically expensive and uses the majority of the brain's energy. This accounts for ~20% of the total energy consumed by the body, though the brain makes up only 2% of body mass [196]. Most of the ATP used in neurotransmission and the maintenance of membrane potential in neurons is produced from oxidative metabolism by mitochondria [196], highlighting mitochondria as arguably the most important organelle for neuronal survival and function.

Neuronal mitochondria are primarily produced in the cell body and are transported to neuronal segments such as various locations within axons and dendrites, *via* anterograde and retrograde transport [197, 198]. This allows them to be positioned in the precise locations of high metabolic demand, such as pre-and post- synapses and neuronal growth cones, where they produce ATP to be used in various vital neuronal functions such as action potential generation and transmission [197, 198].

1.5. Mitochondrial Protein Import and Neurodegeneration

Neurodegeneration occurs due to the progressive degeneration or loss of neuronal cells in specific regions of the brain, leading to problems with movement, known as ataxias, or problems with cognitive function, known as dementias [199, 200]. Neurodegenerative diseases are often age-related disorders and symptoms are most commonly late onset, though symptoms may also present in patients with early onset, genetically determined, familial cases of neurodegeneration [201]. There are five major characteristic features of neurodegeneration [201, 202] (Figure 1.7):

1. Axonal and dendritic degeneration [203-206];
2. Synaptic loss [207-209];
3. The accumulation of toxic, aggregation prone proteins within or surrounding neuronal cells, for example neurofibrillary tangles (NFTs) composed of aggregated Tau in Alzheimer's disease (AD) [200, 210];
4. Mitochondrial dysfunction [211-213];
5. A conserved inflammatory response [214].

While mitochondrial dysfunction has been considered a hallmark of neurodegeneration for decades, it is becoming more evident in recent years that mitochondrial protein import defects may play an important role in the mitochondrial dysfunction associated with neurodegenerative diseases. The evidence highlighting this link in various neurodegenerative diseases is described below, and the specific defects have been summarised in Table 1.2.

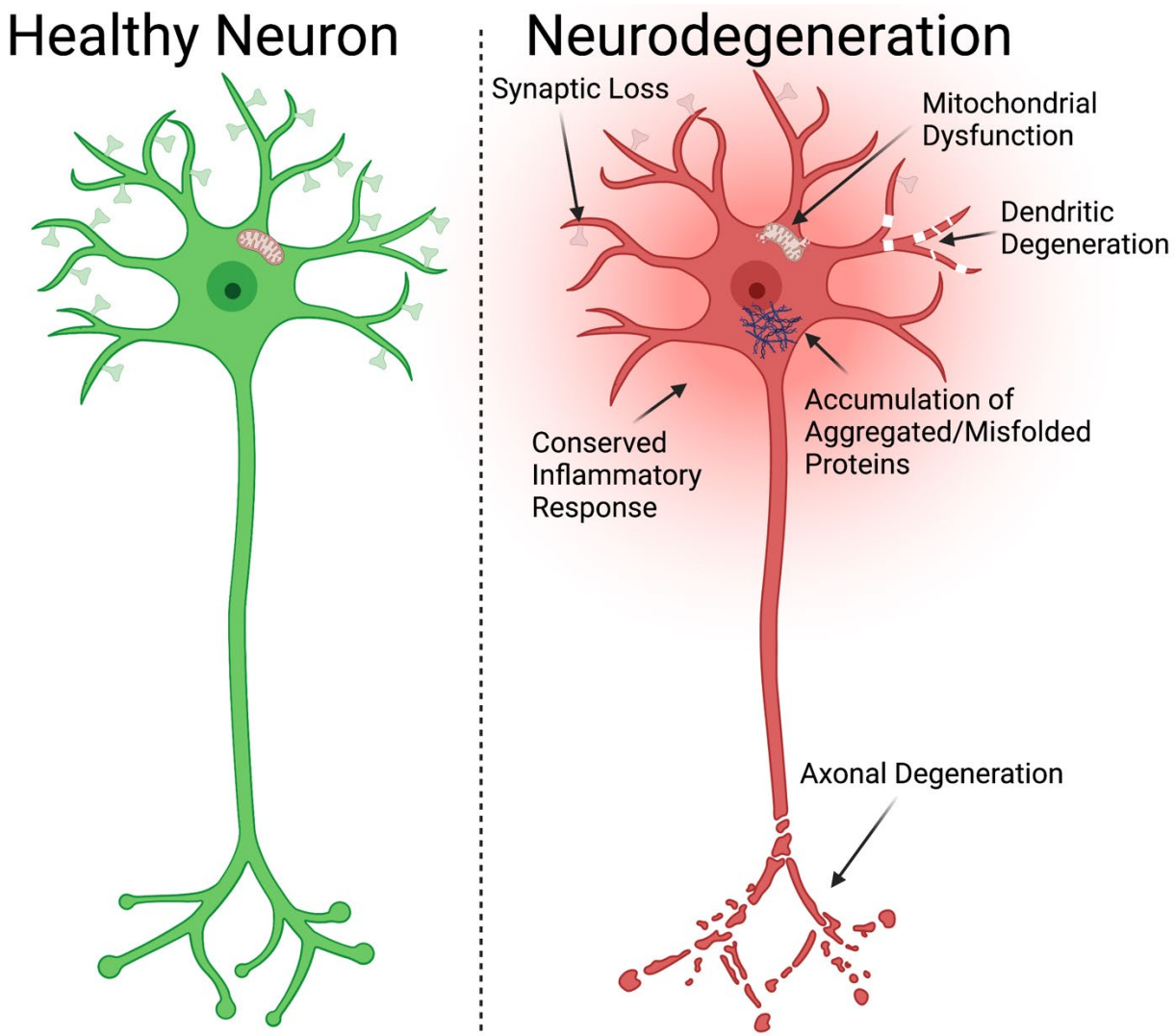

Figure 1.7: Hallmarks of Neurodegeneration
The major hallmarks of neurodegeneration (right, red) are injured and degenerating axons/dendrites, mitochondrial dysfunction, a conserved inflammatory response, synaptic loss, and the accumulation of aggregated or misfolded proteins within or outside of the cell. This is compared to a normal, healthy neuron (green, left). *Created using BioRender.*

Table 1.2: Summary of Import Defects Associated with Neurodegeneration

Pathology	Import Defect(s)	Known Consequence(s)/Rescue Mechanism	Model Organism/System	Reference
Alzheimer's Disease	APP accumulation in TOM40 and TIM23 channels, with higher levels in AD susceptible brain regions.	Inhibition of import of CIV 4 and 5b, and subsequent reduction in CIV activity, leading to increased ROS.	Human AD brains.	[215]
	Chronic, sub-lethal Aβ exposure induces a significant reduction in mitochondrial protein import.	Reduction in Δψ, altered mitochondrial morphology, and increased ROS production.	PC12 cells.	[216]
	Tau accumulation in OMM and IMS, and interactions between N-terminal Tau fragment with OPA1 and Mfn1.	N/A	HEK293T cells, HeLa cells.	[217], [218]
Parkinson's Disease	α-syn localises to and accumulates within mitochondria, mediated by a cryptic non-canonical MTS, in an ATP and Δψ dependent manner.	N/A	Human dopaminergic neuronal cultures, PD brains.	[219]
	A53T version of α-syn is imported more efficiently than wildtype variant.	May account for faster development of cellular abnormalities seen in cells expressing the A53T version of α-syn compared to the wildtype.	Human dopaminergic neuronal cultures, PD brains, A53T mutant alpha-synuclein-inducible PC12 cell lines.	[220], [221]
	Mitochondrial α-syn accumulates at the IMM and interacts with CI.	Reduction in CI activity, increase in ROS production, inducing oxidative stress.	Human dopaminergic neuronal cultures, PD brains, rat *SN* neurons, human neuroblastoma cell line (SK-N-MC cells).	[220]
	S129 phosphorylated α-syn binds tightly to TOM20, inducing loss in TOM20-TOM22 interaction.	Impaired protein import, loss of Δψ, reduced respiratory capacity, and increased oxidative stress. Rescued by *in vivo* knockdown of endogenous α-syn, and by *in vitro* TOM20 overexpression.	SH-SY5Y cells and dopaminergic neurons from *SN* of post-mortem PD patient brains.	[222]
	TOM40 downregulation, corresponding with α-syn accumulation in PD brains.	N/A	Midbrain of PD patients and α-syn transgenic mice.	[223]
	Excessively low levels of mitochondrial import in cells from *PINK1*- and *PARK2*-linked PD patients.	Import defects reversed by phosphomimetic ubiquitin in cells with residual Parkin activity.	Cells from *PINK1*- and *PARK2*-linked PD patients.	[85]

Huntington's Disease	Disease variant of Htt localises to mitochondria and directly interacts with the TIM23 complex.	Inhibited import and subsequent respiratory dysfunction, triggering cell death; rescued by TIM23 overexpression.	Isolated mitochondria from human HD brains, primary neurons expressing Htt variant, forebrain synaptosomal mitochondria in HD mice at early stages of HD.	[224]
	Dysfunctions in MIA pathway associated with mutant Htt: reduced levels and ratio of ALR and CHCHD4.	Reduced import of MIA pathway precursors, CIV assembly defects, deficient respiration, alterations in mtDNA, altered mitochondrial morphology.	Neuronal cell lines.	[225]
Amyotrophic Lateral Sclerosis	Variants of SOD1 accumulate in IMS, matrix, and OMM, and interact with OMM proteins.	Excessive ROS production, mitochondrial dysfunction, and toxic effects on the cells. Rescued by selective IMS targeting of wildtype SOD1.	Transgenic mouse models, spinal cord mitochondria.	[226], [227], [228]
	Increased levels of TOM subunits TOM20, TOM22, and TOM40. 30% reduction in import efficiency.	Changes in CI related protein expression levels.	Rat spinal cord of ALS-linked variant $SOD1^{G93A}$.	[229]
	Novel CHCHD10 mutant, *Q108P*, discovered in a patient with rapidly progressing ALS, almost completely abolishes its import.	Reduced mitochondrial respiratory capacity, an effect which is rescued by CHCHD4 overexpression.	HeLa cells and primary rat embryonic neurons transduced with genomic DNA from a young ALS patient.	[230]

1.5.1. Alzheimer's Disease

AD is the most commonly occurring form of neurodegeneration, and growing evidence links it to mitochondrial dysfunction at all levels of AD neuropathology. AD is characterised by the death or loss of synapses and eventually neurons in specific, susceptible areas of the brain, as well as by the presence of two pathological hallmarks: extracellular senile plaques, and NFTs [231].

1.5.1.1. Amyloid Precursor Protein

Senile plaques are deposits of accumulated amyloid-beta peptide (Aβ), a 40-42 amino acid peptide which is produced by specific, sequential proteolytic cleavages of amyloid precursor protein (APP). The biology of APP processing and its relevance in AD has been reviewed in detail previously [231].

Interestingly, in a study carried out in mitochondria from human AD brains, APP was found to accumulate in the TOM40 channel, forming a stable complex of ~480 kDa (Table 1.2) [215]. It also accumulates with both TOM40 and TIM23 to form a supercomplex of ~620 kDa [215]. Mitochondrial APP levels varied both among patients, corresponding to the severity of AD, as well as across brain regions, with higher levels displayed in the regions of the brain that are more vulnerable to AD: the cortex, hippocampus, and amygdala [215]. Furthermore, the levels of APP accumulation in the mitochondria of AD brains directly correlates with mitochondrial dysfunction [215], suggesting that APP-mitochondrial translocase complex formation and aggregation may in fact be a causative factor in AD progression.

Furthermore, a study in PC12 cells, a cell line derived from a rat adrenal medullary tumour (pheochromocytoma) which are widely used in studies of neuronal differentiation [232], showed that chronic, sub-lethal Aβ exposure induces a significant reduction in mitochondrial protein import [216]. When sustained over long periods, this leads to mitochondrial dysfunction highlighted by a reduction in Δψ, altered mitochondrial morphology, and increased ROS production (Table 1.2) [216]. This negative impact on mitochondrial function is likely due to the loss of important proteins that are usually imported via TOM40, such as proteins necessary for respiratory complex activity and assembly, as well as ROS scavenging proteins.

1.5.1.2. Tau Protein

The second characteristic hallmark of AD, NFTs, are insoluble aggregations made up primarily of hyperphosphorylated Tau protein. NFTs are a characteristic feature of many tauopathies, including frontotemporal lobar degeneration (FTLD), Pick's disease, corticobasal

degeneration (CBD), progressive supranuclear palsy (PSP), and sporadic multiple system tauopathy (primary tauopathies), and Creutzfeldt–Jakob disease and Chronic Traumatic Encephalopathy (CTE) (secondary tauopathies) [233]. AD is also classified as a secondary tauopathy due to the known involvement of other major pathological factors, in this case Aβ accumulation [234].

Tau protein is formed by alternative splicing of the microtubule-associated protein tau (*MAPT*) gene, and is a highly abundant protein in neurons, most of which is localised to the axons, where it mainly functions to bind to microtubules, promoting their assembly and stability (Figure 1.8) [235-237]. Upon binding to microtubules, Tau modulates the activity of motor proteins dynein and kinesin, which in turn regulate transport of cargo, including mitochondria, up and down axons [238-242]. However, the ability of Tau to bind microtubules is highly dynamic and is dependent on Tau isoforms as well as mutations and PTMs. Due to the vital role of Tau in axonal transport, Tau often has pathological roles (Figure 1.8) [234, 243-245].

Mitochondrial function is known to be impaired by abnormal, pathological Tau on various levels, but the mechanism is incompletely understood. Tau accumulation into NFTs was shown to increase retrograde transport of mitochondria (*i.e.,* towards the soma) as well as decreasing complex I activity and ATP levels, and causing defects in mitophagy as well as altered Δψ, and enhancing oxidative stress (Figure 1.8) [217, 242, 246, 247]. The alterations in Δψ particularly suggest that there may also be import defects, since Δψ is vital for mitochondrial protein translocation (*via* both the precursor and carrier pathways).

Studies have shown that different forms of Tau (wildtype, hyperphosphorylated, or caspase-cleaved N-terminal fragment) are localised to various mitochondrial sub-compartments. One study, carried out in HEK293 cells, showed accumulation of Tau in OMM fractions, as well as interactions between the N-terminal fragment of Tau with OPA1 and Mfn1, suggesting that Tau is directly interacting with mitochondria at the OMM and potentially with the IMS (Table 1.2) [217]. This OMM and IMS localisation of Tau was also demonstrated in HeLa cells, where the effect of Tau on ER-mitochondrial contacts was also highlighted [218]. Furthermore, a study in human AD brains showed that total Tau and hyperphosphorylated Tau deposits overlap more with mitochondria, as well as with the ER and the Golgi apparatus, when compared to control brains (Table 1.2) [248]. It is intriguing to observe mitochondrial accumulation of various forms of Tau from the cell line level right up to the human brain level. Whilst, to the best of our knowledge, no studies have specifically looked at the impact of Tau on mitochondrial protein import efficiency, the body of evidence highlighting Tau accumulation in the OMM and IMS suggests this would be an interesting link to follow up, with relevance to all tauopathies.

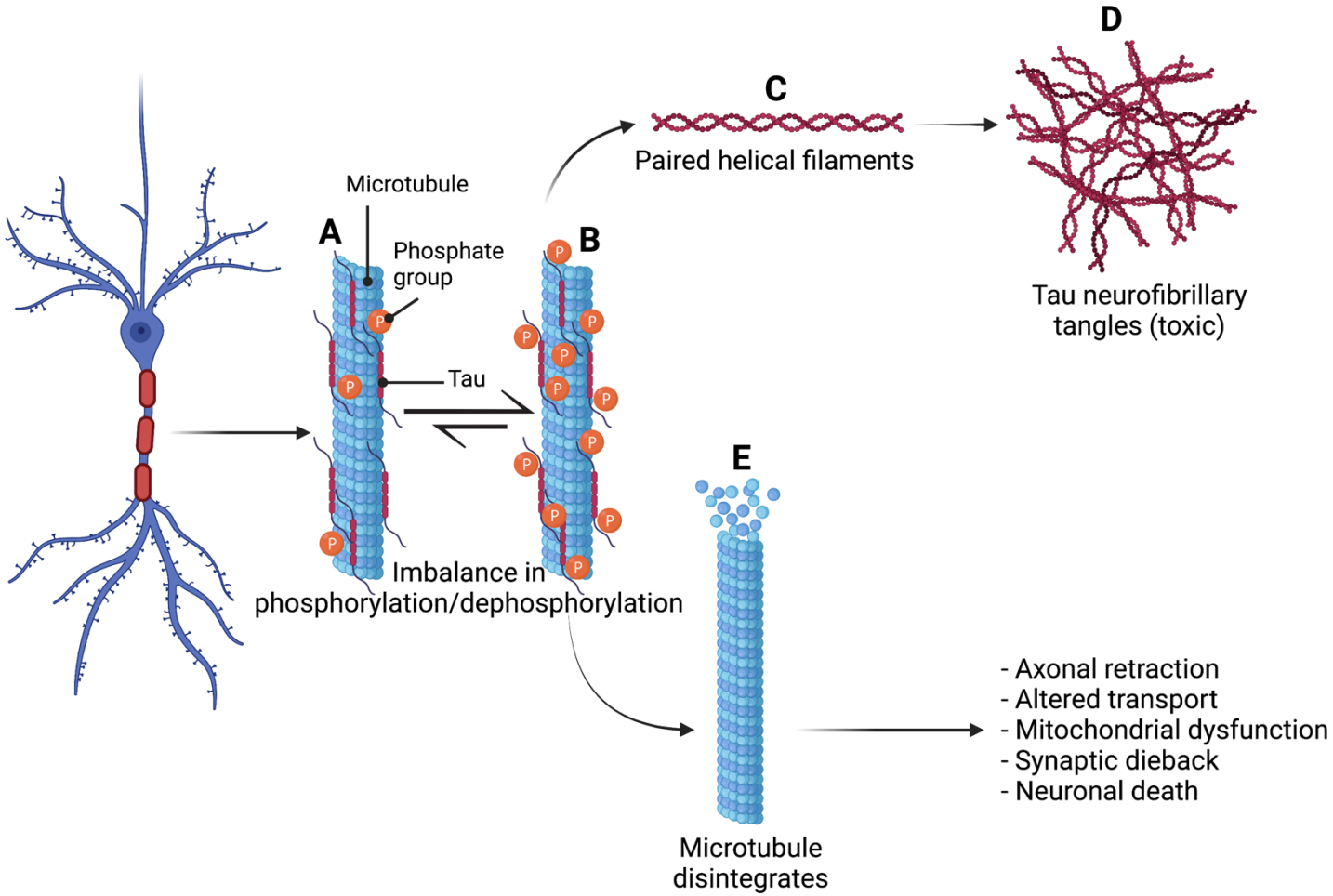

Figure 1.8: Tau Pathogenesis
Tau binds to axonal microtubules and is important for their stability. Tau is consistently phosphorylated and dephosphorylated **(A)**, and if there is an imbalance in its phosphorylation cycles, it can become hyperphosphorylated **(B)**, causing it to detach from microtubules. This leads to the formation of paired helical filaments **(C)**, which eventually aggregate into cytotoxic NFTs **(D)**. Additionally, the detachment of Tau causes microtubules to disintegrate **(E)**, leading to axonal retraction, altered transport of mitochondria, mitochondrial dysfunction, synaptic dieback, and neuronal death. *Schematic created using BioRender.*

1.5.2. Parkinson's Disease

Parkinson's disease (PD) is very closely associated with mitochondrial dysfunction, owing to consistent evidence suggesting reductions in CI activity in PD patient brains and other tissues [249, 250], in addition to genetic links between familial PD and mitochondrial dysfunction [251]. These well characterised mitochondrial abnormalities in PD and potential therapeutic strategies to target them have been reviewed extensively previously [252].

Lewy bodies, which form in the *Substantia Nigra (SN),* are the main pathological hallmark of PD and are made up mainly of aggregated alpha-synuclein (α-syn), an abundant pre-synaptic molecule [253, 254]. Alpha-synuclein is a 140 amino acid molecule which is thought to play a role in neuronal plasticity and synaptic function [253, 255, 256]. The aggregation of α-syn is highly neurotoxic, and studies of transgenic mice overexpressing α-syn have shown that its accumulation can lead to a PD-like phenotype, consisting of the formation of prominent intraneuronal inclusion bodies, loss of dopamine neuron terminals, and motor deficits [257]. Intriguingly, considerable evidence has suggested that neuronal injury caused by α-syn may be mediated by mitochondrial dysfunction and degeneration [219, 220, 258-262].

Multiple studies have shown that α-syn localises to, and accumulates within, mitochondria (Table 1.2) [219, 220, 261, 262]. This is thought to be mediated by a cryptic, non-canonical MTS within the N-terminal 32 amino acids of α-syn [220]. The transport of α-syn into mitochondria does not occur in the presence of oligomycin, which inhibits ATP synthase and thus depletes mitochondrial ATP; or carbonyl cyanide-*m*-lorophenylhydrazone (CCCP), which disrupts the mitochondrial Δψ, highlighting that its import is dependent on both ATP and Δψ, consistent with the import requirements for presequence proteins [220]. Alpha-synuclein with the A53T point mutation, which occurs in rare familial PD cases, is also imported into mitochondria, but with significantly higher efficiency than the wildtype protein [220]. This may account for the faster development of cellular abnormalities seen in cells expressing the A53T version of α-syn compared to the wildtype [221].

It has been shown by EM that the majority of mitochondrial α-syn accumulates at the IMM and that it interacts with CI [220]. This causes a significant reduction in CI activity, as well as an increase in ROS production, inducing oxidative stress [220], which may account for some of the toxic effects on dopaminergic neurons. Importantly, α-syn lacking the N-terminal MTS failed to localise to mitochondria and did not exhibit any of the mitochondrial dysfunctions observed with the wildtype protein [220].

A study carried out in cell models of PD showed that *in vitro* treatment with rotenone leads to an increase in S129 phosphorylation of α-syn [222]. The resulting post-translationally modified α-syn species bound with high affinity to TOM20 molecules, prompting a loss of the critical interaction between TOM20 and TOM22 (Table 1.2) [222]. Consequently, mitochondria had impaired protein import and widespread mitochondrial dysfunction, displayed by a loss of Δψ, reduced respiratory capacity, and increased oxidative stress in SH-SY5Y cells [222]. This α-syn-TOM20 interaction and subsequent loss of import was also detected in the dopaminergic neurons from the *SN* of post-mortem brains of PD patients [222]. The authors highlighted mechanisms for rescuing this disorder, namely *in vivo* knockdown of endogenous α-syn and *in vitro* TOM20 overexpression, both of which preserve mitochondrial import and thus present potential therapeutic strategies for further investigation [222, 263].

It has been shown that the core component of the TOM complex, TOM40, is downregulated in the midbrain of PD patients as well as in α-syn transgenic mice (Table 1.2) [223]. Importantly, levels of TOM20 remained the same, suggesting that this is an effect specific to TOM40, rather than a general reduction in mitochondrial proteins. Furthermore, the reduction in TOM40 levels corresponded with α-syn accumulation in PD brains, inferring a further functional link between α-syn aggregation and mitochondrial import dysfunction [223].

A recent study showed that, in addition to the key roles in mitochondrial quality control and biogenesis already established [264-269], Parkin, an E3 ubiquitin ligase, also plays a part in stimulating mitochondrial protein import, whilst stimulation of import is not achieved by disease-causing Parkin variants (Table 1.2) [85]. Furthermore, the results of this study showed that this effect relies on PINK1-mediated Parkin activation and results in ubiquitylation of TOM40 subunits, as well as an increase in K11 ubiquitin chains on mitochondria [85]. The importance of PINK1-Parkin regulation of mitochondrial import is highlighted by data showing excessively low levels of mitochondrial import in cells from *PINK1*- and *PARK2*-linked PD patients. This effect may be reversed by phosphomimetic ubiquitin in cells with residual Parkin activity, probably by bypassing the need for PINK1-dependent Parkin activation or by enhancing Parkin activity [85].

1.5.3. Huntington's Disease

Huntington's disease (HD) is an autosomal dominant neurological disorder characterised by neuronal loss in the striatal and cortical regions of the brain. The genetic cause of HD is an abnormal expansion of polyglutamine repeats (encoded by the CAG codon) in the huntingtin gene (*HTT*) [270].

N-terminal fragments of variant Huntingtin (Htt) proteins, which form cytotoxic aggregates [271, 272], have been shown to interact directly with mitochondria in cell and mouse models of HD (Table 1.2) [273, 274]. Furthermore, a study showed that, in isolated mitochondria from human HD brains, the disease-associated Htt variant localises to mitochondria and directly interacts with the TIM23 complex, inhibiting import as a result (Table 1.2) [224]. These import defects were consistent in primary neurons expressing the Htt variant as well as in forebrain synaptosomal mitochondria in HD mice at early stages of the disease [224]. Notably, these import defects were not found in liver mitochondria from the same mice, signifying that the import defects are specific to neurons [224]. Additionally, the inhibition of import preceded mitochondrial respiratory dysfunction, and acted as a trigger for cell death, which was rescued upon augmentation of mitochondrial import by overexpression of TIM23 complex subunits, highlighting this pathway as a potential therapeutic strategy against HD [224]. The early detection of impaired import in HD mice [224] suggests that import defects precede the other mitochondrial insults described in HD models, namely: decreased $\Delta\Psi$ [275], reduced respiratory capacity and ATP levels [276, 277], defective calcium buffering function [278], and altered mitochondrial morphology and number [279]. A plausible explanation is that inhibition of import would prevent key respiratory complex proteins from being imported and carrying out their functions, resulting in widespread mitochondrial damage.

The disease associated Htt variant has also been linked to dysfunctions in the MIA pathway (Table 1.2) [225]. In neuronal cell lines, the abundance of MIA pathway proteins was significantly different between disease and control cells [225]. More specifically, ALR and CHCHD4 levels were reduced, and the ratio was altered, whilst cytochrome *c* levels were increased compared to the control group. The abundance of proteins that require the MIA pathway for import was decreased, whilst the abundance of CIV proteins not imported *via* this route, such as MTCO3, was unchanged. This highlights that this effect is specific to MIA substrates, rather than a CIV effect [225]. In cells with a homozygous variant, however, levels of MTCO3 were also reduced [225], suggesting that there may be some CIV assembly defects. The observed MIA pathway defects were accompanied by deficient respiration, alterations in mtDNA, and changes in mitochondrial morphology [225]. This is consistent with what has been shown previously in both HD models and MIA deficient models [280-285].

1.5.4. Amyotrophic Lateral Sclerosis

Amyotrophic lateral sclerosis (ALS) is a motor neuron disease associated with mutations in *SOD1*, the gene coding for ROS scavenging enzyme SOD1 [286, 287]. Characteristic features of mitochondrial dysfunction have been observed across ALS patients, and respiratory chain impairment has been highlighted as a common feature in the muscles of ALS patients, even prior to neuronal deficits being found [288-290]. This finding is consistent across patient samples and experimental systems [291].

A small proportion of wild-type SOD1 is known to localise to the IMS under physiological conditions in both yeast and mammals [292, 293]. Its antioxidant role in detoxifying ROS species produced by the ETC (mainly CI and CIII) is well established [293, 294]. Disease associated variants of SOD1, however, have been shown to accumulate not only in the IMS but also within the matrix and the OMM, where it aggregates and interacts with OMM proteins (Table 1.2) [226, 227]. This SOD1 mislocalisation leads to excessive ROS production and subsequent mitochondrial dysfunction, which can be rescued by selective targeting of wildtype SOD1 to the IMS [228]. Evidence has also highlighted alterations in activity of the respiratory complexes and in mitochondrial calcium buffering capacity to be associated with disease-causing SOD1 variants [278, 295]. A proteomic screen of protein abundance in mitochondria from rat spinal cord of ALS-linked variant $SOD1^{G93A}$ showed vast changes in mitochondrial import and CI related proteins compared to $SOD1^{WT}$ mitochondria (Table 1.2) [229]. Levels of TOM complex subunits TOM20, TOM22, and TOM40 were increased in the affected mitochondria although, surprisingly, *in vitro* import assays highlighted a 30% reduction in protein import levels in these mitochondria compared to wildtype [229].

Furthermore, variants of mitochondrial IMS protein CHCHD10, which is crucial for cristae remodelling, have been linked to progression of ALS as well as frontotemporal dementia [230]. The native version of this protein is imported via the MIA pathway, where disulphide bonds are formed within the CHCHD of the protein [230]. A novel CHCHD10 variant, Q108P, discovered in a patient with rapidly progressing ALS, has been shown to almost completely abolish its import, resulting in reduced mitochondrial respiratory capacity, an effect which is rescued by overexpression of CHCHD4 (Table 1.2) [296]. Interestingly, it was recently demonstrated that the C9orf72 protein, which is often mutated in cases of ALS and frontotemporal dementia, is an IMM protein vital for assembly and stabilisation of CI and is translocated *via* the MIA pathway [297]. Together, these studies demonstrate the importance of mitochondrial protein import and proper respiratory function in the prevention of motor neuron diseases such as ALS, highlighting import pathways as exciting potential targets for treatment.

1.6. Stress Response Pathways

To maintain the integrity and function of the mitochondria, a complex hierarchy of quality control mechanisms exists. This consists of repair mechanisms at the molecular, organellar, and cellular levels *via* a plethora of complex systems including mitochondrial chaperones and proteases, mitochondrial dynamics and distribution, mitochondrial-derived vesicles (MDVs), mitophagy and apoptosis [298]. In addition to the emergence of links between mitochondrial import defects and neurodegenerative diseases, there is also evidence implicating stress response pathways in neurodegeneration. This indicates that these pathways may have either a protective or exacerbating role in disease progression in different models. This section will discuss some of the stress response pathways that cells have developed in response to mitochondrial dysfunction for restoration of mitochondrial import function, respiratory capacity, and mitochondrial and cytosolic proteostasis.

1.6.1. UPR^{mt}

The mitochondrial unfolded protein response (UPR^{mt}) is known to be directly activated in response to impaired proteostasis in the mitochondrial matrix. It was first identified in mammalian cells [299], and has since been extensively studied and characterised in *Caenorhabditis elegans (C. elegans)* [300-303]. The UPR^{mt} is a transcriptional response pathway that eliminates proteotoxic stress and fine-tunes mitochondrial respiration [302, 304].

The sensor for this pathway is stress activated transcription factor (ATFS-1, ATF5 in mammals), which contains both a weak N-terminal MTS and a strong C-terminal nuclear localisation sequence (NLS) [303]. Proteotoxic mitochondrial stress, caused by a variety of mitochondrial stressors including: impairment of the import machinery (*timm23* or *tomm40*(RNAi) or CI inhibition by paraquat application), loss of ETC quality control (*spg-7*(RNAi)), or mtDNA depletion (ethidium bromide application) [303], results in retargeting of ATFS-1 primarily to the nucleus. There, ATFS-1 acts with transcriptional regulators DVE-1 and UBL-5 to induce the production of mitochondrial chaperone proteins HSP-6 and HSP-60, as well as proteases CLPP-1, LONP-1, SPG-7 and YMEL-1, metabolic genes GPD-2 and SKN-1, and core component of the TIM23 complex, TIM17 [304-306]. ATFS-1 is also responsible for repressing the expression of ETC genes, thus shifting expression capacity to increase mitochondrial protein folding, as well as reducing proteotoxic stress from mistargeted proteins in the cytosol [307].

Importantly, the localisation of ATFS-1 is mediated by HAF-1, the previously identified UPR^{mt} regulator and general attenuator of mitochondrial protein import during stress [301]. In the

absence of HAF-1, ATFS-1 is unable to transition to the nucleus under stress conditions, thus failing to activate the UPR^{mt} [301, 303]. It is important to note that ATFS-1 has a relatively weak MTS, meaning that minor effects on mitochondrial protein import efficiency, such as partially depolarised mitochondria, can trigger the stress response pathway, even though some mitochondrial proteins with stronger targeting sequences may still be imported successfully under these conditions [308].

In mammalian cells, the UPR^{mt} is thought to act in a similar way to that described above for *C. elegans*, where transcription factor ATF5 is regulated and triggers a stress response very similar to that described for the *C. elegans* homolog ATFS-1 [309]. However, studies have shown that integrated stress response (ISR) factor ATF4 is also involved in the transcriptional reprogramming of the mammalian UPR^{mt} [310, 311]. It is also thought that the heat shock response (HSR) is activated alongside the UPR^{mt} in what is known as the mitochondrial to cytosolic stress response (MCSR) [300]. The HSR is activated by dysfunctional ETC activity or complex assembly and restores cytosolic proteostasis *via* transcription factor HSF-1 [312].

Given the vast mitochondrial dysfunction described in neurodegeneration, it is not surprising that there is an emerging body of evidence linking the UPR^{mt} to neurodegeneration. In PD, variants of *C. elegans* PINK1 and Parkin orthologs PINK-1 and PDR-1 lead to increased activation of the UPR^{mt}, which mitigates mitochondrial dysfunction caused by the corresponding mutations, subsequently increasing dopaminergic neuron survival [313]. However, a study in *C. elegans* showed that prolonged UPR^{mt} activation can in fact exacerbate mitochondrial dysfunction and dopaminergic cell death by favouring retention of dysfunctional mitochondria [314], which is important to note given the long-term and progressive nature of neurodegenerative diseases. Furthermore, the HSR has been shown to be activated in mouse and cell models of PD [315, 316], and studies have also highlighted heat shock protein overexpression as an attenuator of α-syn aggregation and subsequent dopaminergic cell death [317].

In vivo studies also reveal that the accumulation of ALS SOD1 variant SOD1^{G93A} in the IMS leads to activation of the UPR^{mt} [318], consistent with other studies showing that activation of the UPR^{mt} precedes disease onset and increases throughout disease progression in ALS mutant mice [319]. Similarly, in AD, accumulation of Aβ has been shown to activate the UPR^{mt} [320], and there are high levels of UPR^{mt} marker genes in post-mortem brain samples from AD patients [321]. Interestingly, the inhibition of UPR^{mt} by knockdown of genes coding for key UPR^{mt} proteins HSP-6, HSP-60 and DVE-1 exacerbates AD phenotypes in *C. elegans* [322], suggesting that the UPR^{mt} may play a protective role in AD progression.

Recently, evidence has shown that an earlier form of the UPR^{mt} precedes the classical UPR^{mt} and is activated by the accumulation of unprocessed precursor proteins inside mitochondria, due to impaired processing by MPP [323]. In this case, yeast nuclear transcription factor Rox1 is relocalised to mitochondria, binding to mtDNA and regulating mtDNA transcription and translation, as well as maintaining mitochondrial respiratory and import functions [323].

1.6.2. UPR^{am}

The 'UPR activated by the mistargeting of proteins' (UPR^{am}) is another major stress response pathway that responds to mitochondrial import defects *via* the TIM23 or MIA pathways [324]. It has been well characterised in yeast, and there is some evidence indicating that it also takes place in mammalian cells [324, 325]. In yeast, the trigger for this is not the lack of import of a sensor protein, like ATFS-1 in the UPR^{mt}, but instead the accumulation of cytosolic precursor proteins [324]. The accumulation of cytosolic precursors leads to increased proteasome assembly, triggered by increased activity of proteasome assembly factors Irc25 and Poc4, and subsequent proteasomal degradation of the accumulated cytosolic precursor proteins [324]. This is accompanied by inhibition of protein synthesis, which prevents further accumulation of mistargeted proteins in the cytosol [324].

The UPR^{am} pathway is in part identical to the UPR^{mt} and is probably activated simultaneously alongside the UPR^{mt}; however, they differ in that the UPR^{mt} regulates the abundance of mitochondrial chaperones and proteases, whilst the UPR^{am} regulates the expression of all mitochondrial proteins, as well as enabling the proteasome to clear aggregated proteins [326, 327].

There have been no studies thus far directly implicating the UPR^{am} pathway in neurodegeneration. However, proteasomal degradation *via* the ubiquitin-proteasome system is known to be downregulated in the affected neurons of many neurodegenerative diseases including AD, PD, HD, and ALS; and it is thought that this is mainly caused by the accumulation of cytotoxic protein aggregates [328-330]. For example, in AD, aggregated, ubiquitinated Tau can block entry of unfolded proteins to the 19S catalytic subunit of the proteasome by binding to the recognition site, resulting in impaired proteasomal degradation and enhancing the accumulation of protein aggregates [331].

1.6.3. mPOS

The mitochondrial precursor over-accumulation stress (mPOS) pathway is a mechanism of mitochondria mediated cell death, and has been characterised in yeast [332]. It is usually triggered by any dysfunction that leads to over-accumulation of precursor proteins in the

cytoplasm. Usually, this accumulation would occur as a consequence of import dysfunctions, but it can also be related to other mitochondrial damage, particularly damage that alters IMM integrity such as misfolding of IMM proteins [332]. The mPOS pathway is thought to lead to cell degeneration due to the toxic cytosolic accumulation of misfolded proteins exceeding the cells' capacity to remove these proteins [332]. However, there is a large network of genes responsible for suppressing mPOS and thus promoting cell survival, by means of modulating ribosomal biogenesis, translation of specific transcripts, increasing protein chaperones and turnover, and decapping mRNA [332]. Of these proteins in yeast, Gis2 and Nog2 are particularly important in encouraging cell survival. Gis2 is involved in promoting cap-independent translation whilst Nog2 inhibits the nuclear export of the 60S RNA subunit of the ribosome, promoting cell survival and attenuating mPOS [332-334]. Furthermore, the mPOS pathway can trigger additional stress response pathways within the cell, including the ISR, which restores cellular homeostasis by reducing global protein synthesis, triggered by phosphorylation of eukaryotic translation initiation factor 2 alpha (eIF2α) [335].

Though there have been no specific examples of mPOS in neurodegeneration as of yet, it may have extremely important implications, especially given the mutations in genes of the anti-degenerative network seen in some neurodegenerative diseases such as ALS [336] and PD [337] which have been implicated in suppressing mPOS. The potential association of mPOS with neurodegeneration has been discussed in detail in a recent review [338].

1.6.4. mitoCPR

The mitochondrial compromised protein import response (mitoCPR) pathway was discovered in yeast and is activated when a mitochondrial protein is stalled in the Tom40 channel, inducing mitochondrial import stress and accumulation of proteins on the mitochondrial surface [339]. In yeast, the mitoCPR is activated and transcription factor Pdr3 induces the expression of *CIS1*. Cytosolic protein Cis1 binds to Tom70 and recruits the AAA+ ATPase Msp1, which removes stalled precursor proteins from mitochondrial channels and targets them for proteasomal degradation [339]. This allows mitochondria to maintain their functions under import stress conditions.

This is interesting in the context of AD, especially given that APP, the precursor protein responsible for the production of toxic amyloid plaques in Alzheimer's brains, was shown to accumulate within TOM channels, driving mitochondrial dysfunction in AD [215]. This indicates that the mitoCPR pathway may be defective under these conditions, or may not be sufficient to rescue mitochondrial dysfunction associated with APP-TOM aggregation [340].

1.6.5. mitoTAD

The mitochondrial protein translocation-associated degeneration (mitoTAD) pathway differs from those described already in that it is a quality control pathway that occurs constitutively under physiological rather than stress conditions [341]. In yeast, it is triggered by precursor proteins trapped in the Tom40 channel, sensed by Ubx2, which consistently interacts with the TOM complex under normal conditions, monitoring protein import through Tom40 [341]. If Ubx2 senses that a precursor protein is arrested within the TOM complex, a pool of Ubx2 binds to TOM and recruits the AAA+ ATPase Cdc48 for removal of arrested precursor proteins from the Tom40 channel [341]. The mitoTAD pathway was discovered in yeast, and interestingly, shows similarities to a quality control pathway in the ER, which involves Ubx2 exporting unfolded proteins from the ER [342, 343].

No examples of the mitoTAD pathway have been described in models of neurodegeneration yet. However, as discussed above for the mitoCPR pathway, it is intriguing in the context of studies showing accumulation of proteins in the mitochondrial translocase complexes, including TOM40, in models of neurodegenerative diseases, and further research into this link would be exciting.

1.7. Tunnelling Nanotubes

Tunnelling nanotubes (TNTs) are filamentous, membranous protrusions composed of F-actin, myosin Va, and microtubules, which form connections between neighbouring cells, assisting in long range intercellular communication (Figure 1.9) [344, 345]. They have been shown to mediate the transfer of cargo which includes lipids, nucleic acids, microRNAs, ions, calcium, pieces of plasma membrane, as well as entire organelles such as mitochondria, ER, Golgi, and endosomes [346-349]. Their diameter is determined by the type of cargo they transport, and there are thought to be two distinct types of TNTs, thinner TNTs, which have a diameter of around 50-700 nm (up to 1 μm), and mainly consist of F-actin (Type 1; Figure 1.9), and thicker TNTs whose diameter is over 1 μm and can exceed 3-7 μm for the transport of larger organelles such as mitochondria, and contain microtubules (Type 2; Figure 1.9) [350-352].

The formation of TNTs can be induced by various stressors, including H_2O_2, serum depletion, mitochondrial stress, and cytotoxicity, and relies on p53 gene induction [353]. They are thought to be a cellular stress response mechanism, allowing cells to transfer harmful or required cell substances as well as energy to a neighbouring cell to overcome the stressor. It is not yet known whether they act alongside or independently of other stress response mechanisms. A recent study in PC12 cells showed how transfer of functional, healthy mitochondria *via* TNTs can rescue cells in the early stages of apoptosis [354].

Conversely, a recent study demonstrated how TNTs can be hijacked in disease scenarios, whereby cancer cells use TNTs to obtain mitochondria from neighbouring immune cells [355]. This was inhibited by pharmacological inhibition of TNT assembly, which may represent a novel chemotherapeutic technique [355]. Furthermore, TNTs have been implicated in intercellular transmission of protein aggregates such as prions, which have previously been shown to trigger the formation of TNTs [356-358]. The role of TNTs in disease pathology *via* intercellular transfer of protein aggregates has previously been highlighted as a factor in several neurodegenerative disorders such as AD, HD, PD, and ALS [353, 359, 360].

Regarding Tau, one study showed that, not only is Tau a component of TNTs, whereby it is involved in their establishment *via* its role in microtubule stability, but that it can also be used as a marker of TNTs [360]. Furthermore, in cultured cells and primary neurons, the presence of exogenous Tau species enhances TNT formation, which are subsequently utilised to transfer Tau aggregates between cells [360, 361]. Remarkably, a recent report [362] showed how TNTs can assist in reducing cellular toxicity from α-syn in microglia, by transfer of α-syn fibrils out of diminished cells, as well as transfer of healthy mitochondria from naïve to infected microglia.

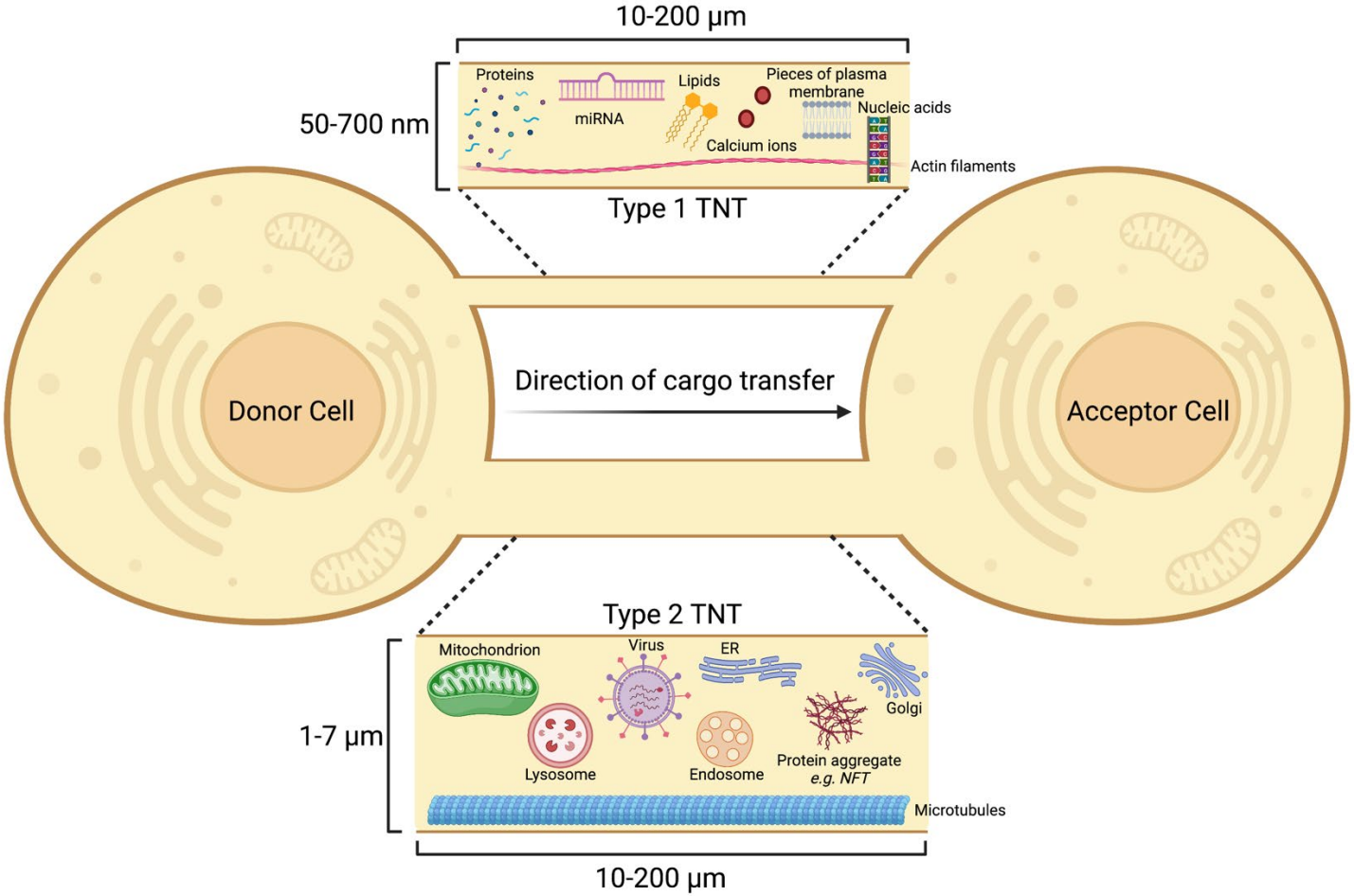

Figure 1.9: Tunnelling Nanotubes
TNTs enable the transfer of cargo between a donor cell and an acceptor cell. There are two types of TNT, both of which can range from 10-200 µm in length. Type 1 TNTs are usually 50-700 nm wide, contain F-actin filaments, and transfer smaller cargo such as proteins, miRNA, lipids, calcium ions, pieces of plasma membrane, and nucleic acids. Type 2 TNTs range from 1-7 µm in diameter and transfer larger cargo. These include mitochondria, endosomes, lysosomes, virus particles, endoplasmic reticulum, Golgi apparatus, and protein aggregates such as NFTs. *Schematic created using BioRender.*

1.8. Aims

The primary goal of this PhD project was to investigate the link between mitochondrial protein import and neurodegeneration, and, specifically, to investigate whether mitochondrial import defects are causative or consequential in neurodegenerative diseases. To do this, I utilised established approaches as well as developing novel means of investigation of mitochondrial protein import in live cell scenarios. The main aims of this thesis were as follows:

1. To develop an assay system to investigate mitochondrial protein import in live mammalian cells in real time (the NanoLuc system).

2. To characterise the impact of failed import on HeLa and neuronal cell health and function by stalling the translocation of a bioengineered precursor protein.

3. To investigate the impact of expressing naturally occurring aggregation prone proteins (variants of the Tau protein) on mitochondrial protein import, as well as on cell health and function in HeLa cells and primary neurons.

4. To examine how cells respond to these import perturbations *via* rescue or repair mechanisms.

1.9. Thesis Overview

In Chapter 3, a technical results chapter is presented, whereby I described the development and optimisation of a cellular based assay system for analysis of mitochondrial protein import in real time in live mammalian cells, using NanoLuc split luciferase technology. I described how this can be utilised to investigate the link between import and disease, as well as the potential for further development into an intact assay system, as well as an inducible intact assay system using CUTE technology.

In Chapter 4, I used the Dihydrofolate Reductase-Methotrexate (DHFR-MTX) system to stall a precursor protein in the presequence pathway. Using this tool, I characterised the impact of failed import on HeLa cells in terms of mitochondrial import, respiratory function, morphology, and dynamics.

Next, in Chapter 5, I moved beyond using engineered precursors and show how disease prone Tau variant Tau^{P301L}, but not its wildtype counterpart, associates with the TOM complex pore forming subunit TOM40. This is in line with alterations in translocase subunit abundance as well as morphological changes which mirror those observed with the trapped precursor.

In Chapter 6, I investigated how import perturbation in the form of precursor stalling and Tau-TOM40 association impacts primary neurons. The data demonstrated phenotypic changes resembling neurodegeneration upon both trapping and expression of Tau^{P301L}, providing a further link between import defects and disease.

Finally, in Chapter 7, I used the precursor trapping approach to investigate a potential cellular rescue mechanism induced by import perturbation. The data showed how import function was rescued by mitochondrial transfer *via* TNTs. This rescue also occurred when import was perturbed by Tau^{P301L} overexpression as well as upon blocking import with TIM23 inhibitor MB20 [363], indicative of a widespread response to mitochondrial import stress.

Chapter 2. Materials & Methods

2.1. Molecular Biology/Cloning

Gene/protein maps and primer sequences were designed using SnapGene software. Constructs were generated by standard cloning techniques with the following vectors: constructs used for HeLa cell expression by transfection were cloned into pEX or pLVX vectors, constructs used for HeLa cell expression by lentiviral infection were cloned into pLVX vectors, and constructs used for primary neuronal expression were cloned into pXLG3-PX vectors (for details of constructs and specific cloning methods, see Appendix 1).

PCR reactions were carried out using Q5 High Fidelity Hot Start DNA Polymerase (New England Biolabs (NEB)), using 20 pmol primers and 200 pg template DNA, as per manufacturers' instructions. PCR products were purified using QIAquick PCR Purification Kit (QIAgen). Restriction digest reactions were carried out using NEB restriction enzymes at 37^{o}C for 45-60 minutes. Ligation reactions were carried out using T4 DNA Ligase (NEB) overnight at 16^{o}C. Transformation was carried out by incubation of 5 µL ligation mix/1 µL plasmid DNA construct in 50 µL competent *E. coli* cells (α-select, XL1-Blue, or BL21-DE3 cells were used, depending on application; all originally sourced from NEB and obtained from lab made stocks, stored at -80^{o}C) for 30 minutes on ice, followed by heat shocking (45 seconds, 42^{o}C), and a further 15 minutes on ice. Cells were recovered by incubating in 250 µL LB media at 37^{o}C for 1 hour at 200 rpm, followed by plating 25-250 µL of recovered cells on LB-agar plates containing appropriate antibiotic.

Plasmids were prepared by mini or maxi preps using commercially available kits (Qiagen and Promega, respectively) following manufacturers' instructions, and verified by DNA sequencing using Eurofins Genomics TubeSeq service.

Commonly used buffers are detailed in Table 2.1.

Table 2.1: Compositions of Commonly Used Buffers

Buffer Name	Use	Composition
LB	Bacterial growth (molecular biology)	2.5% (w/v) Miller Luria-Bertani Broth (LB) granules (Fisher Scientific) in ddH2O
LB-agar	Bacterial growth (molecular biology)	2.5% (w/v) LB powder, 2% (w/v) agar (Gibco) in ddH2O
2X YT	Bacterial growth (protein purifications)	2X YT powder (Sigma) (16 g/L tryptone, 10 g/L yeast extract, 5 g/L NaCl) in ddH2O
TK (low salt)	Protein purification (soluble proteins)	20 mM tris base (Merck), 50 mM KCl (Merck) (pH 8.0)
TK + Urea	Protein purification (insoluble proteins)	20 mM tris, 50 mM KCl, 6 M urea (Sigma) (pH 8.0)
TK + Glutathione	Protein purification (elution from GST column)	20 mM tris, 50 mM KCl, 20 mM glutathione (Sigma) (pH 8.0)
TK + Imidazole	Protein purification (elution from Nickel column)	20 mM tris, 50 mM KCl, 1M imidazole (Sigma) (pH 8.0)
TK (high salt)	Protein purification (elution from S/Q columns)	20 mM tris, 1 M KCl (pH 8.0)
HBSS imaging buffer	Live, intact cell assays (NanoLuc, live cell microscopy)	1 X HBSS (Thermo), 5 mM D-(+)-glucose (Sigma), 10 mM HEPES (Santa Cruz), 1 mM MgCl2 (Sigma), 1 mM CaCl2 (Fisher Scientific) (pH 7.4)
Mannitol respiration buffer	Permeabilised cell or mitochondrial assays (NanoLuc, oxygraphy)	225 mM mannitol (Sigma), 10 mM HEPES, 2.5 mM MgCl2, 40 mM KCl, 2.5 mM KH_2PO_4 (Sigma), 0.5 mM EGTA (Sigma) (pH 7.4)
Permeabilised cell assay master mix	Permeabilised cell NanoLuc assay	1X mannitol respiration buffer (above), 5 mM succinate (Sigma), 1 µM rotenone (Sigma), 0.1 mg/ml creatine kinase (Sigma), 5 mM creatine phosphate (Sigma), 1 mM ATP (Sigma), 0.1% (v/v) Prionex (Sigma), 3 nM rPFO (purified in house), 20 µM GST-Dark (purified in house), 1:800 furimazine (Nano-Glo® Luciferase Assay System; Promega)
Transfer buffer	Western blotting	336 mM tris, 260 mM glycine (Severn Biotech), 140 mM tricine (Sigma), 2.5 mM EDTA (Sigma)
TBS-T	Western blotting	20 mM tris, 1.5 M NaCl (Honeywell), 1X triton X-100 (Sigma) (pH 7.6)
IP Buffer	Immunoprecipitations	0.1 M tris HCl (Roche), 0.15 M NaCl, phospholipids (Avanti Polar Lipids; 0.03mg/ml PE; 0.03mg/ml PG; 0.09mg/ml PC), 1X cOmplete ULTRA Protease Inhibitor Cocktail (Roche)
Mowiol mounting medium	Mounting coverslips for confocal microscopy	9.6% (w/v) Mowiol® 40-88 (Sigma), 24% (w/v) glycerol (Sigma), 0.1 M tris (pH 8.5)

2.2. Protein Purification

Protein expression was carried out exactly as described previously [364]. A single colony of transformed BL21 (DE3) bacteria was grown as a pre-culture in LB with appropriate antibiotic overnight (37°C, 200 rpm). Pre-cultures were used to inoculate a secondary culture at a 1:100 dilution, in 1-8 L 2X YT supplemented with appropriate antibiotic. Secondary cultures were grown until mid-log phase, then induced with 1 mM IPTG or 0.2% (w/v) Arabinose and grown for a further 3 hours. Cells were harvested by centrifugation, resuspended in TK buffer (Table 2.1), cracked in a cell disruptor and clarified by centrifugation.

2.2.1. GST-tagged Recombinant Perfringolysin (rPFO)

rPFO is a selective cytolysin [365], used as a permeabilisation agent in permeabilised cell NanoLuc import assays.

Supernatant (soluble fraction) was loaded onto a 5 mL GSTrap 4B column (GE Healthcare) and the column was washed with TK buffer until the absorbance of the flow through ceased to decrease any further. The peptide was eluted using 10 μM reduced glutathione. Eluted fractions were pooled and loaded onto a 5 mL anionic exchanger (Q- column; GE Healthcare). A salt gradient of 0-1 M was applied over 20 minutes and the protein was eluted in 5 mL fractions. The fractions containing the protein were confirmed by SDS-PAGE with Coomassie staining, then pooled and spin concentrated. The final protein concentration was determined by A280. The protein was aliquoted, snap frozen, and stored at -80^{o}C.

2.2.2. GST-Dark Peptide

GST-Dark is an inactive version of the HiBit peptide of the NanoLuc enzyme (DarkBiT; [366]) fused to GST. It is used to quench any cytosolic LgBit in import assays, preventing background signal from cytosolic binding of HiBit and LgBit.

GST-Dark was prepared as described previously [364]. Supernatant was loaded onto a GSTrap 4B column and purification was carried out exactly as for rPFO. The GSTrap was the only column required for preparation of GST-Dark. Analysis, yield, and freezing was carried out exactly as for rPFO.

2.2.3. His-tagged Su9-EGFP-HiBit

Su9-EGFP-HiBit is a precursor protein with a Subunit 9 MTS (Su9), an EGFP reporter domain, and a HiBit peptide (the small peptide of the NanoLuc enzyme, also known as pep86; [367]). It is used in permeabilised cell NanoLuc assays as the precursor protein whose import into mitochondria is monitored.

Inclusion bodies (insoluble fraction) were solubilised in TK buffer supplemented with 6 M urea (Table 2.1) before loading onto a 5 mL HisTrap HP column (GE Healthcare). The column was washed with TK + 6 M urea and TK + 6 M Urea + 50 mM imidazole. The protein was eluted in 300 mM imidazole. Eluted fractions containing the desired protein were pooled and loaded onto a 5 mL cationic exchanger (S- column; GE Healthcare). A salt gradient of 0-1 M was applied over 20 minutes and the protein was eluted in 5 mL fractions. Imidazole was removed by spin concentration, followed by dilution in TK buffer containing 6 M urea. Analysis, yield, and freezing were carried out exactly as for rPFO.

2.2.4. His-SUMO--Su9-ACP1-D-ACP1-D-DHFR-Myc

His-SUMO--Su9-ACP1-D-ACP1-D-DHFR-Myc is a precursor protein with a Su9 MTS, an ACP1 region, and a DHFR trapping motif. D (DeadBiT) is a scrambled version of HiBit, which does not bind to LgBit or produce bioluminescent signal. This protein was used for acute, *in vitro* trapping using the DHFR-MTX system in permeabilised cells prior to NanoLuc analysis.

His-SUMO--Su9-ACP1-D-ACP1-D-DHFR-Myc was produced as described previously [108]. It was expressed by induction with IPTG, and cells were grown for a further 18 hours prior to harvesting. Subsequently, proteins from the soluble fraction were purified using a Nickel column as for Su9-EGFP-6xHis-HiBit, and finally contaminants were removed by size exclusion chromatography using a HiLoad 16/60 Superdex gel filtration column (Cytiva, UK). The SUMO tag was cleaved from the protein using Ulp1 protease following purification, and the eluted sample passed through a Nickel column to separate the SUMO-His tag from the protein.

2.3. Cell Culture

Cell culture media compositions are detailed in Table 2.2.

2.3.1. HeLa/HEK293T Cell Culture

HeLa cells (cultured in glucose media; HeLaGLU) and HEK293T cells were maintained in glucose media (Table 2.2). For experiments where cells were required to have OXPHOS activity, HeLa cells were cultured in galactose media (HeLaGAL; Table 2.2). Cells were considered mature at 70-90% confluency and split or plated for experimental procedures at this timepoint. Cells were washed extensively in Hanks' Balanced Salt Solution (HBSS; Invitrogen) and detached by incubation (2-5 minutes) in Trypsin-EDTA solution (0.05% trypsin, 0.02% EDTA; Invitrogen). Trypsin was inactivated by the addition of complete DMEM, and cells were plated as required for experimental procedures. Cells were maintained in T75 ventilated flasks in humidified incubators at 37^{o}C with 5% CO_2.

2.3.2. Primary Neuronal Culture

Primary neuronal culture was carried out following established lab protocols, as described previously [368]. Primary hippocampal and cortical neurons were isolated from embryonic day 18 (E18) Han Wistar rat pups. Pregnant Han Wistar rats, bred in-house at the University of Bristol Animal Services Unit, were anaesthetised using isoflurane with pure oxygen flow and humanely killed by means of cervical dislocation, following Home Office Schedule 1 regulations. Isolated neurons were washed extensively in HBSS and dissociated by incubation with 10% (v/v) Trypsin-EDTA solution at 37^{o}C for 15 or 9 minutes, for cortical or hippocampal neurons, respectively. Cells were grown in plating media (Table 2.2). After 2-3 hours, plating medium was removed and replaced with feeding medium (Table 2.2). For biochemistry, cortical neurons were seeded at a density of 500,000 cells per well and for imaging experiments, hippocampal neurons were seeded at a density of 100,000 cells per well, where one well represents a ~35 mm surface. All plates (containing sterile coverslips if appropriate) were incubated with poly-L-lysine (PLL, 0.5 mg/mL or 1 mg/mL for plastic or glass, respectively, in sterile borate buffer (1 mM borax and 5 mM boric acid)) overnight, extensively washed with tissue culture grade H2O and incubated overnight in plating medium prior to plating cells, to aid adhesion. Cells were kept in humidified incubators at 37^{o}C with 5% CO2.

Table 2.2: Cell Culture Media Compositions

Media Name	Use	Composition
Glucose media	HeLaGLU/ HEK293T cell culture	1X high glucose DMEM (Gibco; 11965092), 10% FBS (Thermo), 1% penicillin streptomycin (P/S; Sigma)
Galactose media	HeLaGAL cell culture	1X glucose free DMEM (Gibco; 11966025), 10% FBS, 1% P/S, 10 mM D-(+)-galactose (Sigma), 1 mM sodium pyruvate (Gibco)
FBS free glucose media	CUTE assay optimisation	1X high glucose DMEM, 1% P/S
Charcoal stripped FBS glucose media	CUTE assay optimisation	1X high glucose DMEM, 10% charcoal stripped FBS (Gibco; 12676029), 1% P/S
Seahorse media	Seahorse respirometry assays	Seahorse XF assay medium (Agilent), 1 mM pyruvate (Agilent), 2 mM glutamine (Agilent), 10 mM D-(+)-galactose
Opti-MEM	Transfection of HeLa cells	1X Opti-MEM (Gibco; 31985070)
Freezing media	Freezing down HeLa/HEK293T cells	1X DMEM (high glucose or glucose free, depending on cells), 10% FBS, 10% DMSO (Sigma)
Plating media	Plating neuronal cells (for first 3 hours until cells adhered)	1X neurobasal medium (Gibco; 21103049), 5% horse serum (Thermo), 2% B27 supplement (Gibco), 1% GlutaMAX™ (Thermo), 1% P/S
Feeding media	Neuronal cell culture (after first 3 hours)	1X neurobasal medium, 2% B27, 0.4% GlutaMAX™, 1% P/S
Plain neurobasal	Transfection of primary neurons	1X neurobasal medium

2.4. Transfection of Cells

2.4.1. HeLa Cell Transfection

HeLa cells were plated and grown up to 70-80% confluency. At this point, cells were transfected with 0.5-2.5 µg of the desired DNA using Lipofectamine 3000 reagent (Thermo Fisher Scientific), following the manufacturers' protocol. Cells were then grown for a further 24-72 hours prior to experimental analysis.

2.4.2. Neuron Transfection

Primary neurons were transfected at 7 days *in vitro* (DIV7) with 0.5-1 µg of the desired DNA using Lipofectamine 2000 reagent (Thermo Fisher Scientific), at a ratio of 1.5 µL per 1 µg DNA. Coverslips with adhered neurons were washed in plain neurobasal medium and transferred to dishes containing plain neurobasal medium, to which the transfection mix was added. 45 minutes after transfection, coverslips were washed again to remove all remaining DNA and lipofectamine from cells and returned to their conditioned growth media. Neurons were then maintained for a further 7 or 14 days prior to fixation.

2.5. Lentivirus Production & Transduction

2.5.1. Lentivirus Production

Lentiviral particles were produced in HEK293T cells by addition of a mixture of DNAs (27.2 µg DNA to be produced, and packaging vectors pMDG2 (6.8 µg) and pAX2 (20.4 µg)) and 1 µg/µL pEI transfection reagent in OptiMEM media (Gibco) to HEK293T cells in a T75 flask, followed by incubation for 6 hours at 37^{o}C, 5% CO_2. Media was then changed to complete DMEM, and cells incubated for 72 hours to allow lentivirus particle production. Lentivirus particles were harvested at 48 and 72 hours for maximum yield, pooled, spun down at 4000 xg for 5 minutes to remove dead cells, and concentrated by adding Lenti-X concentrator (Takara Bio) at a 1:3 ratio and incubating at 4^{o}C for at least 1 hour. Lentivirus was then pelleted by centrifugation at 4000 xg for 45 minutes. Pellets were resuspended in plain DMEM at 1:50 of initial supernatant volume and aliquoted and stored at -80^{o}C until required.

2.5.2. Lentiviral Transduction

For lentiviral transduction, 5-150 µL concentrated lentivirus (optimised by titration of each batch) was added dropwise to cell media when cells were at 70-80% confluency and incubated for 24-72 hours (HeLa cells) or 1-2 weeks (primary neurons) prior to experimental analysis.

2.6. SRB Assay

For analysis of cell density based on cellular protein content, the sulforhodamine B (SRB) assay was used [369]. Cells were fixed with ice cold 1% (v/v) acetic acid in methanol overnight at -20°C. Fixative was aspirated and plates were allowed to dry at 37°C before proceeding to the next step. SRB (0.5% (w/v) in 1% (v/v) acetic acid in dH2O) was incubated in wells (37°C, 30 minutes). SRB was then aspirated, and unbound stain removed by cells extensive washing using 1% acetic acid, prior to drying plates at 37°C. Bound protein stain was solubilised by shaking incubation with 10 mM Tris (pH 10; 15 minutes, RT). Absorbance was read on a microplate reader with a 544/15 nm filter.

2.7. Total Protein Cell Lysis

For extraction of total protein lysate, cells were washed extensively with HBSS, and RIPA buffer (Sigma, supplemented with 1 mM PMSF) was added (200 µL for ~35 mm surface, scaled up or down appropriately). Cells were scraped on ice into Eppendorf tubes, which were incubated for 1 hour on a rotating wheel at 4°C, prior to spinning down at 10,000 xg for 15 minutes at 4°C. Supernatant (containing proteins) was stored at -20°C. If protein concentration was required, this was obtained by carrying out a BCA assay (Pierce™ BCA Protein Assay Kit, Thermo Fisher Scientific), following manufacturer's instructions.

2.8. Western Blotting Analysis

Following total protein extraction, protein samples were heated to 95°C for 5 minutes in the presence of LDS (1X, supplemented with 50 mM DTT). 10-30 µL of total protein was loaded on 4-12% BOLT gels (Thermo Fisher Scientific), separated (200 V, 24 minutes), and transferred onto polyvinylidene difluoride (PVDF) membranes (activated with methanol; Thermo Fisher Scientific) with transfer buffer (Table 2.1) using a semi-dry Pierce Power Station transfer system (Thermo Fisher Scientific; 25 V, 2.5 mAmp, 10 min). Membranes were blocked for 1 hour in milk or BSA (5% w/v in TBS-T; Table 2.1) and incubated in 5% milk or BSA containing the appropriate primary antibody (Table 2.3; 4°C, overnight). Membranes were washed extensively with TBS-T and probed with appropriate secondary antibody (Table 2.4) in 2.5% milk or BSA (RT, 1 hour). Membranes were washed with TBS-T, incubated with ECL substrate (GE Healthcare), and developed using an Odyssey Fc Imaging System (LI-COR). Analysis and quantification were carried out using Image Studio Lite software.

Table 2.3: Primary Antibodies

Protein	Supplier	Catalogue Number	Host Species/Clonality	Application	Dilution	Preparation
Ankyrin G	UC Davis/NIH NeuroMab facility	75-146	Mouse Monoclonal	ICC	1:500	BSA
ATP5A	Abcam	ab14748	Mouse Monoclonal	WB	1:1000	Milk
β-actin	Sigma-Aldrich	A2228	Mouse Monoclonal	WB/ICC	1:10,000/1:1000	Milk/BSA
DRP1	BD Biosciences	6111113	Mouse Monoclonal	WB	1:1000	Milk
DRP1 phospho-S616	Cell Signalling Technology	4494	Rabbit Monoclonal	WB	1:1000	BSA
Gephyrin	Synaptic Systems	147111	Mouse Monoclonal	WB	1:1000	Milk
GFP	Sigma-Aldrich	G1544	Rabbit Polyclonal	WB	1:2000	Milk
NanoLuc	Promega (kind gift)	N/A	Rabbit Polyclonal	WB	1:2000	Milk
PSD95	EMD Millipore	AB1596	Mouse Monoclonal	WB/ICC	1:1000/1:500	Milk/BSA
Synaptophysin	Merck Millipore	573822	Mouse Monoclonal	WB	1:1000	Milk
TIM23	Invitrogen	PA5-71877	Rabbit Polyclonal	WB	1:1000	Milk
TOM20	Santa Cruz Biotechnology	sc-17764	Mouse Monoclonal	WB	1:1000	Milk
TOM40	Thermo Fisher Scientific	PA5-57575	Rabbit Polyclonal	WB	1:1000	Milk
Tubulin-α	BioRad	MCA78G	Rat Monoclonal	ICC	1:400	BSA

Table 2.4: Secondary Antibodies

Antibody	Conjugate	Supplier	Catalogue Number	Application	Dilution
Anti-mouse	HRP	Invitrogen	SA5-10276	WB	1:10,000
	DyLight 800	Invitrogen	SA5-10176	WB	1:10,000
	Cy2	Jackson ImmunoResearch	715-225-150	ICC	1:400
	Cy3	Jackson ImmunoResearch	715-165-150	ICC	1:400
	Cy5	Jackson ImmunoResearch	715-175-151	ICC	1:400
Anti-rabbit	HRP	Invitrogen	31462	WB	1:10,000
	Alexa Fluor 790	Invitrogen	A11374	WB	1:10,000
	Cy2	Jackson ImmunoResearch	711-225-152	ICC	1:400
	Cy3	Jackson ImmunoResearch	711-165-152	ICC	1:400
	Cy5	Jackson ImmunoResearch	711-175-152	ICC	1:400
Anti-rat	Alexa Fluor 488	Invitrogen	A-11006	ICC	1:1000
	DyLight 650	Invitrogen	SA5-10029	ICC	1:500

2.9. Fluorescence Microscopy

2.9.1. Fixed Cell Confocal Microscopy

Transfected or infected cells were grown to confluency on glass coverslips, stained with 100 nM MitoTracker® Deep Red FM (Thermo Fisher Scientific; where appropriate - see figure legends) then washed in HBSS and fixed in 4% (v/v) paraformaldehyde (PFA) with 2% (w/v) sucrose (sucrose used for neurons only, to retain osmolarity), for 12 minutes at 37°C. Coverslips were then washed extensively in HBSS, and PFA was quenched using 100 mM Glycine.

If staining with antibodies (immunocytochemistry), cells were permeabilised by incubation in 0.1% (v/v) Triton-X in HBSS for 5 minutes, washed in HBSS and blocked in 3% (w/v) BSA in HBSS for 30 minutes. Coverslips were incubated on a drop of primary antibody in 3% BSA overnight at 4°C. Coverslips were washed extensively in HBSS and incubated with the appropriate secondary antibody (2 hours, RT) in 3% BSA, then washed again.

Coverslips were then dipped in dH2O and mounted on 5 µL mounting medium containing DAPI (VECTASHIELD Antifade Mounting Medium, Vector Laboratories) or Mowiol® mounting medium (Table 2.1) where DAPI was not suitable. Coverslips were left to dry overnight and imaged using a Leica confocal microscope (SP5II or SP8) and Leica Application Suite X (LAS X) software platform, in the Wolfson Bioimaging Facility.

2.9.2. Live Cell Confocal Microscopy

Cells were grown to confluency on 35 mm glass bottomed dishes (Corning). Cells were washed in HBSS and incubated in imaging buffer (Table 2.1) with 25 nM tetramethylrhodamine (TMRM) for 30 minutes at 37°C to obtain mitochondrial staining (where applicable). Cells were imaged immediately using a Leica SP8 confocal microscope and LAS X software platform, at 37°C.

2.9.3. Live Cell Structured Illumination Microscopy

SR-3D SIM is a widely used optical super resolution technique [370-373]. Here, it was used to obtain greater resolution when investigating mitochondrial morphology and aggregated proteins at mitochondrial membranes. Cells were grown to confluency on glass coverslips prior to staining with 100 nM MitoTracker Green™ (Thermo Fisher Scientific) for 30 minutes at 37°C. Coverslips were washed in HBSS and incubated in DMEM in Attofluor™ Cell Chambers (Invitrogen) for live imaging on an OMV v4 microscope (GE Healthcare). SIM was carried out in collaboration with Dr Wolfgang Hübner at the University of Bielefeld.

2.9.4. Long Term Live Cell Imaging (IncuCyte)

For long term live cell imaging, HeLa cells expressing red/green fluorophores (details in figure legends) were transferred to 24 well plates (VWR) on the morning of the assay and left to attach for 2 hours prior to transferring plates to the IncuCyte. Cells were imaged on an IncuCyte ZOOM (Essen Biosciences) in the University of Bristol Wolfson Bioimaging Facility, at 37^{o}C, 5% CO2 with 488- and 565-mm lasers. Images were collected every 30 minutes for 48 hours, and 9 positions were imaged per well.

2.9.5. Light Microscopy Image Analysis

All image analysis was performed using the FiJi image processing package [374, 375]. All the relevant plugin files are included as a zip file in Appendix 2. All macros were written by Dr Stephen Cross (Wolfson Bioimaging Facility, University of Bristol), within the FiJi plugin Modular Image Analysis (MIA) package version 0.21.0, which is publicly accessible on GitHub with a linked version specific DOI from Zenodo [376]. Where data was analysed manually, data was randomised/blinded by a colleague prior to manual analysis.

2.9.5.1. Mitochondrial Morphology Analysis

Mitochondrial pre-processing, as well as branch and network analysis was carried out using plugins developed by Dr Stephen Cross and Dr Richard Seager, exactly as described previously [377].

Analysis of mitochondrial width was carried out by manual measurement. Data was blinded and the same region of mitochondria was measured in each cell (100 x 100 pixels at 2 ‘o’ clock relative to the nucleus) to maintain unbiased results. Five measurements were taken across each mitochondrion (parallel to cristae) and averaged to obtain an average width for the given mitochondrion. An equal number of mitochondria were analysed for each condition.

Circularity analysis was carried out using a macro in the MIA package, written by Dr Stephen Cross, included in the appendix. This macro classifies mitochondria, providing a circularity index, where a value of 1 represents a perfect circle.

Cristae were counted manually and normalised to the length of the mitochondrion. Data was randomised and regions selected as detailed for thickness analysis.

2.9.5.2. Membrane Potential Analysis

TMRM analysis of mitochondrial membrane potential was done based on a published protocol [378]. Briefly, an average of the first 10 frames (TMRM fluorescence where images were captured by live confocal microscopy over 2 minutes) was taken, then the mitochondria were thresholded and their intensity measured. The average of the final three frames (after carbonyl cyanide m-chlorophenylhydrazone (CCCP) treatment to dissipate the $\Delta\Psi$) was subtracted as a control and the intensity of the subtracted image was re-measured. Batch processing was achieved using a macro written by Dr Stephen Cross within the MIA package.

2.9.5.3. Aggregate Analysis

Aggregation analysis was achieved using a macro written by Dr Stephen Cross on images acquired by SIM, also within the MIA package 0.21.0. Mitochondria (channel 1) are detected in 2D within a region of interest (ROI, *i.e.,* a transfected cell) and the pixel intensity of the trapping substrate (channel 2) is measured as a 4-pixel wide strip at the edge of the mitochondrion. The background channel 2 intensity (intensity at 10-14 pixels from the edge of the mitochondrion) is subtracted from the raw intensity surrounding the mitochondrion, to account for differing expression levels between cells. This provides values for the intensity directly surrounding mitochondria, and after thresholding, these values highlight the proportion of mitochondria within a cell or population of cells that have trapped protein on their outside.

2.9.5.4. Neuronal Morphology Analysis

Analysis of neuronal complexity (number of processes, *i.e.,* axon and dendrites) was carried out by manually counting the number of processes protruding from the soma (at a given distance from the soma, see indications on images by circles). This was carried out on randomised data, where expression of the protein of interest had been confirmed (prior to randomisation) and all processes were highlighted using an mCherry cytosolic marker.

Axons in transfected cells were identified using an Ankyrin G stain. Following identification of the axon to be measured, the length of the axon was measured by tracing the length of the axon, highlighted by the mCherry cytosolic stain, using the Simple Neurite Tracer (SNT) component of the Neuroanatomy plugin in FiJi. Synapses were counted manually. First, data was randomised, and dendrites were identified. The dendrite of interest was measured using the SNT plugin (as above) and the synapses along the region of interest were counted manually. Functional synapses were identified using PSD95 stain colocalisation with spines (shown in mCherry channel). A total of 5 dendrites were analysed per cell and an average was taken for each cell.

2.10. Cryo-Electron Tomography (cryo-ET)

Cryo-ET is a specialised application of cryo-electron microscopy (cryo-EM) used to create 3D reconstructions, or tomograms, of larger objects such as protein complexes or whole organelles in a sample. Samples are imaged as they are tilted, resulting in a tilt-series of 2D images, which can be reconstructed to form a 3D reconstruction of the object of interest [379]. In this study, cryo-ET was used for visualisation of microtubules/cargo within TNTs.

2.10.1. Sample Preparation

Grids (lacey carbon films on 200 µm gold mesh, Quantifoil) were glow discharged (2 mA and 1.5-1.8x10^{-1} $mbar^{-1}$; GloQube Plus Glow Discharge System, Quorum) for 1 minute. Grids were sterilised for 1 hour under UV light in a cell culture laminar flow hood. Grids were then washed extensively in HBSS and coated with 10 µL 25 µg/mL fibronectin (incubated at 37°C, 1 hour). Excess fibronectin was blotted from the grid before washing with HBSS. A suspension of 1 million cells/mL was prepared, and 10 µL was added to each grid. Cells were left to attach to grids by incubation at 37°C, 5% CO2 for 2 hours. Grids were then placed into 35 mm dishes containing cell culture medium, and cells were incubated for 24 hours prior to lentiviral transduction as appropriate (described in figure legends). Following transduction, cells were incubated for a further 48 hours prior to freezing. Grids were plunge frozen using a Leica EM GP automatic plunge freezer and stored in liquid nitrogen prior to imaging.

2.10.2. Cryo-ET Imaging

Cells on grids were imaged using a cryo-capable 120 kV Tecnai 12 microscope at The University of Exeter (Living Systems Institute), in collaboration with Dr Vicki Gold and Dr Mathew McLaren. Tomograms were processed using the IMOD tomography package.

2.11. NanoLuc Assay

The NanoLuc system is a split luciferase-based system developed by Promega [367]. It has been developed into a means to monitor import in yeast mitochondria previously [108, 364]. Here, it is developed into a means to monitor mitochondrial protein import in live mammalian cells for the first time.

2.11.1. Intact Cell Assay

HeLa cells were seeded in 6-well plates (300,000 cells/well), transfected with pLVX-EF1a—eqFP670-P2A-Cox8a-LgBit and incubated for 24 hours at 37°C. After 6 hours, cells were pre-treated with 100 nM MTX (where applicable, see figure legends). 24 hours after seeding, cells were infected with pLVX--Su9-EGFP-HiBit lentivirus and incubated at 37°C for 24 hours. Cells were detached using Trypsin and seeded on 96-well plates (20,000 cells/well). Cells were incubated for 16 hours at 37°C. Cells were then washed extensively with HBSS and incubated in HBSS imaging buffer prior to the addition of furimazine in Live Cell System Buffer (1:20; Promega) at a 1:5 ratio. Luminescent signal was analysed using a microplate reader collecting all wavelengths in the absence of light.

2.11.2. Permeabilised Cell Assay

Cells were seeded in 6-well plates (300,000 cells/well), transfected with eqFP670-P2A-Cox8a-LgBit, and incubated for 48 hours at 37°C (with additional lentiviral transduction carried out 24 hours after LgBit transfection, where appropriate). Cells were detached using Trypsin and seeded on 96-well plates at 30,000 cells/well. Cells were incubated for 16 hours at 37°C. Cells were washed extensively with HBSS and incubated in HBSS imaging buffer (Table 2.1). A fluorescence read was taken at 605/670nm using a BioTek Synergy Neo2 plate reader for normalisation of results against eqFP670 expression. Cells were then incubated in permeabilised cell assay master mix (Table 2.1). Drugs or inhibitors were added to individual wells as described in figure legends. A baseline read of background luminescent signal was taken prior to injection of purified substrate protein (Su9-EGFP-HiBit) to 1 µM final concentration, followed by a further bioluminescence read corresponding to import, lasting 30 minutes. Bioluminescence was read using a BioTek Synergy Neo2 plate reader (Agilent) or a CLARIOstar Plus plate reader (BMG LabTech).

2.12. CUTE Assay

The controlled unmasking of targeting elements (CUTE) assay system is a trafficking regulation system that relies on the reversible masking of the signal sequence responsible for directing the protein to its target organelle [380]. Here, it is used as an add-on to the intact NanoLuc system for monitoring mitochondrial protein import, to mask the MTS, rendering import inducible and thus enabling real-time visualisation in the intact cell system.

Cells were cultured as described earlier. Where necessary, media was replaced with FBS free glucose media, or with charcoal stripped FBS glucose media and cells were grown for 24 hours prior to seeding. Cells were seeded on 13 mm coverslips in 12-well plates (100,000 cells/well) and grown for 12 hours prior to transfection with 1 µg SLC5A6 (where appropriate, see figure legends). 12 hours later, cells were transfected with 1-10 µg Streptavidin and 0.5-1 µg Streptavidin-IRES-Su9/Cox8a-SBP-EGFP-HiBit (CUTE construct; either co- or pre-transfected, see figure legends), and, where required, treated with 40 µM Biotin. Cells were incubated for a further 24 hours (see figure legends), then fixed and analysed by confocal microscopy.

2.13. Mitochondrial Respiratory Function Analysis

2.13.1. Oroboros Oxygraph Assay

Cells were grown to confluency in 75 cm flasks and detached with 0.05% Trypsin, which was inactivated by the addition of complete DMEM. Cells were washed with HBSS and resuspended in mannitol respiration buffer (Table 2.1). Respiratory function assays were carried out by adding 1 mL of cells (5 million/mL) to 1 mL of mannitol respiration buffer in a closed chamber. Drugs were added as indicated in figure legends and respiratory function was measured as a function of oxygen slope and oxygen consumption, using an Oroboros oxygen electrode machine.

2.13.2. Seahorse Assay: Mitochondrial Stress Test

Cells were seeded in 6-well plates (200,000 cells/well) and infected with the appropriate lentivirus, as described in figure legends. The day prior to the assay, cells were detached by trypsinisation, counted, and seeded at 10,000 cells/well in 96 well Seahorse XF cell culture plates (Agilent). The sensor cartridges were hydrated overnight with tissue culture grade H_2O in a non-CO_2 incubator at 37^{o}C as per manufacturer's instructions. On the day of the assay, H2O in the sensor plate was replaced with Seahorse XF Calibrant (Agilent) and cells were washed with HBSS and incubated in Seahorse media (Table 2.2). Both sensor and cell plates were incubated in a non-CO_2 incubator at 37^{o}C for 1 hour prior to the assay. The sensor plate was loaded with oligomycin (15 µM for 1.5 µM final concentration in wells; injector A), CCCP (5 µM for 0.5 µM final; injector B) and antimycin A and rotenone (5 µM/5 µM for 0.5 µM/0.5 µM final; injector C). The sensor plate was calibrated in the machine prior to loading cells and running a mitochondrial stress test using a Seahorse XFe96 (Agilent). Following assays, cells were washed and fixed in 1% acetic acid in methanol at -20^{o}C overnight for SRB assays, which were used for normalising data to protein content.

2.14. Mitochondrial Isolations

Confluent cells were harvested by trypsinisation, pelleted, and washed extensively with HBSS. Pellets were freeze-thawed to weaken membranes. Subsequently, mitochondrial isolation was performed using Mitochondrial Isolation Kit for Cultured Cells (Abcam; ab110170) following manufacturers' instructions. Mitochondrial protein concentration was calculated using BCA assays.

2.15. Immunoprecipitations

Following mitochondrial isolation, mitochondria were gently lysed using 4.5g/g GDN in IP buffer (Table 2.1). GFP-tagged proteins were isolated using 10 µL GFP-trap beads (Chromotek), and Myc-tagged proteins were isolated using 10 µL Myc-Trap beads (Chromotek). Beads were washed extensively in IP buffer by centrifugation (4000 rpm, 1.5 minutes) and removal of supernatant. Supernatant (lysed mitochondrial sample) was incubated on a rotating wheel with beads overnight at 4^{o}C. Subsequently, beads were washed in IP buffer. After washing, supernatant was removed, and samples were analysed by Western blotting or mass spectrometry.

2.16. Tandem Mass Tagging Mass Spectrometry

Tandem mass tagging mass spectrometry (TMT-MS) is a highly sensitive, high throughput technique used for quantification of relative protein abundance between samples [381]. Here it was used for comparison of protein levels between samples subjected to trapping or Tau variant expression. Following immunoprecipitation as described above, beads were sent directly to the Proteomics Facility at the University of Bristol for TMT-MS analysis. Phospholipids and protease inhibitor were removed for the final wash steps to prevent sample contamination.

2.17. Statistical Analysis

GraphPad Prism 7 software was used to perform statistical analysis on results of all quantitative experiments, as detailed in figure legends. Unpaired t-tests or one or two-way ANOVA tests with multiple comparisons (Tukey's post hoc test) were used to calculate and determine statistical significance between observed differences, as appropriate (details in figure legends). A p-value less than 0.05 was considered significant for all experiments, in line with Graph Pad style P value format ($p^{ns}>0.05$ (not significant), $p^{*}\leq0.05$, $p^{**}\leq0.01$, $p^{***}\leq0.001$, $p^{****}\leq0.0001$). Statistical analysis for TMT-MS data was carried out by Dr Phil Lewis.

Chapter 3. The NanoLuc System to Monitor Mitochondrial Import

3.1. Introduction

Since most proteins required for mitochondrial function are encoded by nuclear DNA and synthesised by cytoplasmic ribosomes, efficient translocation of proteins into mitochondria is critical [64]. Furthermore, in recent years, impaired mitochondrial protein import has been highlighted as a key mechanism in a range of pathologies, including many neurodegenerative disorders (see Table 1.2). Therefore, a complete and detailed understanding of the mechanistic details of these processes, and how they go wrong in disease scenarios, is vital for target validation in drug discovery and for improving outcomes in such diseases.

Until recently, monitoring protein translocation was only possible by carrying out end-point time course assays *in vitro* in isolated mitochondria, and detection of import has relied on radioactivity and Western blotting-based outputs [130, 382, 383]. Whilst these assays have been helpful in improving our understanding of protein translocation, they are inefficient and time consuming. Moreover, they do not offer real-time readouts allowing for analysis of the kinetics of import and are not necessarily representative of what is happening within the whole cell scenario.

Various alternative methods have been proposed over the past couple of decades, which attempt to achieve real-time monitoring of protein translocation, but all have various limitations and drawbacks, as discussed previously [364, 367]. For example, split-fluorophore systems have been attempted [384], but these are reliant on slow chromophore maturation which obscures the dynamics of import. Similarly, β-galactosidase assays have been used to monitor nuclear and plasma membrane protein translocation [385], and could in theory be applied to mitochondria. However, these assays rely on reporter oligomerisation and product accumulation, hindering its ability to monitor dynamic import processes. Technology such as SNAP-tags can improve the time resolution of standard Western blotting based import assays [386], but these are still laborious and do not represent real-time import. Thus, there has been a real need for new quick and efficient experimental systems allowing for real-time monitoring of mitochondrial protein import into isolated mitochondria, as well as within live mammalian cell systems.

NanoLuc Binary Technology (NanoBiT) is a highly sensitive, specific, and stable bioluminescence-based reporter system that utilises a small luciferase subunit derived from a deep-sea shrimp [387]. This technology was originally developed by Dixon *et al.* at Promega [367] to monitor protein-protein interactions within living cells. It is a split luciferase, complementation-based system that relies on the binding of LgBit (also known as 11S), an 18 kDa fragment of NanoLuc, and SmBiT (pep114), a small, 1.3 kDa peptide of 11 amino acids,

which is the final β-strand of NanoLuc [367]. The resulting fully functional NanoLuc enzyme can convert furimazine to furimamide, producing a bioluminescent signal that can be read with a plate reader [367, 388]. HiBit (also known as pep86) is a high-affinity variant of SmBiT (Kd 0.7 nM vs. 190 μM, respectively), also developed by Promega [367].

Recently, our lab utilised this technology and developed it into a means to monitor protein transport across biological membranes [364]. Here, the data demonstrated how this can achieve considerably enhanced time resolution, which allows measurement of kinetic parameters based on import traces. Importantly, it reduces the timescale of data acquisition from days (for classical assays involving radioactivity and/or western blotting) to minutes.

Its versatility was demonstrated by utilising it for monitoring of protein import in mitochondria isolated from yeast cells (concept shown in Figure 3.1), as well as to monitor translocation *via* the bacterial Sec system [364]. In a follow up study, the yeast NanoLuc system was used in collaboration with mathematical based modelling approaches to further define the kinetic parameters underlying mitochondrial protein import in mitochondria isolated from yeast cells [108]. Here, the authors used the NanoLuc system to show how the two major driving forces for import through the $TIM23^{MOTOR}$ complex, Δψ and ATP hydrolysis, contribute to import, and the high level of dependency on the specific properties of the precursor protein [108].

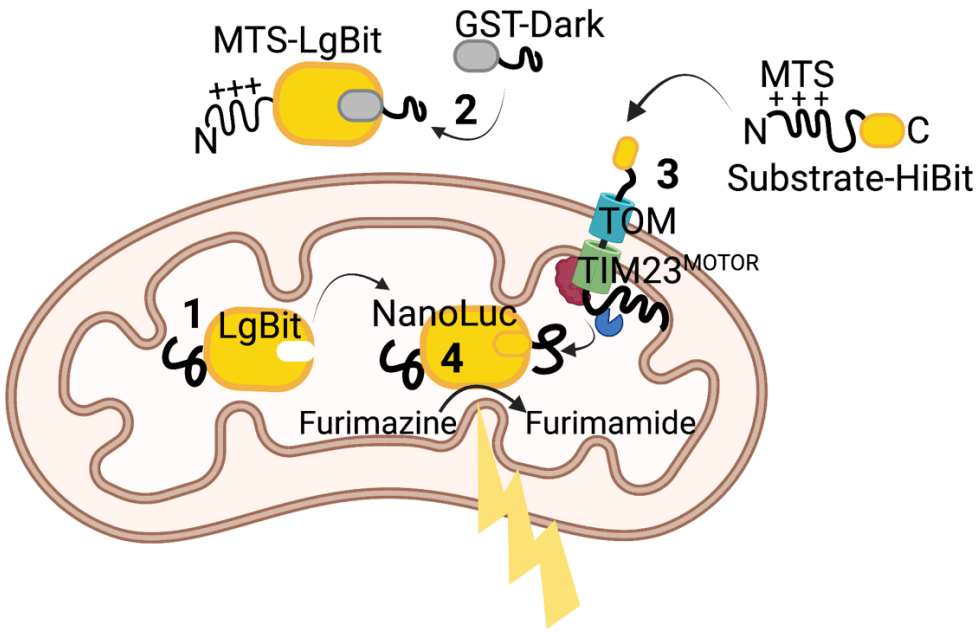

Figure 3.1: NanoLuc System to Monitor Mitochondrial Import in Isolated Yeast Mitochondria
Yeast mitochondria expressing mitochondrially targeted LgBit (MTS-LgBit, MTS is cleaved in the matrix leaving LgBit) are isolated *(1)*. GST-dark is added to bind non-mitochondrial LgBit, decreasing background signal *(2)*. A HiBit-tagged substrate protein (containing an N-terminal MTS) is added and is targeted to the mitochondrial matrix *(3)*. The MTS is cleaved and the HiBit peptide binds to LgBit in the matrix, forming NanoLuc *(4)*. This Converts furimazine to furimamide producing a luminescent signal. *Diagram created using BioRender.*

3.2. Aims

Using the same principles as previously described when the system was employed to monitor import in isolated yeast mitochondria (Figure 3.1) [108, 364], the aims of this part of my PhD project were to further develop the NanoLuc system for use in whole mammalian cells. Then, using this optimised technology, my overall aim was to further understand mitochondrial protein import in a whole cell scenario and how this may fail in disease.

The NanoLuc system relies on the expression of the LgBit protein and its localisation to the mitochondrial matrix, aided by an MTS, and the subsequent successful import of a protein containing a HiBit peptide tag into mitochondria, where it binds to LgBit to form the NanoLuc enzyme. The mammalian cell NanoLuc import assay system can be further split into two sub-systems: the intact cell system, which has a potential add-on using Controlled Unmasking of Targeting Elements (CUTE) technology, and the permeabilised cell system, each of which have their own advantages and caveats depending on the application (discussed below).

The main aims of this chapter were:

1. To develop the NanoLuc assay system into a means of monitoring import in an intact cell scenario, in HeLa cells.

2. To utilise CUTE technology as an add-on to the intact NanoLuc assay system, to allow kinetic details to be obtained from this assay.

3. To develop the NanoLuc assay system to monitor import in a permeabilised cell scenario, in HeLa cells.

3.3. Results: The Intact Cell NanoLuc System

The intact cell NanoLuc assay system follows the same principles as described previously (Figure 3.1) [364], but here, it was carried out in intact mammalian cells, rather than in isolated mitochondria from yeast cells. This updated version of the import assay undoubtedly provides more information of the biological process, especially in the context of cell physiology. Overall, the intact assay allows the comparison of import efficiency between cell types or conditions and provides information on the amount of protein imported into the mitochondria compared to a control, however it does not allow for analysis of the kinetics of import.

3.3.1. Optimisation of NanoLuc Component Expression

LgBit is inherently impossible to image or detect either on a microscope or plate reader because it lacks fluorescence or luminescence activity prior to complementation. Therefore, to confirm efficient transfection, cells were first transfected with DNA coding for eqFP670-P2A-Cox8a-LgBit (Figure 3.2). The P2A motif is a member of the 2A family of self-cleaving peptides that allows ribosome hopping between the eqFP670 and Cox8a-LgBit components. Characteristically, these peptides are 18-22 amino acids long, and contain a conserved core C-terminal motif (**DxExNPGP**) [389]. These peptides induce ribosomal hopping during protein translation, achieved by ribosomal skipping of the peptide bond between the proline and glycine residues [389]. The 2A peptides are each derived from different viral families, and P2A, with a sequence of **ATNFSLLKQAGDVEENPGP**, is derived from the porcine teschovirus-1 2A [389]. Theoretically, the P2A motif allows the equimolar expression of both components [390]. This allowed normalisation of the readouts to the transfection efficiency of the LgBit containing plasmid in cells, to normalise against batch-to-batch expression variability. This is achieved by carrying out an initial fluorescence read, quantifying the fluorescence intensity of eqFP670 (also known as near-infrared fluorescent protein (NiRFP) [391]) far-red probe.

EqFP670 is expressed on the same construct as LgBit but is retained in the cytosol (as shown in Figure 3.2 and Figure 3.3). Contrarily, the LgBit component is targeted to the mitochondrial matrix using a Cox8a MTS, a common bioengineering strategy in cell biology [64, 392]. Cox8a is a widely used MTS, from human cytochrome c oxidase subunit viii [393, 394]. We engineered MTS-LgBit downstream of the P2A motif to avoid potential perturbations associated with having a considerable stretch of amino acids at the C-terminus of LgBit, as this may hinder HiBit binding and NanoLuc activity.

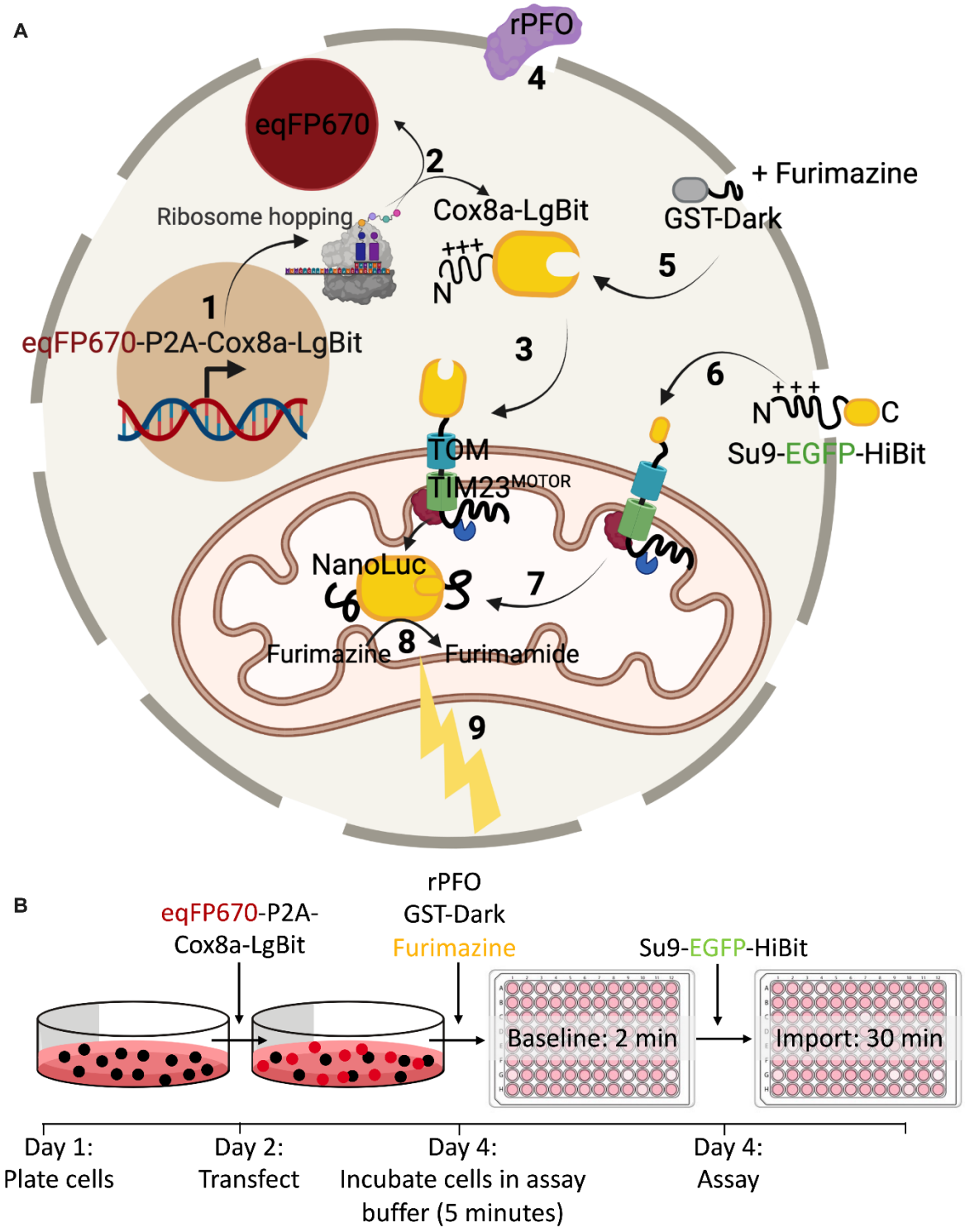
A
rPFO
4
eqFP670
2
Ribosome hopping
Cox8a-LgBit
+ Furimazine
GST-Dark
5
1
eqFP670-P2A-Cox8a-LgBit
3
6
Su9-EGFP-HiBit
TOM
TIM23MOTOR
NanoLuc
7
Furimazine
8
Furimamide
9
B
eqFP670-P2A-
Cox8a-LgBit
rPFO
GST-Dark
Furimazine
Su9-EGFP-HiBit
Baseline: 2 min
Import: 30 min
Day 1:
Plate cells
Day 2:
Transfect
Day 4:
Incubate cells in assay
buffer (5 minutes)
Day 4:
Assay

Figure 3.2: Intact Cell NanoLuc Assay System to Monitor Mitochondrial Protein Translocation
(A) Schematic showing the concept of intact NanoLuc import assay system in live mammalian cells. DNA encoding eqFP670 (far red fluorophore) and Cox8a-LgBit is transcribed in the nucleus and translated in the cytosol *(1)*, where ribosome hopping owing to the P2A motif leads to the production of cytosolic eqFP670 and mitochondrially targeted Cox8a-LgBit *(2)*. Cox8a-LgBit is imported into the mitochondrial matrix *via* the presequence pathway *(3)*. DNA coding for Su9-EGFP-HiBit is subsequently transcribed *(4)*, synthesised on cytoplasmic ribosomes *(5)*, and imported *via* the presequence pathway to the matrix *(6)*. Here, it binds to LgBit to form NanoLuc *(7),* which converts furimazine to furimamide *(8),* producing a bioluminescent signal as a readout of import *(9).* Importantly, eqFP670-P2A-Cox8a-LgBit and Su9-EGFP-HiBit expression are staggered by 24 hours. *Diagram created using BioRender.*
(B) Experimental outline of the intact NanoLuc assay. On day 1, cells are plated, and are subsequently transfected with DNA coding for eqFP670-P2A-Cox8a-LgBit on day 2. EqFP670 and Cox8a-LgBit expressing cells are transduced with DNA coding for Su9-EGFP-HiBit on day 3. On day 4, the day of the assay, a fluorescence read at 605/670 (ex/em) is taken for normalisation, media is replaced with assay buffer containing furimazine, and incubated for 5 minutes prior to carrying out an endpoint read for luminescence corresponding to protein import.

To characterise the optimal expression time for the LgBit containing protein, expression tests were carried out by Western blotting with an antibody against full length NanoLuc, but which also detects LgBit, on lysates from HeLaGAL cells, expressing Cox8a-LgBit for 24, 48 and 72 hours. The data shows that cells transfected with 0.5 µg of DNA per 100,000 cells have an optimal expression at 48 hours (Figure 3.3A). Confocal images of cells after 48 hours (Figure 3.3B) show an acceptable transfection efficiency but a relatively heterogenous population, *i.e.,* cells expressing high and low levels of eqFP670 and, consequently, Cox8a-LgBit. HeLa cells cultured in galactose medium (HeLaGAL) were used here, and throughout this thesis, unless otherwise specified. This is because HeLa cells cultured in glucose containing medium (HeLaGLU) are not reliant on their mitochondria for energy, since they are highly glycolytic, and thus do not respond to mitochondrial perturbations [395]. HeLaGAL cells, on the other hand, rely on mitochondrial OXPHOS for cellular energy, and therefore are sensitive to mitochondrial dysfunction [395]. HeLaGAL cells are therefore commonly used cultures in mitochondrial biology research.

Regarding the HiBit-tagged protein, transduction by lentiviral infection was performed 24 hours after the initial LgBit transfection. The HiBit protein contains a Su9 MTS, a commonly used MTS that encodes the first 69 amino acids of subunit 9 of the F0-ATPase of *Neurospora crassa* [392, 396], and an EGFP reporter domain preceding the HiBit tag (Su9-EGFP-HiBit). Like that described above for LgBit, expression tests carried out on cells expressing Su9-EGFP-HiBit by Western blotting (Figure 3.3C) showed that protein expression is sufficiently high after 24 hours. Confocal images show the signal is colocalised with TMRM, a cell permeant dye that accumulates within mitochondria with intact membrane potentials, commonly used as a fluorescent probe for identification of mitochondria [397]. This indicates good targeting to the mitochondrial compartment at 24 hours (Figure 3.3D).

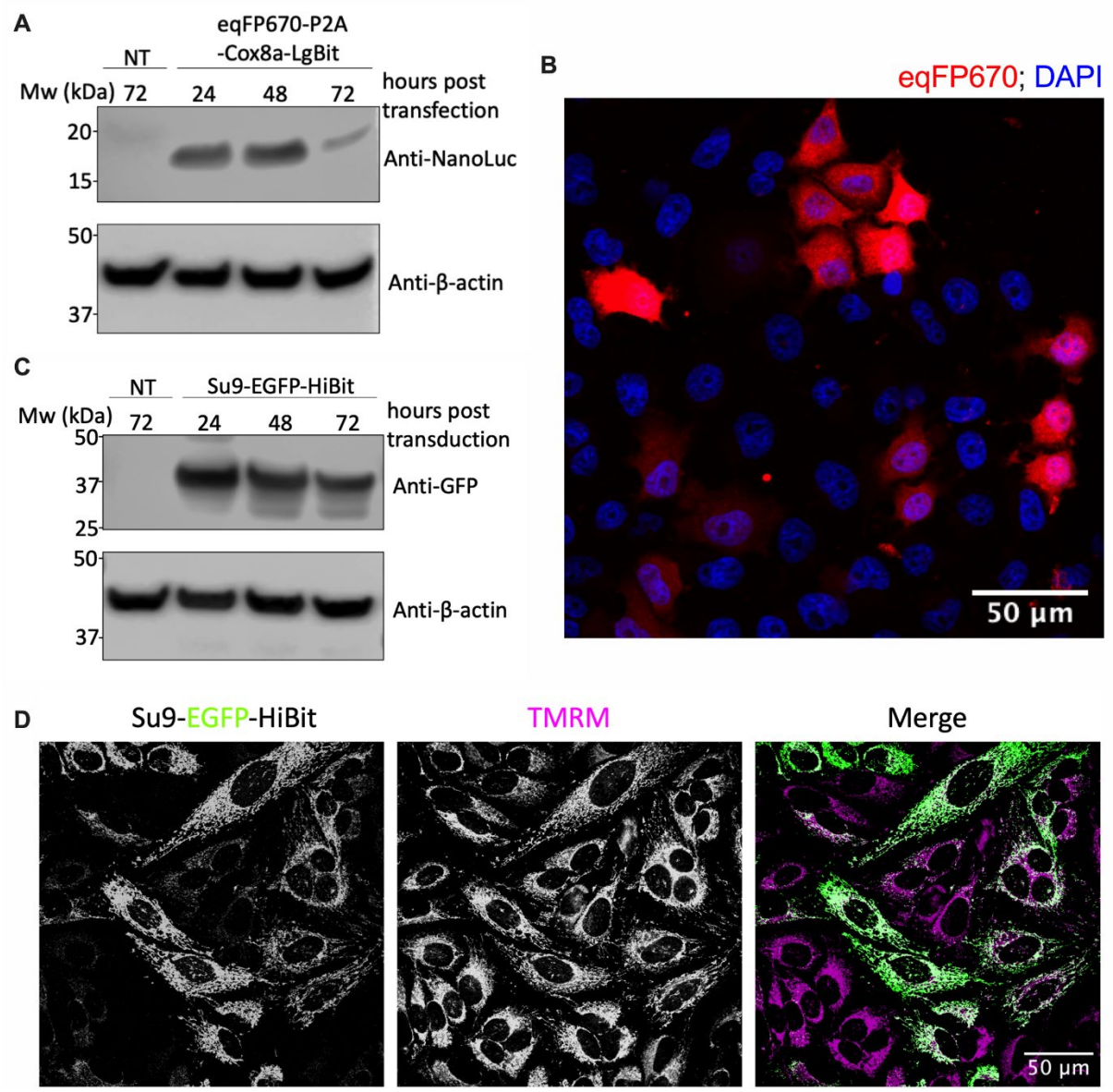

Figure 3.3: Optimisation of LgBit and HiBit Expression
(A) Western blot showing levels of Cox8a-LgBit expressed in HeLa cells. Cell samples were taken 24, 48, and 72 hours after transfection of cells with 1 µg eqFP670-P2A-Cox8a-LgBit DNA (per well in a 6 well plate), and an untransfected (NT) control sample was taken at the 72-hour timepoint. 30 µg of total cell lysate was loaded onto a protein gel and the membrane was probed against anti-NanoLuc for assessment of Cox8a-LgBit expression, as well as a β-actin loading control. *N=3*.
(B) Confocal microscopy image showing eqFP670 expression (red) in the cytosol of HeLa cells. Cells were transfected with 0.5 µg eqFP670-P2A-Cox8a-LgBit DNA (per well in a 12 well plate) and fixed 48 hours after transfection. Nuclei are indicated with DAPI (blue). Fixed cells on coverslips were mounted on slides and imaged using a confocal microscope. Scale bar is 50 µm. *N=3*.
(C) Western blot showing levels of Su9-EGFP-HiBit expressed in HeLa cells. Cell samples were taken 24, 48, and 72 hours after transduction of cells with Su9-EGFP-HiBit lentivirus, and an untransduced (NT) control sample was taken at the 72-hour timepoint. 30 µg of total cell lysate was loaded onto a protein gel and the membrane was probed against anti-GFP for measurement of Su9-EGFP-HiBit expression, as well as a β-actin loading control. *N=3*.
(D) Confocal microscopy image showing Su9-EGFP-HiBit expression (green) in the mitochondria of HeLa cells. Cells were infected with Su9-EGFP-HiBit lentivirus and imaged live 24 hours after transduction on a confocal microscope. TMRM staining indicates mitochondria (magenta). *N=3*.

3.3.2. *The Intact System Quantifies Import but not Kinetics*

Therefore, under our experimental design cells are incubated for a total of 48 hours prior to analysis of import efficiency on a microplate reader, in order to obtain maximal expression of both proteins (Figure 3.2). This produces end point measurements of import efficiency over a 24-hour period (Figure 3.4). This signal is directly proportional to the amount of HiBit-tagged protein successfully imported into mitochondria because the signal becomes negligible when cells express LgBit or HiBit alone or are untransfected (NT) (Figure 3.4).

Although this system yielded a signal corresponding to complementation of the LgBit and HiBit fragments of NanoLuc within the mitochondrial matrix, in this state, there was no capacity for the system to be used to obtain kinetic information relating to import. Rather, it provides a '*black and white*' picture of whether the protein has been imported efficiently into mitochondria. This has some potentially useful applications, for example in high throughput drug screening assays, but there was potential for it to be further developed into a system capable of kinetic analysis. This is of particular interest for this project which focusses on further understanding import mechanisms. To this end, I investigated the possibility of using the CUTE system as an add-on to the intact NanoLuc system, to allow us to monitor import in intact cells in an inducible manner, providing the ability to visualise import in real time.

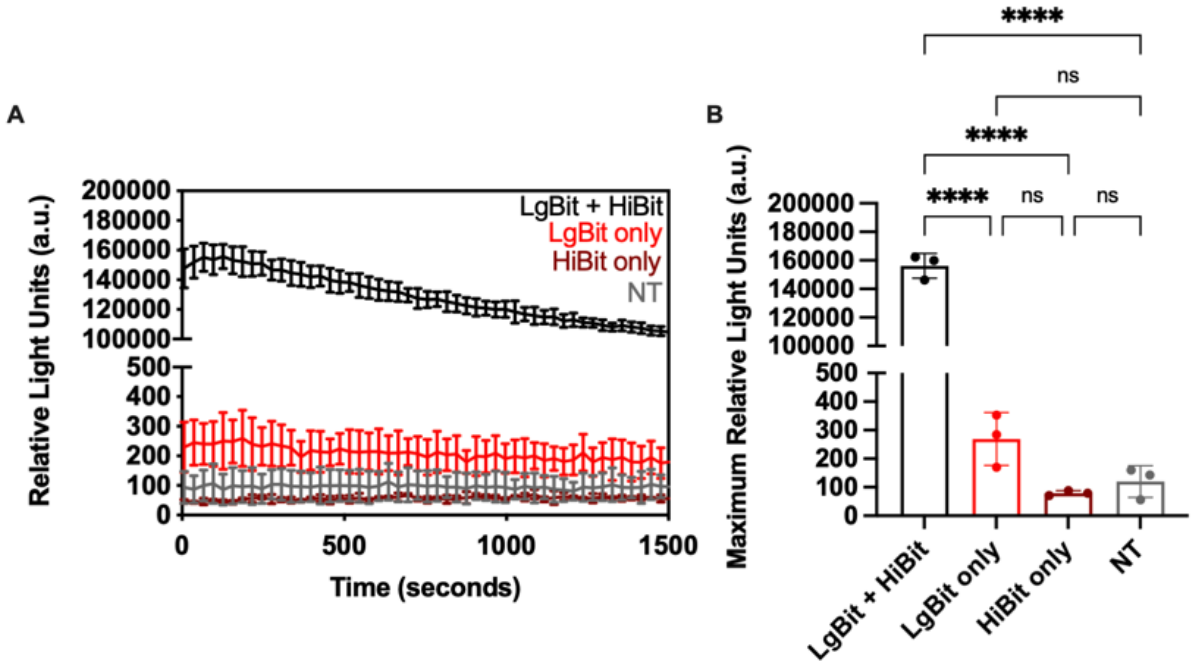

Figure 3.4: Intact Cell NanoLuc System Quantifies Import but does not Report Kinetics
(A) Import read corresponding to mitochondrial protein import using the intact NanoLuc assay system. Cells expressing LgBit and HiBit (black), LgBit only (red), HiBit only (deep red/maroon) or untransfected control cells (NT, grey) were subjected to import assays and luminescence was measured 5 minutes after furimazine addition over a period of 30 minutes. *Average, raw data displayed with error bars representing SD. N=3 biological replicates, each with n=3 technical replicates.*
(B) Maximum amplitude from (A) plotted as bar graphs to show relative import in different conditions. *Error bars display SD. One-way ANOVA with Tukey's post hoc test was used to determine significance.*

3.4. Results: The Controlled Unmasking of Targeting Elements (CUTE) System

The CUTE system was first developed by Abraham *et al.,* in 2016 [380]. It is a trafficking regulation system that relies on the reversible masking of the signal sequence responsible for directing the protein of interest (POI) to its target organelle. The CUTE system is a modification of the early retention using selective hooks (RUSH) system [398], in which the POI is trapped in a compartment by an organelle-resident membrane protein that serves as a hook. Both systems take advantage of the differential affinity of streptavidin for the streptavidin binding protein (SBP) and biotin. Essentially, the unmasking or release of the POI from the streptavidin-SBP interaction is achieved by addition of biotin to the cells.

These approaches are directly relevant to my project since they would allow me to carry out real-time NanoLuc assays to monitor the import event in intact cells. Moreover, it would avoid potential off target effects of permeabilising cells, which may pose problems, particularly in primary neurons in which the dynamic modulation of membrane potential is integral to function. We decided to move forward with the CUTE system since early, unpublished work (communicated *via* conference poster presentation) from a different laboratory showed that ~ 50% of the POI in the RUSH system was already translocated to the mitochondrial matrix prior to the biotin pulse.

Our modified CUTE system was designed as follows: the POI was engineered with an MTS (Su9 in this case) positioned at the N-terminus, followed directly by a 38 aa SBP domain [399], a reporter protein (EGFP) and a HiBit peptide (referred to hereafter as the CUTE construct or protein; Figure 3.5). To mask the MTS signal, cytosolic streptavidin is expressed within the cells and binds to the SBP domain [380, 399]. This renders the protein incapable of being targeted to the mitochondria. To induce import, the system is flooded with biotin, and the high affinity of the streptavidin-biotin interaction means that SBP is displaced from streptavidin, unmasking the MTS, and allowing release of the protein and subsequent translocation to mitochondria (Figure 3.5).

The streptavidin and CUTE proteins are encoded on the same plasmid, but are expressed as independent proteins, due to their separation by an internal ribosome entry site (IRES). IRES elements allow for translation initiation in a cap-independent manner [400, 401]. They are commonly used in molecular biology to allow expression of multiple genes under the same promotor, in a similar manner to that described previously for 2A-peptides [402]. This was done to ensure all cells expressed both proteins (or neither). Theoretically, this should eliminate background signal associated with unbound CUTE protein which would be transported to mitochondria in the absence of streptavidin.

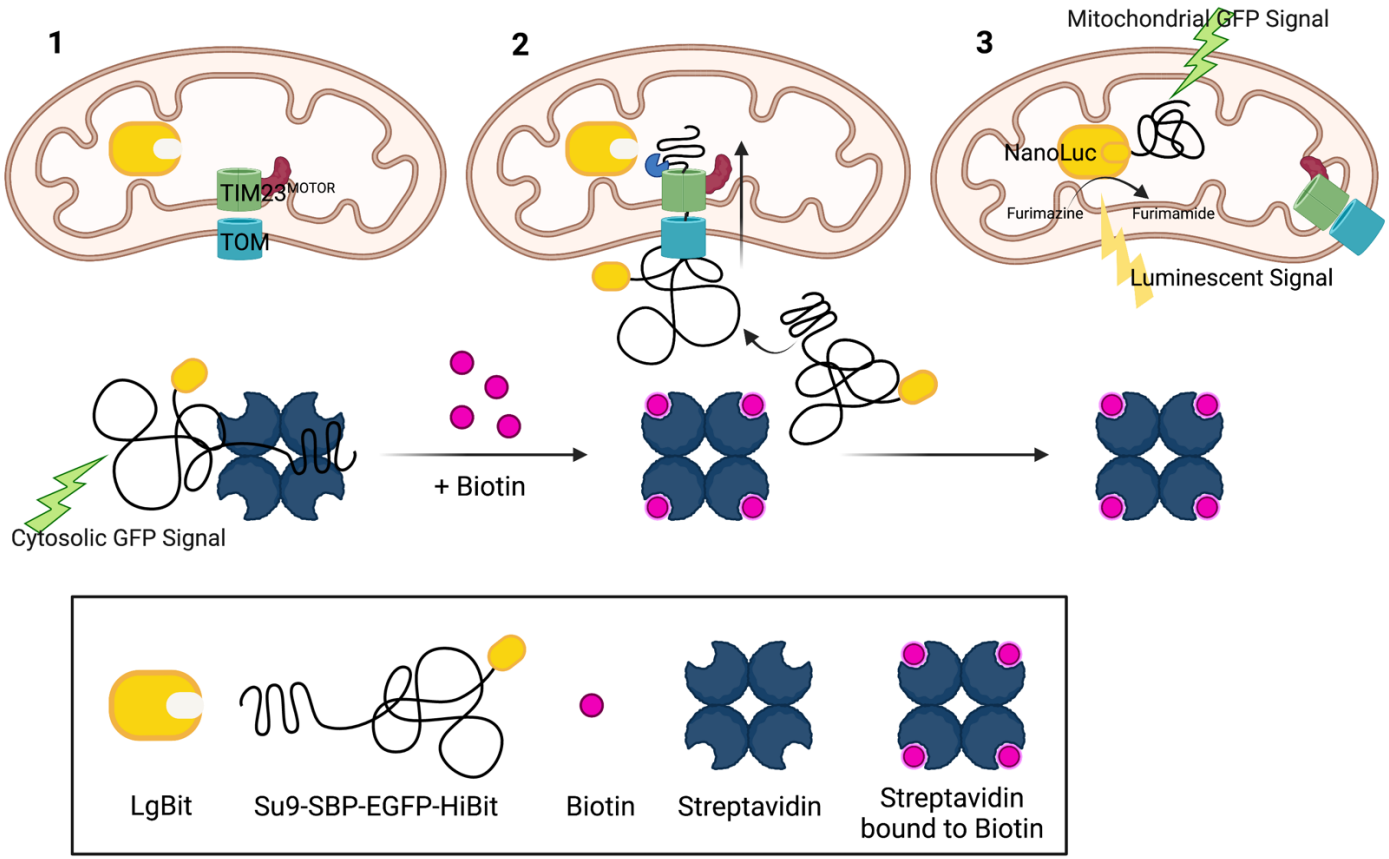

Figure 3.5: CUTE System as an add-on to the Intact NanoLuc Assay
(1) LgBit is expressed in the mitochondrial matrix as described for the intact system. Subsequent transfection induces expression of a construct coding for streptavidin and Su9-SBP-EGFP-HiBit. The SBP binds to streptavidin at four binding sites, which masks the MTS (Su9). *(2)* Addition of biotin, which has higher affinity for streptavidin than SBP, displaces the Su9-SBP-EGFP-HiBit, allowing it to be targeted to the mitochondrial matrix. *(3)* Once imported, HiBit binds to LgBit, forming NanoLuc, which converts furimazine to furimamide and produces a bioluminescent signal. Additionally, the localisation of the GFP signal allows assessment of the system by confocal microscopy. *Schematic created using BioRender*.

3.4.1. POI Localises to Mitochondria in Absence of Biotin

First, the CUTE construct was expressed in HeLa cells in the absence or presence of 40 µM biotin. Confocal microscopy showed that, unexpectedly, the CUTE protein was localised to mitochondria even in the absence of biotin (Figure 3.6A). Although DMEM is biotin free, supplemented FBS may contain trace levels of biotin which may be enough to saturate streptavidin binding, thus preventing masking of the SBP containing protein. To eliminate this possibility, the CUTE construct was expressed in cells cultured in media containing normal FBS, charcoal stripped FBS, or no FBS, all in the absence of exogenously added biotin (Figure 3.6B). Charcoal stripped FBS has previously been shown to eliminate biotin from FBS, and has been used to study the effects of biotin deficiency on mitochondria [403]. However, in our experimental setup, the CUTE protein still appeared to be imported into mitochondria under all conditions, indicating that trace levels of biotin in FBS was not the issue.

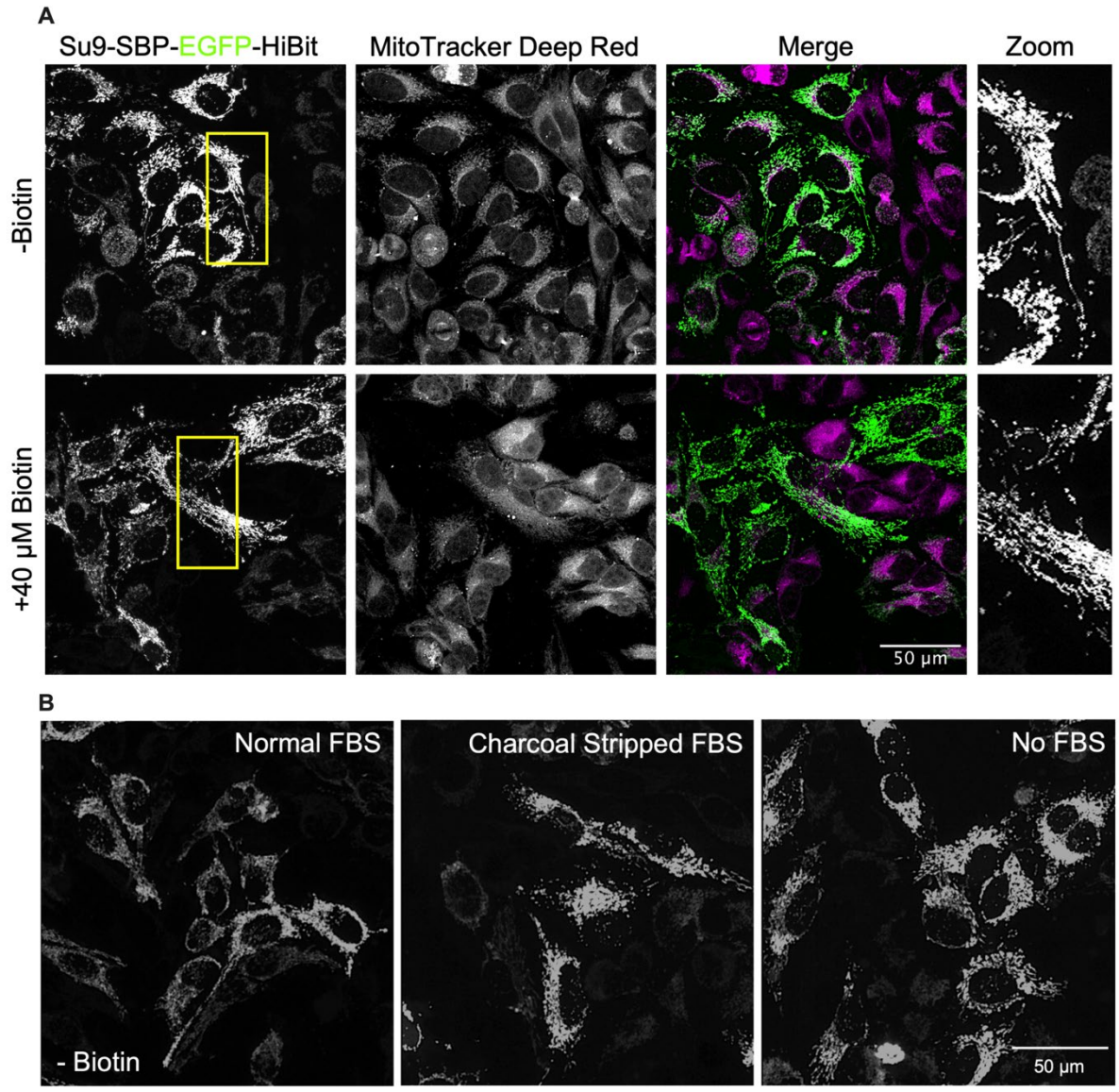

Figure 3.6: CUTE Protein Localises to Mitochondria in the Presence and Absence of Biotin
(A) CUTE protein (Su9-SBP-EGFP-HiBit; green) localisation in the absence and presence of exogenously added biotin. HeLa cells were subjected to expression of the CUTE construct for 24 hours in the presence of absence of 40 µM biotin. Mitochondria were stained with MitoTracker Deep Red (magenta), then cells were fixed and visualised by confocal microscopy. Scale bar is 50 µm. Zoom is shown to highlight mitochondrial structures. *N=3*.
(B) CUTE localisation in cells cultured in various forms of FBS. HeLa cells were grown in normal FBS, charcoal stripped FBS, or no FBS, for 24 hours prior to expression of the CUTE construct, in the absence of biotin. After a further 24 hours, cells were fixed and EGFP localisation visualised by confocal microscopy. Scale bar is 50 µm. *N=3*.

3.4.2. MTS Masking Depends on MTS and SBP: Streptavidin Ratio

The yeast Su9 MTS is a very long (207 bp/ 69 aa/ 7.5 kDa) and 'strong' MTS, in terms of its mitochondrial targeting, as discussed previously [404, 405]. Thus, I anticipated that it may be resistant to trapping by streptavidin binding as:

1) It may be too long to be fully masked by the four molecules binding.
2) It may be translocated directly to mitochondria upon translation, outcompeting the binding of streptavidin.

To assess if this was indeed the case, the Su9 MTS was substituted for a shorter (75 bp/ 25 aa/ 2.7 kDa), weaker MTS, Cox8a (Figure 3.7A). CUTE protein localisation in HeLa cells expressing CUTE proteins containing either Su9 or Cox8a targeting sequences was compared by confocal microscopy (Figure 3.7B).

I also hypothesised that the streptavidin levels may not be high enough to fully saturate the SBP, as higher streptavidin: SBP ratios had been used previously [380]. Streptavidin was cloned onto a separate construct, and a range of SBP: streptavidin ratios were tested in cells, ranging from 1:1 to 1:5, in the presence or absence of biotin (Figure 3.7B). Expressing the new Cox8a-CUTE protein in HeLa cells cultured in media containing charcoal stripped FBS with various SBP: streptavidin ratios led to an increase in the cytoplasmic localisation of CUTE protein by around 50% in the absence of biotin (not quantified; Figure 3.7B). Both factors seemed to have a compounding effect on CUTE protein trapping in the cytosol. I therefore decided to use the Cox8a MTS in combination with a higher (1:5) SBP: streptavidin ratio going forwards.

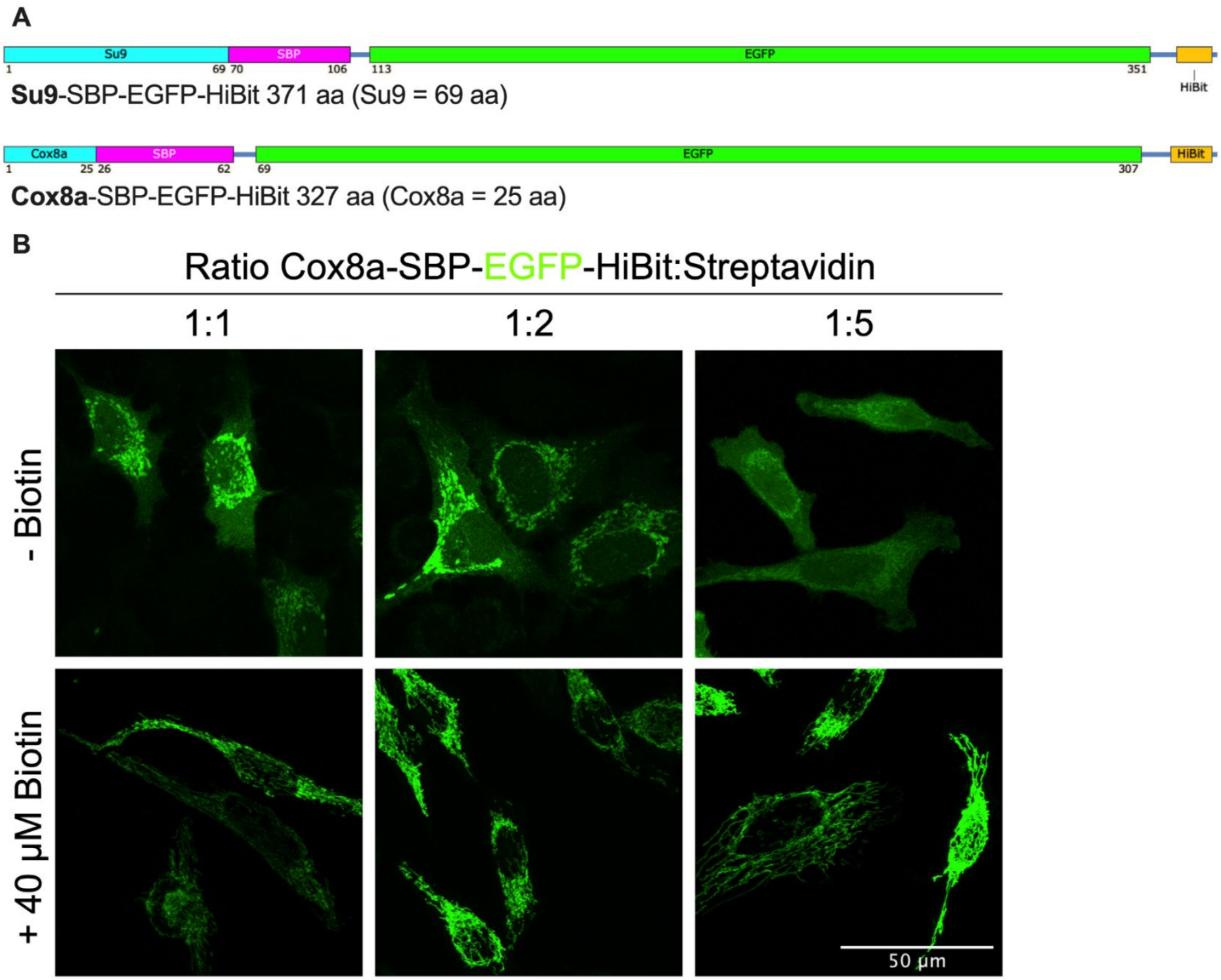
A
Su9
SBP
EGFP
1
69 70
106
113
351
HiBit
Su9-SBP-EGFP-HiBit 371 aa (Su9 = 69 aa)
Cox8a
SBP
EGFP
HiBit
1
25 26
62
69
307
Cox8a-SBP-EGFP-HiBit 327 aa (Cox8a = 25 aa)
B
Ratio Cox8a-SBP-EGFP-HiBit:Streptavidin
1:1
1:2
1:5
- Biotin
+ 40 µM Biotin
50 µm

Figure 3.7: Cox8a MTS and Increased Streptavidin Improve CUTE Cytosolic Trapping

(A) Comparison of CUTE proteins with altered MTS. The original CUTE protein (Su9-SBP-EGFP-HiBit; top schematic) had a very long, strong MTS of 69 amino acids. The new CUTE protein (Cox8a-SBP-EGFP-HiBit; bottom schematic) had a shorter MTS (25 amino acids). *Protein schematics created using SnapGene.* **(B)** Representative confocal images of HeLa cells with altered ratios of SBP: streptavidin with Cox8a-CUTE construct. HeLa cells were transduced with varying ratios of streptavidin--IRES--Cox8a-SBP-HiBit: streptavidin (1:1, 1:2 and 1:5) and incubated in the presence or absence of 40 μM biotin for 24 hours, prior to fixation and visualisation of EGFP localisation (green) by confocal microscopy. Scale bar is 50 μm. *N=3*.

3.4.3. SLC5A6 Improves Speed of Unmasking and Translocation

Clearly, ~50% cytoplasmic localisation in the absence of biotin was not perfect. Nonetheless, I predicted that it would be sufficient to visualise import into mitochondria using the NanoLuc assay *if* transport occurred immediately following biotin addition. Therefore, a time course assay was undertaken to investigate how long it takes for translocation of the CUTE protein to mitochondria following biotin addition (Figure 3.8).

Unfortunately, this experiment highlighted the slow relocation to mitochondria following biotin supplementation, taking at least four hours to complete translocation (Figure 3.8 A (top panel) and B (blue)). Ideally, for the assay to work optimally, it would require translocation within a matter of minutes (<30 minutes). Of course, the maturation time of EGFP will play a part when trying to visualise this by confocal microscopy, which will not be an issue when reading bioluminescence, but this should not cause it to take in excess of four hours. Indeed, the maturation time of EGFP has previously been shown to be ~60 minutes [406] so a maximum translocation and maturation time of ~90 minutes when using confocal microscopy would be sufficient to assume the assays would work in NanoLuc format.

It has been shown previously that the sodium-dependent multi-vitamin transporter SLC5A6 is required for, and drastically improves efficiency and speed of, biotin uptake and transport in HeLa cells [407]. Therefore, I overexpressed SLC5A6 prior to expression of CUTE and streptavidin, and biotin treatment, to see if this would speed up translocation (Figure 3.8 A (bottom panel), quantified in B (purple)). The overexpression of SLC5A6 does indeed speed up translocation. Two hours after biotin addition, the construct is localised to mitochondria in the majority of cells (73%, compared to only 29% in the absence of SLC5A6, Figure 3.8). This implies that the CUTE system may be fast enough for use with the intact NanoLuc assay to monitor mitochondrial protein import in real-time.

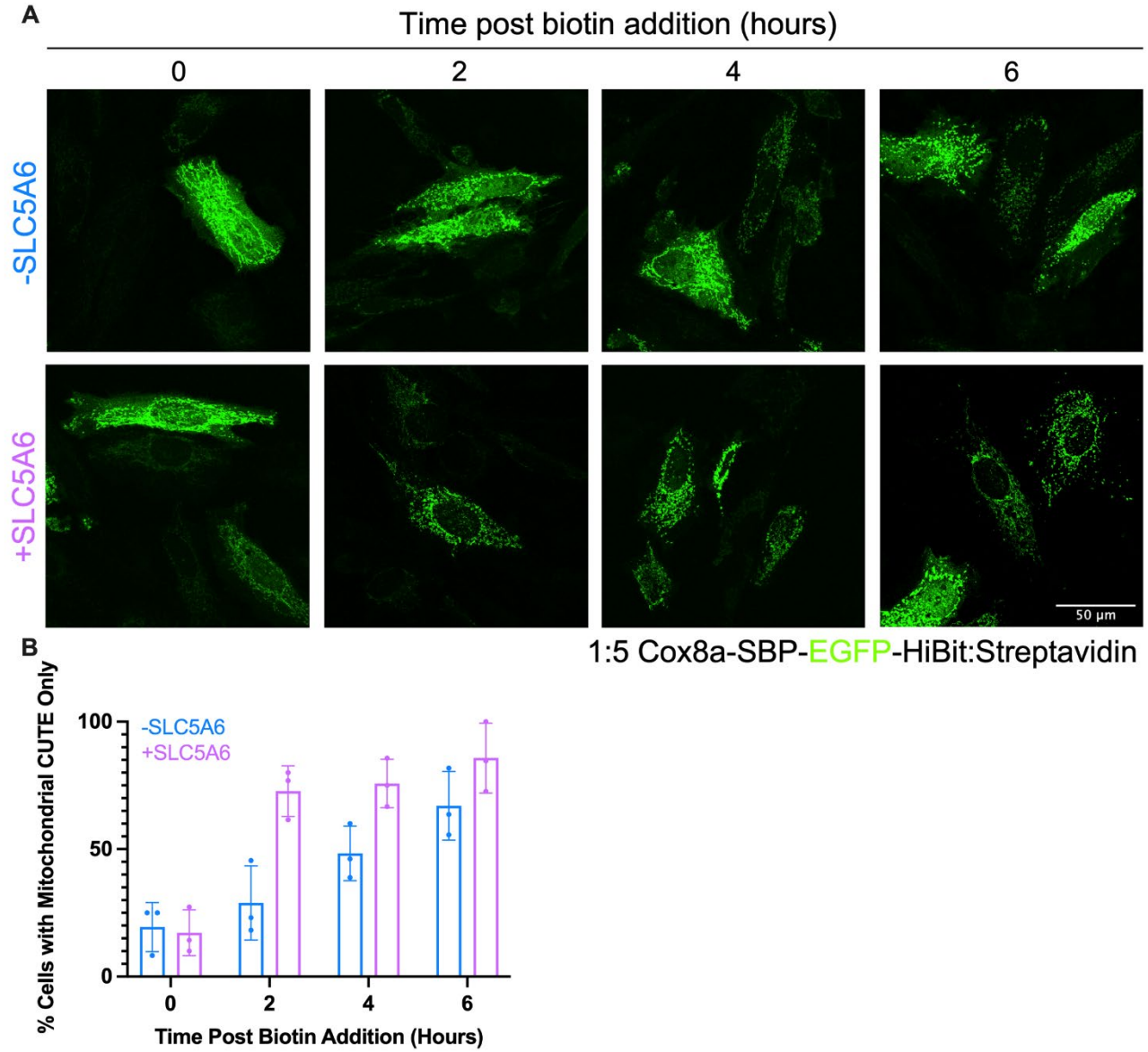
A
Time post biotin addition (hours)
0
2
4
6
-SLC5A6
+SLC5A6
50 µm
1:5 Cox8a-SBP-EGFP-HiBit:Streptavidin
B
% Cells with Mitochondrial CUTE Only
100
50
0
-SLC5A6
+SLC5A6
0
2
4
6
Time Post Biotin Addition (Hours)

Figure 3.8: SLC5A6 Speeds up CUTE Mitochondrial Import
(A) Time course showing CUTE localisation after addition of biotin. HeLa cells were subjected to expression of Cox8a-SBP-EGFP-HiBit and streptavidin (1:5 ratio) with or without SLC5A6. After 24 hours, 40 µM biotin was added, and cells were fixed at 0-, 2-, 4- and 6-hours following addition of biotin. The localisation of the CUTE protein was then visualised by the EGFP fluorescence (green), using a confocal microscope. Scale bar is 50 µm. *N=3 biological replicates*.
(B) Quantification of (A). Cells without (blue) or with (purple) SLC5A6 expression were categorised based on whether they displayed EGFP signal solely from the mitochondria. *20 cells were counted per condition for each biological replicate, giving a total of n=60 cells per condition. Error bars show SD.*

However, this led to the requirement for expression of four separate DNA constructs in cells for NanoLuc-CUTE assays: LgBit, SLC5A6, Streptavidin (at a 1:5 ratio compared to CUTE), and Su9-SBP-EGFP-HiBit. This poses numerous problems, the first being excessive cell death due to subsequent transfections, lipofectamine reagent and the expression of toxic DNA repeatedly in cells. This means there may not be enough viable cells expressing all proteins to carry out assays. In initial attempts, excessive cell death following transfections prevented me from being able to carry out NanoLuc assays. The second problem this poses is potential off target effects of this toxicity on cells. Is the system now showing us physiological responses, or are the cells and mitochondria simply subject to high levels of stress and death due to this expression overload?

In its current state, the intact NanoLuc assay system is not sufficient to obtain the data output required for real-time monitoring of mitochondrial import in live mammalian cells. Therefore, I focussed on development of the permeabilised cell system as a contingency plan.

3.5. Results: The Permeabilised Cell NanoLuc System

In principle the permeabilised assay system is largely the same as the intact system, with use of plasma membrane permeabilisation which provides capacity for kinetic analysis of the import process. In the permeabilised assays, the LgBit component was targeted to the matrix using a Cox8a MTS, and after 48 hours of expression (as optimised previously; Figure 3.3A and B), read outs were normalised to the expression of eqFP670 in cells (full experimental set up and schematic shown in Figure 3.9). The individual aspects of the permeabilised set up as well as their optimisation and characterisation are described in detail in the following section.

3.5.1. Optimisation of Key Components of the Permeabilised Cell System

Prior to assays, cell plasma membranes were permeabilised using 3 nM purified recombinant perfringolysin (rPFO), a cholesterol-dependent, selective cytolysin [365] which forms pores in the plasma membrane, allowing solutes and proteins up to 200 kDa to enter [408, 409]. Its efficiency was characterised by respirometry using an Oroboros oxygraph to measure the oxygen consumption rate in cells in response to various respiratory chain substrates. This was done to ensure that, following rPFO treatment, plasma membranes were permeable to substrates without compromising mitochondrial integrity or respiratory function (Figure 3.10A).

The respirometer trace shown in Figure 3.10A demonstrates that prior to addition of rPFO, mitochondria did not respond to stimulation of the respiratory chain using 5 mM succinate and 1 mM ADP, which are charged molecules and thus cell impermeable. Once 3 nM rPFO was added, the rate of oxygen consumption increases rapidly, showing that the mitochondria are indeed utilising the substrates, demonstrating that the cell plasma membrane is permeabilised. The very slight reduction in the slope following addition of 10 µM cytochrome *c* and recovery of the slope (from 122 pmol/(s*ml) to 108 pmol/(s*ml)) shows that, whilst the plasma membrane is permeabilised, the mitochondria remain intact and have not been permeabilised or burst by rPFO at this concentration. Finally, following addition of 1 µM antimycin A, which inhibits OXPHOS at the Complex III level, the oxygen slope is quickly depleted, showing that the mitochondria are respiring normally in the presence of rPFO (Figure 3.10A).

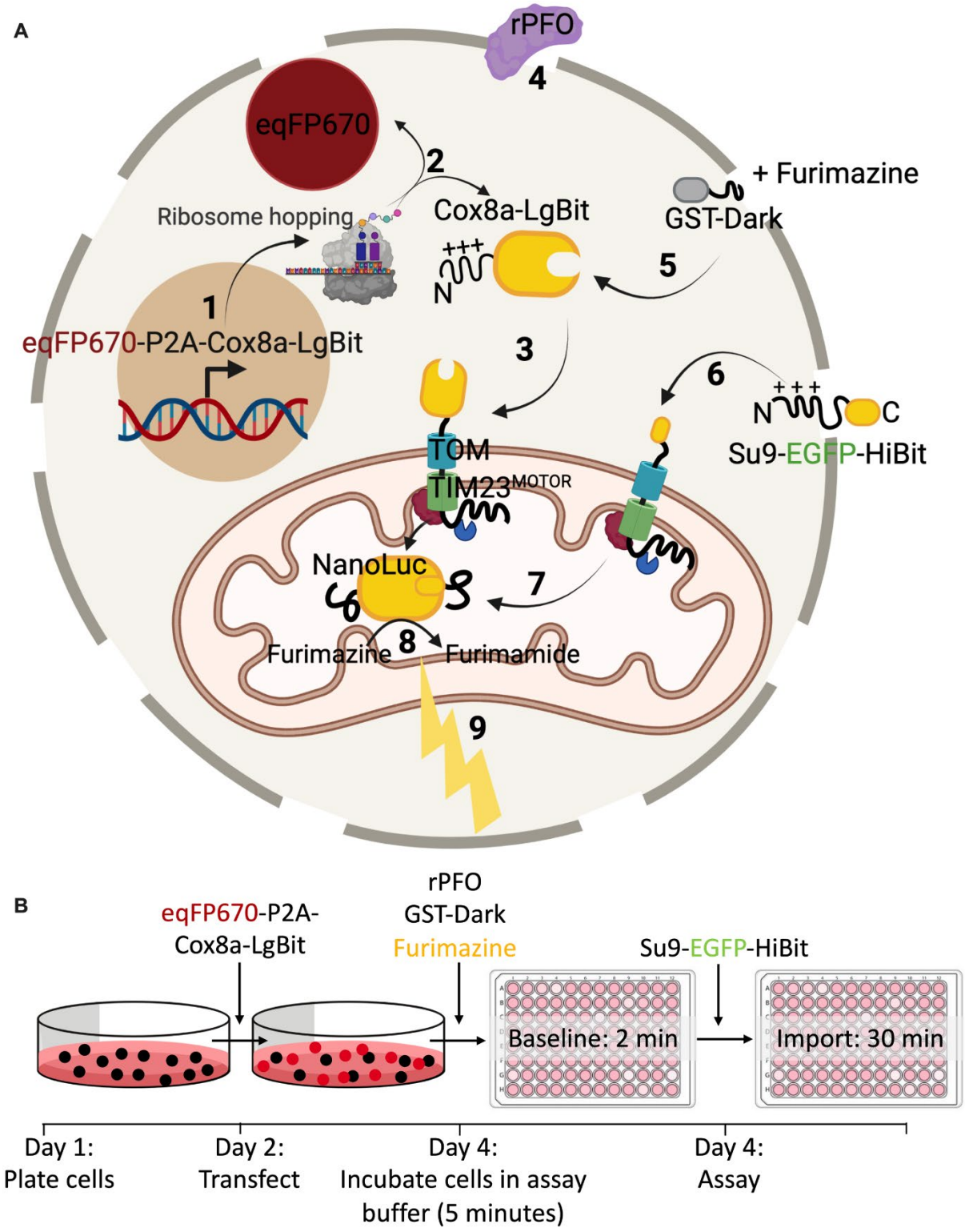
A
rPFO
4
eqFP670
2
+ Furimazine
Ribosome hopping
Cox8a-LgBit
GST-Dark
5
1
eqFP670-P2A-Cox8a-LgBit
3
6
Su9-EGFP-HiBit
TOM
TIM23MOTOR
NanoLuc
7
8
Furimazine
Furimamide
9
B
eqFP670-P2A-
Cox8a-LgBit
rPFO
GST-Dark
Furimazine
Su9-EGFP-HiBit
Baseline: 2 min
Import: 30 min
Day 1:
Plate cells
Day 2:
Transfect
Day 4:
Incubate cells in assay
buffer (5 minutes)
Day 4:
Assay

Figure 3.9: Permeabilised Cell NanoLuc Assay System: Experimental Outline
(A) Schematic showing the concept of the permeabilised NanoLuc import assay system in live mammalian cells. DNA encoding eqFP670 (far red fluorophore) followed by a P2A region and Cox8a-LgBit is transcribed in the nucleus and translated in the cytosol *(1)*, leading to the production of cytosolic eqFP670 and mitochondrially targeted Cox8a-LgBit *(2)*. Due to its MTS, Cox8a-LgBit is translocated to the mitochondrial matrix *via* the presequence pathway *(3)*. At the time of the assay, import buffer containing 3 nM rPFO is added, which perforates the plasma membrane *(4)* whilst retaining intact mitochondria. This allows other substrates, drugs, furimazine, and proteins to enter the cells. One such protein is GST-dark, which binds any remaining cytosolic LgBit *(5)*, preventing background signal from cytosolic binding. Following a baseline read, a HiBit containing precursor is added (in this case Su9-EGFP-HiBit; *(6)*) which is translocated into mitochondria where is binds to LgBit *(7)*, forming the fully functional NanoLuc enzyme, which converts furimazine to furimamide *(8)*, producing a bioluminescent signal corresponding to import *(9)*. *Diagram created using BioRender.*
(B) Experimental outline of the permeabilised NanoLuc assay. On day 1, cells are plated, and are subsequently transfected with DNA coding for eqFP670-P2A-Cox8a-LgBit on day 2. On day 4, the day of the assay, media is replaced with assay buffer containing furimazine, rPFO, and GST-dark and incubated for 5 minutes prior to carrying out a 2-minute baseline read, followed by injection of Su9-EGFP-HiBit and a 30-minute kinetic import read for luminescence corresponding to protein import.

To reduce background signal, I adopted an early approach used in our lab by adding GST-dark peptide to the reaction [364]. GST-dark peptide is a fusion of GST and an inactivated form of the HiBit, containing a point mutation at a critical catalytic arginine residue (DarkBiT). This mutation prevents catalysis by the NanoBiT complex when LgBit binds to DarkBiT [364, 366]. Purified GST-Dark was added to a final concentration of 20 μM (20-fold higher than HiBit; Figure 3.10B, quantified in C), which reduces but does not obliviate, background luminescence by binding to any residual LgBit in the cytosol or as a result of cell death. This prevents LgBit from binding to HiBit, ensuring that the luminescent signal is solely produced by the formation of mitochondrial NanoLuc [364]. Figure 3.10 (panel B, black trace, quantified in C) shows that there is a large amount (~60%) of signal coming from cytoplasmic binding of LgBit and HiBit. When this is eliminated by the addition of GST-Dark (red trace), the resulting trace displays the sigmoidal shape expected for a typical import curve (Figure 3.10C).

At the same time as rPFO and GST-Dark addition to cells, furimazine was added at a dilution of 1:800, as determined by a titration experiment to determine the optimal concentration (Figure 3.10D, quantified in E). At higher concentrations (over 1:200), furimazine has an inhibitory effect on mitochondrial import, probably through inhibition of mitochondrial respiration (Figure 3.10D and E). This is in line with what was shown previously in our lab using the yeast system [364].

Mitochondria were energised by the addition of 5 mM succinate, and 1 μM rotenone was added to inhibit respiratory complex I, ensuring all energy is produced via complex II. This is standard for *in vitro* mitochondrial assays, as blocking complex I allows maximal respiration via complex II. This is because if complex I is active, oxaloacetate can build up which strongly inhibits complex II. In addition, an ATP regeneration system (composed of ATP, creatine kinase and creatine phosphatase) was added to ensure that ATP levels remain constant for the duration of the assay. Prionex, a biocompatible polymer used for protein stabilisation, is also added. All these components were incorporated in a master mix in a mannitol-based buffer, chosen to maintain mitochondrial function.

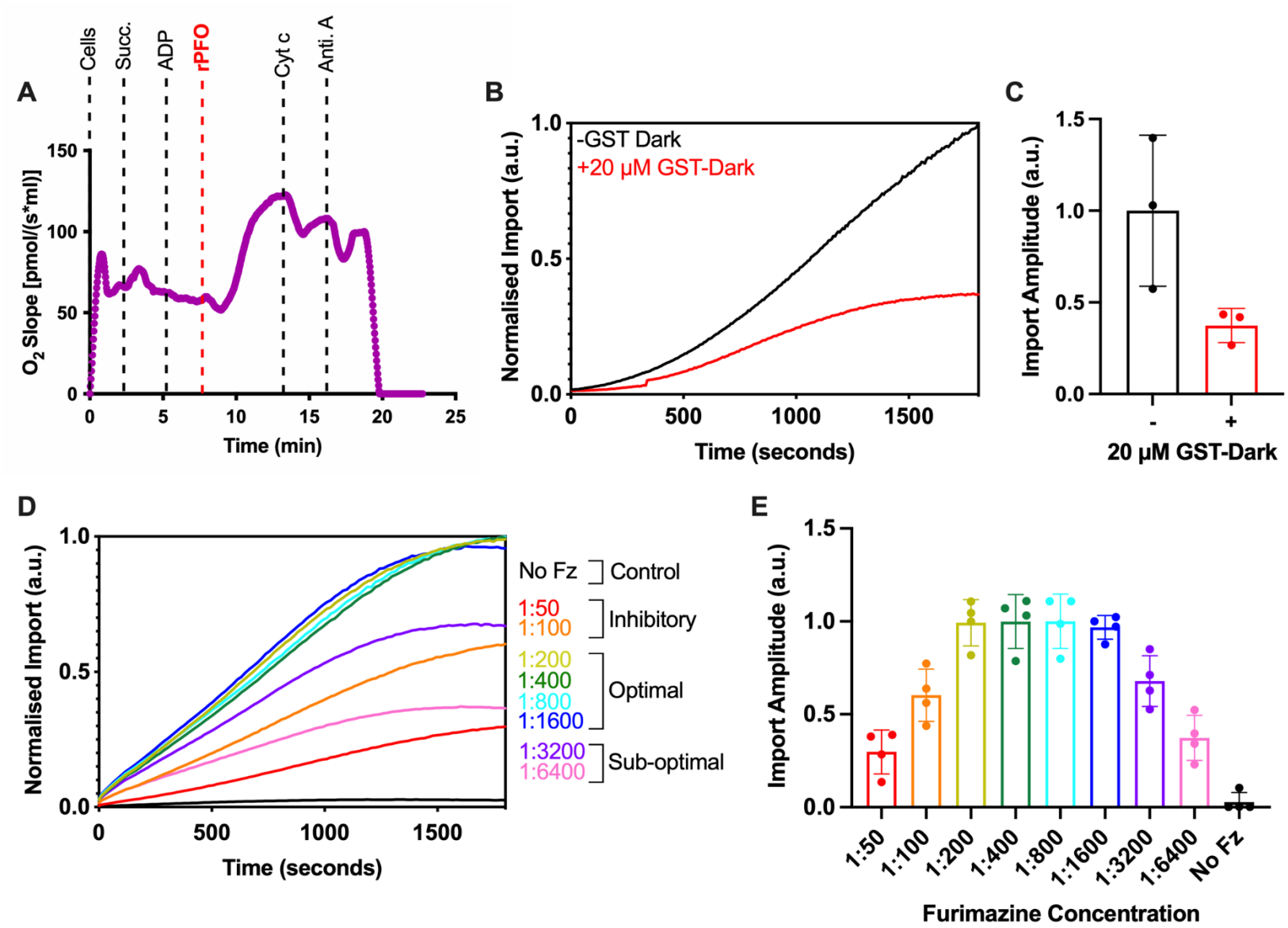
A
Cells
Succ.
ADP
rPFO
Cyt c
Anti. A
O_2 Slope [pmol/(s*ml)]
Time (min)
B
-GST Dark
+20 µM GST-Dark
Normalised Import (a.u.)
Time (seconds)
C
Import Amplitude (a.u.)
20 µM GST-Dark
D
Normalised Import (a.u.)
Time (seconds)
No Fz
Control
1:50
1:100
Inhibitory
1:200
1:400
1:800
1:1600
Optimal
1:3200
1:6400
Sub-optimal
E
Import Amplitude (a.u.)
Furimazine Concentration

Figure 3.10: Permeabilised Cell NanoLuc Assay Optimisation: rPFO, GST-Dark, and Fz
(A) Oroboros oxygraph trace showing mitochondrial respiration in response to various stimuli/poisons in HeLa cells. Cells are stimulated by addition of 5 mM succinate (Succ) and 1 mM ADP prior to addition of 3 nM rPFO, which allows the substrates to access mitochondria. Cytochrome *c* (Cyt c; 10 µM) and antimycin A (Anti. A; 1 µM) are subsequently added, and the impact of these respiratory chain substrates on the oxygen consumption of the cells is measured. *Representative trace shown. N=3 biological replicates*.
(B) Average traces from the NanoLuc import assay in the absence (black) or presence (red) of 20 µM GST-Dark, added to cells 5 minutes prior to the assay. Normalisation was as described in (A). *N=3 biological replicates, each with n=3 technical replicates.*
(C) Maximum amplitude plotted from average import traces displayed in (B). *Error bars display SD.*
(D) Various concentrations of furimazine (Fz; concentrations indicated as ratios of furimazine: assay buffer) were added to the import assay to determine the most suitable concentration. Fz was applied to cells for 5 minutes prior to starting the assay, the NanoLuc assay was then carried out with a chasing precursor (Su9-EGFP-HiBit). Resulting average traces are shown. Background was removed and data was normalised to cellular eqFP670 expression, and the maximum amplitude from the run, to allow comparison between runs regardless of raw values. *N=4 biological replicates, each with n=3 technical replicates.*
(E) Maximum amplitude plotted from average import traces displayed in (D). *Error bars display SD.*

3.5.2. The Permeabilised Cell NanoLuc Assay Depends on ATP and PMF

As an import substrate, the precursor protein Su9-EGFP-6xHis-HiBit was cloned and purified in urea *i.e.,* unfolded. This protein contains the Su9 MTS for targeting to the mitochondrial matrix, as well as an EGFP reporter domain for fluorescence-based experiments. The 6xHis motif is important for purification of the protein by immobilised metal affinity chromatography using a nickel column. Finally, at the C-terminus, there is the small, 11 amino acid HiBit component of the NanoLuc enzyme. This substrate protein was injected into wells at a final concentration of 1 µM. The MTS triggers the localisation of this substrate protein to the mitochondrial matrix, as shown by the luminescent signals obtained under basal, energised conditions (Figure 3.11 A, black trace; maximum import amplitude quantified in B).

To characterise the specificity of the assay system for import via the presequence pathway, cells were treated with 1 µM antimycin A (CIII inhibitor; A) and 5 µM Oligomycin (ATP synthase inhibitor, O). Together, these drugs inhibit the respiratory chain and ATP synthesis/hydrolysis, and thus, protein translocation *via* the presequence pathway will be perturbed, since it requires both a PMF and ATP to function (see Figure 1.4). The impact of these inhibitors on respiratory function, analysed by a seahorse respirometer, is shown in Figure 3.11C for reference. Figure 3.11 (panel A, red trace; quantified in B) shows that import of the precursor protein is decreased by ~70% in the presence of AO. Also, in the presence of AO, the shape of the curve is no longer sigmoidal, and therefore probably reflects non-specific binding of the precursor to LgBit outside of the mitochondria.

Furthermore, addition of CCCP (titration shown in Figure 3.11D, quantified in E), which collapses the Δψ (Figure 1.4 and Figure 3.11C), reduces import in a concentration dependent manner. Taken together, these data confirm that the luminescent signal is indeed representative of the requirements of the presequence import pathway: ATP hydrolysis and the PMF [137, 410-412]. As an additional control, in the absence of the HiBit containing import substrate (Figure 3.11A, orange trace; quantified in B), there was no signal whatsoever. Together, this data confirms that the luminescent signal is due to the formation of NanoLuc in the mitochondrial matrix.

I further investigated the specificity of the assay system as well as highlighting an application for the system, by treating cells with several drugs known to target various components of the import machinery (Figure 3.11F, quantified in G). Cells were incubated for five minutes prior to beginning NanoLuc assays (acute treatment) with the following small molecules:

- SW02 (also known as 115-7c), enhances (agonist) the activity of mtHSP70 [413] (used at 20 μM).
- VER-155008, inhibits (competitive) mtHSP70 by targeting of its ATPase binding domain [414] (used at 20 μM).
- MKT077, inhibits (allosteric) mtHSP70 by binding to its nucleotide binding domain [415] (used at 20 μM).
- MB10, inhibits import of precursor proteins via the presequence pathway by targeting TIM44 (subunit of PAM and $TIM23^{MOTOR}$ complexes) [383] (used at 30 μM).
- MB6, selectively inhibits mitochondrial protein import via the MIA pathway by inhibition of ALR oxidase activity [416] (used at 10 μM).

All drug treatments induced a reduction in mitochondrial import efficiency (Figure 3.11F and G), unsurprisingly, in the cases of VER, MKT077, and MB10. However, what was unanticipated was that SW02, which enhances the ATPase activity of Hsp70 [413], also led to a reduction in import efficiency, albeit only a subtle reduction. This is likely because SW02 treatment uncouples ATPase from transport. The dramatic effects of MB6 on import efficiency were also surprising, considering that the imported substrate, Su9-EGFP-HiBit, does not require the MIA pathway for import, being a mitochondrial matrix protein. This is an interesting finding that requires further experimentation in future. Whilst all the drugs have an impact on the amplitude, there are also variations in the shape of the curve. Interestingly, SW02 seems to accelerate the initial phase whilst the others seem to slow it down. This should be investigated further by kinetic analysis using the NanoLuc assay system.

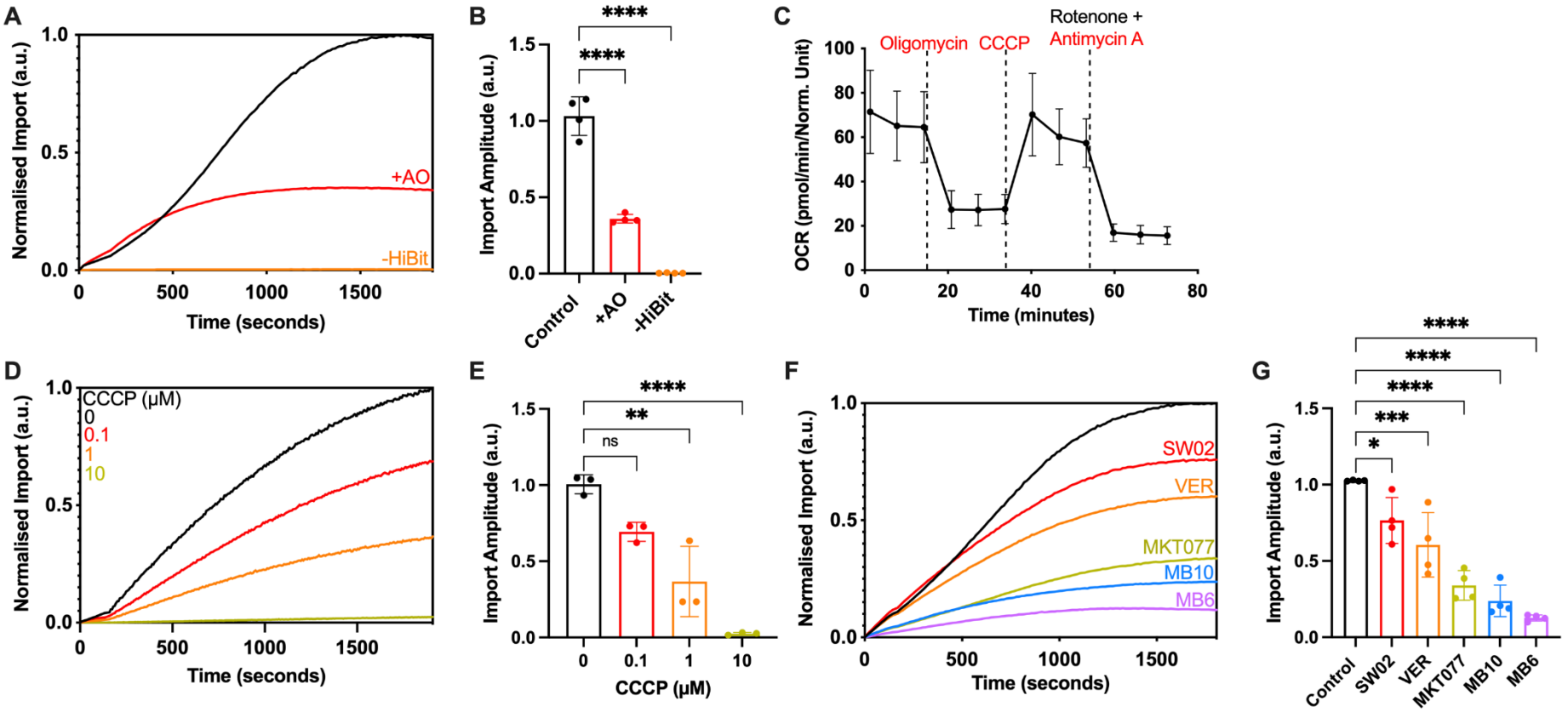
A
Normalised Import (a.u.)
1.0
0.5
0.0
0
500
1000
1500
Time (seconds)
+AO
-HiBit
B
Import Amplitude (a.u.)
****
****
1.5
1.0
0.5
0.0
Control
+AO
-HiBit
C
OCR (pmol/min/Norm. Unit)
Oligomycin
CCCP
Rotenone +
Antimycin A
100
80
60
40
20
0
0
20
40
60
80
Time (minutes)
D
Normalised Import (a.u.)
CCCP (μM)
0
0.1
1
10
1.0
0.5
0.0
0
500
1000
1500
Time (seconds)
E
Import Amplitude (a.u.)
****
**
ns
1.5
1.0
0.5
0.0
0
0.1
1
10
CCCP (μM)
F
Normalised Import (a.u.)
SW02
VER
MKT077
MB10
MB6
1.0
0.5
0.0
0
500
1000
1500
Time (seconds)
G
Import Amplitude (a.u.)
****
****
****
***
*
1.5
1.0
0.5
0.0
Control
SW02
VER
MKT077
MB10
MB6

Figure 3.11: Permeabilised NanoLuc Assay Monitors Import *via* the Presequence Pathway
(A) NanoLuc import trace in the absence (black) or presence (red) of PMF inhibitor AO (1 µM antimycin A, 5 µM oligomycin), or in the absence of HiBit containing precursor (orange). AO was applied to appropriate wells for 5 minutes prior to starting the assay, the NanoLuc assay was then carried out to monitor the import of precursor (Su9-EGFP-HiBit). Resulting normalised average traces are shown. *N=4 biological replicates, each with n=3 technical replicates.*
(B) Maximum amplitude plotted from average traces shown in (A). *Error bars display SD. One-way ANOVA and Tukey's post hoc test were used.*
(C) Mitochondrial stress test showing oxygen consumption rate (OCR) of cells when subjected to various respiratory chain substrates. HeLaGAL cells were grown for 48 hours prior to carrying out mitochondrial stress tests on a Seahorse XFe96. 1.5 µM oligomycin, 0.5 µM CCCP, 0.5 µM antimycin A, and 0.5 µM rotenone were added and their impact on mitochondrial oxygen consumption was measured. Data was normalised to cell density according to an SRB assay. *N=6 biological replicates, each with n=3 technical replicates.*
(D) NanoLuc import traces in the presence of 0-10 µM CCCP. CCCP was applied to cells for 5 minutes prior to starting the assay, the NanoLuc assay was then carried out, measuring the import of a precursor protein (Su9-EGFP-HiBit). Resulting normalised average traces are shown. *N=3 biological replicates, each with n=3 technical replicates.*
(E) Maximum amplitude plotted from average traces shown in (D). *Error bars display SD. One-way ANOVA and Tukey's post hoc test were used to determine significance.*
(F) NanoLuc import traces in the presence of small molecule inhibitors of the import machinery. No drug (black), SW02 (20 µM, red), VER (20 µM, orange), MKT077 (20 µM, green), MB10 (30 µM, blue), or MB6 (10 µM, purple) were applied to cells for 5 minutes prior to starting the assay, the NanoLuc assay was then used to monitor import of a purified precursor (Su9-EGFP-HiBit). Resulting normalised average traces are shown. *N=4 biological replicates, each with n=3 technical replicates.*
(G) Maximum amplitude plotted from average traces shown in (F). *Error bars display SD. One-way ANOVA and Tukey's post hoc test were used to determine significance.*

3.6. Discussion

The main aim of this chapter was to develop, optimise, and characterise the NanoLuc system into a means to monitor mitochondrial protein import of precursor proteins in a live, mammalian whole cell system. The key findings from this chapter are:

- The intact assay system is a good first assay system for identifying changes in import in response to a variable (*i.e.,* a cell line, mutation, or drug) and could be useful in high throughput screening such as drug screens.

- The CUTE system would be a useful addition to the intact system, allowing real-time visualisation of the import event, and analysis of kinetics, however this system is not fully functional at this point and requires further optimisation.

- The permeabilised NanoLuc system is an effective means of monitoring mitochondrial import in real-time in live, mammalian cells and could be further exploited to obtain kinetic details about import.

- The permeabilised NanoLuc assay system is dependent on ATP and the PMF, and is sensitive to various import inhibitors, indicating that it is specifically measuring import *via* the presequence pathway.

3.6.1. The Intact Cell NanoLuc System

In this chapter, I used the NanoLuc split luciferase assay system, which has previously been developed into a means to monitor mitochondrial protein import in mitochondria isolated from yeast cells [364]. I adapted and developed it as a means to monitor mitochondrial protein import in intact mammalian cells. This has several advantages over traditional import assays, which have only been possible in isolated mitochondria and rely on Western blotting or radioactivity for readouts. The intact NanoLuc system (Figure 3.2) is carried out in whole, intact cells, thus is a direct representation of what is going on in these cells. Furthermore, the data acquisition time is much quicker, that is, following the cell set up, acquiring the readouts on the plate reader takes seconds, as opposed to days spent Western blotting. This is also advantageous over other split reporter based assays such as the split-GFP assay, which has some of the same advantages as the NanoLuc assay, but has a significant time lag associated with the maturation of the GFP fluorophore [417]. The sensitivity of the NanoLuc assay is also extremely high, allowing for the identification of subtle changes in import between samples.

Finally, it would be feasible to use this assay in a high throughput manner, for example to allow for screening of drug libraries very quickly and easily.

However, there are several limitations to this assay system. Firstly, in its current state, there is no way to remove background signal from the readouts, which may meaningfully impact on the specificity and sensitivity of the intact assay. This needs to be tested by investigating the impact of inhibition of import, such as by addition of AO or inhibition of the TOM or TIM complexes by small molecule inhibitors. This would both determine the dynamic range of the system and identify any background signal. To overcome background issues, one option would be to express the GST-dark peptide, used in the permeabilised assay system (Figure 3.10C and D) and previously [364, 366], prior to expression of the HiBit protein. This would bind to any cytosolic or extracellular LgBit, preventing non-mitochondrial NanoLuc complementation.

Another option would be to use a degron motif, such as a PEST domain, on the MTS-LgBit. A PEST domain is a polypeptide sequence rich in proline (**P**), glutamic acid (**E**), serine (**S**), and threonine (**T**), which is considered a signature of short-lived proteins, destined for degradation via the ubiquitin-mediated proteolytic pathway [418]. More specifically, a PEST region can be defined as a hydrophilic stretch of 12 or more amino acids, uninterrupted by positively charged residues, which contain at least one proline, one glutamic acid or aspartic acid, and one serine or threonine residue, and is usually flanked by histidine, lysine, or arginine residues. PEST sequences can vary considerably in length, secondary structure, and precise sequence, and some proteins are known to contain multiple different PEST sequences within their polypeptide chain [418]. Promega, the developers of NanoLuc, show how a PEST domain (with the sequence **SHGFPPEVEEQAAGTLPMSCAQESGMDRHPAACASARINV**) can be used to destabilise reporters very quickly and lead to a significantly higher signal-to-noise ratio compared to non-destabilised reporters [419]. This Promega PEST domain was cloned onto the LgBit DNA, however, due to time constraints following lab shutdowns during the Covid-19 lockdown periods, this part of the project was not taken any further. However, it would be a useful experiment to carry out in future. A possible limitation of this approach is that the long stretch of amino acids from the PEST domain may interfere with NanoLuc complementation. If this were the case, a linker domain could be useful in preventing occlusion and thus allowing binding of HiBit.

Recently, another luminescence-based reporter system was developed and used to monitor the regulation of import by PINK1-Parkin and to investigate how import efficiency varies between control and disease patient cells [85]. This system is a bioluminescence resonance energy transfer (BRET) based system which utilises the fusion between *Renilla reniformis*

GFP and luciferase proteins (RGFP and RLuc) to produce a bioluminescent signal which is induced by cleavage of the MTS in the mitochondrial matrix following the addition of RLuc substrate coelenterazine (CLZ) [85, 420]. The authors use a PEST sequence [85], which seems to function successfully in eliminating background signal from unimported protein. However, though import traces are displayed whereby the production of the bioluminescent signal is monitored in real time, the system is essentially monitoring the formation of the signal due to the addition of the substrate, CLZ [85]. This is very similar to our intact NanoLuc assay system, whereby the actual import event is not being monitored in real-time. The reliance on MTS cleavage is another limitation of this study since it is possible for the precursor to have the MTS cleaved in transit or if it were trapped in the import machinery (so long as the MTS has entered the matrix). From this point of view, the readout from the intact NanoLuc assay system is a more reliable indication of import since it only reports on fully imported proteins.

Overall, the intact cell system has great potential as a way of quantifying changes in import without off-target effects on cells associated with permeabilisation and compromised cell membranes. In some cell types, for example neurons, this would be a significant problem since interfering with dynamic changes in membrane potential will impact on their signal transduction, function, and viability. Thus, an optimised intact system would be ideally suited for investigating mitochondrial import in neuronal cells. However, the intact assay system does not, in its current state, allow real-time visualisation of import and consequently we cannot investigate the import process by this means, limiting the data we can really obtain about the different stages of the import event. To do this, the system needs to be adapted to provide the ability to monitor the import event as it happens, which is why the next step was to attempt to tie-in the CUTE technology with the intact cell NanoLuc assay system.

3.6.2. The CUTE System

To overcome the inability of the intact system to visualise the import event in real-time and obtain kinetic information, I decided to apply CUTE technology. CUTE has been used previously to allow organelle-level specific targeting of proteins in a controlled manner [380]. It was originally developed as a mechanism to control trafficking through the endocytic and coat protein complex I (COPI; ER to Golgi trafficking) systems, and the authors also showed how it could be used to control peroxisomal and nuclear protein import [380]. It has since been developed as a reversible association with motor proteins (RAMP) system whereby the reversible masking of targeting sequences by streptavidin-SBP binding allows regulation of the positioning of entire organelles within cells [421]. This works by binding of an organellar SBP containing protein to motor protein associated streptavidin. Biotin releases this, allowing monitoring of organelle movement within cells [421]. This system has exciting potential for

application to various biological questions, including monitoring mitochondrial transport in neurons, or trafficking of aggregation prone proteins, such as Tau, in disease models.

The CUTE system is based on the same principles previously described for the RUSH system. The RUSH system relies on a hook protein which is stably anchored in the donor compartment and is bound to streptavidin, and a reporter protein with an SBP domain [398]. It has been used to analyse transport characteristics of various Golgi and plasma membrane proteins by live imaging [398]. It has also been used to investigate the trafficking, assembly, and regulation thereof of kainate receptors in primary neurons [422]. However, the fact that the CUTE system does not rely on the use of hooks which must be anchored stably somewhere within the cell is a major advantage over the RUSH system, and this one of the reasons for selection of the CUTE system for this project.

Unfortunately, while a few studies have shown both the CUTE and the RUSH systems to be useful tools for monitoring protein trafficking *via* various transport pathways [380, 398, 423], this has only been done using live fluorescence-based imaging. Combining this system with NanoLuc technology posed a variety of challenges, some of which were not fully overcome within the scope of this PhD project. After overcoming issues associated with poor or incomplete masking of the mitochondrial signal sequence (Figure 3.8), the major outstanding problems was excessive toxicity and cell death associated with expressing a large quantity of DNA within the cells.

To circumvent problems associated with excessive toxicity in intact NanoLuc-CUTE assays, one option would be to utilise a cell line which naturally expresses high levels of SLC5A6, such as U2OS cells (standardised value = 1.06579 from BioGPS Cell Line Gene Expression Profiles dataset; [424-426]). Another option would be to express some DNA as lentivirus, increasing the cells capacity to express the various DNAs, or to create a stable cell line.

A cell line stably expressing eqFP670-P2A-LgBit was attempted throughout the course of this project, but due to unknown factors, lentiviral expression of this DNA in HeLaGAL cells (but not in HEK293T cells) was not successful. Furthermore, one possible way forward would be to re-clone the constructs into a single composite vector, for example inserting the SLC5A6 before the IRES residue on the CUTE construct (as Streptavidin is expressed separately already). Following this, the NanoLuc-CUTE assay may be functional in intact cells, which would have the added benefit of not needing to permeabilise cells.

Alternatively, there are other approaches that could, in theory, be used in the place of the CUTE system, with the same outcome of providing inducibility to the intact NanoLuc assay

system. A recent study showed how transport can be controlled using a photo-responsive light-oxygen-voltage (LOV) domain, which sequesters a protein in a particular location within the cell [427]. Blue light illumination can be used to reversibly release the sequestered protein, in a similar way to the addition of biotin in the CUTE or RUSH systems. The authors showed how this system allows for time-resolved monitoring of nuclear-cytoplasmic shuttling of transcription factors [427], and it is likely this mechanism could be adapted to investigate mitochondrial protein translocation. However, the authors tethered their light-responsive LOV domain to TOM20 on the OMM [427], and so if this system was to be applied to investigate mitochondrial protein import, an alternative tethering site would be chosen so as not to have any impact on the import pathways, such as the KDEL receptors of the Golgi apparatus [428].

Due to the time constraints of this PhD project, the CUTE system was not developed into a fully functional state, and other potential systems, such as the optogenetic-release system [427], were unfortunately not yet published at the time I carried out the cloning at the beginning of the project. Therefore, the permeabilised cell NanoLuc assay system was used as a contingency to allow for kinetic monitoring of mitochondrial import in a whole cell system.

3.6.3. The Permeabilised Cell NanoLuc Assay System

Finally, to visualise the import event in real-time with the capacity to obtain kinetic data as opposed to the endpoint read provided by the intact system (Figure 3.4), I developed a permeabilised cell NanoLuc assay system for monitoring mitochondrial import in live mammalian (HeLa) cells (Figure 3.9). Characterisation of this system allowed confirmation that this system monitors import *via* the presequence pathway, as it is highly dependent on ATP and the PMF (Figure 3.11 A-B and D-E, respectively) and is sensitive to a number of small molecule import inhibitors (Figure 3.11 F-G).

This system is based on the same concepts as described for the intact system, and as previously described in yeast mitochondria [108, 364]. It was modified to allow entry of a recombinant HiBit-tagged precursor, as well as drugs unable to permeate the plasma membrane, by rPFO permeabilisation. Whilst this is a perceivable limitation of the system, characterisation of the impact of rPFO showed that there was no negative impact on their respiratory capacity, and specifically addition of cytochrome *c* showed that mitochondria remain intact, indicative of fully functional import pathways (Figure 3.10A). In addition, a benefit to this system is that mitochondrial isolation does not need to be performed, which damages the organelle despite how careful the operator is. Although it lacks cytosolic factors which are likely lost or diluted upon permeabilisation, it is still a more complete system than isolated mitochondria. Additionally, most import studies are carried out in yeast as it is

relatively easy to obtain sufficient material compared to in mammalian cells. This system reduces the amount of sample required, as well as the sample handling and loss/damage during mitochondrial isolation. This should allow more studies to directly investigate import processes in mammalian cells going forwards.

The data presented here demonstrates that this system has several benefits over classical import assays. As with the intact system, the data acquisition time is reduced significantly from a matter of days to ~30 minutes, which our assays show is the maximum time required to visualise the entire import assay, as we can gather from the plateau of the import curves (Figure 3.11). Furthermore, it allows rapid time resolution with a complete a full cycle of reads in ~4 seconds (though this is of course dependent on the number of reads being taken and would be faster still if no injection were required). Although not as simply as the intact system, due to the necessity of injecting a purified protein into the wells and the time this would take, this system does have the capacity to be used in a high throughput manner. However, this would have some impact on the level of kinetic data one could obtain, that is, the kinetic resolution of the lag phase would be compromised by the time taken to inject the protein into several wells. This could be overcome somewhat by manual injection of proteins with a multichannel pipette or even an automated pipettor.

The permeabilised cell NanoLuc assay system can provide insight into the kinetics of import. Not only can it report information on the amount of import that has taken place (amplitude, as is also possible with the intact system), but the data can be used to determine the rate, number of steps, and rate of each step of import. This has been discussed in detail in a recent study from our lab using isolated yeast mitochondria [108]. It would be very interesting to carry out a similar study on the kinetics of import in live mammalian cells, especially neurons where, among other functions, mitochondria play key roles in the maintenance of synaptic transmission and plasticity. Finally, the sensitivity of this assay system is much higher than what has been previously possible, and this allows us to detect very small changes in any of the stages of import.

This system has several potential applications in terms of monitoring mitochondrial protein import in mammalian cells. Firstly, it could be used as a secondary screening system for drugs, identified as impacting import using the intact system, to further characterise their effect on import, and yield kinetic information relating to the various stages of import. This is demonstrated in my data, where I took a number of small molecules that have been shown previously to inhibit import via various mechanisms and characterised their impact on the import of our precursor protein (Su9-EGFP-HiBit) *via* the presequence pathway (Figure 3.11F and G). Likewise, it could be used as a screening system to investigate the impact of the

aggregation prone proteins or disease-related mutations characteristic of neurodegenerative diseases (Table 1.2) on import. This will be discussed further in future chapters.

Looking beyond the presequence pathway, this system could be altered to investigate the import of proteins *via* the various other mitochondrial protein translocation pathways (see Figure 1.5). To this end, a current PhD student in the lab is utilising this system to investigate the import of PINK1, with the ultimate goal of investigating how this is dysregulated or altered in PD. Aside from monitoring mitochondrial protein import, the NanoLuc assay system has various other applications, for example binding assays, which have been exploited in the past in our lab and others, for various applications both *in vitro* and *in vivo* [429-432].

Another interesting example of how NanoLuc technology can be applied to answer important, current, biological questions in mammalian cells became clear to us during the Covid-19 pandemic. We decided to exploit the NanoLuc system to enable us to characterise the binding of the coronavirus to mammalian cells. To do this, I utilised the mammalian LgBit containing construct used here, and tagged LgBit with hACE2, the receptor protein that the Spike protein of the coronavirus binds to [433]. The hACE2 signal sequence was placed at the N-terminus of LgBit, with a flexible linker between to allow NanoLuc complementation, and the rest was at the C-terminus. This allows its targeting to the plasma membrane without perturbing the binding of HiBit to LgBit. The HiBit peptide was cloned onto the Spike protein in various locations and purified in suspension mammalian cells to produce the recombinant proteins. The principle of this is that the binding between HiBit and LgBit would provide information on the conformational changes of the Spike protein since it would only bind in a particular conformation. This project is ongoing but has the potential to yield interesting results with regards to the kinetics of Spike-hACE2 binding and could also be used as a drug screen for small molecules that may inhibit binding and thus infection.

3.6.4. Summary

The data so far highlights that the permeabilised NanoLuc assay system is a useful means of monitoring protein import into mitochondria in live mammalian cells. The system has several useful applications, and I will use this system in the following chapters to answer the questions integral to my PhD project. Broadly, how are mitochondrial protein import pathways dysregulated in the progression of neurodegenerative diseases?

Chapter 4. Exploring the Impact of Failed Import *via* Precursor Stalling

4.1. Introduction

In recent years, numerous studies have described examples of how disease-related, aggregation prone proteins interact with the translocation machinery of mitochondrial import pathways, leading to defective mitochondrial and cellular functions and phenotypic changes associated with neurodegeneration [215, 216, 219-221, 223-225, 229]. Some studies even go as far as to show how targeting import can reverse or reduce these detrimental effects [85, 222, 230]. These studies highlight the potential for import defects and specific translocation machinery to be targeted therapeutically in the treatment of neurodegenerative diseases, and shine light on the importance of dissecting the critical link between mitochondrial import and neurodegeneration.

Notwithstanding these studies describing translocase-aggregated protein interactions and their association with neurodegenerative disease, systematic mechanistic studies of the impact of aggregation on the translocation machinery have not yet been published. Since these aggregation prone proteins affect multiple cellular pathways [434-436], this is important when determining which disease phenotypes are attributable to disruption of mitochondrial import. Defining which pathological steps are mediated by mitochondrial import dysfunction would be key towards obtaining a better understanding of disease progression as well as in the design of potential therapeutic interventions.

To investigate the impact of aggregation prone proteins on cell health and function, I used the DHFR-MTX trapping system to model an aggregated or stalled precursor, as is commonly seen in neurodegenerative diseases. Precursor trapping using the DHFR-MTX trapping system has been used in the past to investigate the properties and kinetics of mitochondrial protein import [437-440]. A recent study in our lab showed how this system can be exploited to obtain information on the turnover of protein import *via* the presequence pathway [108]

This system traps a precursor in transition through the mitochondrial presequence pathway [439]. Briefly, an MTS (Su9) containing protein with a reporter region (EGFP or mScarlet) followed by DHFR, was expressed in cells in the presence or absence of MTX (Figure 4.1). In the absence of MTX, the protein is imported *via* the presequence pathway to the matrix where the signal sequence can be cleaved by MPP, forming the mature protein. In the presence of 100 nM MTX, MTX binds to the DHFR motif, sequestering it in its folded state and causing it to become stalled in the TOM40 and TIM23 pores, due to the long Su9-Reporter region ahead of DHFR. This stalled precursor blocks import sites, presumably preventing other precursor proteins from being imported *via* the blocked sites (Figure 4.1).

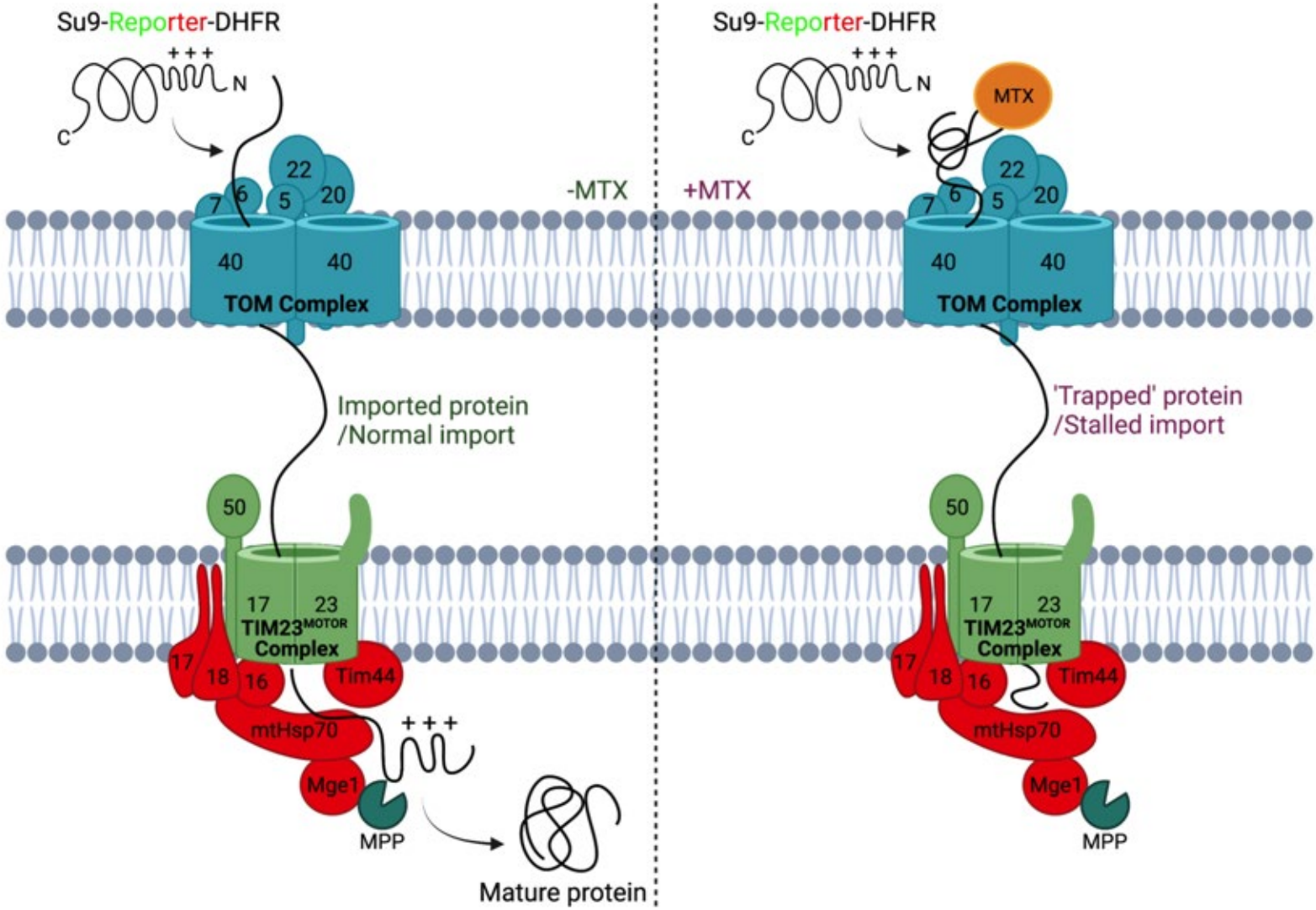
Su9-Reporter-DHFR
+++
N
C
-MTX
+MTX
MTX
22
7
6
5
20
40
40
TOM Complex
Imported protein
/Normal import
'Trapped' protein
/Stalled import
50
17
23
TIM23MOTOR
Complex
17
18
16
Tim44
mtHsp70
Mge1
MPP
Mature protein

Figure 4.1: Modelling Failed Precursor Import using the DHFR-MTX Affinity System
In the absence of MTX (*left*), the precursor protein (Su9-Reporter-DHFR) is imported into mitochondria *via* the presequence pathway. In the mitochondrial matrix, the MTS is cleaved by MPP, and it folds to form the mature protein. In the presence of MTX (*right*), MTX binds to DHFR in the cytosol, preventing it from unfolding, and thus preventing it from crossing the TOM40 channel. Since the protein contains a long Su9-Reporter region before the DHFR, this region will form a plug through the TOM40 and TIM23 channels, mimicking a stalled or aggregated precursor protein within the presequence pathway. *Schematic created using BioRender.*

4.2. Aims

The overarching aim of the work described in this chapter was to investigate the impact of failed import of a precursor protein within the presequence pathway, mimicking what has been seen in neurodegenerative diseases (see Table 1.2 for a full breakdown of mitochondrial import defects associated with neurodegeneration) [215, 222, 224]. I used the DHFR-MTX system to stall the DHFR containing precursor protein within the TOM40 and TIM23 channels of the presequence pathway, which allowed exploration of the impact of failed precursor import on HeLa cells.

The main aims of this chapter were:

1. To characterise the DHFR-MTX trapping system as a model of failed precursor import in HeLa cells.
2. To explore the impact of failed import by precursor trapping on HeLaGAL cells in terms of:
    - Mitochondrial import function,
    - Mitochondrial morphology and dynamics,
    - Respiratory function,
    - Associated proteins/pathways.

4.3. Results

4.3.1. DHFR-MTX Trapping Captures the Precursor Protein in Transit

To test if the DHFR-MTX trapping system efficiently stalls import of a DHFR containing precursor protein, I expressed the precursor Su9-EGFP-DHFR-HiBit in cells for 48 hours in the presence or absence of 100 nM MTX. As a control for off target effects associated with MTX treatment, I expressed the same protein, only lacking the MTS: EGFP-DHFR-HiBit. The HiBit peptide is irrelevant in this context, however due to its small size it does not interfere with expression or trapping, and thus this construct was created to be compatible with the NanoLuc assay system. After 48 hours, mitochondria were stained using TMRM and the localisation of the protein reporter under the various conditions was determined using live-cell confocal microscopy (Figure 4.2A).

The presequence-lacking protein EGFP-DHFR (labelled as -MTS) is localised to the cytoplasm in the absence and presence of MTX. As expected, in the absence of MTX, the precursor protein (Su9-EGFP-DHFR; +MTS) is imported into mitochondria. In the presence of 100 nM MTX, however, the protein is mainly cytosolic, with some indication of mitochondrial expression (Figure 4.2A). This mitochondrial localised fraction could correspond to the trapped protein stuck to the import sites of mitochondria, however the resolution obtained from confocal microscopy was insufficient to distinguish between mitochondrial sub-compartments. Therefore, it is unclear from these images whether this does indeed correspond to the trapped protein aggregates, or to protein that has bypassed the trapping mechanism and been imported.

To further test whether the trapping was successful, I separated the cytosolic and mitochondrial fractions from HeLaGAL cells expressing precursor protein Su9-EGFP-DHFR-HiBit in the presence or absence of 100 nM MTX and carried out Western blotting analysis of these fractions (Figure 4.2B). A large proportion of the protein is localised to mitochondria in the absence of MTX, whilst in the presence of MTX, only a small proportion of this protein is mitochondrial (Figure 4.2B). The fact that a portion of this protein is still present in the mitochondrial fraction suggests it is not cleared from the import sites of these mitochondria. However, there are relatively low levels of this protein expressed in the cytosolic fraction of these cells, suggesting that some of this protein may have been degraded by a cellular stress response mechanism *i.e.,* proteasomal degradation.

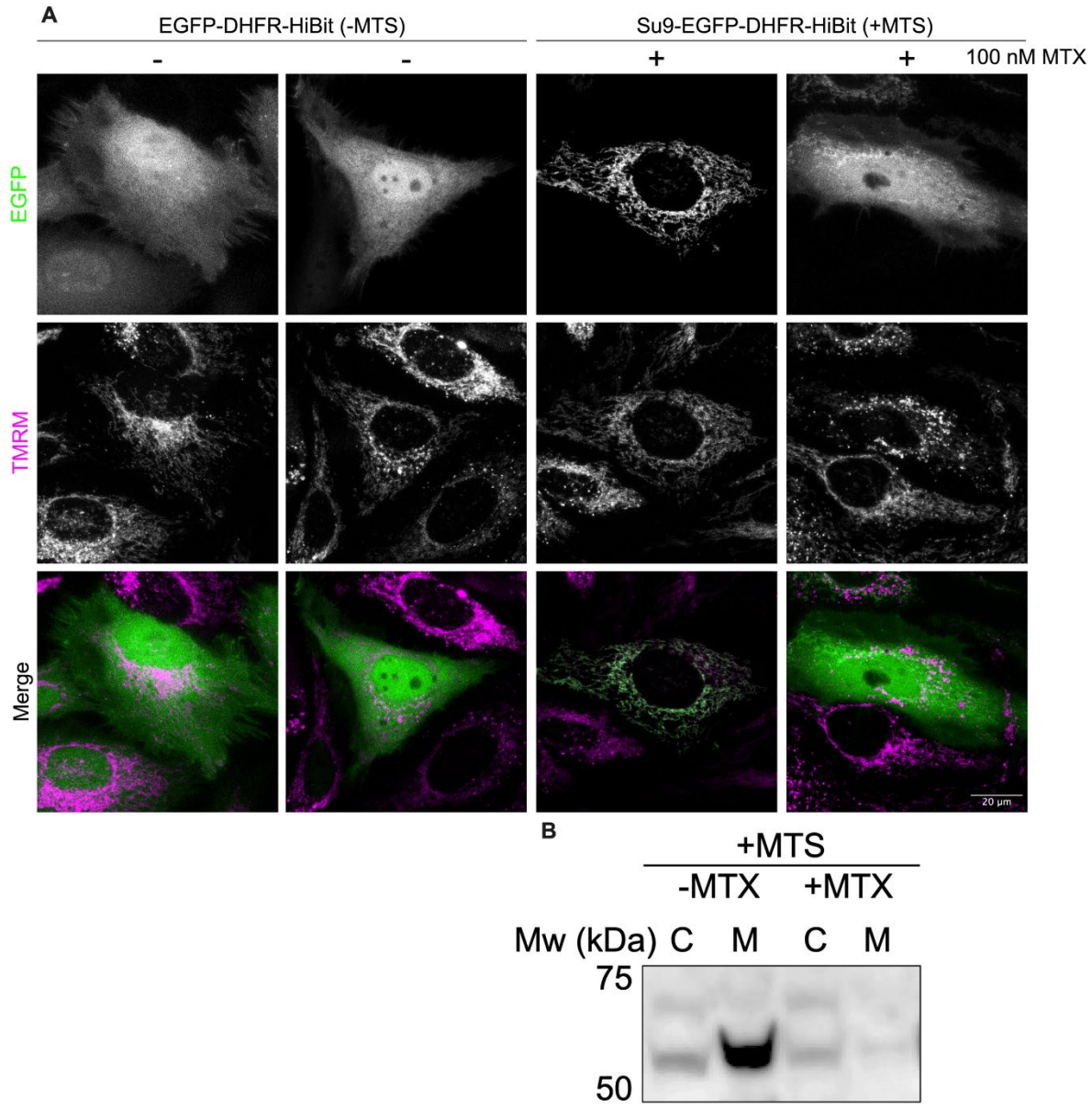

Figure 4.2: DHFR-MTX Trapping System Prevents DHFR-Precursor Import
(A) Confocal microscopy of HeLaGAL cells treated with 100 nM MTX (or with vehicle; DMSO only) overnight prior to expression of EGFP-DHFR-HiBit (-MTS; green) or Su9-EGFP-DHFR-HiBit (+MTS; green) for 48 hours. Mitochondria were stained with 25 nM TMRM (magenta). *N=3*.
(B) Western blot showing expression of Su9-EGFP-DHFR-HiBit (+MTS) in the cytosolic and mitochondrial fractions of HeLaGAL cells in the presence or absence of 100 nM MTX. The levels of Su9-EGFP-DHFR-HiBit in each fraction was visualised by probing with an anti-GFP antibody. *N=3*.

To confirm that the trapped precursor observed in the mitochondrial fractions in Figure 4.2 was due to the accumulation of this protein around the membranes, I used SR 3D-SIM (Figure 4.3) to obtain higher resolution images of mitochondria after trapping (Figure 4.4). HeLaGAL cells were pre-treated with 100 nM MTX (or DMSO) for 12 hours prior to expression of Su9-mScarlet-DHFR for a further 48 hours. Mitochondria were then stained with 100 nM MitoTracker Green for 30 minutes at 37^{o}C prior to imaging. SIM was carried out in collaboration with Dr Wolfgang Hübner, at the University of Bielefeld, Germany.

SIM is a wide-field type setup that uses illumination in a known pattern (usually stripes) to excite the sample (unknown pattern), and the resulting fluorescence emission pattern for stripes at a range of rotations is collected (Figure 4.3) [370]. This 'structured illumination' allows the diffraction limit to be overcome, allowing for the increased resolution. This produces raw images known as Moiré patterns, which can be reconstructed to give the SIM images relating to the structure of the sample (Figure 4.3), providing a ~2-fold improvement in the resolution [371-373, 441]. SIM is not optimised for imaging diffuse signals of low contrast (*i.e.,* diffuse cytoplasmic mScarlet fluorescence). Such signals can lead to artefacts in the reconstructed data, which can be reduced by application of a high Wiener filter [371]. This was necessary in my images since potential artefacts from the diffuse mScarlet signal in cells subjected to trapping would prevent recognition of actual accumulations of this protein around mitochondria. However, this can affect SIM resolution, as can be observed in the mitochondrial channel (Figure 4.4A), and this is something to take into consideration with regards to this technique and the resulting data [371, 442]

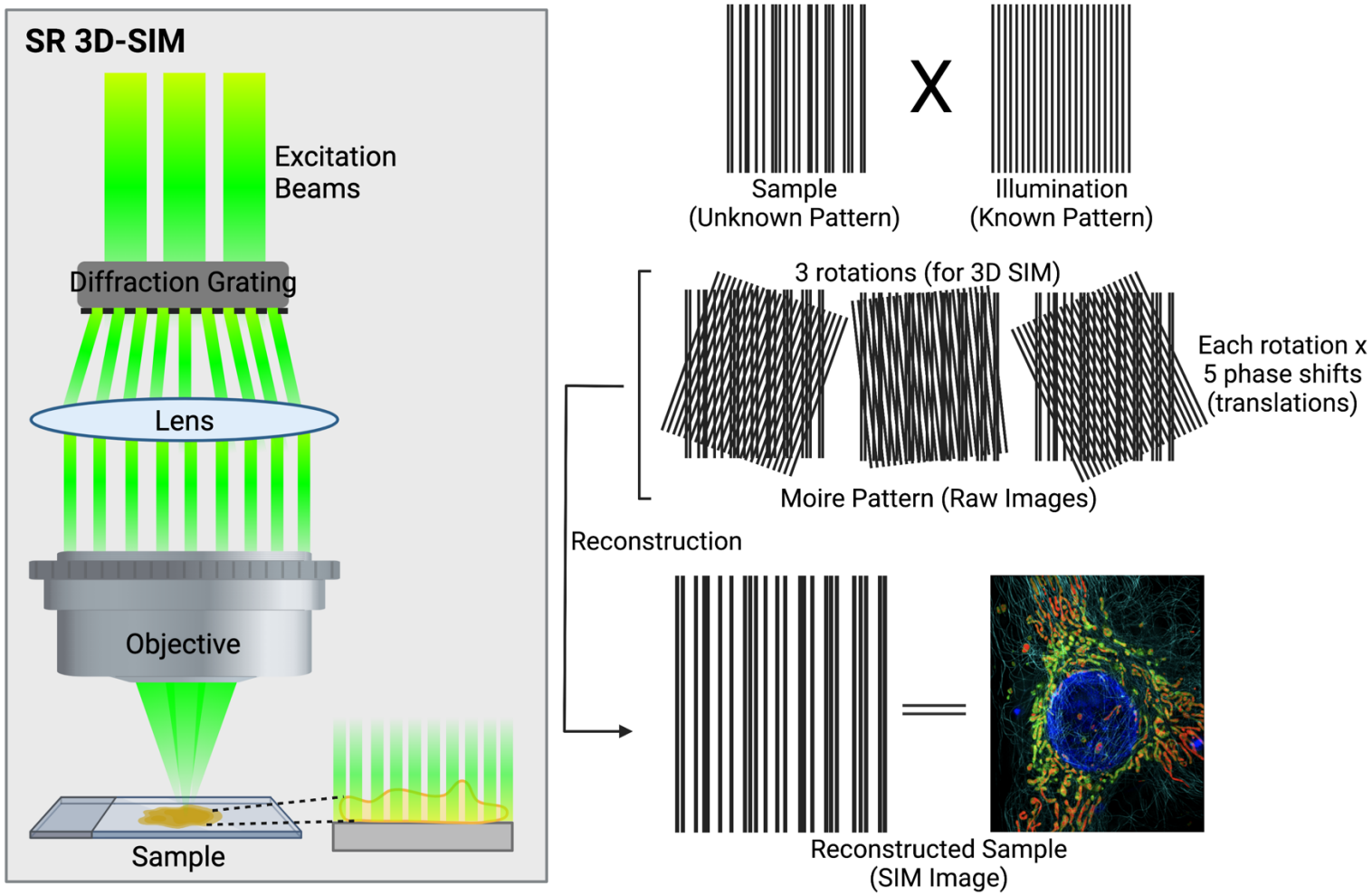

Figure 4.3: Principle of SR 3D-SIM
In a SR 3D-SIM setup, a diffraction grating, positioned in the illumination aperture of the excitation beams path generates illumination in a known pattern (structured illumination). This in turn excites the sample, and the pattern produced by the sample (with an unknown pattern) illuminated by the known pattern of the illumination stripes creates a low frequency pattern, known as a Moiré pattern or Moiré fringe. For reconstruction, several images are acquired using different orientations of the known illumination pattern, achieved by translations and rotations of the diffraction grating. For a 3D image, this requires 5 translations and 3 rotations, totalling 15 raw images. The reconstruction of these raw images produces a final, super-resolved SIM image.

Nevertheless, after application of the high Wiener filter, the resulting images were still of high enough resolution to visualise the accumulation of high mScarlet fluorescence around the outside of a population of mitochondria, indicative of protein stalling when HeLaGAL cells were treated with 100 nM MTX (Figure 4.4). This is indicated by arrows (Figure 4.4A, bottom middle panel) and has been quantified in terms of pixel intensity (Figure 4.4B). This shows the exclusion of the trapped precursor from the inside of the mitochondria in the cells expressing the trap (Figure 4.4B), compared to the inclusion of Su9-mScarlet-DHFR in the mitochondrial matrix when MTX is not present (Figure 4.4C). In combination with the confocal and biochemistry data presented in Figure 4.2, these data indicate that the trapped precursor is excluded from mitochondria, and that the DHFR-MTX trapping mechanism effectively stalls the precursor protein in the import sites of a population of mitochondria.

To determine the proportion of mitochondria per cell which were surrounded by the stalled precursor following two days of trapping, I carried out automated analysis of the SIM images. Analysis of the pixel intensity of the SIM images using a FiJi macro (described in Section 2.9.5.3) showed that an average of 43% of mitochondria per cell are surrounded by the trapped precursor, suggesting that their import sites are blocked (Figure 4.4D). It is important to note that the percentage of surrounded mitochondria was highly variable between cells, and there is a large range, as highlighted in the quantification shown in Figure 4.4D. Therefore, this data should be used as an indication of the expected proportion of mitochondria subjected to trapping, rather than a definitive value.

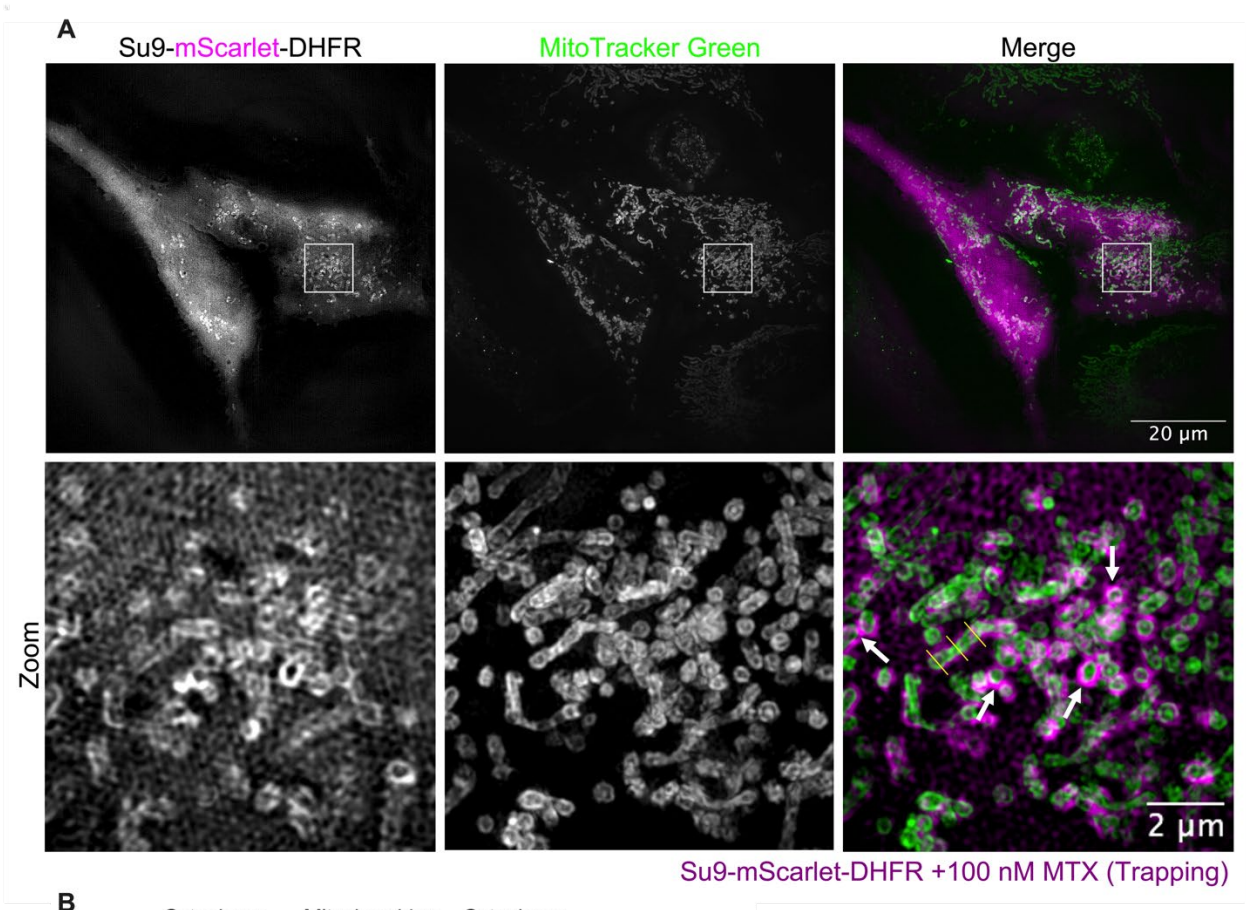
A
Su9-mScarlet-DHFR
MitoTracker Green
Merge
20 µm
Zoom
2 µm
Su9-mScarlet-DHFR +100 nM MTX (Trapping)

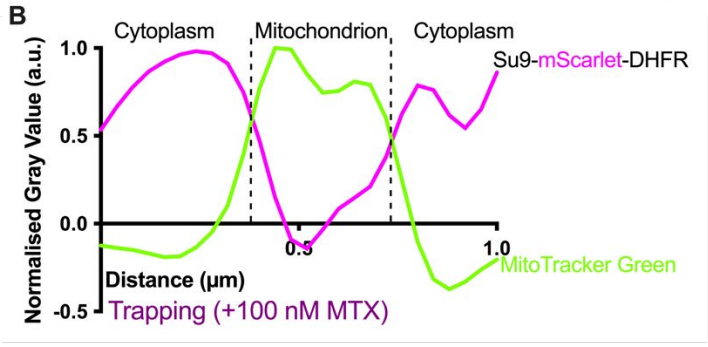
B
Cytoplasm
Mitochondrion
Cytoplasm
Su9-mScarlet-DHFR
MitoTracker Green
Normalised Gray Value (a.u.)
1.0
0.5
0.0
-0.5
0.5
1.0
Distance (µm)
Trapping (+100 nM MTX)

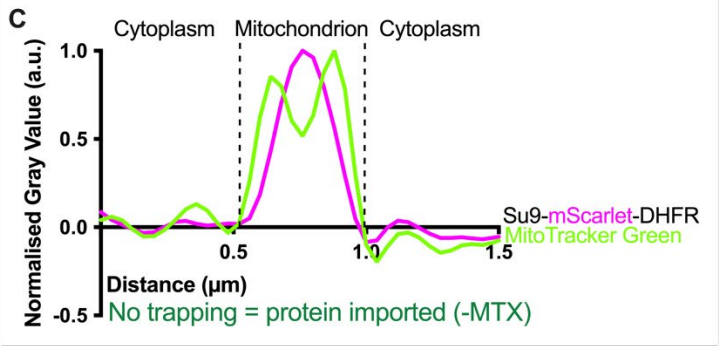
C
Cytoplasm
Mitochondrion
Cytoplasm
Su9-mScarlet-DHFR
MitoTracker Green
Normalised Gray Value (a.u.)
1.0
0.5
0.0
-0.5
0.5
1.0
1.5
Distance (µm)
No trapping = protein imported (-MTX)

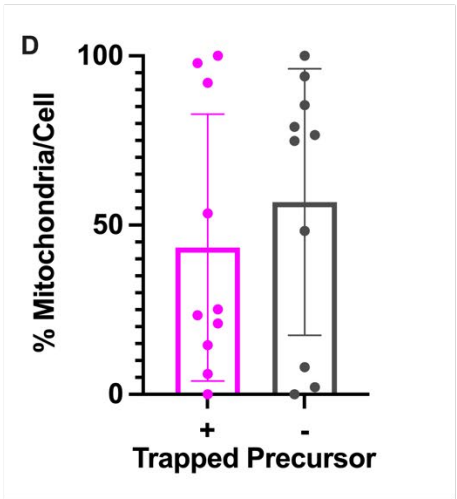
D
% Mitochondria/Cell
100
50
0
+
-
Trapped Precursor

Figure 4.4: The Stalled Precursor Accumulates around the OMM of ~43% of Mitochondria
(A) SIM showing trapping substrate accumulation around mitochondrial membranes in HeLaGAL cells expressing Su9-mScarlet-DHFR (mScarlet; magenta) in the presence or absence of 100 nM MTX. Mitochondria are shown by MitoTracker Green staining (green). Images were reconstructed and aligned. Arrows show aggregates of trapping construct surrounding mitochondria (as represented in pixel intensity plot in panel B). *N=3*.
(B) Plot of average pixel intensity across a mitochondrion surrounded by trapped precursor (highlighted by arrows in panel A zoom merge, with example yellow cross sections showing how pixel intensity was plotted) in cells subjected to the trapping insult.
(C) Plot of average pixel intensity across a mitochondrion not subjected to the trapping insult, where the precursor is imported into mitochondria, displayed as a comparison.
(D) Quantification of the % of mitochondria per cell with (magenta) or without (grey) trapped precursor surrounding them. *Analysis was done using a FiJi plugin, described in Section 2.9.5.3. Each point represents the average from the mitochondria in an individual cell. 10 cells were analysed (the low sample size is due to the diffuse background signal and high Wiener filter meaning that cells had to be selected carefully to avoid artefacts in the analysis). Analysis included a total of 883 mitochondria.*

4.3.2. Acute but not Chronic Trapping Reduces Mitochondrial Import Function

To characterise the impact of a stalled precursor (DHFR-MTX system) on the import of other precursor proteins, I carried out import assays using the NanoLuc system. HeLaGAL cells were allowed to express eqFP670-P2A-Cox8a-LgBit for 24 hours prior to overnight pre-treatment with 100 nM MTX (or DMSO only), and lentiviral expression of Su9-mScarlet-DHFR. 48 hours later cells were subjected to import assays whereby the import of a chasing precursor protein was monitored (Figure 4.5A). After precursor trapping for 48 hours (chronic trapping) there appeared to be no change in the import of the chasing precursor (Figure 4.5A).

To test whether the normal import function in the presence of precursor stalling was due to insufficient trapping capacity of DHFR-MTX, I performed the same experiment with acute trapping, *i.e.,* precursor trapping *in vitro* over the course of 10 minutes. Cells were subjected to expression of eqFP670-P2A-Cox8a-LgBit for 72 hours prior to permeabilising with 3 nM rPFO. A purified trapping substrate, Su9-ACP1-DHFR, was added and incubated with cells for 10 minutes in the presence or absence of 100 nM MTX. The NanoLuc assay was then carried out exactly as before. The import traces show that after acute trapping, the import of the chasing precursor protein is reduced by 37% (Figure 4.5B). Together, these data indicate that a cellular mechanism may help restore import function following chronic trapping.

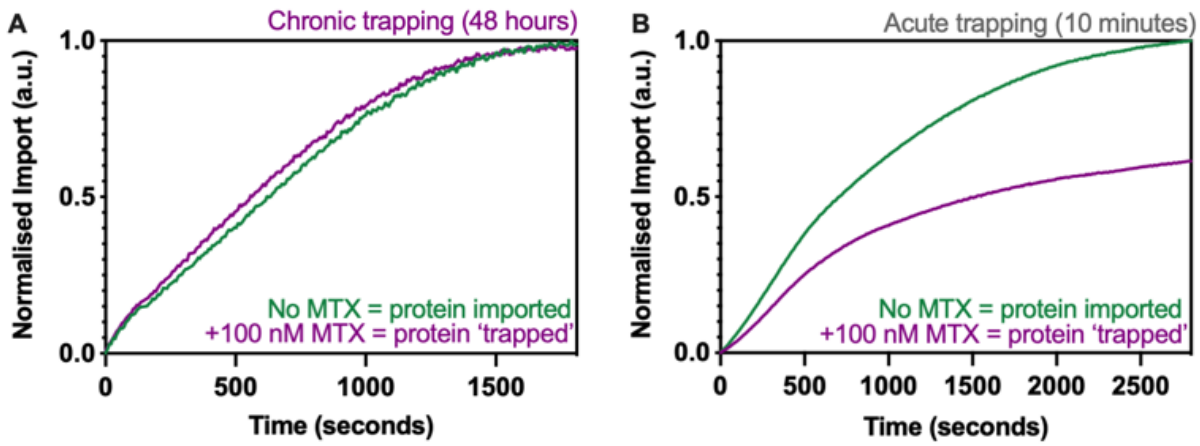

Figure 4.5: Acute but not Chronic Trapping Reduces Import of a Chasing Precursor Protein
(A) NanoLuc import trace after chronic trapping. LgBit expressing HeLaGAL cells were subjected to expression of Su9-mScarlet-DHFR in the presence (purple) or absence (green) of 100nM MTX for 48 hours prior to carrying out NanoLuc import assays to monitor import of precursor protein Su9-EGFP-6xHis-HiBit. *Traces were normalised to eqFP670 fluorescence (as a marker of LgBit expression levels), technical replicates averaged, then normalised to the maximum value for the given run, and finally normalised to the +/- MTX (-MTS) control. N=3 biological replicates, each with n=3 technical replicates.*
(B) NanoLuc import trace after acute trapping. HeLaGAL cells expressing LgBit were permeabilised using 3 nM rPFO prior to incubation (RT, 10 minutes) with 1 µM trap substrate, in the presence (purple) or absence (green) of 100 nM MTX. NanoLuc import assays were carried out and traces normalised as above. *N=3 biological replicates, each with n=3 technical replicates.*

4.3.3. Precursor Stalling Leads to Mitochondrial Fission and Alters Cristae

Using the DHFR-MTX system, I used SIM to characterise the impact of precursor stalling on mitochondrial morphology. HeLaGAL cells were subjected to pre-treatment (overnight) with (+MTS +MTX) or without (+MTS -MTX) 100 nM MTX, prior to transduction with DNA coding for precursor protein Su9-mScarlet-DHFR. Cells were incubated for 48 hours before staining mitochondria with MitoTracker Green. Cells were visualised live by SR 3D-SIM (Figure 4.6). The fact that not all cells expressed Su9-mScarlet-DHFR provided an internal control for the effects of MTX treatment on cells (NT +MTX). The resulting images were reconstructed, aligned, and processed to obtain a clear representation of mitochondria (Figure 4.6).

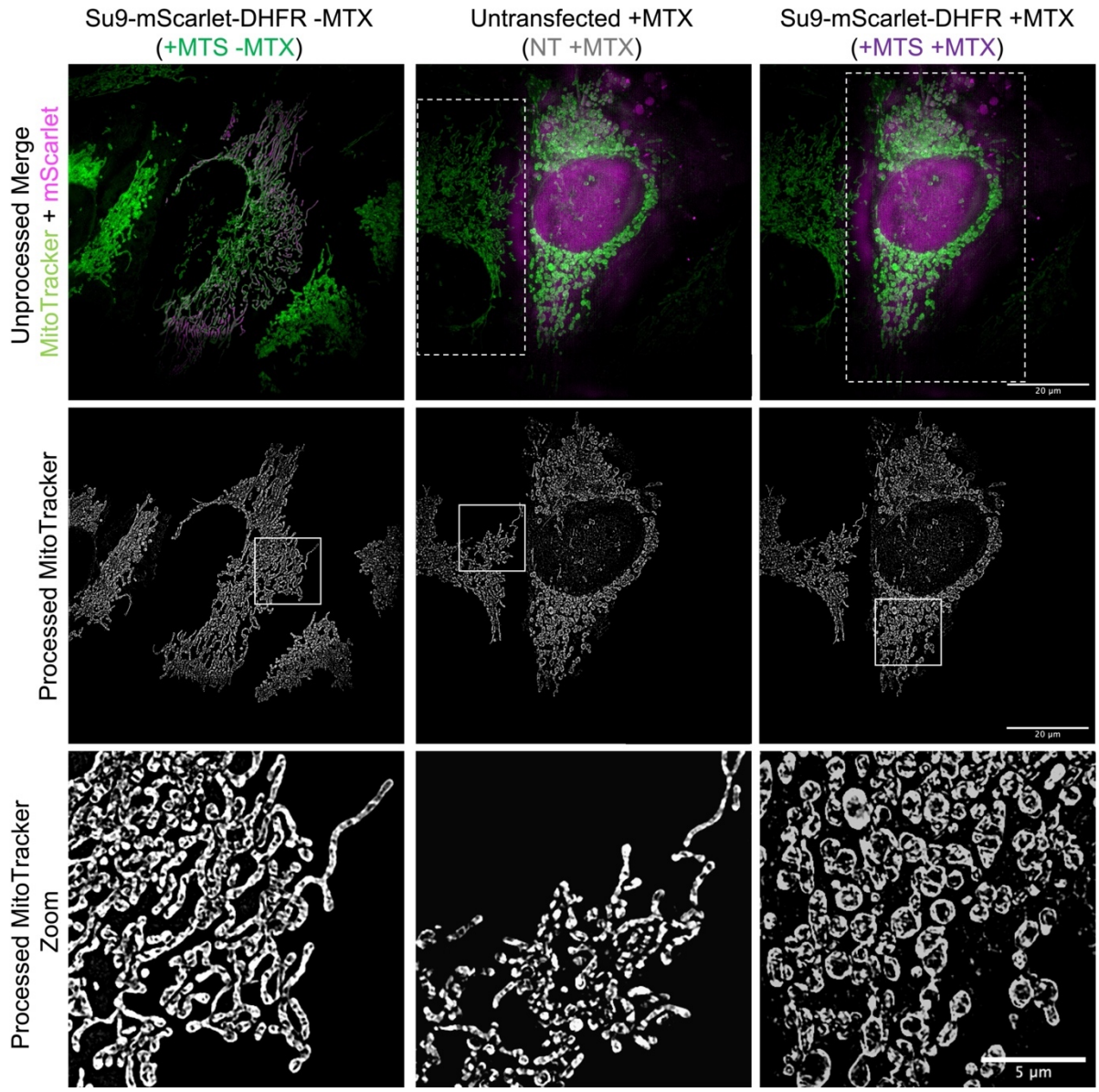

Figure 4.6: Mitochondrial Morphology is Altered Following Trapping
SIM showing mitochondria of HeLaGAL cells subjected to trapping (+MTS +MTX) or not (+MTS -MTX). Untransfected cells in the same well as cells subjected to trapping were used as an internal control for MTX treatment (NT +MTX). The top row shows a merge of MitoTracker Green (green) and mScarlet (magenta) prior to processing. The middle row shows mitochondria (MitoTracker Green channel only) after processing, allowing for clearer visualisation of the mitochondrial morphology. The bottom panel shows a zoom of an area of mitochondria (highlighted in the middle panel) to give a clearer view of mitochondrial morphology. *Images are representative of N=3 biological repeats*.

Mitochondrial morphology was analysed in terms of the average number of branches in a mitochondrial network, which gives an indication of the complexity of the mitochondrial network, as well as mitochondrial dynamics, since a less branched/smaller network is indicative of increased fission (Figure 4.7). A 'mitochondrial network' represents a single connected structure of fused, branched mitochondria within a cell. This was quantified using a FiJi macro, which was developed and described in detail previously [377]. All mitochondrial imaging analysis was carried out as described in Section 2.9.5, and links to macros can be found in Appendix 2.

Figure 4.7A shows that, following trapping, there is a reduction in the average number of branches, from an average of 6 branches/mitochondrial network when the protein is imported (+MTS -MTX) and 7.5 in untransfected cells exposed to MTX (NT +MTX), to 3.6 following trapping (+MTS +MTX). Considering the extremities, the data was further analysed to acknowledge the maximum number of branches in a mitochondrial network. Figure 4.7B shows that in the presence of stalled precursor, the maximum number of branches is 61, whilst when the protein is imported, it is 116, and untransfected cells treated with MTX have a maximum of 134 branches per network. This highlights a reduction in the complexity of mitochondrial networks following precursor trapping.

Next, I expanded the analysis to investigate the width of mitochondria in response to failed precursor import. The mitochondrial width is quantified by measuring directly across the mitochondria, as indicated by MitoTracker Green staining. This analysis was carried out manually on blinded data. Figure 4.7C shows that, after chronic trapping, mitochondria are wider, with an average width of 0.53 μm, compared to 0.49 μm for cells with imported precursor, and 0.48 μm for untransfected, MTX treated cells. This analysis was expanded to quantify the circularity of mitochondria. Circularity analysis was automated, using a FiJi plugin. The data shows that following trapping mitochondria have a higher circularity index (0.61) compared to those where trapping has not occurred (0.55 and 0.51 for +MTS -MTX and NT +MTX, respectively).

Overall, these morphological changes suggest that mitochondria with a stalled precursor may undergo increased fission. It is well established that an increase in mitochondrial fission causes mitochondrial connectivity to decrease, resulting in short, round mitochondria [14, 443]. Additionally, an altered fission: fusion ratio, specifically increased fission, is associated with conditions that compromise mitochondrial function, such as depletions of mtDNA or treatment with mitochondrial toxins [444, 445]. Perturbation of the import machinery is therefore likely to have a similar impact.

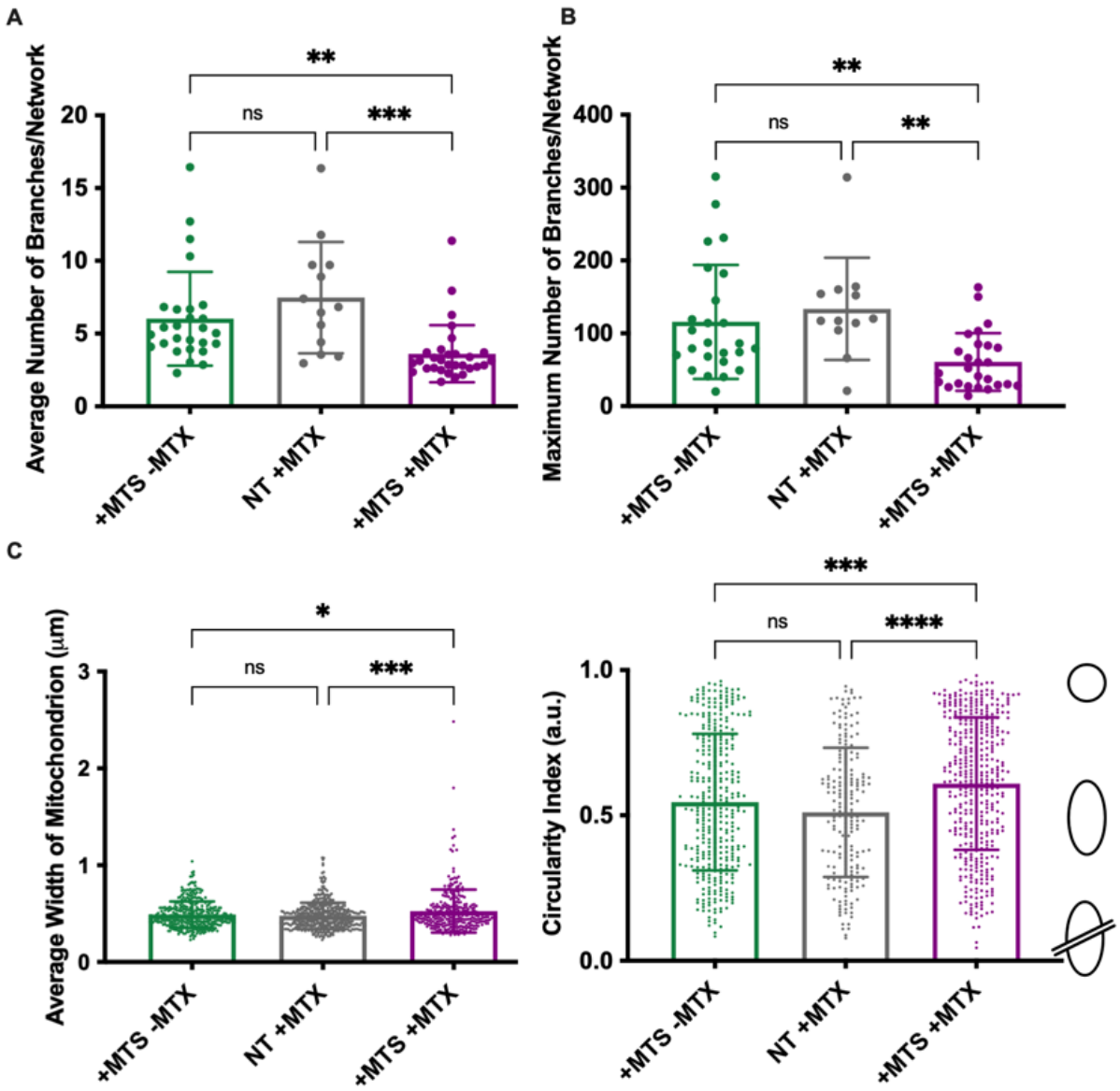

Figure 4.7: Mitochondria Subjected to Trapping are Circularised and Less Elongated
(A) Quantification of the average number of mitochondrial branches of representative images shown in Figure 4.6, for cells expressing Su9-mScarlet-DHFR in the absence of MTX (imported precursor, +MTS +MTX; green), internal control cells (untransfected but in the presence of 100 nM MTX; NT +MTX; grey), and transfected cells in the presence of MTX (trapped precursor, +MTS +MTX; purple). *Each point represents an individual cell from a separate z-stack. N=27, 13, 30 cells for different conditions, respectively, taken from 3 independent biological repeats (N=3). Error bars show SD. Error bars show SD. One-way ANOVA and Tukey's post hoc test were used to determine significance.*
(B) Quantification of the maximum number of mitochondrial branches in a network. *As for (A).*
(C) Quantification of the width of a mitochondrion, conditions as for (A). *Each point represents an individual mitochondrion, as an average of 5 measurements taken for any one mitochondrion, from a square taken from a separate z-stack (example squares in Figure X (bottom panel). N=360, 470, 315 mitochondria, from 20 cells for each condition, respectively, taken from 3 independent biological repeats (N=3). Error bars show SD. One-way ANOVA and Tukey's post hoc test were used to determine significance.*
(D) Quantification of the circularity of a mitochondrion. *Each point represents an individual mitochondrion, and circularity was calculated using a FiJi plugin. N=359, 199, 434 mitochondria, respectively, taken from 3 independent biological repeats (N=3). Error bars show SD. One-way ANOVA and Tukey's post hoc test were used to determine significance.*

Accordingly, I analysed the abundance of fission related protein DRP1 in these cells. During mitochondrial fission, DRP1 is recruited to the OMM, where it assembles into spiral-like oligomers, which constrict mitochondria via its GTPase activity [17]. However, mitochondria-DRP1 interactions are regulated by various PTMs. Specifically, phosphorylation of DRP1 at Serine 616 (p-DRP1 S616) promotes mitochondrial fission, whilst phosphorylation at Serine 637 (p-DRP1 S637) inhibits it [27]. Though Western blotting analysis showed that the abundance of total DRP1 was unchanged in HeLaGAL cells following chronic trapping (Figure 4.8A, quantified in B), the abundance of DRP1 phosphorylated at S616 was higher after trapping (Figure 4.8C and D). This is consistent with increased fission of mitochondria subjected to trapping compared to their control counterparts. This justifies the morphological changes highlighted by SIM (Figure 4.6 and Figure 4.7).

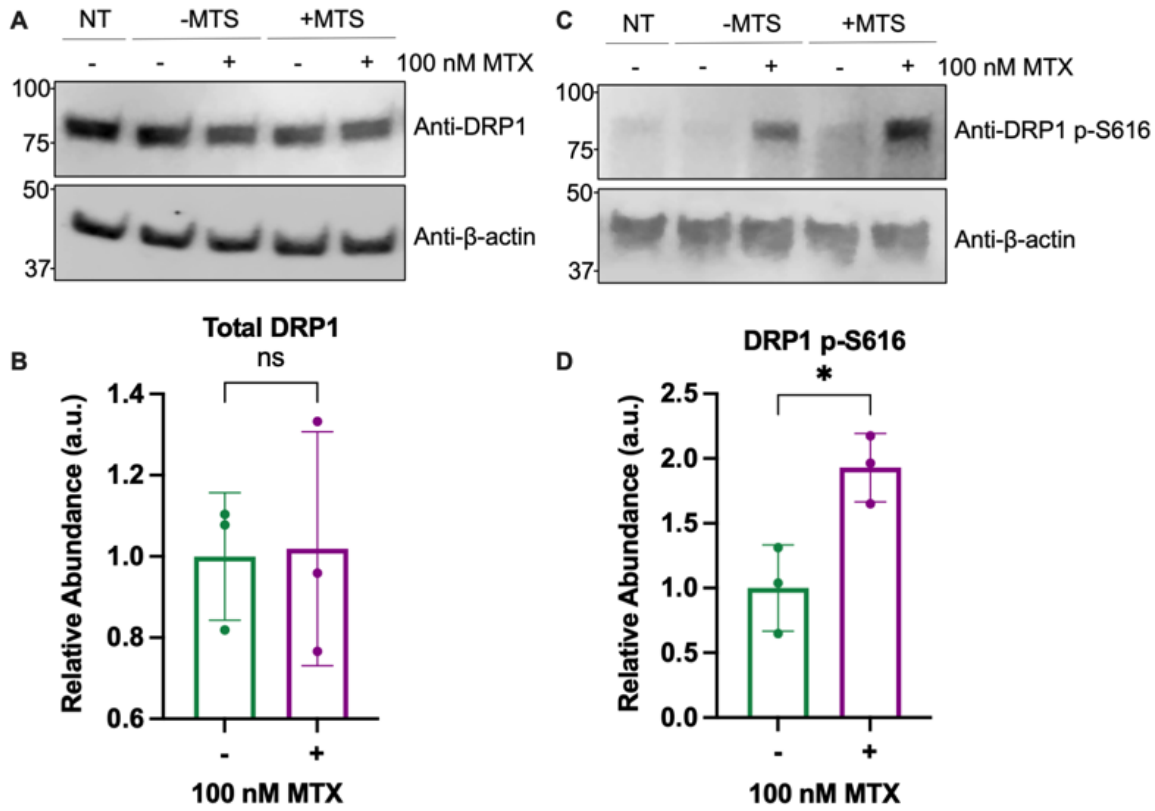

Figure 4.8: Phosphorylation of DRP1 at S616 is Increased Following Precursor Trapping
(A) Representative Western blots showing abundance of total DRP1 in whole cell lysates from HeLa cells expressing EGFP-DHFR-HiBit, Su9-EGFP-DHFR-HiBit, or untransduced (NT) cells in the absence of presence of 100 nM MTX. β-actin is used as a loading control. *N=3 biological replicates*.
(B) Quantification of (A). Expression levels were normalised to β-actin loading control, then further normalised to their respective -/+MTX control, to account for changes associated with MTX treatment. *Error bars show SD. Unpaired t-test was used to determine significance.*
(C) Representative western blots showing abundance of p-S616 DRP1. Conditions exactly as in (A).
(D) Quantification of (C). Normalised as in (B). *Unpaired t-test was used to determine significance.*

I next analysed the number of cristae per mitochondrion (Figure 4.9A). This was done by selecting an area of cell containing mitochondria from pre-processed images of blinded SIM data (representative images shown in Figure 4.6). I then manually isolated and measured mitochondria, counted the number of cristae on the given length of mitochondrion, and normalised to the length of said mitochondrion. The data show that trapping leads to a significantly increased number of cristae per micron of mitochondrion, compared to when the precursor is imported (3.5 compared to 2.9, or 2.2 for untransfected cells treated with MTX; Figure 4.9A). The fact that MTX alone reduces the number of cristae, whilst trapping increases it, implies that the effect of trapping may be even greater in the absence of this unspecific, off target effect. Together, these changes are indicative of mitochondrial remodelling, which is often highlighted as a hallmark of various diseases [446].

Since mitochondria have more cristae following precursor trapping, I hypothesised that there may also be alterations in the assembly and/or function of the respiratory chain complexes, which reside on the crista IMM [447]. Therefore, I investigated the respiratory capacity of these cells, by carrying out mitochondrial stress tests *via* high resolution respirometry using a Seahorse respirometer (Figure 4.9B). HeLaGAL cells were pre-treated with 100 nM MTX or vehicle, prior to expression of Su9-EGFP-DHFR-HiBit (+MTS) or EGFP-DHFR-HiBit (-MTS) by lentiviral transduction and incubation for 48 hours. The respiratory capacity of these cells was subsequently measured in response to the addition of various respiratory chain substrates and inhibitors. Figure 4.9B shows that there was no change in the oxygen consumption rate (OCR) of these cells in response to trapping, suggesting that these cells do not have altered respiratory function or complexes, or that respiratory function has been rescued. It is important to note that subtle effects may be diluted by untransduced cells in these experiments. Although lentiviral expression was used to minimise this, expression levels were not quantified and therefore this cannot be discounted.

I also investigated the ΔΨ in these cells in response to trapping by analysing TMRM intensity, as has been described previously [378]. TMRM accumulation in mitochondria is dependent on a functional PMF, and therefore is commonly used as a measure of the ΔΨ [378]. Cells were subjected to precursor trapping, with conditions and controls exactly as described above. 25 nM TMRM was used for mitochondrial staining, and cells were imaged live on a confocal microscope over 2 minutes. 10 μM CCCP was then added to dissipate the ΔΨ, and cells were imaged for a further 2 minutes. Following quantification of ΔΨ using a FiJi plugin, it was clear that precursor trapping did not alter the ΔΨ (Figure 4.9C-D).

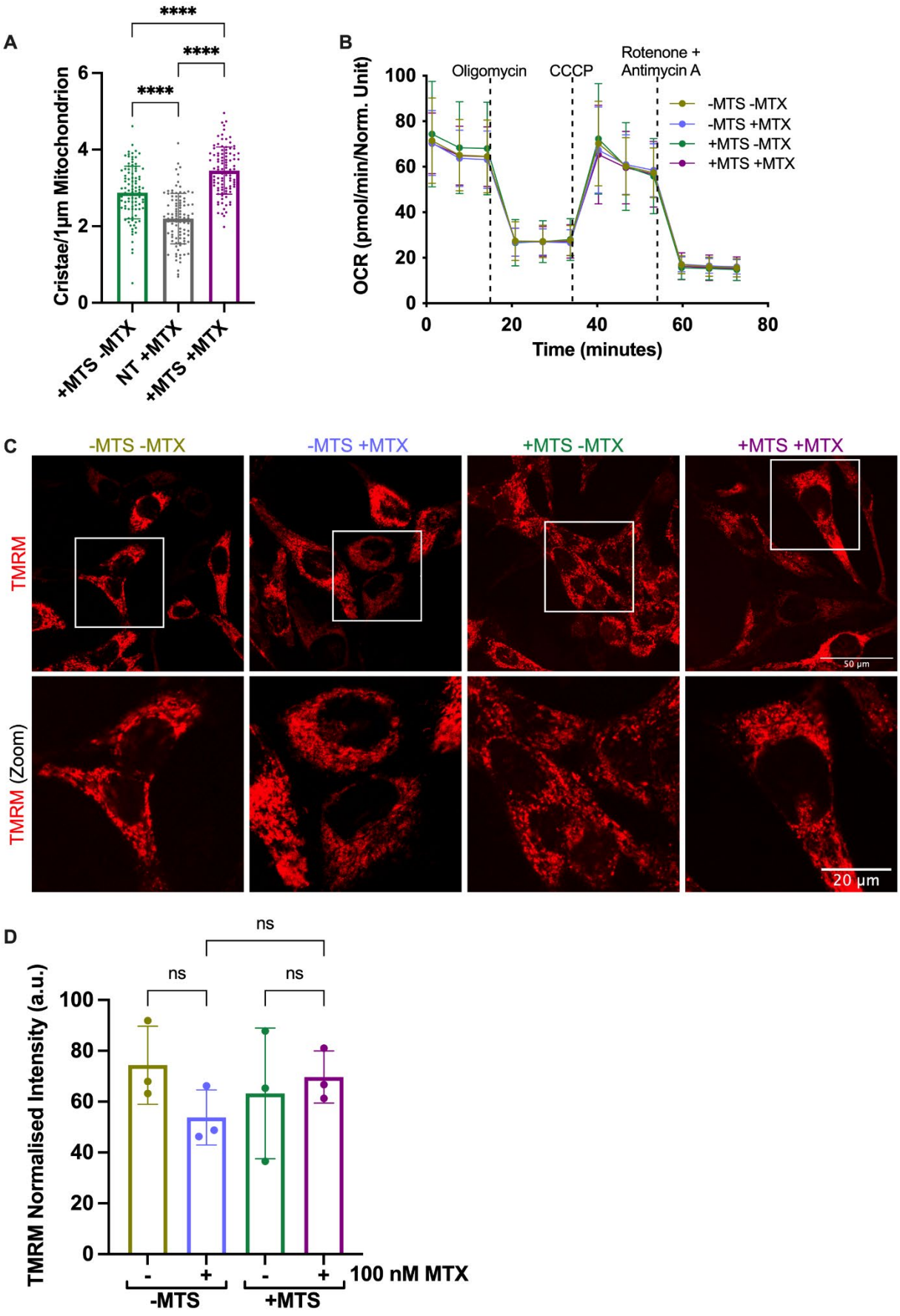
A
****
****
****
Cristae/1µm Mitochondrion
0
2
4
6
+MTS -MTX
NT +MTX
+MTS +MTX
B
Oligomycin
CCCP
Rotenone +
Antimycin A
OCR (pmol/min/Norm. Unit)
0
20
40
60
80
100
Time (minutes)
-MTS -MTX
-MTS +MTX
+MTS -MTX
+MTS +MTX
C
-MTS -MTX
-MTS +MTX
+MTS -MTX
+MTS +MTX
TMRM
TMRM (Zoom)
50 µm
20 µm
D
ns
ns
ns
TMRM Normalised Intensity (a.u.)
0
20
40
60
80
100
-
+
-
+
100 nM MTX
-MTS
+MTS

Figure 4.9: Precursor Trapping Alters Cristae Abundance but Respiration is Unchanged
(A) Quantification of the number of cristae per 1 µm mitochondrion (for representative SIM images shown in Figure 4.6). *Each point represents an individual mitochondrion, and cristae were counted by eye on blinded data. N=100 mitochondria, 10 cells for each condition (10 mitochondria chosen at random per cell), taken from N=3 biological repeats. Error bars show SD. One-way ANOVA and Tukey's post hoc test were used to determine significance.*
(B) Mitochondrial stress test showing OCR of cells subjected to various respiratory chain substrates. HeLaGAL cells expressing EGFP-DHFR-HiBit (-MTS) or Su9-EGFP-DHFR-HiBit (+MTS) were grown in the presence (+MTX) or absence (-MTX) of 100 nM MTX for 48 hours prior to mitochondrial stress tests (Seahorse XFe96 analyser). Data is normalised to total protein content as determined by SRB assays. *N=6 biological replicates, each with n=3 technical replicates*. *Error bars show SD*.
(C) Confocal microscopy images showing mitochondrial ΔΨ (TMRM staining) of HeLaGAL cells expressing EGFP-DHFR-HiBit (-MTS) or Su9-EGFP-DHFR-HiBit (+MTS) +/- MTX. CCCP was added after 2 minutes to control for background fluorescence not relating to ΔΨ. *N=3 biological replicates*.
(D) Quantification of (C). Analysis was carried out using an automated macro on FiJi. *Error bars show SD. One-way ANOVA and Tukey's post hoc test were used to determine significance.*

4.3.4. Enhancement of Proteins Associated with the Trapped Precursor

Finally, to facilitate exploration of other pathways that might be activated by import disturbance, TMT-MS was utilised to enable identification of proteins associated with the trapped precursor. Cells were pre-treated with MTX (or DMSO) and subjected to lentiviral expression of Su9-EGFP-DHFR-HiBit for 48 hours. Cells were harvested and mitochondria isolated and lysed gently with glyco-diosgenin amphiphile (GDN; Figure 4.10A). Interacting proteins were isolated using a GFP-trap. The pulldown was validated by Western blotting (Figure 4.10B). Beads were then sent for TMT-MS, which provided a broad overview of proteins associated with the trapped precursor. A volcano plot showing protein enhancement in the -MTX *vs* +MTX samples, with some proteins of interested highlighted for reference, is shown in Figure 4.10. These proteins of interest and their cellular functions are detailed in Table 4.1. It is important to note that these highlighted proteins are a selection of proteins picked out manually, and there may be other proteins of interest worthy of investigation within the dataset, as shown in full in Appendix 3.

Interestingly, the associated proteins include several proteins important for respiratory complexes assembly and function, as well as mitochondrial morphology and dynamics. Additionally, enhanced proteins included those involved in stress response pathways, particularly associated with the proteasome. Finally, various proteins that have previously proven important in cytoskeleton regulation as well as TNT signalling and/or formation were enhanced in association with the trapped precursor. These provide clues into which cellular pathways may be activated in response to precursor stalling. A full representation of all significantly enhanced proteins is provided in Appendix 3, along with PANTHER analysis of correlated cellular pathways.

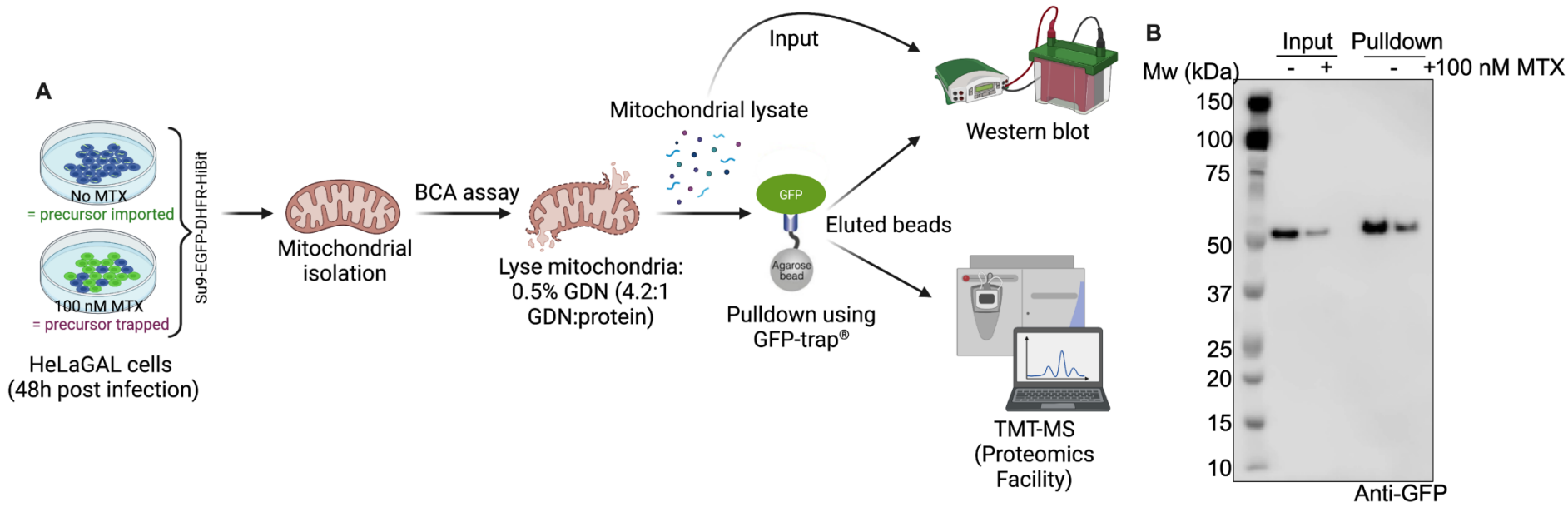

Figure 4.10: Proteomic Analysis of Proteins Associated with Trapped Precursor: Setup
(A) Experimental outline for GFP-pulldown assays. HeLaGAL cells were subjected to lentiviral expression of Su9-EGFP-DHFR-HiBit in the presence or absence of 100 nM MTX for 48 hours. Mitochondria were isolated and mitochondrial protein content was assessed using a BCA assay. Equal amounts of mitochondria were lysed using 0.5% GDN at a ratio of 4.2:1 (GDN: protein). A fraction of mitochondrial lysate was saved as an input control, and the rest was loaded onto GFP-trap agarose beads, to pull-down proteins associated with the GFP tagged protein of interest. The resulting beads conjugated to proteins associated with GFP-tagged proteins were analysed by Western blotting and sent for TMT-MS.
(B) Representative Western blot showing GFP-tagged protein in the input and pulldown samples. Samples were prepared as in (A) and probed against a GFP antibody to validate IP. *N=3*.

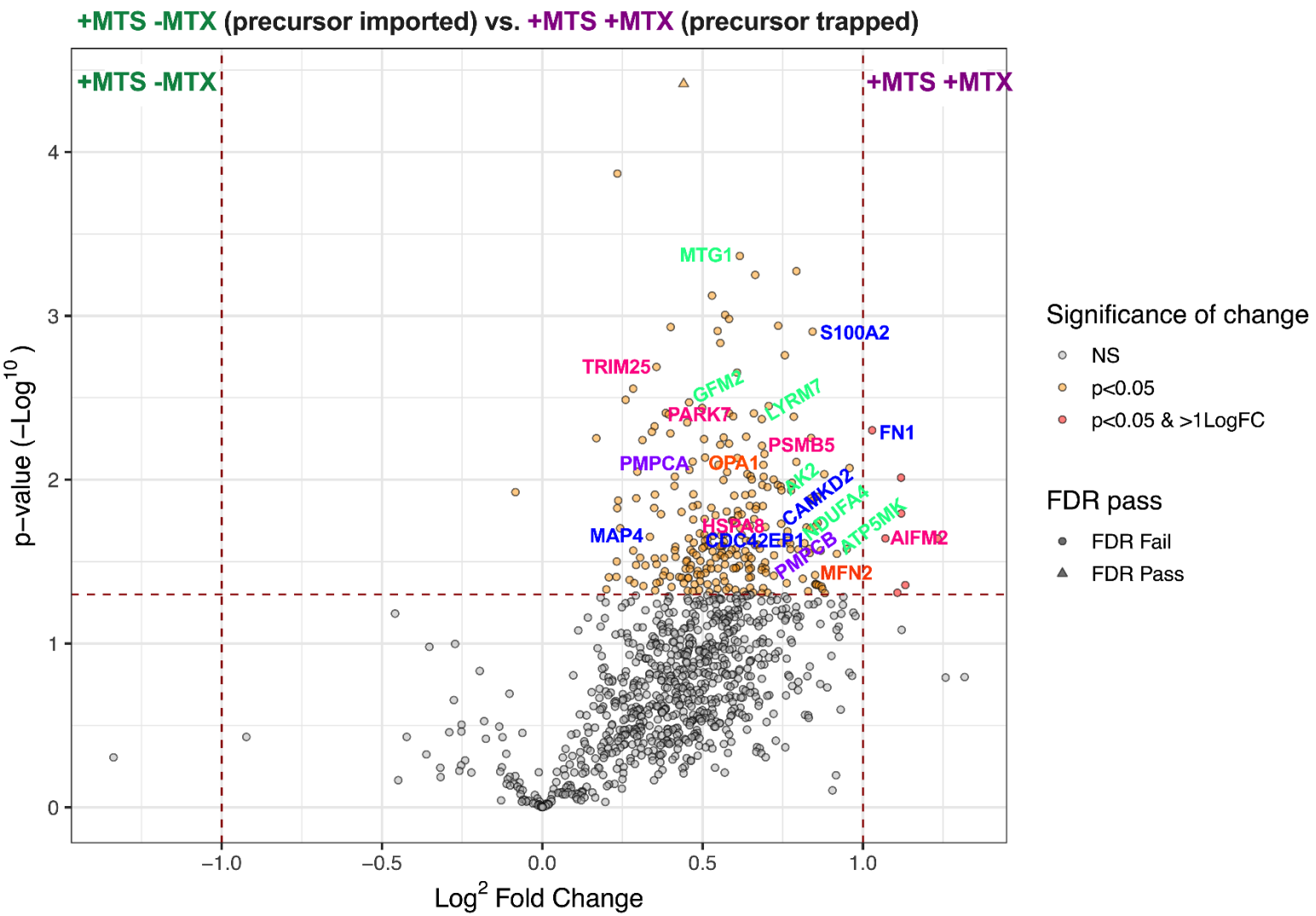

Figure 4.11: Enhancement of Proteins Associated with Trapped Precursor
Volcano plot showing proteins enhanced in pulldown samples from proteins with imported precursor (+MTS -MTX, left) compared to those with the trapped precursor (+MTS +MTX, right). Some proteins of potential relevance are highlighted by gene names on the volcano plot. *N=3.*

Table 4.1: Proteins of Interest with Enhanced Association to Trapped Precursor

Pathway of Interest	Gene	Protein	Function	Log^2 FC	T-Test
Respiratory Complexes Assembly/ Function	MTG1	Mitochondrial ribosome associated GTPase 1	Regulation of mitochondrial ribosome assembly and translational activity [448].	0.62	4.31E-04
	GFM2	Ribosome-releasing factor 2, mitochondrial	Mitochondrial GTPase, mediates ribosome disassembly [449].	0.39	4.00E-03
	ATP5MK	ATP synthase membrane subunit K	Regulates mitochondrial ATP synthesis [450, 451].	0.87	2.71E-02
	NDUFA4	Cytochrome c oxidase subunit NDUFA4	Mitochondrial ETC [452].	0.82	2.44E-02
	AK2	Adenylate kinase 2, mitochondrial	ATP metabolism/ADP biosynthesis [453].	0.73	1.08E-02
	LYRM7	Complex III assembly factor LYRM7	Chaperone in CIII assembly [454].	0.66	3.94E-03
Mitochondrial Dynamics	MFN2	Mitofusin-2	OMM GTPase, mediates fusion [455].	0.85	4.33E-02
	OPA1	Dynamin-like 120 kDa protein, mitochondrial	Mitochondrial morphology mediator [42].	0.69	6.97E-03
Mitochondrial Protein Processing	PMPCA	Mitochondrial-processing peptidase subunit α	MTS cleavage [456, 457].	0.47	7.76E-03
	PMPCB	Mitochondrial-processing peptidase subunit β		0.66	2.51E-02
Cytoskeleton Assembly/ Dynamics *TNT Formation/ Signaling/ Activity*	S100A2	Protein S100-A2	Calcium sensor and modulator [458]	0.84	1.25E-03
	CAMK2D	Calcium/calmodulin-dependent protein kinase type II subunit delta	Calcium signaling [459]	0.68	2.64E-02
	FN1	Fibronectin	Cell adhesion and motility, involved in TNT formation [460, 461].	1.12	9.72E-03
	MAP4	Microtubule associated protein 4	Promotes microtubule assembly [462].	0.42	2.57E-02
	CDC42EP1	Cdc42 effector protein 1	Actin cytoskeleton organization; known to induce membrane extensions in fibroblasts [463].	0.5	2.62E-02
Stress Response Pathways	AIFM2	Ferroptosis suppressor protein 1	Mitochondrial stress signaling [464].	1.12	1.61E-02
	PARK7	Parkinson's disease protein 7	Mitochondrial stress response(s) [465, 466].	0.58	3.93E-03
	TRIM25	E3 ubiquitin/ISG15 ligase TRIM25	Ubiquitin E3 ligase [467].	0.36	2.05E-03
	PSMB5	Proteasome subunit β type 5	Component of the 20S core proteasome [468].	0.69	6.21E-03
	HSPA8	Heat shock cognate 71 kDa protein	Molecular chaperone, involved in mitochondrial import and stress responses [165, 469].	0.51	2.36E-02

4.4. Discussion

4.4.1. Key Findings

The main aim of this chapter was to investigate the impact of failed precursor import on cells in terms of their health and function, and to examine how this may be related to import defects observed in neurodegeneration. The key findings from this chapter are:

- The DHFR-MTX trapping system is a useful means of modelling failed precursor import.
- Precursor trapping leads to a reduction in import function when carried out acutely, whilst import function is unchanged when trapping is done chronically.
- Stalling the import of a precursor protein induces changes in mitochondrial morphology, increased fission, and increased cristae abundance.
- Precursor trapping has no impact on respiratory function or membrane potential under examined conditions.
- Trapping leads to a significant shift in proteins associated with the precursor, including many involved in cellular stress response and repair mechanisms.

4.4.2. DHFR-MTX Trapping to Model Failed Import

Several recent reports have linked failed import or aggregation of proteins within mitochondria, and specifically import sites, to neurodegenerative diseases. Examples of this are studies showing that APP and Htt variants associate with translocase subunits, an association which is correlated with mitochondrial dysfunction, a common hallmark of neurodegenerative disease [215, 224]. However, this link has not yet been dissected in a system where the mitochondrial and cellular effects can be directly correlated to the import perturbation. This is important considering the many cellular pathways that have been found to be associated with disease prone proteins. Thus, I considered characterisation of the impact of a stalled protein on cells by the DHFR-MTX trapping system was an essential first step in dissecting the link between import dysfunction and neurodegeneration. Modelling the association of a precursor with translocase subunits synthetically allows control and understanding of the import perturbation mechanism, without the limitations of other impacts on the cells associated with expression of naturally occurring aggregation prone proteins. Here, I characterised this system, showing that the trapped precursor is still associated with ~43% of mitochondria per

cell after trapping for 48 hours. I then went on the investigate the impact of this on mitochondria in terms of import, morphology, dynamics, respiratory function, and protein abundance.

4.4.3. Failed Import Impact on Mitochondria

4.4.3.1. Mitochondrial Import

First, I used the NanoLuc system to monitor import of a chasing precursor protein *via* the presequence pathway in HeLaGAL cells subjected to precursor trapping for 48 hours (chronic trapping). Surprisingly, the resulting import trace showed that trapping in this manner had no impact on import efficiency (Figure 4.5A). This was an unexpected finding, since we predicted that stalling a precursor within the translocation channels would block the subsequent import of proteins at least partially, *i.e.,* the blockage incurred by the captured DHFR containing precursor would saturate a percentage of channels, leaving less (if any) import sites available for import of other proteins.

However, acute trapping (trapping for 10 minutes *in vitro*) led to a reduction in import of ~37% (Figure 4.5B). This indicates that, over a short time scale, the DHFR-MTX trapping mechanism does block chasing precursors from entering mitochondria, in line with what has previously been shown *in vitro* [470]. The fact that import is only reduced by 37% could suggest that the trapping substrate is not saturating at this level, or that the time of trapping (10 minutes) was not long enough for the trapping substrate to reach and become captured in all import sites. To test this possibility, titration of the trapping substrate concentration as well as the trapping incubation time should be tested, to identify the maximum possible effect of trapping in this manner on import efficiency. Alternatively, there could be competition from the chasing precursor leading to release of the trapped precursor from some of the translocase sites. It is important to consider that cells incubated with the DHFR containing precursor in the absence of MTX would have imported this protein, which may be responsible for a reduction in their import capacity for subsequent precursors, giving the false impression of a lower dynamic range. This is because precursor import is likely to diminish Δψ and ATP availability, both of which are vital for subsequent import (as shown in this system in Figure 3.11) [137, 410-412]. Nonetheless, the fact that import is reduced following acute but not chronic trapping is indicative of the involvement of a cellular rescue or clearance mechanism.

4.4.3.2. Mitochondrial Morphology

Using the precursor trapping system as a model of failed import, I went on to investigate the impact of failed import on mitochondrial morphology, by SR 3D-SIM. The data shows that stalling a precursor protein in the presequence pathway causes mitochondrial remodelling in terms of increased fission and cristae remodelling (Figure 4.6, Figure 4.7, Figure 4.8 and Figure 4.9). Furthermore, mitochondrial morphology related proteins MFN2 and OPA1 were shown to associate with the trapped precursor (Figure 4.11 and Table 4.1), though the exact mechanism by which this affects morphology is unclear.

Alterations in cristae biogenesis and structure as well as in mitochondrial dynamics have been implicated in several neurodegenerative diseases [471-474], as well as respiratory chain dysfunction [475]. The changes associated with cristae abundance are particularly interesting and warrant further investigation. This could include investigation into the mitochondrial contact site and cristae organising system (MICOS) complex, required for cristae junction formation [476], as well as investigation into cristae structure. However, this would require much higher resolution imaging, such as electron microscopy, which would need to be carried out on slices due to the cell thickness.

4.4.3.3. Mitochondrial Respiratory Function

Despite observing altered mitochondrial morphology including in cristae prevalence, there was no alteration in the $\Delta\Psi$, or the respiratory capacity of mitochondria subjected to precursor trapping (Figure 4.9). Proteomic analysis showed several proteins involved in respiratory complex assembly and function associated with the trapped precursor (Figure 4.11 and Table 4.1). These data were initially surprising considering it was previously assumed that the trapped precursor would block import of other proteins into mitochondria. Considering that the respiratory complexes are made up of subunits encoded by both nuclear and mitochondrial DNA, which must be tightly regulated and synchronised for proper assembly and function of respiratory complexes (see Figure 1.4) [1, 477, 478], perturbing import would be expected to have a knock on effect on respiratory function.

One explanation could be that there is low respiratory complex turnover, and therefore the complexes assembled prior to trapping were still fully functional at this timepoint. Consistent with this, a previous study investigating Htt impact on import showed that import dysfunction precedes defects in respiratory capacity [224]. Alternatively, this data may provide further evidence for a compensatory or rescue mechanism which maintains respiratory function in response to import perturbation.

4.4.4. Cellular Response to Import Stress: Hypotheses

Although acute precursor trapping correlates with a reduction in import function, when trapping is carried out chronically, mitochondrial import function appears normal (Figure 4.5). In addition, despite alterations in mitochondrial morphology, dynamics, and cristae, respiratory function is unchanged following trapping (Figure 4.6-Figure 4.9). Together, this data is indicative of a compensatory or clearance mechanism. There are several possible rationalisations for this, some of which are:

4.4.4.1. Lateral Insertion of the Precursor into the OMM

The data shown in Figure 4.2 shows that the stalled precursor is retained in the mitochondrial fraction, and it appears to accumulate around the OMM, at least in a proportion of mitochondria (Figure 4.4). In line with this, proteomic analysis showed MPP subunits PMPCA and B associated with the trapped precursor (Figure 4.11 and Table 4.1), which suggests that the MTS is reaching the matrix, and therefore is likely still trapped within import sites. However, this data does not necessarily confirm that the precursor is retained within the import sites in these cells. The trapped precursor could have been cleared from import sites and laterally inserted in the OMM or anchored to the outside of mitochondria. This could be tested by carrying out mitochondrial sub-fractionation and/or IPs on crosslinked mitochondrial samples.

4.4.4.2. Activation of a Stress Response Mechanism

Alternatively, there may be a stress response mechanism activated which clears the stalled precursor from mitochondrial translocation channels. Various stress response mechanisms induced by import perturbations have been described in the literature and are discussed in detail in Section 1.6. The result shown in Figure 4.2B further indicates this possibility, whereby the overall abundance of the trapping substrate was very low in the presence of MTX. This suggests that it may have been targeted for proteasomal degradation, or there may be alterations in transcription and translational processes, as has been detailed previously as a response to import stress [324]. This is consistent with the proteomic analysis shown in (Figure 4.11 and Table 4.1), which highlights association of the trapped precursor with proteins involved in stress responses involving the proteasome, such as the UPR^{am}. Unfortunately, further investigation of this mechanism was not within the scope of this thesis, especially since many of these stress response mechanisms have not yet been characterised in mammalian cells. However, it would be interesting to investigate activation of these mechanisms, by observing abundance as well as localisation of stress response marker proteins, in direct response to failed import modelled by the DHFR-MTX system.

4.4.4.3. Activation of a Compensatory Mechanism i.e., Mitochondrial Transfer

An alternative explanation is that the precursor does block import sites, but there is a compensatory mechanism at play, offsetting the reduced import capacity of these mitochondria. An example of such a mechanism could be intercellular mitochondrial transfer from neighbouring healthy cells (*i.e.,* untransduced cells with normal mitochondrial import function). This may also be evidenced by the fact that we only see protein aggregates around a population of mitochondria (Figure 4.4A, quantified in D) and not around all mitochondria. Recent studies have described how TNTs are formed in response to various stressors and are involved in mitochondrial transfer as a response to the stress factor [354, 355, 362]. Although this has not yet been studied with respect to mitochondrial import dysfunction, this could represent a means of compensating for the import perturbation induced by trapping. Interestingly, the proteomic screen (Figure 4.11 and Table 4.1) showed enhancement of calcium signalling proteins CamKIID and S100A2. Calcium signalling via the Ca^{2+}/Wnt pathway has been shown to regulate TNTs previously [459]. Additionally, cytoskeleton related proteins, required for TNT formation, such as Microtubule associated protein 4 and Cdc42 effector protein 1 were enhanced [354, 479, 480]. Finally, cell adhesion protein fibronectin, which has also been implicated in TNT formation and activity, associated with the trapped precursor [461]. This will be investigated further in Chapter 7.

4.4.5. Summary

The data in this chapter highlights the usefulness of stalling an engineered precursor to model failed import in cells. Using this system, I showed how chronic failed import leads to mitochondrial morphological changes and altered dynamics (increased fission), despite no changes in mitochondrial import or respiratory function. This suggests the activation of a stress response mechanism, which may rescue cells subjected to the trapping insult. This will be investigated further in Chapter 7. These results are informative in terms of determining the impacts of translocase blockage associated with neurodegenerative disease and allow us to obtain mechanistic insight into which changes can be directly linked to the import deficit in these scenarios. This disease link will be investigated further in Chapter 5 (in terms of a pathological protein) and Chapter 6 (impacts on primary neurons).

Chapter 5. Association of Tau^{P301L} with Mitochondrial Import Pathways

5.1. Introduction

As discussed in Chapter 4, numerous recent studies have described how disease-related, aggregation prone proteins interact with the translocation machinery of the presequence pathway, leading to mitochondrial dysfunctions including import and respiratory chain defects. For example, a recent study showed that, in mitochondria isolated from human AD patient brains, APP accumulates within mitochondria, forming stable complexes with TOM40, as well as with both TOM40 and TIM23 [215].

Similarly, a study showed import defects in mitochondria isolated from HD mice as well as in primary neurons expressing disease associated Htt variant, suggesting that import dysfunction is an early event in HD onset [224]. Furthermore, the authors showed that, in primary neurons, disease associated Htt protein aggregates within mitochondria and interacts with the TIM23 complex. This inhibits import and induces respiratory dysfunction as a result, which eventually triggers cell death [224]. The observed import and respiratory defects are rescued by overexpression of TIM23 [224].

A separate study in dopaminergic neurons from post-mortem PD patient brains, as well as in SH-SY5Y cells, showed how α-syn, when phosphorylated at S129, binds to TOM20. TOM20 is a vital receptor of the TOM complex, and this association perturbs the interaction between TOM20 and TOM22, impairing import and respiratory function as a result [222]. The SH-SY5Y cell line was originally derived and subcloned from the SK-N-SH neuroblastoma cell line, and serves as a common model for neurodegenerative diseases, since culturing these cells with specific supplements allow for their differentiation into certain types of neurons [481]. Additionally, the authors report that the import and respiratory chain defects can be rescued by either *in vivo* knockdown of endogenous α-syn, or *in vitro* TOM20 overexpression [222]. Together, these studies highlight the potential for import defects and translocation machinery to be targeted therapeutically in the treatment of neurodegenerative diseases.

Microtubule associated protein Tau is another aggregation prone protein associated with neurodegenerative diseases [233]. Studies in various model systems, from cell lines right up to human AD brains, showed that Tau often associates with mitochondria at the OMM and IMS [217, 218, 248]. One study showed association of Tau N-terminal fragment with mitochondrial fusion mediators OPA1 and Mfn1 [217]. Another study described the accumulation of Tau in the OMM and IMS and showed how Tau may have a role in misregulation of ER-mitochondria contacts and Ca^{2+} signalling in disease scenarios [218]. Despite these studies implicating Tau in mitochondrial dysfunction, it has not yet been studied with regards to its impact on mitochondrial import function.

5.2. Aims

The overarching aim of the work described in this chapter was to move beyond using a modified precursor to model failed import and mirror the analysis conducted in Chapter 4, but with a naturally occurring aggregation prone protein. I chose to investigate aggregation prone Tau, since its implications on import have not yet been directly studied, although several studies have observed Tau variant association with mitochondria [217, 218, 248].

I chose to use Tau^{P301L} in this study since this is the most common variant associated with disease [482, 483], and has been linked to mitochondrial deficiencies in the past [234]. **P301L**, P301S, and ΔK280 mutations in Tau encoding gene MAPT are commonly observed in frontotemporal dementia with parkinsonism-17 (FTDP-17). These forms of Tau all have the PHF6* hexapeptide motif present [484], which causes enhanced β-sheet propensity. This correlates with a lower affinity for microtubules and Tau is more likely to assemble into filaments. This enhances Tau aggregation and increases the likelihood of accelerated NFT formation [244, 485]. Therefore, the Tau^{P301L} variant is commonly used as a model of disease-prone Tau and has been well characterised in cell and mouse model systems [483, 486-488].

The main aims of this chapter were:

1. To investigate the impact of overproducing the aggregation prone protein variant Tau^{P301L} on HeLa cells in terms of its impacts on mitochondrial import.

2. To explore the impact of Tau^{P301L} overexpression on mitochondrial morphology and respiratory function.

5.3. Results

5.3.1. Disease Prone Tau Variant Tau^{P301L} Forms Aggregates in HeLaGAL Cells

The first step was to test the expression and localisation of Tau^{WT} and Tau^{P301L} variants in my experimental setup. Confocal microscopy was carried out on HeLaGAL cells overexpressing Myc-Tau^{WT} or Myc-Tau^{P301L}, where the POI was visualised by immunofluorescent staining against an antibody targeting Myc.

The resulting images showed the Tau signal diffuse throughout the cytoplasm in cells expressing both Tau variants. Additionally, cells displayed areas of high signal intensity, indicative of Tau protein aggregates, which were present in HeLaGAL cells overexpressing both wildtype and disease-prone Tau. The proportion of cells with Tau^{P301L} aggregates is higher (60%) than those with Tau^{WT} aggregates (17.5%; Figure 5.1A, quantified in B). Due to the limited resolution, it is not clear from these images whether a proportion of the Myc signal, or indeed the aggregated protein, correlates with or is excluded from mitochondria (identified by co-expression of mito-DsRed).

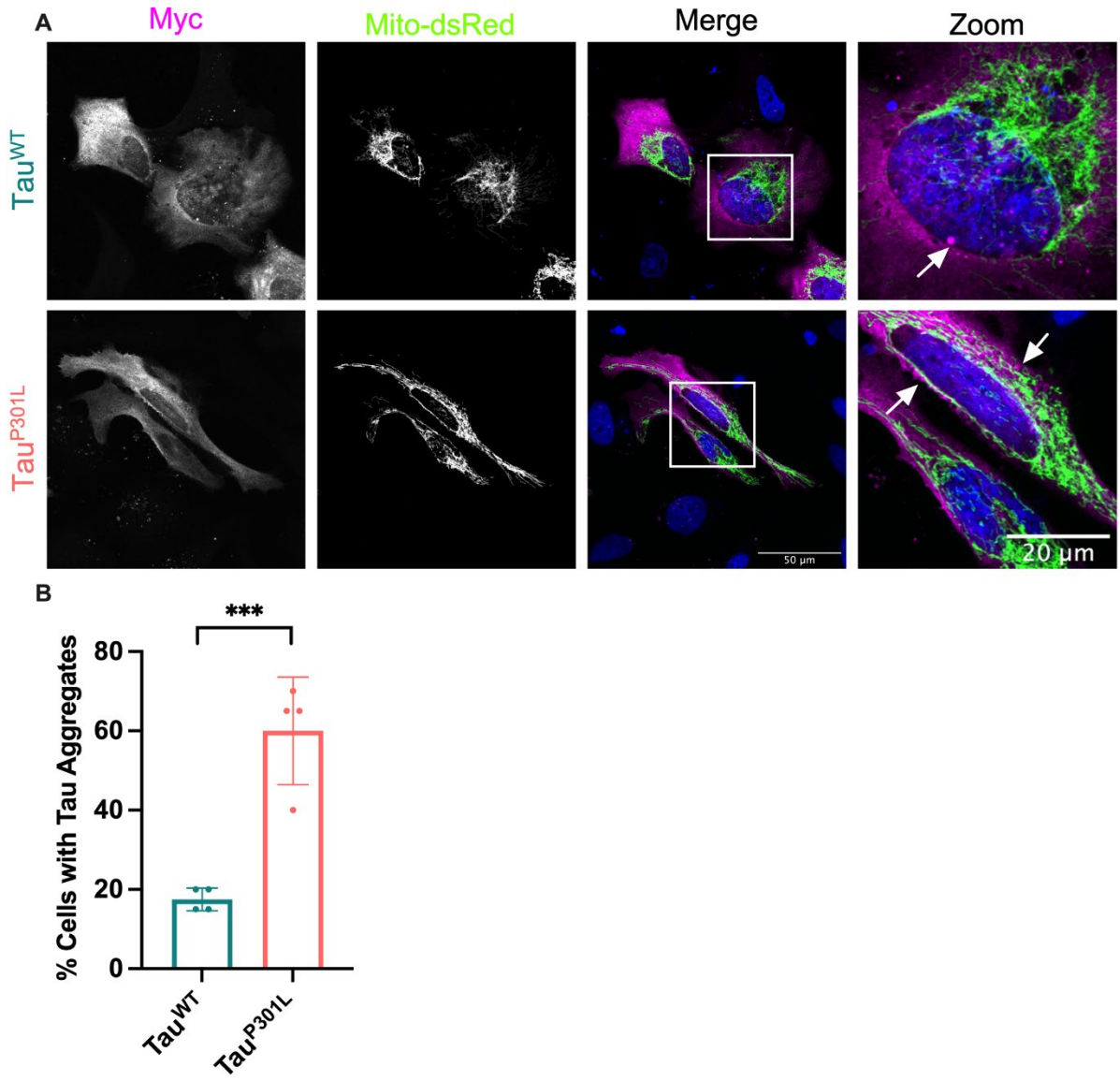

Figure 5.1: Both Tau Variants Form Aggregates in HeLaGAL Cells
(A) Representative confocal microscopy images of HeLaGAL cells expressing Myc-Tau^{WT} or Myc-Tau^{P301L} (Myc staining shown in magenta) and mito-dsRed (mitochondria; green). Nuclei are stained with DAPI (blue). *N=4 biological replicates.*
(B) Quantification of the percentage of cells with Tau aggregates. *Data was blinded, and percentages were taken from 4 biological replicates, each representing the average from 10 images containing at least 10 cells. Error bars show SD. Unpaired t-test was used to determine significance.*

5.3.2. Mitochondrial Tau^{P301L} is Increased Despite Fewer Translocases

To further investigate correlation between the Tau variants and mitochondria, I carried out Western blotting analysis on mitochondrial and cytosolic fractions isolated from cells expressing Myc-Tau^{WT}, Myc-Tau^{P301L}, or a GFP only control (Figure 5.2A-C). The Western blots showed that, in HeLaGAL cells overexpressing Myc-Tau^{P301L}, there was a higher proportion of the Tau protein localised to mitochondria compared to those expressing Myc-Tau^{WT} or GFP (Figure 5.2A, quantified in B). To test whether this increased localisation of Tau^{P301L} to mitochondria correlates with altered import pathways, I expanded this analysis to include translocase subunits (Figure 5.2A, quantified in C). Overall, mitochondria from cells overexpressing Tau^{P301L} had lower levels of mitochondrial translocase subunits TOM20 and TIM23 compared to control cells (Figure 5.2A and C), but there was no change in TOM40 abundance. Together, these data are indicative of import changes, potentially defects, associated with Tau^{P301L}.

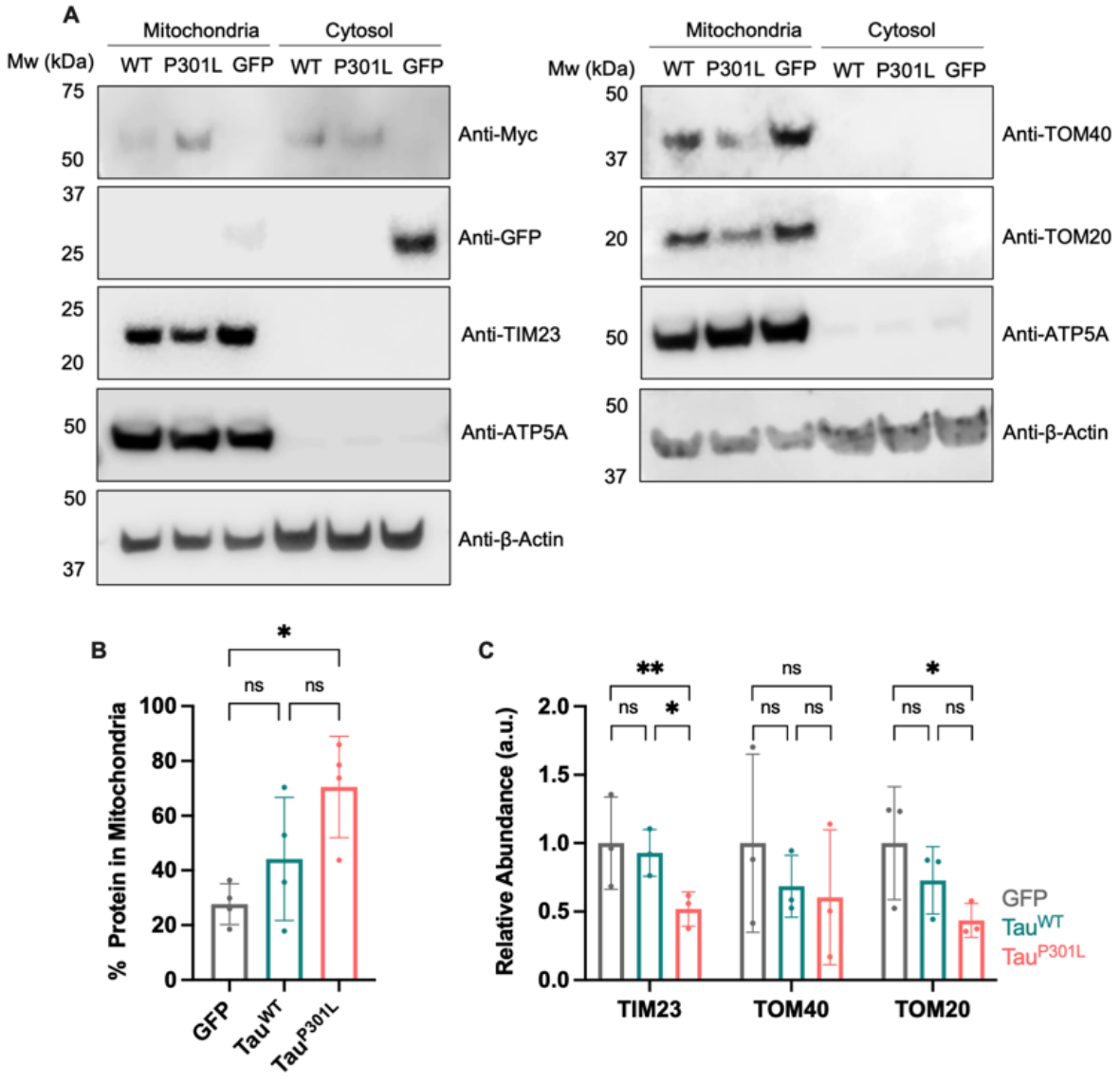

Figure 5.2: Tau^{P301L} Expression Alters Mitochondrial Import in HeLaGAL Cells
(A) Western blots showing relative protein abundance in mitochondria and cytosol of HeLaGAL cells expressing GFP, Tau^{WT} and Tau^{P301L}. Localisation of GFP, Tau^{WT} and Tau^{P301L} was analysed by probing for GFP or Myc. Translocase subunits abundance was analysed by probing for TIM23, TOM40, and TOM20. ATP5A and β-actin were used as loading controls for mitochondria and cytosol, respectively. *N=4 (GFP/Myc) and N=3 (translocases) biological replicates.*
(B) Quantification of % GFP, Tau^{WT} or Tau^{P301L} in mitochondrial fraction. Normalised to loading controls. *Error bars show SD. One-way ANOVA and Tukey's post hoc test were used to determine significance.*
(C) Quantification of translocase subunits (TIM23, TOM40, TOM20). *As in (B).*

5.3.3. Tau^{P301L} Associates with the TOM40 Channel in HeLaGAL Cells

I proceeded to investigate the interaction between Tau^{P301L} and the translocation machinery of the presequence pathway by carrying out Myc-trap pulldown assays on mitochondria isolated from cells expressing Myc-GFP, Myc-Tau^{WT}, or Myc-Tau^{P301L} (experimental outline is shown in Figure 5.3A). Examining the quantities of the mitochondrial translocation machinery co-purified with the Myc-tagged protein showed that Tau^{P301L}, but not its wildtype counterpart or the GFP control, associates with TOM40 in the mitochondria of HeLaGAL cells (Figure 5.3B). This is consistent with previous reports which showed Tau^{P301L} accumulation in the OMM and IMS [217, 218], and suggests that it may be associated with the translocation channel in a similar way to the trapped precursor.

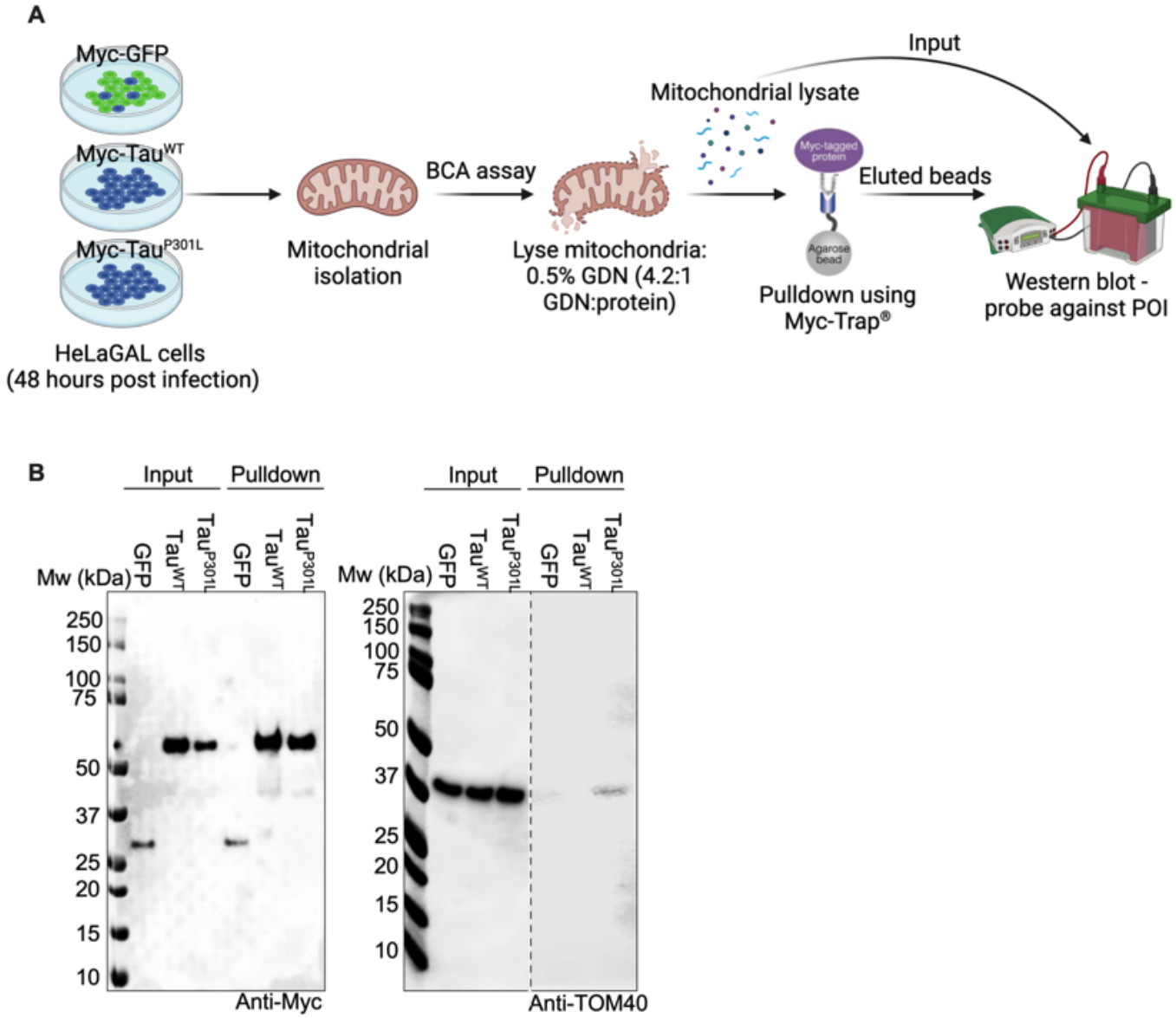
A
Myc-GFP
Myc-Tau^WT
Myc-Tau^P301L
HeLaGAL cells
(48 hours post infection)
Mitochondrial isolation
BCA assay
Lyse mitochondria:
0.5% GDN (4.2:1
GDN:protein)
Mitochondrial lysate
Input
Myc-tagged protein
Agarose bead
Pulldown using
Myc-Trap®
Eluted beads
Western blot -
probe against POI
B
Input
Pulldown
GFP
Tau^WT
Tau^P301L
Mw (kDa)
250
150
100
75
50
37
25
20
15
10
Anti-Myc
Anti-TOM40

Figure 5.3: Tau^{P301L} Associates with TOM40
(A) Experimental outline for Myc-pulldown assays on mitochondria from Tau variant expressing cells. HeLaGAL cells were subjected to lentiviral expression of Myc tagged GFP, Tau^{WT}, or Tau^{P301L} for 48 hours prior to harvesting cells. Mitochondria were isolated from cells and mitochondrial protein content was assessed using a BCA assay. Equal amounts of mitochondria were lysed using 0.5% GDN at a ratio of 4.2:1 (GDN: protein). A fraction of mitochondrial lysate was saved as an input control, and the rest was loaded onto Myc-trap agarose beads, to pull-down proteins associated with the Myc tagged protein of interest. The resulting beads conjugated to proteins associated with Myc-tagged proteins were analysed by Western blotting.
(B) Western blots showing expression of Myc tagged GFP, Tau^{WT}, and Tau^{P301L}, and TOM40, in input and pulldown samples from experiment described in (A). Representative Western blots are shown. *N=4*.

5.3.4. *Import Activity is Unchanged in HeLaGAL Cells Overexpressing Tau^{P301L}*

To test whether the association between TauP301L and TOM40, as well as the reduced abundance of translocase subunits TOM20 and TIM23, alters import function, I used the permeabilised cell NanoLuc assay system (as described in Figure 3.9) to assess import efficiency in cells expressing TauP301L, TauWT, and GFP (control). HeLaGAL cells were first subjected to LgBit expression, then, after 24 hours, were infected with lentivirus for expression of Myc-TauP301L, Myc-TauWT, or Myc-GFP. Following a further 48-hour incubation, import assays were carried out using the permeabilised cell NanoLuc assay system, to monitor the import of the Su9-EGFP-6xHis-HiBit precursor protein in cells expressing the various Tau variants.

The data displayed in Figure 5.4 demonstrates that exposure to Tau variants had no significant impact on the import of a precursor protein. This was unexpected, considering the reduction in translocase subunits in the mitochondria of Tau^{P301L} expressing cells, as well as association between Tau^{P301L} and key import channel subunit TOM40. However, this is consistent with what was observed following chronic precursor trapping (Figure 4.5), and together, these results are indicative of a rescue mechanism responding to import stress within these cells.

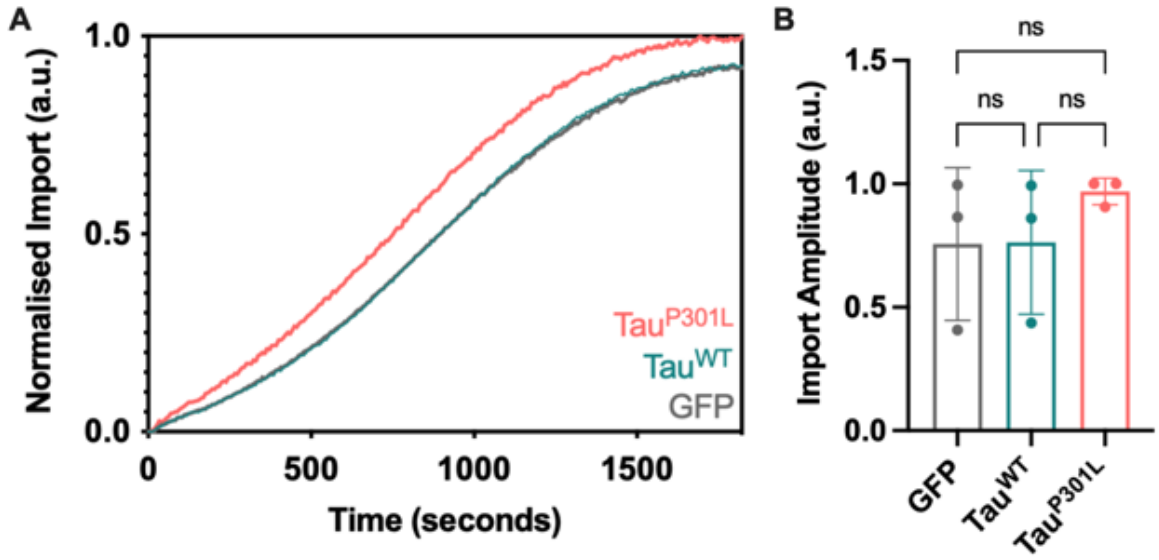

Figure 5.4: Import is Unchanged in HeLaGAL Cells Exposed to Tau^{P301L}-TOM40 Association
(A) NanoLuc import assay trace showing import of a precursor protein in HeLaGAL cells expressing GFP, Tau^{WT}, or Tau^{P301L}. Averaged, normalised traces are shown (normalised to eqFP670 expression and max amplitude/run). *N=3 biological repeats, each with n=3 technical replicates*.
(B) Maximum import amplitude plotted from import traces. *Error bars display SD. One-way ANOVA with Tukey's post hoc test were used to determine significance.*

5.3.5. Mitochondrial Network is Less Complex in Cells Expressing Tau^{P301L}

In line with the similar TOM40 pore blocking mechanism observed after trapping as well as when we express Tau^{P301L} (Figure 4.1 and Figure 5.3), I wondered whether the mitochondrial morphological changes observed after stalling the import of a modified precursor, Su9-mScarlet-DHFR (Figure 4.6), would be mirrored following Tau^{P301L} association with TOM40 (Figure 5.3). To examine this, I carried out confocal microscopy on cells co-expressing mito-dsRed with either GFP, Tau^{WT}, or Tau^{P301L}, and imaged the fixed cells on a confocal microscope (Figure 5.5). Unfortunately, due to time constraints and Covid-related travel restrictions, I was unable to carry out SIM, which limits the resolution of data and subsequent analysis capabilities.

Nonetheless, analysis of mitochondrial branching showed that cells expressing Tau^{P301L} have significantly fewer branches per mitochondrial network on average, when compared to mitochondria from cells expressing Tau^{WT} or GFP (3.9 compared to 5.9 and 6.6, respectively; Figure 5.5B). The maximum number of branches per network is also reduced to 127.3 for Tau^{P301L}, compared to 276.9 for Tau^{WT} and 298.3 for GFP (Figure 5.5C).

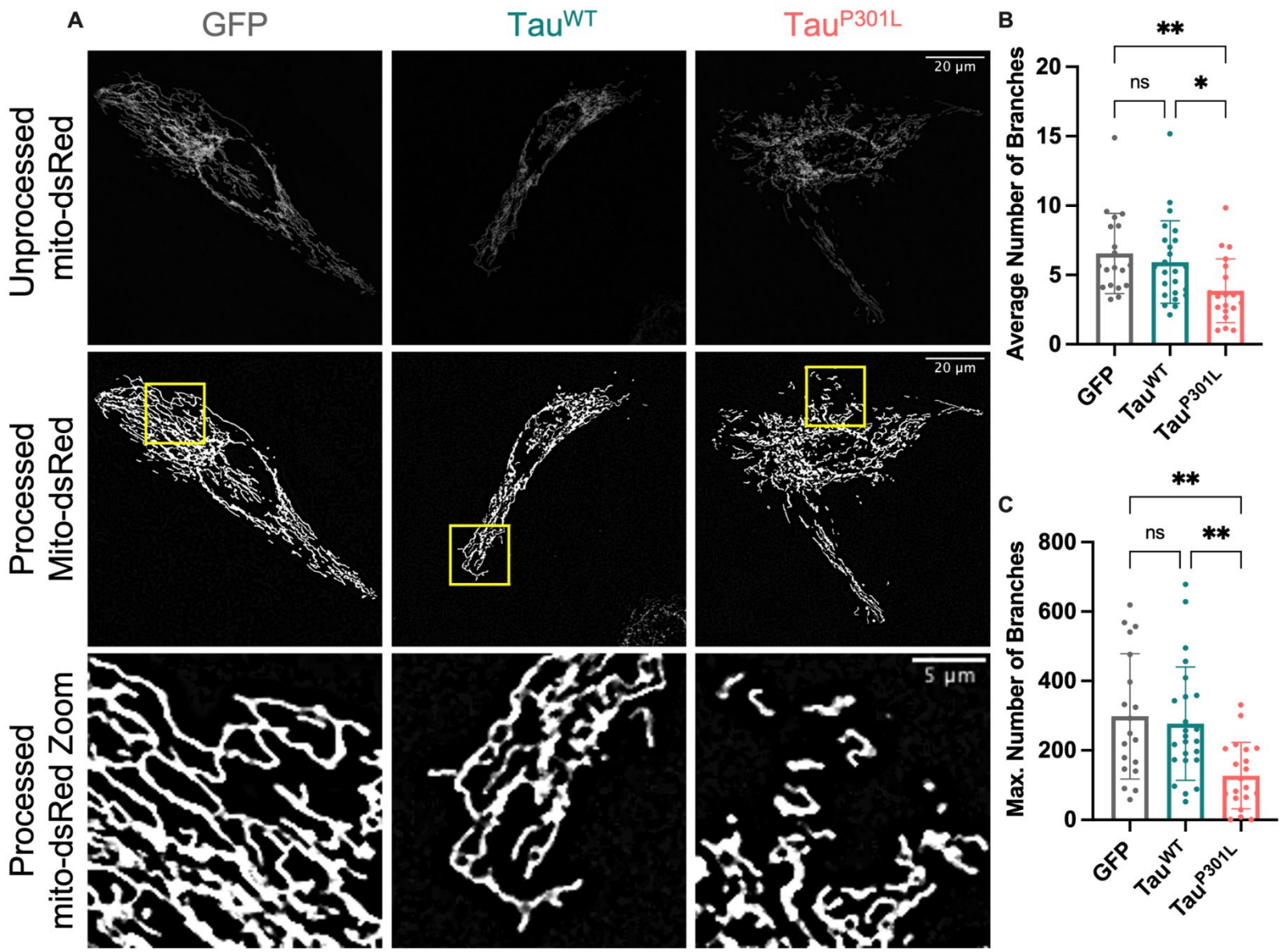
A
GFP
TauWT
TauP301L
Unprocessed mito-dsRed
Processed Mito-dsRed
Processed mito-dsRed Zoom
20 µm
20 µm
5 µm
B
Average Number of Branches
**
ns
*
GFP
TauWT
TauP301L
C
Max. Number of Branches
**
ns
**
GFP
TauWT
TauP301L

Figure 5.5: Mitochondrial Branching is Decreased in HeLaGAL Cells Expressing Tau^{P301L}
(A) Confocal microscopy showing mitochondria in HeLaGAL cells expressing mito-dsRed and GFP (left, grey), Tau^{WT} (middle, teal) or Tau^{P301L} (right, pink). The top panel shows mito-dsRed (mitochondria) prior to processing. The middle panel shows mitochondria after processing, allowing for clearer visualisation of the mitochondrial morphology. The bottom panel shows a zoom of an area of mitochondria (highlighted in the middle panel) to give a clear view of mitochondrial morphology. *Representative images taken from N=5 biological repeats.*
(B) Quantification of the average number of mitochondrial branches. Representative images shown in (A). *Each point represents an individual cell from a separate z-stack. N=20, 24, 23 for different conditions, respectively, taken from 5 independent biological repeats (N=5). Error bars show SD. One-way ANOVA and Tukey's post hoc test were used to determine significance.*
(C) Quantification of the maximum number of mitochondrial branches in a network. *As in (B).*

5.3.6. Respiratory Function is Unchanged in Tau^{P301L} Cells

Next, I investigated the respiratory capacity of these cells by carrying out mitochondrial stress tests using high resolution respirometry on a Seahorse XFe96 analyser. HeLaGAL cells were subjected to expression of Myc-GFP, Myc-Tau^{WT}, or Myc-Tau^{P301L} by lentiviral infection for 48 hours prior to carrying out Seahorse assays. Figure 5.6A shows that there is no alteration in the OCR of these cells in response to Tau variant overexpression. As mentioned for trapping, even with lentiviral transduction, not all cells will be expressing the protein of interest and the effect may be somewhat diluted by untransduced cells. Alternatively, respiratory function may have been rescued at this point.

Furthermore, analysis of TMRM signal showed that the ΔΨ of cells expressing Tau^{WT} or Tau^{P301L} was unchanged compared to the GFP control (Figure 5.6B and C). These data mirror those described earlier for cells subjected to precursor trapping (Figure 4.9), consistent with a common pathway.

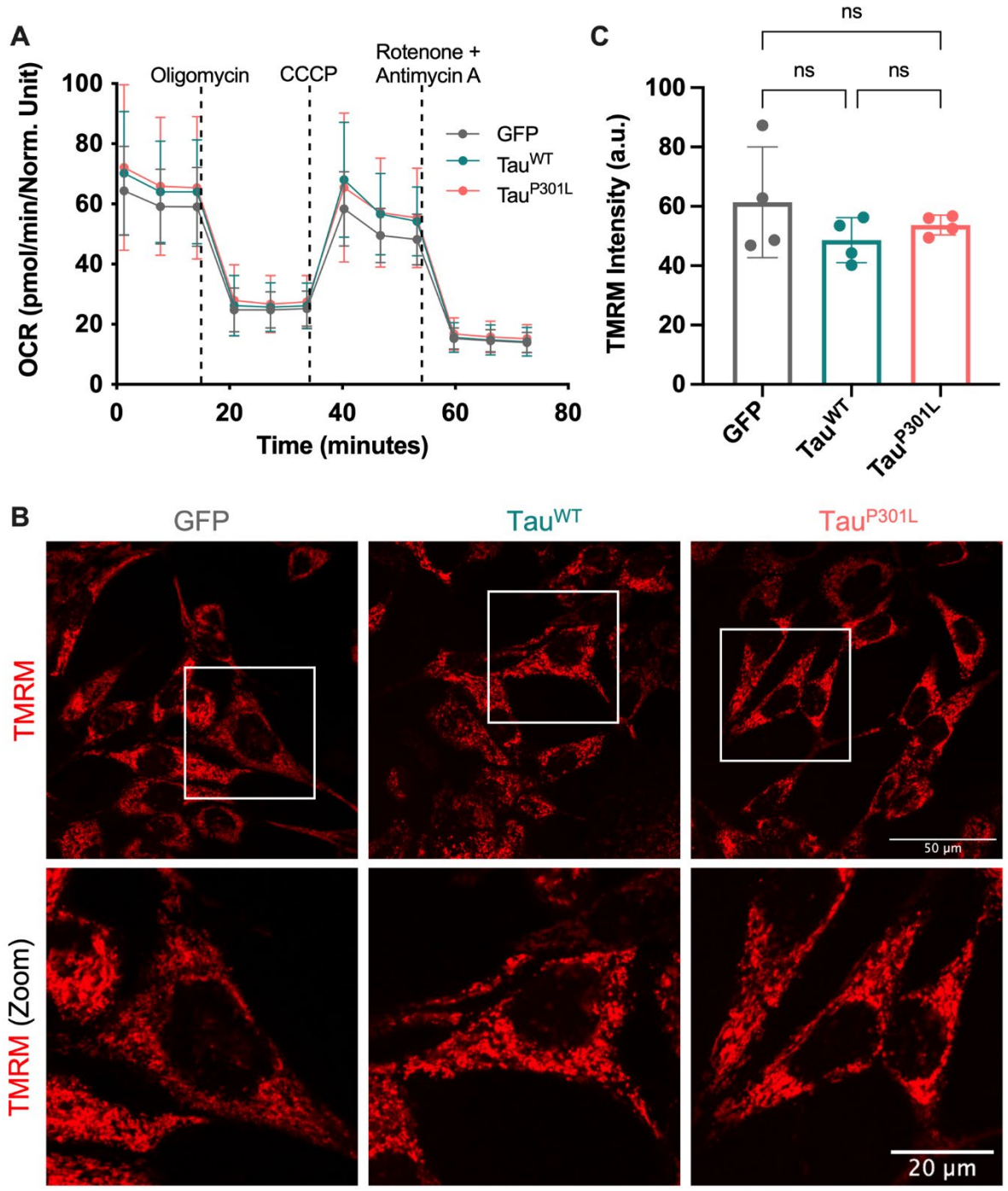

Figure 5.6: Tau Variants have no Impact on Mitochondrial Respiratory Function or ΔΨ
(A) Mitochondrial stress test (Seahorse XFe96 analyser) showing OCR of HeLaGAL cells expressing Myc-GFP, Myc-Tau^{WT}, or Myc-Tau^{P301L}. Data is normalised to protein content as determined by SRB assays. *Error bars show SD. N=6 biological replicates, each with n=3 technical replicates.*
(B) Representative confocal images showing TMRM fluorescence (red) in the mitochondria of HeLaGAL cells expressing Myc-GFP, Myc-Tau^{WT}, or Myc-Tau^{P301L}. CCCP was added after 2 minutes to control for background fluorescence. *N=4 biological replicates.*
(C) Quantification of (B). Analysis was carried out using a macro on FiJi (described in Section 2.9.5.2). *Error bars show SD. One-way ANOVA and Tukey's post hoc test were used to determine significance.*

5.4. Discussion

5.4.1. Key Findings

The main aim of this chapter was to investigate the impact of disease prone Tau variant Tau^{P301L} on the mitochondrial import apparatus, as well as on mitochondrial morphology and function. The key findings from this chapter are:

- Tau^{P301L} localises partially to mitochondria, associating with TOM40 and leading to alterations in mitochondrial translocase abundance, despite no changes in import function.

- Tau^{P301L} overexpression is associated with changes in mitochondrial morphology (less branched mitochondria) but not in respiratory function, mirroring what was observed with precursor trapping.

5.4.2. Tau^{P301L} Expression and Localisation in HeLaGAL Cells

Having characterised the impact of failed import on mitochondria using an engineered trapping substrate, I next wanted to investigate the physiological relevance of this in terms of disease prone protein association with import machinery. To this end, I decided to investigate the impact of disease prone variant Tau^{P301L} on mitochondria. Tau^{P301L}, being the most frequently observed mutation in patients with FTD as well as being associated with AD, has been extensively characterised previously [482, 483, 487, 489]. Although it is known to localise to the IMS and OMM [217, 218], no direct associations with the translocation machinery have yet been discovered.

Initial imaging experiments were carried out to confirm the localisation of the Tau variants. The confocal data shown in Figure 5.1 demonstrated an increase in Tau aggregates in cells overexpressing the Tau^{P301L} variant compared to the wildtype variant (which still has aggregates in ~20% of cells). These aggregates appear to be distributed throughout the cell, and it is difficult to determine from these images whether any of the aggregates are colocalising with mitochondria. The Western blotting data in Figure 5.2 indicates that a fraction of Tau does indeed localise to mitochondria, to a greater extent in Tau^{P301L} cells. To corroborate this by microscopy, SIM would be useful. These experiments are currently being undertaken by our collaborators at the University of Bielefeld.

5.4.3. Tau^{P301L} Impacts on Mitochondria

5.4.3.1. Mitochondrial Import

The fact that the data shows an increased localisation of Tau^{P301L} to the mitochondria (Figure 5.2), and that it associates with TOM40 (Figure 5.3), suggests that it is likely to be localised to the OMM, as has been shown previously [217, 218]. A recent study used NanoLuc technology in binding assays to investigate extracellular Tau entry into the cytosol in HEK293 and neuronal cells [432]. Using Tau-HiBit proteins kindly gifted from the authors of this study, I attempted to confirm the submitochondrial localisation of the Tau variants by NanoLuc import assays. Unfortunately, these experiments were unsuccessful, likely due to unpredictable aggregation behaviour of the Tau proteins, which will impact on NanoLuc formation. These experiments, or simpler experiments such as mitochondrial sub-fractionation using a detergent titration and Western blotting analysis, would be useful future work to confirm the submitochondrial localisation of Tau in these cells.

The association between Tau^{P301L} and TOM40 (Figure 5.3) is in accordance with previous studies showing TOM40 association with similar aggregation prone proteins characteristic of neurodegeneration, such as APP, Huntingtin, and alpha-synuclein [215, 220, 224]. To further dissect this interaction, it would be interesting to examine whether the association between Tau^{P301L} and TOM40 is dependent on energised mitochondria, and whether it is associated with active TOM-TIM23, by repeating the pulldown on samples prepared in the presence of CCCP or small molecule TOM/TIM23 inhibitors (such as those described in Figure 3.11).

Together, these data indicate that Tau^{P301L} is correlated to aberrant mitochondrial translocation pathways, however, the results are not clear cut. Overexpressing Tau^{P301L} in HeLaGAL cells leads to no change in the import of a precursor protein (Figure 5.4), despite a reduction in the expression of key translocase subunits TOM20 and TIM23 (Figure 5.2A and C). This incongruence between import function and translocase subunits expression has been observed previously [229], however there is currently no clear explanation, and it warrants further investigation. It may suggest that there is a stress response mechanism initiated due to the Tau^{P301L} association with import sites, that accounts for the normal import of the chasing precursor observed when Tau^{P301L} is overexpressed. As discussed above with regards to the DHFR-MTX induced import perturbation, this will be investigated in detail in Chapter 7.

5.4.3.2. Mitochondrial Morphology

Considering the association between Tau^{P301L} and TOM40, the fact that the mitochondrial morphological changes, that is a reduction in mitochondrial network complexity (Figure 5.5), mirror those observed with precursor trapping (Figure 4.6) suggests that this may be a direct result of the association with import sites in these cells. However, the precise mechanism linking precursor association with import sites and morphological changes remains unclear and requires further investigation.

These data are particularly intriguing since the changes here directly oppose what has been shown previously, whereby Tau was shown to increase levels of various fusion proteins and trigger DRP1 mislocalisation, leading to elongation of the mitochondrial network [246, 490]. Here, my data suggests fragmentation of the mitochondrial network, however this cannot be confirmed definitively, since proteins associated with mitochondrial dynamics were not directly investigated. Consistent with this speculation, a study carried out in cortical neurons from $tau^{-/-}$ KO mice, showed that expression of disease-associated Tau variants (pseudo-phosphorylated or caspase cleaved Tau) induced mitochondrial fragmentation associated with a reduction in OPA1 expression [491]. Together, these studies and my data suggest there may be a multitude of distinct pathways by which Tau associates with and alters mitochondrial dynamics, and these need to be unravelled further to improve understanding of the relationship between Tau and mitochondria in physiological and disease scenarios. Further parameters to analyse mitochondrial morphology, as done for trapping with DHFR-MTX, would be helpful in further dissecting the mechanism behind this. These experiments are currently being carried out by our collaborators in Bielefeld.

5.4.3.3. Mitochondrial Respiratory Function

Despite the association between Tau^{P301L} and the TOM40 channel, as well as the reduction in translocase subunits, there is no change tor respiratory function. This is surprising considering the functional interplay between respiratory complexed assembly and function and translocation pathways [1], but is consistent with the overall normal import function in these cells. This data also mirrors that observed in cells with a trapped precursor and provides further evidence for activation of a stress response mechanism induced by perturbation of mitochondrial import sites.

5.4.4. Implications in Disease

It would be interesting to investigate whether the interaction between Tau^{P301L} and TOM40 is conserved in primary neuronal cells. This is because this association may provide a vital link between mitochondrial import failure and neurodegeneration, which could have therapeutic potential, especially considering recent work on mitochondrial disaggregases [492]. AAA+ protein Skd3 was shown to disaggregate α-syn fibrils *in vitro* [492]. This shows its potential as a therapeutic in synucleinopathies. Although it has only been studied with respect to α-syn so far, a similar approach could have the potential to reduce or remove proteins aggregates such as Tau^{P301L} (shown in HeLa cells (Figure 5.3) but not yet observed in primary neurons), APP [215], or Huntingtin [224] from mitochondrial import sites, reducing the toxic effects on cells. This could be tested using the DHFR-MTX model system.

The Tau-TOM40 IP experiments were attempted in primary neuronal cultures, but due to the large quantities of starting material (comparatively limited number of neurons can be isolated from the brains of rat embryos) required for the experiments, a clear result was not obtained in the timeframe of this PhD. Nevertheless, the evidence highlighting a Tau-TOM40 interaction in HeLa cells indicates that the DHFR-MTX trapping system is a useful tool for further investigation into the impact of failed impact on cells in terms of neurodegenerative disease.

5.4.5. Summary

The data in this chapter highlights a strong link between failed import and pathological Tau. Much of the data mirrors what was shown for trapping, highlighting that the effects are likely to be directly linked to the association of Tau^{P301L} or DHFR-MTX with TOM40. The importance of this link in primary neurons will be explored in Chapter 6. Finally, the data here provides further evidence for a potential rescue mechanism involved in cell survival and mitochondrial function following import perturbations, which was first noticed with precursor trapping and will be explored further in Chapter 7.

Chapter 6. The Role of Mitochondrial Import in Neuronal Health & Disease

6.1. Introduction

Neurodegeneration involves the progressive loss of neurons in specific regions of the brain. This precise neuronal loss is the determining factor responsible for the symptoms observed in patients, that is problems with movement (ataxias) or cognition (dementias) [199, 200]. On a cellular level, there are a multitude of phenotypic changes or hallmark features observed in cells at all stages of neurodegeneration (Figure 1.7) [201, 202]. These disease phenotypes are important in modelling neurodegeneration, as well as identifying contributary factors at all levels of research. In addition, these features are essential for the identification of clinical biomarkers or therapeutic intervention pathways at early stages of neurodegeneration.

One of the most widely conserved phenotypes amongst neurodegenerative diseases is the accumulation of aggregated proteins in neurons, which are highly cytotoxic and eventually kill the cells [200]. An example is senile plaques and NFTs in AD [210]. More recently, studies have begun to associate the accumulation of these protein aggregates with another characteristic feature, mitochondrial dysfunction [211-213]. This was discussed in detail in Chapter 5, where the data presented showed association of aggregation prone Tau^{P301L} with key TOM pore forming subunit, TOM40. This is akin to what has been shown previously for both APP and Htt, key players in aggregate accumulation in AD and HD, respectively [215, 224]. Aside from import defects, mitochondrial dysfunction associated with neurodegeneration is very broad and includes: OXPHOS deficiencies, excessive ROS production, changes in mitochondrial dynamics, aberrant mitophagy, and mtDNA mutations [211-213, 493].

Disease related neuronal phenotypic changes involve alterations in axons and dendrites. In neurodegeneration, axonal and dendritic injury occurs and results in degeneration and eventually loss of both axons and dendrites [494]. Additionally, damage or loss of synapses results in dysfunctional neuronal transmission, associated with cognitive and movement deficits [207-209]. Finally, recent research has begun to associate a conserved inflammatory response with neurodegeneration, whereby alterations in cytokine signalling and phagocytosis as well as immune cell proliferation are all thought to be key features in neurodegeneration associated immune pathway dysregulation [214, 495].

Though these phenotypic changes are relatively well characterised, the complexity of neurodegenerative disease renders it difficult to determine which phenotypic changes are attributable to which cellular mechanistic changes. For example, since the accumulation of aggregated proteins are known to affect many cellular pathways, it is difficult to determine which of these disease phenotypes, if any, are attributable to the impacts of aggregated proteins on mitochondrial import.

6.2. Aims

In Chapter 4, I showed how the DHFR-MTX trapping system can be used to model failed import in the precursor pathway. Then, in Chapter 5, I showed how disease prone Tau variant Tau^{P301L} acts similarly to the engineered trapped precursor, associating with TOM40 and leading to similar phenotypic changes. These data provide a strong, direct link between import defects and Tau pathogenesis, and the next step was to explore this link further in terms of neurodegenerative disease and associated phenotypic changes. To do this, I investigated the impact of perturbing mitochondrial import in a direct, isolated manner by trapping with DHFR-MTX or in an indirect, contextualised manner by expressing Tau^{P301L} in primary neurons. The goal was that this would allow determination of which of the phenotypic features observed following Tau overexpression can be correlated with its impacts on the import machinery, albeit in an indirect manner.

The main aims of this chapter were:

1. To study the impact of precursor trapping and Tau variant overexpression on neuronal viability.

2. To explore how neuronal morphological changes are associated with import perturbation.

3. To investigate the impacts of precursor trapping and Tau^{P301L} overexpression on synapse abundance and localisation.

6.3. Results

6.3.1. Neuronal Viability is Unaffected by Import Insults

First, I carried out viability assays over a period of 15 days on primary cortical neurons, to investigate the impact of precursor trapping or Tau^{P301L} overexpression on neuronal viability (Figure 6.1). DIV5 primary cortical neuronal cultures were subjected to lentiviral transduction, for expression of EGFP-DHFR-HiBit, Su9-EGFP-DHFR-HiBit (+/- MTX pre-treatment), Myc-GFP, Myc-Tau^{WT} or Myc-Tau^{P301L}. Cells were subsequently fixed at various timepoints, and cell density was analysed in terms of cellular protein content by SRB assays. Figure 6.1A shows that, though there was a significant reduction in neuronal growth correlated with MTX treatment, the trapping insult itself had no further impact on neuronal viability. Similarly, overexpression of Tau^{WT} or Tau^{P301L} proteins in neurons had no impact on neuronal viability or growth (Figure 6.1B).

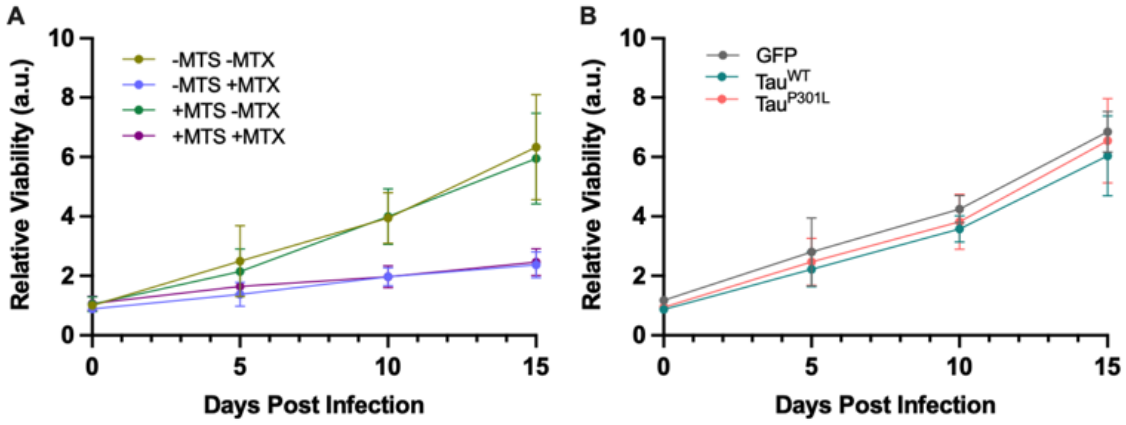

Figure 6.1: Import Perturbations do not Impact Neuronal Viability
(A) Viability of primary cortical neurons expressing EGFP-DHFR-HiBit (-MTS) or Su9-EGFP-DHFR-HiBit (+MTS) +/- MTX, as determined by cell density, quantified by SRB assays. Data was normalised to the average reading for the 0 days post infection timepoint, to give relative viability of the neurons in response to the varying expression/treatment. *N=4 biological replicates. Error bars show SD.*
(B) As in (A), for cells expressing GFP, Tau^{WT}, or Tau^{P301L}.

6.3.2. Precursor Trapping Leads to Reduced Neuronal Complexity

Next, to investigate the impact of precursor trapping on neuronal morphology, I carried out confocal microscopy on DIV21 primary hippocampal neurons following 7 days of trapping. DIV21 neurons equate to 'mature' neurons with spines and fully formed synapses, as has been established previously [496, 497]. Therefore, this age was chosen to allow analysis of synapses and neuronal complexity. Axons are identified by staining for Ankyrin G, a scaffolding protein important in formation of the initial segment of the axon [498]. Ankyrin G is an established and commonly used marker of the initial segment (the proximal base) of the axon and used as an identification tool in differentiating between axons and dendrites in neuronal imaging.

Neuronal complexity was measured by counting the number of processes per cell. That is, the number of processes directly extending from the cell soma, counted by overlapping processes at a given radius from the soma (highlighted by the circle drawn in Figure 6.2A). The data showed that there is a reduction in the number of processes per cell following trapping (7.2 (+MTS +MTX) compared to 12.3 (+MTS -MTX), 11.3 (-MTS +MTX) and 14 (-MTS -MTX); Figure 6.2A, quantified in B).

Axon length was measured using the Simple Neurite Tracer (SNT) plugin on FiJi (described in Section 2.9.5.4), using the mCherry whole cell (cytosolic) stain as a fluorescent marker. Figure 6.2 (panel A, quantified in C) shows that trapping reduces axonal length, from an average of 239 µm in Su9-EGFP-DHFR-HiBit expressing cells without MTX to 148 µm following trapping (Su9-EGFP-DHFR-HiBit +MTX). This was not due to MTX treatment, as shown by the -MTS controls, where in the absence of MTX axons are on average 279 µm, compared to 300 µm in the presence of MTX. Taken together, these data indicate a reduction in neuronal complexity directly associated with failed precursor import.

Additionally, observation of the localisation of the trapping protein (EGFP channel, top panel) highlights that this protein is localised mainly to the area around the soma in the presence of MTX (*i.e.,* when the precursor is trapped). This is in comparison to the same protein (Su9-EGFP-DHFR-HiBit; +MTS) in the absence of MTX, where it appears to be localised to mitochondria around the whole neuron, extending to the distal axon and dendrites.

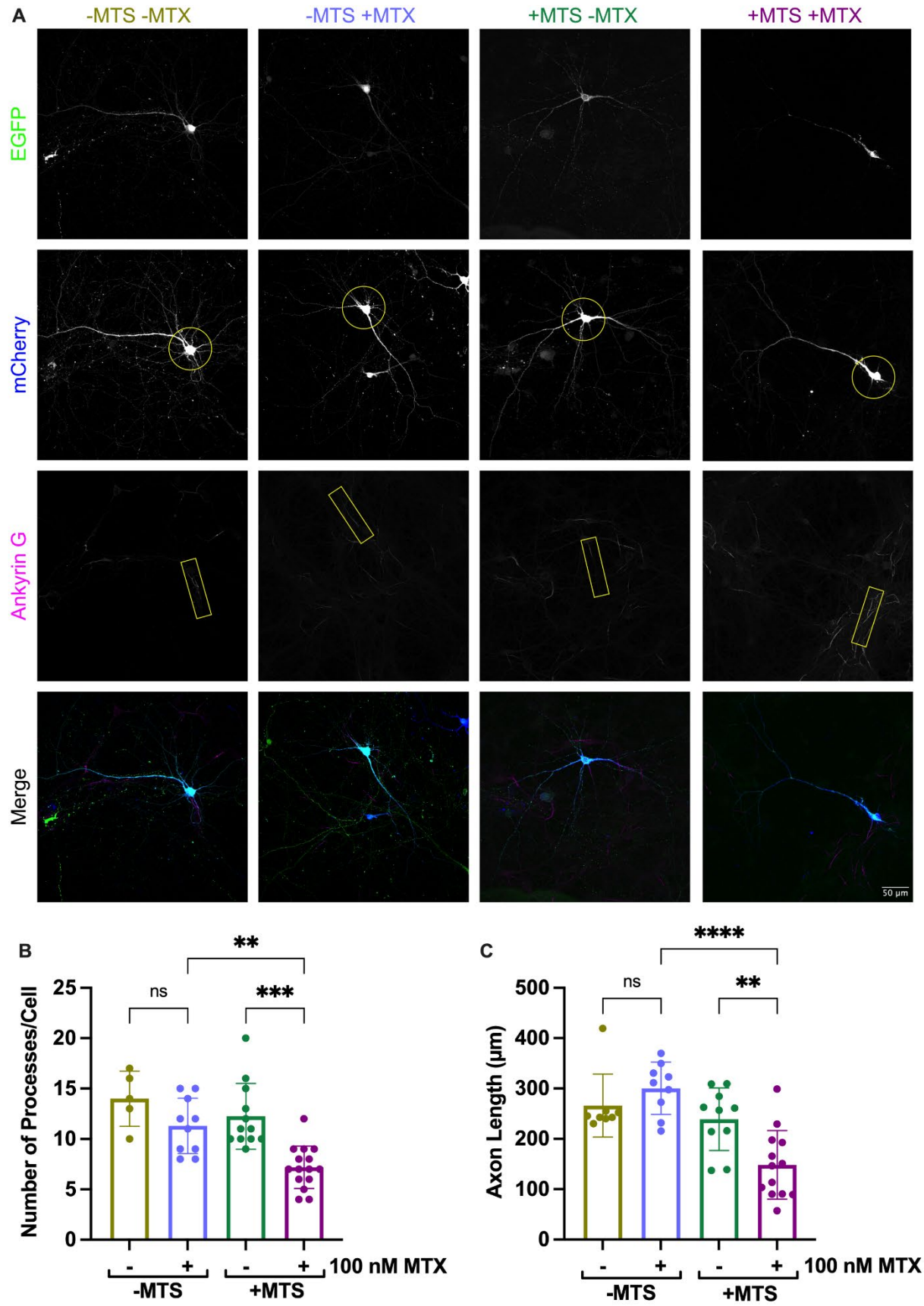
A
-MTS -MTX
-MTS +MTX
+MTS -MTX
+MTS +MTX
EGFP
mCherry
Ankyrin G
Merge
50 µm
B
Number of Processes/Cell
ns
**
***
100 nM MTX
-MTS
+MTS
C
Axon Length (µm)
ns
****
**
100 nM MTX
-MTS
+MTS

Figure 6.2: Neurons Subjected to Trapping have Fewer Processes and Shorter Axons
(A) Representative confocal images showing the morphology of DIV21 primary hippocampal neurons expressing mCherry (whole cell cytosolic marker; blue; circle used to highlight complexity in second panel down *i.e.,* the number of processes that cross the circle is representative of number of processes per cell) as well as EGFP-DHFR-HiBit (-MTS; green; top panel) or Su9-EGFP-DHFR-HiBit (+MTS; green; top panel) +/- MTX. Axons were stained with Ankyrin-G (magenta; highlighted by box in third panel down). *N=5 biological replicates*.
(B) Quantification of the number of processes per cell. *Each data point represents an individual cell (cells were only analysed if the entire cell could be identified separately from surrounding cells). Error bars show SD. One-way ANOVA and Tukey's post hoc test were used to determine significance.*
(C) Quantification of axonal length. *Cells were only analysed if the axon could be clearly identified. Statistical analysis as in (B).*

6.3.3. Tau^{P301L} Overexpression Causes Reduced Neuronal Complexity

For hippocampal cells overexpressing Tau variants, analysis of neuronal morphology in terms of neuronal complexity and axon length was carried out exactly as described above for cells subjected to precursor trapping. It is important to note that whilst Tau is often used as an axonal marker due to its abundance in axons (bound to microtubules), overexpression leads to widespread distribution throughout the neuron. Therefore, in our lab, it is not used as an axonal marker. This can be seen in the images displayed in Figure 6.3 (top panel) and may also explain why Myc-tagged Tau provides seemingly better resolution of neuronal complexity compared to GFP. In addition to this, it is likely that cells express the different proteins at varying abundances and localisations, and therefore the mCherry channel was used for analysis purposes.

Firstly, looking at neuronal complexity, there is a clear reduction in the number of processes per cell in cells expressing Tau^{WT}, and an even greater reduction in cells overexpressing Tau^{P301L} (Figure 6.3 panel A; quantified in B) compared to the GFP control. GFP control cells have an average of 16.6 processes per cell, whilst cells overexpressing Tau^{WT} and Tau^{P301L} have 12.6 and 8.3, respectively (Figure 6.3B). This is indicative of reduced neuronal complexity associated with Tau aggregation.

In terms of axon length, Figure 6.3 (panel A; quantified in C) shows that there was no change associated with overexpression of Tau variants. Hippocampal cells expressing GFP had an average axon length of 267 μm, compared to 274 and 267 μm for cells expressing Tau^{WT} and Tau^{P301L}, respectively.

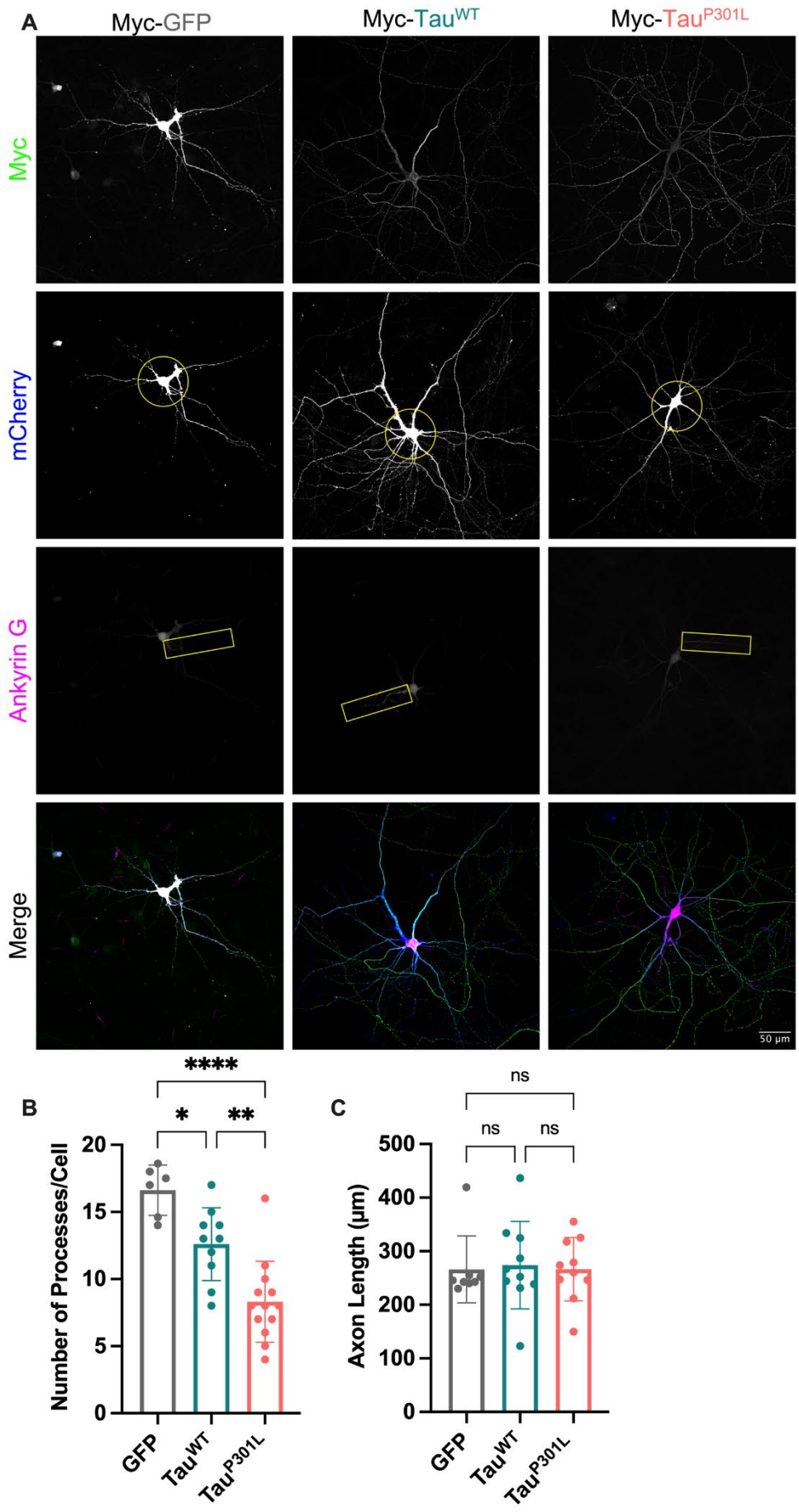
A
Myc-GFP
Myc-TauWT
Myc-TauP301L
Myc
mCherry
Ankyrin G
Merge
50 µm
B
****
*
**
Number of Processes/Cell
20
15
10
5
0
GFP
TauWT
TauP301L
C
ns
ns
ns
Axon Length (µm)
500
400
300
200
100
0
GFP
TauWT
TauP301L

Figure 6.3: Neuronal Complexity is Reduced in Cells Expressing Tau^{P301L}

(A) Representative images showing morphology of DIV21 primary hippocampal neurons expressing mCherry (whole cell cytosolic marker; blue) and Myc tagged GFP, Tau^{WT}, or Tau^{P301L} (Myc, green), taken by confocal microscopy. Axons were stained for Ankyrin-G (magenta). Circles and boxes as in Figure 6.2. *N=4 biological replicates*.

(B) Quantification of number of processes per cell. *Each data point represents an individual cell (cells were only analysed if the entire cell could be identified separately from surrounding cells). Error bars show SD. One-way ANOVA and Tukey's post hoc test were used to determine significance.*

(C) Quantification of axon length. *Cells were only analysed if the axon could be clearly identified. Statistical analysis is as above*.

6.3.4. Cells Subjected to Precursor Trapping have Fewer Synapses

Next, I expanded the neuronal morphological analysis to investigate the number of synapses per dendrite. This was done by pre-treatment of primary hippocampal cells with 100 nM MTX, followed by co-transfection of DIV14 neurons with DNA coding for mCherry (used as a whole cell marker, allowing measurement of process length) and Su9-EGFP-DHFR-HiBit (+MTS) or EGFP-DHFR-HiBit (-MTS). Cells were incubated with the stalled precursor (or control) for 7 days. At DIV21, cells were fixed, and synapses were stained with synaptic marker post-synaptic density protein 95 (PSD95). PSD95 is the major scaffold protein involved in the organisation of postsynaptic signalling complexes in excitatory neurons [499]. These signalling complexes comprise glutamate receptors, ion channels, signalling enzymes and adhesion proteins, and are therefore vital in neurotransmission [500]. PSD95 is commonly used as a marker of excitatory (glutamatergic) post-synapses, due to its abundance. The resulting images were analysed by manual counting on blinded data to quantify the number of synapses per dendrite, as described in Section 2.9.5.4.

The data indicated that perturbing import by precursor trapping induces a reduction in the number of synapses per dendrite (Figure 6.4). When the precursor is trapped, there is an average of 1.8 synapses per 10 µm dendrite, compared to 4.2 when the substrate is not trapped (Figure 6.4B). The controls highlight that this reduction in synapses is correlated to the precursor trapping and not MTX treatment, since in the absence of a presequence (-MTS) there is no significant change in the number of synapses based on the presence of MTX. Specifically, there are 4.1 and 3.6 synapses per cell in the absence or presence of MTX, respectively (Figure 6.4B).

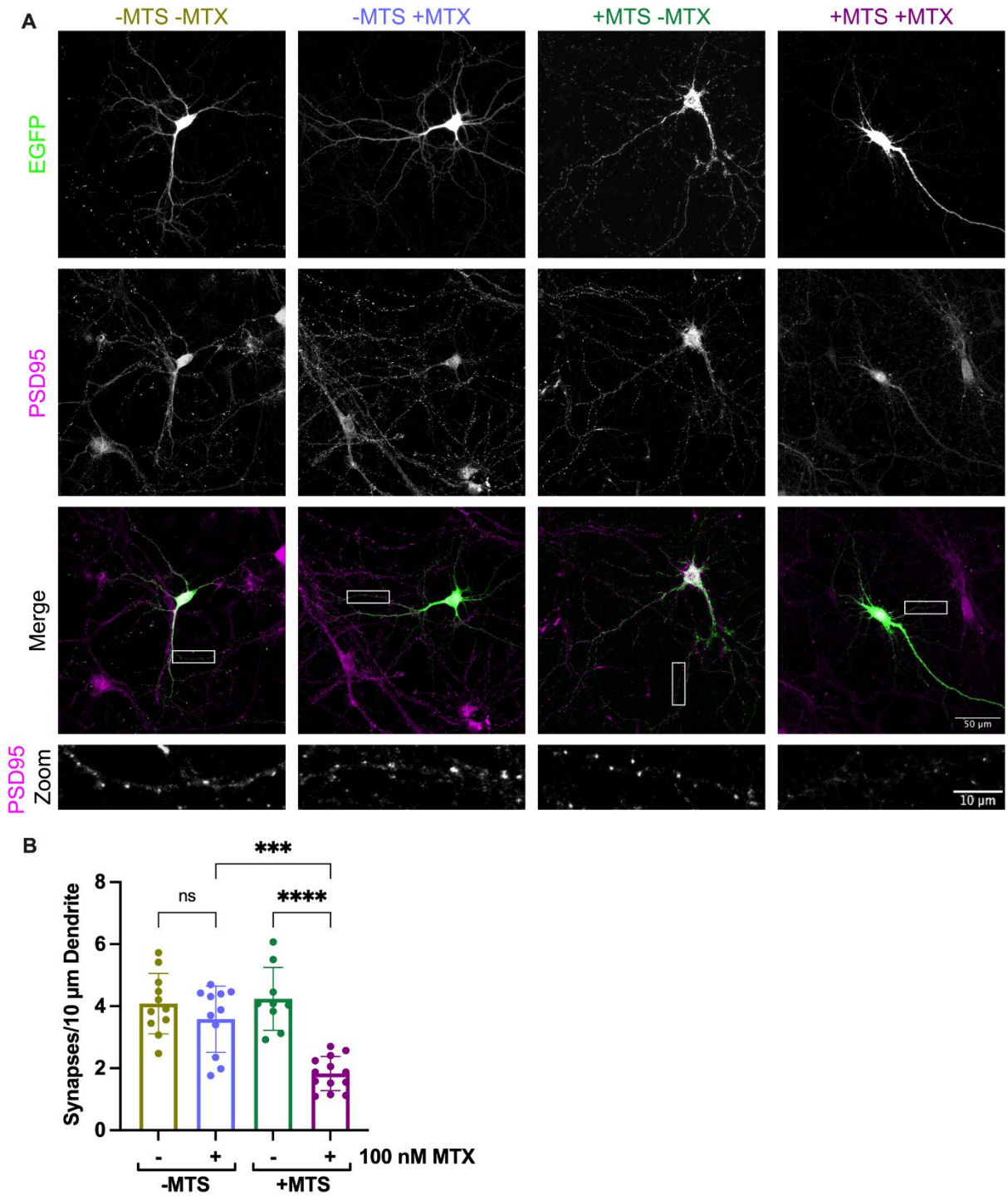

Figure 6.4: Synapse Abundance is Reduced in Cells Subjected to Trapping
(A) Representative confocal microscopy images showing synaptic staining of DIV21 primary hippocampal neurons expressing EGFP-DHFR-HiBit (-MTS) or Su9-EGFP-DHFR-HiBit (+MTS; EGFP shown in green, top panels) in the absence or presence of 100 nM MTX (-/+MTX). PSD95 staining shows synapses (magenta, second panel from top, also shown in zoom). *N=5 biological replicates*.
(B) Quantification of the average number of synapses per 10µm dendrite. Synapses were counted manually on blinded data. *Each data point represents an individual cell. Error bars show SD. One-way ANOVA and Tukey's post hoc test were used to determine significance.*

From the imaging data, it is not clear whether the reduction in dendritic synapse abundance is due to a reduction in the overall abundance or the localisation of synaptic proteins. To investigate this, I carried out Western blotting analysis of whole cell lysates from DIV21 primary cortical neurons expressing EGFP-DHFR-HiBit or Su9-EGFP-DHFR-HiBit in the absence or presence of MTX for one week (Figure 6.5). I probed for synaptic markers PSD95, Synaptophysin, and Gephyrin. PSD95 is an excitatory (glutamatergic) post-synaptic protein, described above. Synaptophysin is an integral membrane protein localised to presynaptic secretory vesicles, commonly used as a marker of excitatory pre-synapses [501]. Gephyrin is a scaffolding protein central to the organisation and structure of inhibitory neuronal post-synapses [502]. It is commonly used as a marker of inhibitory (GABAergic) synapses.

Western blotting analysis and subsequent quantification showed that the overall cellular abundance of all three synaptic marker proteins remained constant regardless of precursor trapping (Figure 6.5). This suggests that the reduction in synapses shown in Figure 6.4 is due to altered localisation of PSD95, rather than its overall abundance in the cells.

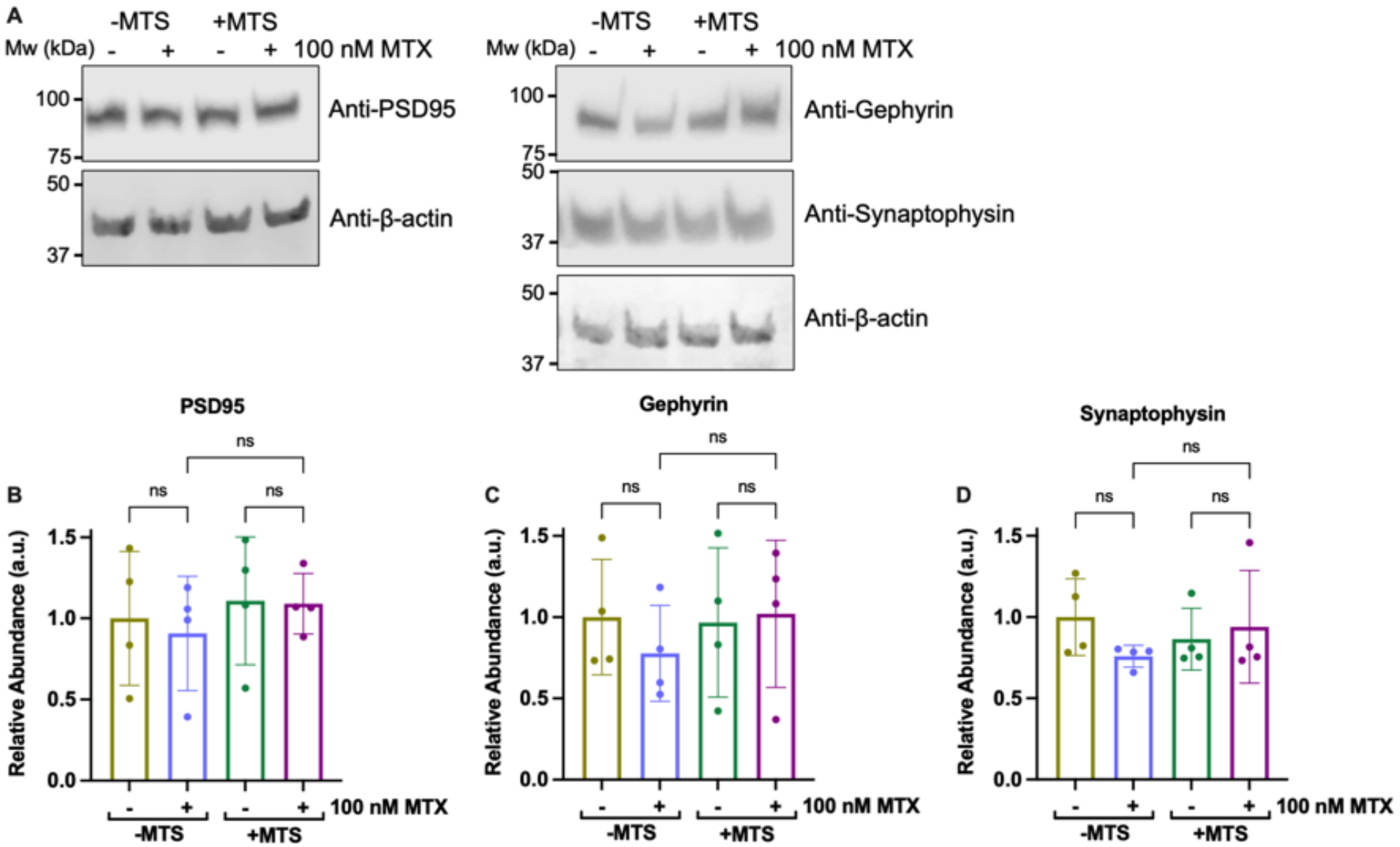
A
-MTS
+MTS
Mw (kDa) - + - + 100 nM MTX
100
75
Anti-PSD95
50
37
Anti-β-actin
-MTS
+MTS
Mw (kDa) - + - + 100 nM MTX
100
75
Anti-Gephyrin
50
37
Anti-Synaptophysin
50
37
Anti-β-actin
PSD95
B
Relative Abundance (a.u.)
1.5
1.0
0.5
0.0
ns
ns
ns
- + - + 100 nM MTX
-MTS
+MTS
Gephyrin
C
Relative Abundance (a.u.)
1.5
1.0
0.5
0.0
ns
ns
ns
- + - + 100 nM MTX
-MTS
+MTS
Synaptophysin
D
Relative Abundance (a.u.)
1.5
1.0
0.5
0.0
ns
ns
ns
- + - + 100 nM MTX
-MTS
+MTS

Figure 6.5: Precursor Trapping has no Impact on Synaptic Protein Overall Abundance
(A) Western blots showing total cellular abundance of PSD95, Gephyrin, and Synaptophysin in DIV21 cortical neurons after 7 days of expression of EGFP-DHFR-HiBit (-MTS) or Su9-EGFP-DHFR-HiBit (+MTS) +/- MTX. β-actin was used as a loading control. *N=4 biological replicates.*
(B) Quantification of PSD95 abundance. Normalised to β-actin. *Error bars show SD. One-way ANOVA and Tukey's post hoc test were used.*
(C) Quantification of Gephyrin abundance. *As in (B).*
(D) Quantification of Synaptophysin abundance. *As in (B).*

6.3.5. Cells Overexpressing Tau^{P301L} Display Altered Synaptic Protein Localisation

The investigation into synapse number and synaptic protein localisation was replicated with cells expressing Tau variants. To quantify the number of synapses per dendrite, primary neurons were subjected to expression of Myc tagged GFP, Tau^{WT}, or Tau^{P301L} for 1 week prior to fixation. At DIV21, cells were fixed and stained for synapses (PSD95) and Tau expression (Myc). Subsequent analysis showed that, in neurons expressing Tau^{P301L}, there is an average of 1.8 synapses per 10 µm dendrite, which is significantly lower than cells expressing GFP or Tau^{WT}, both of which have an average of 3.4 synapses per 10 µm dendrite.

As for trapping, Western blotting analysis was carried out, to confirm whether the reduction in synapses was due to altered abundance or localisation of synaptic marker proteins. Similarly, there was no change in the overall levels of PSD95, Gephyrin, or Synaptophysin in whole cell lysates from cortical cells expressing GFP, Tau^{WT} or Tau^{P301L} (Figure 6.7). This indicates that the reduction in PSD95 expression at dendritic spines, *i.e.,* synapse abundance, demonstrated in Figure 6.6, is due to a change in the localisation of synaptic proteins rather than a reduction in their overall abundance.

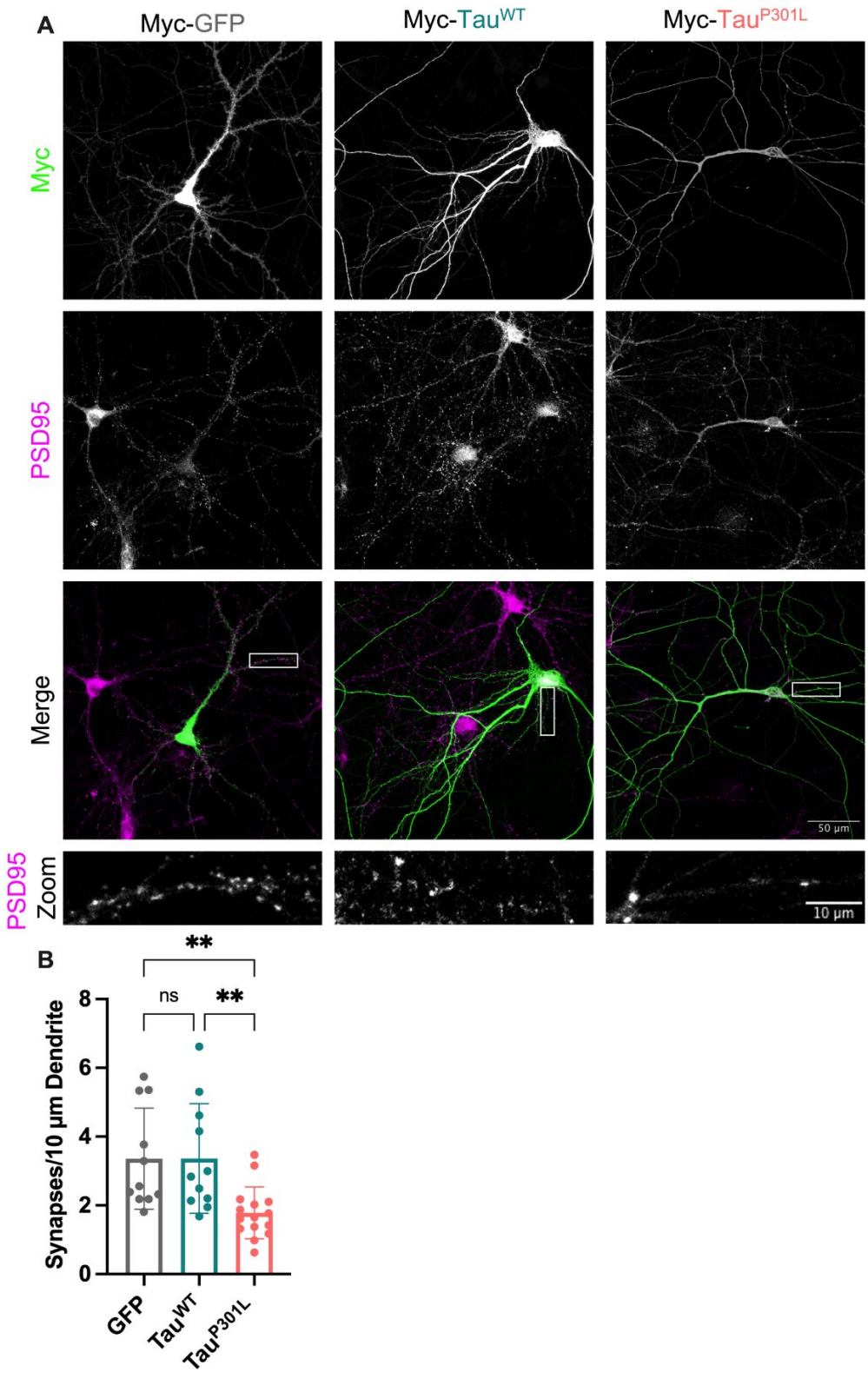

Figure 6.6: Synapse Abundance is Reduced in Hippocampal Neurons Expressing Tau^{P301L}
(A) Representative confocal microscopy images showing synaptic staining of DIV21 primary hippocampal neurons expressing Myc tagged GFP, Tau^{WT}, or Tau^{P301L} (Myc; green). PSD95 staining shows synapses (magenta). *N=5 biological replicates*.
(B) Quantification of the average number of synapses per 10µm dendrite. Synapses were counted manually on blinded data. *Each data point represents an individual cell. Error bars show SD. One-way ANOVA and Tukey's post hoc test were used to determine significance.*

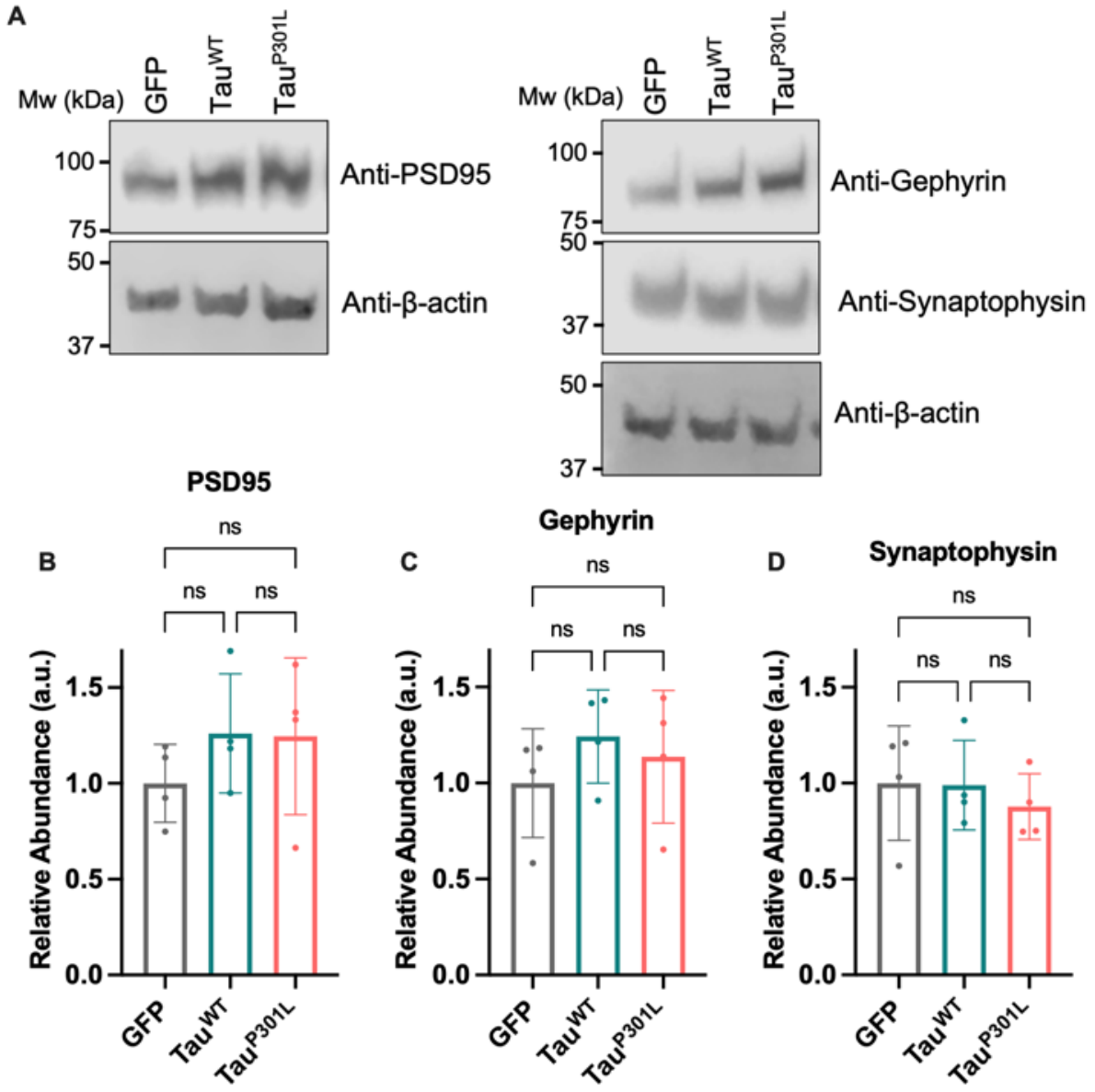

Figure 6.7: Synaptic Marker Expression is Unchanged with Tau Variants
(A) Representative Western blots showing levels of PSD95, Gephyrin, and Synaptophysin in DIV21 cortical neurons after 7 days of expression of Myc-GFP, Myc-Tau^{WT}, or Myc-Tau^{P301L}. β-actin was used as a loading control. *N=4 biological replicates.*
(B) Quantification of PSD95 relative abundance. Normalised to β-actin. *Error bars show SD. One-way ANOVA and Tukey's post hoc test were used to determine significance.*
(C) Quantification of Gephyrin relative abundance. *As in (B).*
(D) Quantification of Synaptophysin relative abundance. *As in (B).*

6.4. Discussion

6.4.1. Key Findings

The main aim of the work described in this chapter was to investigate the impact of failed precursor import on primary neurons in terms of their viability and morphology, to explore how import perturbations may be related to neurodegeneration. The key findings from this chapter are:

- Neuronal viability is unaffected by import perturbation resulting from precursor trapping or Tau^{P301L} overexpression.
- Both insults (trapping and Tau^{P301L}) are associated with changes in neuronal morphology, resembling features observed in models of neurodegeneration.
- Both import insults lead to changes in synapse abundance, which correlates with altered localisation of synaptic proteins.

6.4.2. Import Insults and Neuronal Viability

First, I investigated the impact of precursor trapping and overexpression of Tau variants on neuronal viability (Figure 6.1). This was carried out in cortical neurons over a period of 15 days, and in this timeframe, neither insult had an observable impact on neuronal viability, measured as a function of cellular protein content (where only living (adhered) cells are measured, with the assumption that protein content will be consistent between conditions). This result is not surprising, considering that neurodegenerative diseases progress over years, and neuronal death is the last feature in disease, thus we probably would not expect to see death at this early stage.

6.4.3. Import Insults and Neuronal Morphology: Hints at Neurodegeneration?

Both the reduction in neuronal complexity and the reduced number of synapses per process were visualised with both the precursor trapping (Figure 6.2 and Figure 6.4) and Tau^{P301L} (Figure 6.3 and Figure 6.6) insults. This suggests that these phenotypic features, characteristic of neurodegenerative disease [208, 209, 503, 504], may indeed be at least partially a result of failed import of proteins into mitochondria. Furthermore, the reduction in axonal length observed after precursor trapping could indicate axonal degeneration, another phenotypic feature of neurodegeneration [505]. To confirm this, cells should be imaged, and axons measured at consistent timepoints following trapping, to ascertain that the axon is indeed degenerating rather than growing more slowly.

Figure 6.4 and Figure 6.6 show that both trapping and Tau^{P301L} overexpression are associated with a reduction in the number of synapses per 10 µm of dendrite, as indicated by PSD95 staining. This is despite no reduction in the overall abundance of synaptic marker proteins PSD95, Gephyrin, and Synaptophysin in whole cell lysates (Figure 6.5 and Figure 6.7). This indicates that, though synaptic proteins are still expressed in cells exposed to precursor trapping or Tau^{P301L} overexpression, these proteins are not properly localised to the synapses. This investigation of synaptic protein abundance and localisation could be expanded further to include key players in neurotransmission: ionotropic glutamate receptors (N-methyl-D-aspartate (NMDA), α-amino-3-hydroxy-5-methyl-4-isoxazolepropionic acid (AMPA), and kainate (KA) receptors) [506]. These receptors are central to synaptic transmission and plasticity [506], and therefore examining changes in their abundance, localisation, and activation following import perturbation would provide further information on synaptic function in response to import failure. Previous studies have also shown defects in mitochondrial trafficking, morphology and respiratory function associated with synaptic instability, dysfunction, and disease [507-510]. From a functional perspective, the link between mitochondrial import perturbation and synaptic function could be further investigated by electrophysiology.

The fact that precursor trapping induces a more severe phenotype than Tau^{P301L}, specifically reduced axonal length as well as reductions in synapses and neuronal complexity, is in line with the severity of the insult on import. The DHFR-MTX precursor trapping mechanism is specifically designed to form a plug within import sites, whilst we assume that Tau^{P301L} aggregates within the IMS as well as within the TOM40 pore, and thus probably does not perturb import to the same extent.

6.4.4. Perturbed Import and Neuronal Mitochondria

Future work should include examining the impact of import failure on neuronal mitochondria, in terms of their morphology, density, and localisation. Bearing in mind the complex organisation and high energy demands of neurons, proper mitochondrial function and localisation is vital for maintenance of neuronal homeostasis and function [511]. For example, some synaptic proteins are translated locally in a highly energy consuming process that requires mitochondria docked at synapses as an ATP source [512]. Thus, mitochondrial import defects are likely to have a huge knock-on effect on synaptic function. It would be interesting to investigate this directly by examination of mitochondrial localisation and synaptic function following precursor trapping. For example, differences between axonal and dendritic mitochondria (in terms of localisation, morphology, and function) could be measured, as well as investigating whether mitochondria subjected to trapping are retrieved to the soma.

Considering the changes observed when perturbing import in isolated neuronal cells, it would be interesting to expand this to investigate the impact on a whole organism, which would provide further insight into its role in neurodegeneration. For example, this could be carried out in *Caenorhabditis elegans* or *Drosophila melanogaster*. These are easily tractable organisms with relatively short life cycles, simple but well characterised nervous systems, and mitochondrial function closely conserved with that of humans [513-518]. The insult (precursor trapping or Tau^{P301L} overexpression) could be induced in all mitochondria, or specifically in neuronal mitochondria. This would allow exploration of how defective import in neuronal mitochondria impacts on the entire organism in terms of its viability, behaviour, and function.

6.4.5. Summary

The work presented in this chapter highlights the usefulness of the DHFR-MTX trapping system in investigating import defects related to neurodegenerative disease. These data strengthen the link between import defects and Tau pathologies, as discussed in previous chapters. The data presented here begins to build an understanding of how phenotypes associated with neurodegeneration may be associated with disruption of mitochondrial import. Defining which pathological steps are mediated by mitochondrial import dysfunction is key towards better understanding of disease progression and in the design of potential therapeutic interventions, and therefore this is an area that merits further exploration.

Chapter 7. Import Function Rescue *via* Intercellular Mitochondrial Transfer

7.1. Introduction

When mitochondrial protein import is impaired, there are detrimental effects on not only the mitochondria, but the entire cell and organism. This is even more pronounced in high energy consuming cells such as neurons, and compelling evidence highlights a strong link between mitochondrial import failures and neurodegeneration [1]. In line with this, I showed that the disease prone Tau variant Tau^{P301L} partially localises to mitochondria where it associates with the vital translocation gateway subunit TOM40 (Chapter 5). The data highlighted how this alters mitochondrial morphology and neuronal complexity in a similar manner to synthetic blockage of the TOM40 channel using the DHFR-MTX precursor trapping system (Chapter 4). Despite these changes, there was no apparent change to import efficiency or respiratory function in cells subjected to chronic precursor trapping or Tau^{P301L} association with TOM40, indicative of a cellular rescue or repair mechanism at play.

Many stress response mechanisms have been described as responses to impaired mitochondrial import. These include the UPR^{mt} [299], the UPR^{am} [324], mitoTAD [341], mitoCPR [339], and mPOS [332] pathways (described in detail in Section 1.6). These pathways have mainly been characterised in yeast but are mostly thought to be conserved in mammalian cells. They have been shown to have protective effects in restoration of mitochondrial respiratory function, and cytosolic proteostasis.

Mitochondrial transfer has also been highlighted as a key mechanism in revitalisation of cells subjected to mitochondrial defects. This has been shown to occur endogenously *via* microvesicles (MVs) [519-524], gap junctions [519, 525, 526], endocytosis [527], tumour microtubules [528], and internalisation [525, 529-532], and more recently, tunnelling nanotubes (TNTs) [346]. TNTs are filamentous, membranous protrusions which form connections between neighbouring cells and assist in long range communication and transfer of cellular cargo [344-346]. They are thought to act as a cellular stress response mechanism as well as being implicated in disease propagation [353, 355, 356, 533]. It is not yet known whether they act alongside or independently of other stress response mechanisms. Notably, a recent study in PC12 cells showed how transfer of functional, healthy mitochondria *via* TNTs can rescue cells in the early stages of apoptosis [354]. Interestingly, another recent report also showed how TNTs can assist in reducing cellular toxicity from alpha-synuclein in microglia, by transfer of alpha-synuclein fibrils out of diminished cells, as well as transfer of healthy mitochondria from naïve to infected microglia [362]. Interestingly, proteomic analysis of proteins associated with the trapped precursor highlighted the involvement of various TNT associated proteins (Figure 4.11 and Table 4.1).

7.2. Aims

In this chapter, the overarching aim was to investigate how cells respond to import stress in terms of compensatory mechanisms. I utilised the previously characterised DHFR-MTX system of precursor trapping to model failed import. This allowed investigation and characterisation of the impact of failed import on TNT formation and activity.

The main objectives of this chapter were:

1. To investigate the impact of precursor trapping on TNT formation, using the DHFR-MTX system to model failed import.

2. To characterise mitochondrial transfer *via* TNTs as a rescue mechanism following import failure.

3. To investigate whether the same rescue effect is visualised following Tau^{P301L} association with TOM40.

4. To explore whether this represents a widespread cellular response to perturbation of mitochondrial protein import *via* the presequence pathway.

7.3. Results

7.3.1. Cells Subjected to Mitochondrial Precursor Trapping Form TNTs

The first step was to investigate whether there was an observable compensatory or rescue mechanism implicated following trapping, that could account for the disparity in the import function of cells exposed to chronic *vs.* acute trapping (Figure 4.5). Cell morphology was investigated by carrying out confocal microscopy on fixed cells after co-expressing the trapped precursor as well as an mCherry cytosolic marker. After trapping for 48 hours (chronic trapping), cells appear to form thin, elongated outward extensions or protrusions which are stable after fixation (Figure 7.1A). Quantification showed that in HeLaGAL cells subjected to trapping (+MTS +MTX), 66% of cells have these protrusions, compared to only 24% when the precursor is imported (+MTS -MTX; Figure 7.1B). This effect is not due to MTX treatment, as in cells expressing the DHFR protein without the MTS (EGFP-DHFR-HiBit; -MTS), only 30% of cells treated with MTX form protrusions, compared to 25% in untreated (-MTS -MTX) cells, which does not represent a significant change (Figure 7.1B).

Interestingly, these protrusions only form following precursor trapping when HeLa cells are cultured in galactose containing medium (HeLaGAL), but not when the cells are cultured in glucose containing medium (HeLaGLU; Figure 7.1A, quantified in B). When HeLa cells are grown in galactose based medium, glutamine accounts for ~98% of ATP production, which forces cells into OXPHOS [395]. This causes cells to become reliant on their mitochondria in a similar manner to that observed in brain or muscle cells. Moreover, galactose cultured cells have previously been shown to reveal mitochondrial dysfunction whereas glucose cultured cells do not [395]. This data therefore suggest that the formation of these cellular protrusions is a direct consequence of disrupting mitochondrial protein import, likely sensed *via* a cellular stress response pathway in response to import stress in cells dependent on mitochondrial function for ATP production.

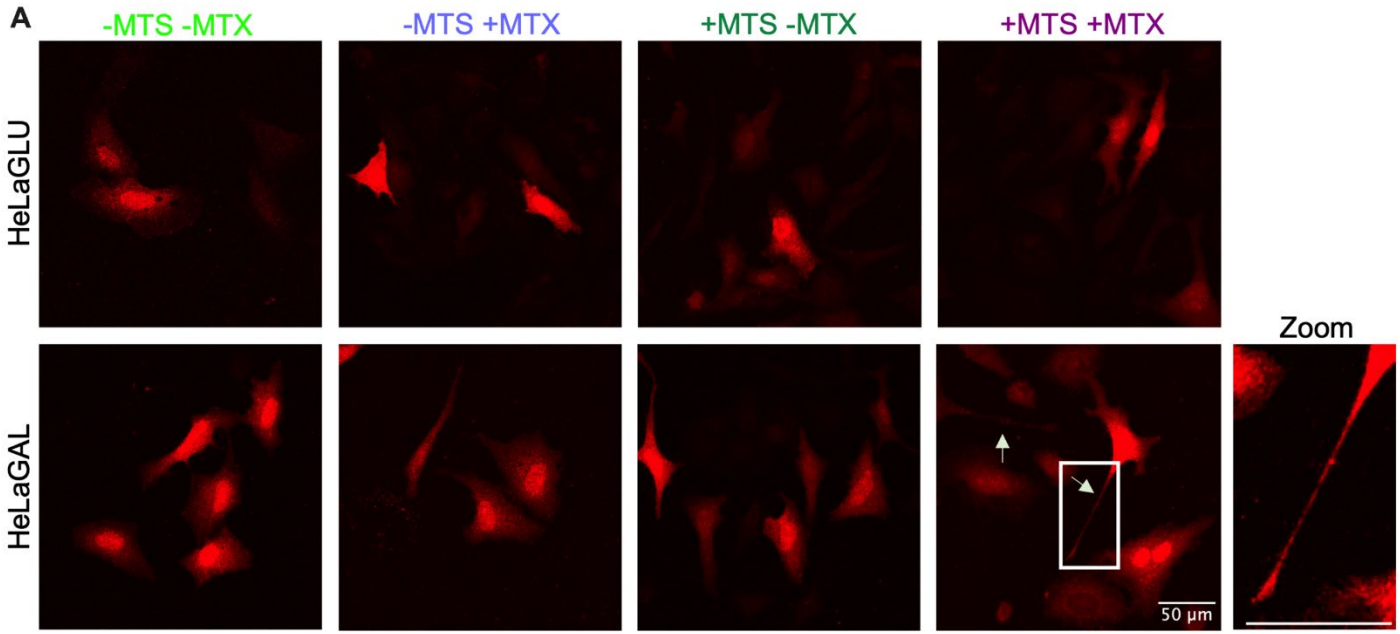
A
-MTS -MTX
-MTS +MTX
+MTS -MTX
+MTS +MTX
HeLaGLU
HeLaGAL
Zoom
50 µm

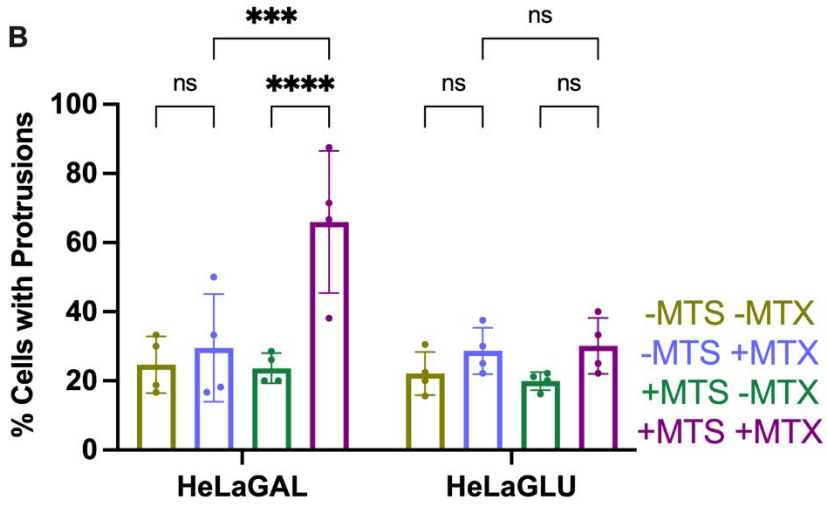
B
***
ns
ns
****
ns
ns
100
80
60
40
20
0
% Cells with Protrusions
HeLaGAL
HeLaGLU
-MTS -MTX
-MTS +MTX
+MTS -MTX
+MTS +MTX

Figure 7.1: Precursor Trapping Induces Protrusion Formation in HeLaGAL Cells
(A) Representative fixed cell confocal images showing cell morphology of HeLaGLU or HeLaGAL cells subjected to expression of mCherry (red) as well as EGFP-DHFR-HiBit (-MTS) or Su9-EGFP-DHFR-HiBit (+MTS) in the absence (-MTX) or presence (+MTX) of 100 nM MTX. Arrows point to protrusions, and box highlights region of interest displayed in zoom. *N=4 biological replicates*.
(B) Quantification of the proportion of cells with protrusions. *Error bars show SD. Two-way ANOVA and Tukey's post hoc test were used.*

Next, I characterised the composition of these protrusions by immunocytochemistry, staining for cytoskeletal markers tubulin-α and β-actin. Tubulin-α forms a heterodimer with tubulin-β for microtubule formation, whilst β-actin is the major cytoskeletal isoform of F-actin [534-536]. Confocal microscopy showed that the protrusions contain microtubules and are decorated with actin (Figure 7.2A).

Since the protrusions are relatively thin compared to the rest of the cell, I attempted to obtain further information on their structure by carrying out cryo-ET. HeLaGAL cells were grown on gold grids and subjected to precursor trapping for 48 hours prior to freezing grids. The samples were visualised on an electron microscope and tomograms reconstructed.

The resulting images showed that the protrusions contain highly organised structures resembling microtubules (Figure 7.2, example 1), consolidating the results of the ICC. Furthermore, some protrusions visualised by cryo-ET contained round, membranous structures, resembling organelles (Figure 7.2, example 2). Due to the low resolution of the tomograms, it is not clear what this organelle is, however it appears round and is surrounded by a membrane, suggesting it could be a mitochondrion, a lysosome, a peroxisome, or a vacuole.

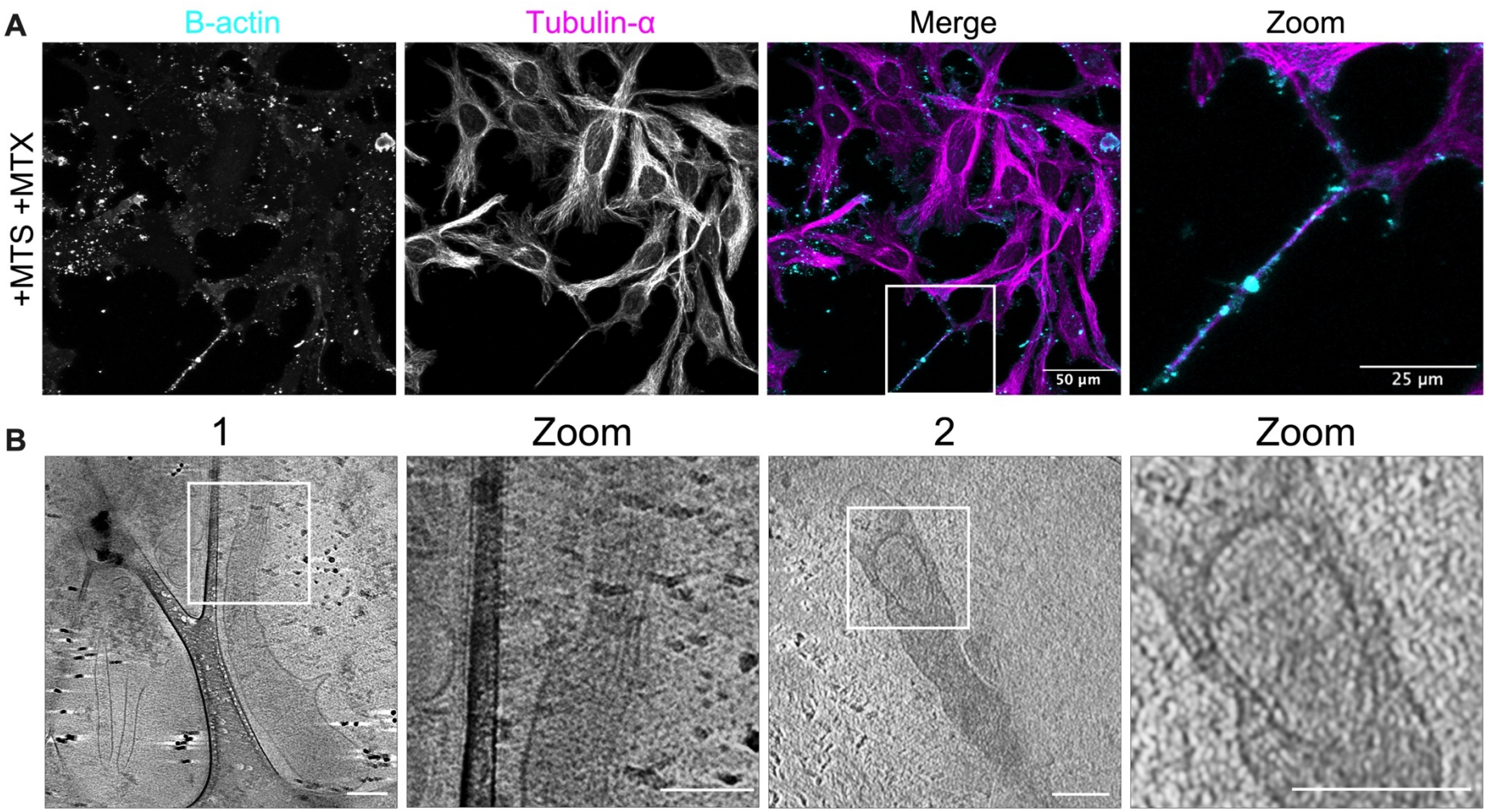

Figure 7.2: Protrusions are Composed of Tubulin and Actin and Contain Cellular Structures
(A) Tubulin and actin staining of protrusions. HeLaGAL cells were subjected to trapping for 48 hours to induce protrusion formation. Cells were then fixed and stained with antibodies against β-actin and tubulin-α and visualised by confocal microscopy. *N=4.*
(B) Cryo-ET of protrusions. HeLaGAL cells subjected to trapping were grown on gold grids, frozen and visualised by cryo-EM. Tomograms were reconstructed to allow visualisation of protrusions. Scale bar is 1 µm. *N=1.*

These data suggest that the protrusions could represent TNTs. This is because type 2 TNTs (thicker in diameter to facilitate transport of larger cargo such as whole organelles) are known to be composed of microtubules and actin filaments, and to transport whole organelles, including mitochondria, between cells [344-347].

To confirm this, I tested whether protrusions still form when treated with various drugs known to inhibit TNT formation. Cytochalasin B and D have previously been shown to inhibit filopodia formation in a specific manner, by competing with Ena/VASP actin cytoskeletal regulatory proteins at the filopodia tip, blocking actin polymerisation [537, 538]. More recently, Cytochalasin B was repurposed and shown to inhibit TNT formation and consequent organelle transport in PC12 cells when used at a concentration of 350 nM [539]. Several studies have also shown how treatment with Cytochalasin D inhibits TNT formation [353, 540-542]. The lowest concentration it was shown to inhibit TNT formation at was 50 nM [542]. I therefore used 50 nM to minimise potentially damaging off target effects. Nocodazole is an inhibitor of microtubule formation [543-545] and has also been shown to inhibit TNT formation at nanomolar concentrations in previous studies [546, 547]. In line with this, I treated cells with 100 nM Nocodazole. It is important to note that, being microfilament-disrupting agents, these inhibitors will disrupt many other normal cellular processes, including cell motility, morphology, size, adherence, and secretion [548, 549]. Despite this, they are commonly used as TNT inhibitors, however, to minimise off-target effects, I kept the concentrations as low as possible.

Cells were subjected to precursor trapping, and either treated with DMSO only (NT), Cytochalasin B, Cytochalasin D, or Nocodazole. Cells were fixed, stained for tubulin-α, and imaged by confocal microscopy (Figure 7.3A). Actin polymerisation inhibitor Cytochalasin B had no significant impact on the formation of protrusions. Cytochalasin D reduced the percentage of cells with protrusions from 75% (NT) to 44% (41% reduction; Figure 7.3A, quantified in B). Microtubule inhibitor Nocodazole reduced protrusion formation even further down to only 17% (77% reduction; Figure 7.3A, quantified in B). It is noteworthy that cells treated with Nocodazole appear to have altered overall morphology, appearing rounder than the other cells, suggesting that it may have some toxic effects. However there does not appear to be a reduction in cell density in Nocodazole treated cells (Figure 7.3A; bottom panel). Overall, these data further corroborate that the protrusion structures represent TNTs, specifically type 2 TNTs, which are composed of microtubules as well as actin and transfer larger organelles such as mitochondria between cells in response to stress [350].

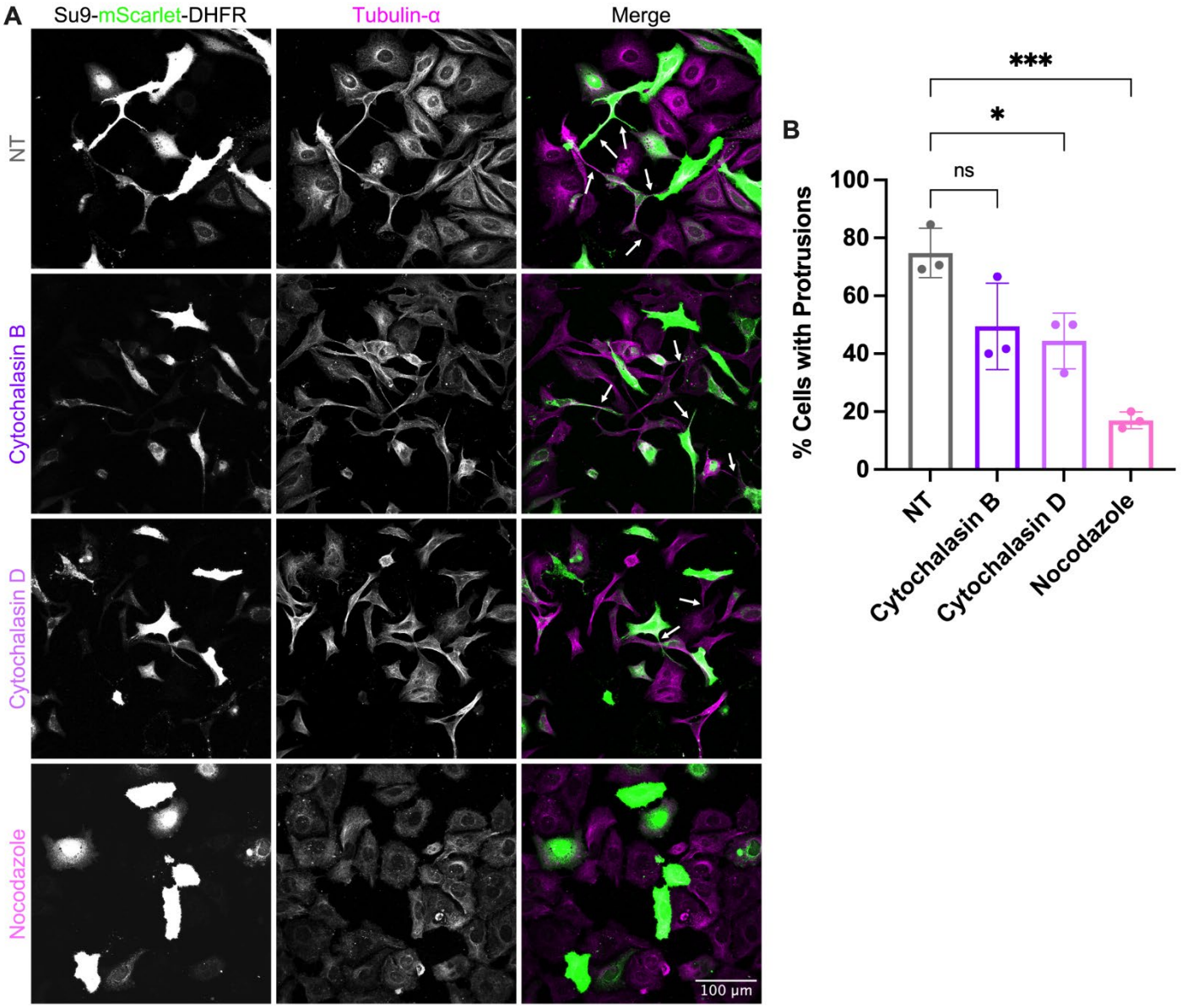
A
Su9-mScarlet-DHFR
Tubulin-α
Merge
NT
Cytochalasin B
Cytochalasin D
Nocodazole
100 µm
B
***
*
ns
% Cells with Protrusions
100
80
60
40
20
0
NT
Cytochalasin B
Cytochalasin D
Nocodazole

Figure 7.3: Protrusion Formation is Decreased by Cytochalasin D and Nocodazole
(A) Representative confocal images of HeLaGAL cells exposed to precursor trapping in the presence of TNT inhibitors. HeLaGAL cells were subjected to trapping (Su9-mScarlet-DHFR +100 nM MTX; green) and either untreated (NT; DMSO only), or treated with 350 nM Cytochalasin B, 50 nM Cytochalasin D, or 100 nM Nocodazole for 48 hours. Cells were fixed and stained for tubulin-α as a marker of the cytoskeleton. *N=3 biological replicates.*
(B) Quantification of the proportion of cells with protrusions. *Error bars show SD. One-way ANOVA and Tukey's post hoc test were used to determine significance.*

7.3.2. TNTs Transfer Mitochondria Intercellularly in Response to Import Failure

Consistent with Type 2 TNTs, the cryo-ET data (Figure 7.2B) suggests that in my setup, TNTs transport membranous organelles. However, it is unclear whether the structure in the tomogram represents a mitochondrion. To explore whether mitochondria are transported *via* TNTs, I referred to the SIM data obtained previously while investigating mitochondrial morphology in response to precursor trapping. Here, HeLaGAL cells were subjected to trapping (using Su9-mScarlet-DHFR + 100 nM MTX) for 48 hours prior to mitochondrial staining with MitoTracker Green and live imaging using SR 3D-SIM. The data showed that TNTs form between a challenged cell (with trapped precursor surrounding mitochondria and diffuse in the cytosol; magenta) and a healthy neighbouring cell (untransfected, no cytosolic marker). The TNTs also contain mitochondria (green), which appear to be traveling along the TNTs between the cells (Figure 7.4A).

To test whether these mitochondria are being transferred between cells, I carried out co-culture experiments in HeLaGAL cells. First, I expressed the trapped precursor (Su9-mScarlet-DHFR; magenta = challenged mitochondria), and in a separate batch of cells, expressed a mitochondrial GFP marker (Su9-EGFP; green = healthy mitochondria). After 24 hours of expression, cells were washed thoroughly to remove any residual DNA in the medium. The cells were then detached by trypsinisation, counted, mixed at a 1:1 ratio, and re-seeded on coverslips. After 48 hours, these cells were fixed and imaged. The images showed challenged cells, that is those with the stalled precursor (magenta cytosolic stain), that also contained healthy mitochondria (green) from the cells not subjected to trapping (Figure 7.4B, example 1).

To confirm that mitochondria were being transferred and not the cytosolic protein, I repeated the experiment exactly as before, but where the cells subjected to trapping had a mitochondrial marker (mito-dsRed; magenta) rather than the cytosolic marker. This marker was expressed prior to lentiviral expression of the trapping protein, to allow it to enter mitochondria. Again, some cells end up with both mitochondrial stains, indicating that the mitochondria are transferred between cells (Figure 7.4B, example 2). A limitation of this experiment was the inability to visualise the transfer event in action, and therefore the next logical step was to capture the mitochondrial transfer event by live imaging.

I carried out live imaging, using an IncuCyte system, on co-cultured cells directly after re-seeding, which allowed an image to be taken every 30 minutes over 48 hours. Although this does not represent fully live/real-time imaging *per se*, I anticipated that this would allow visualisation of the mitochondrial transfer event without photobleaching cells. The cells were cultured and stained as described in Figure 7.4B (example 2). The resulting data demonstrate the transfer of healthy mitochondria (green) to cells subjected to the trapping insult (red), which mix with the cells own mitochondria, visualised by yellow mitochondria. This highlights the directionality of transfer, that is transfer of viable mitochondria to challenged cells presumably *via* TNTs, following precursor trapping (Figure 7.4C). It is notable that the transfer of compromised mitochondria from cells subjected to trapping to healthy cells was not observed in these experiments.

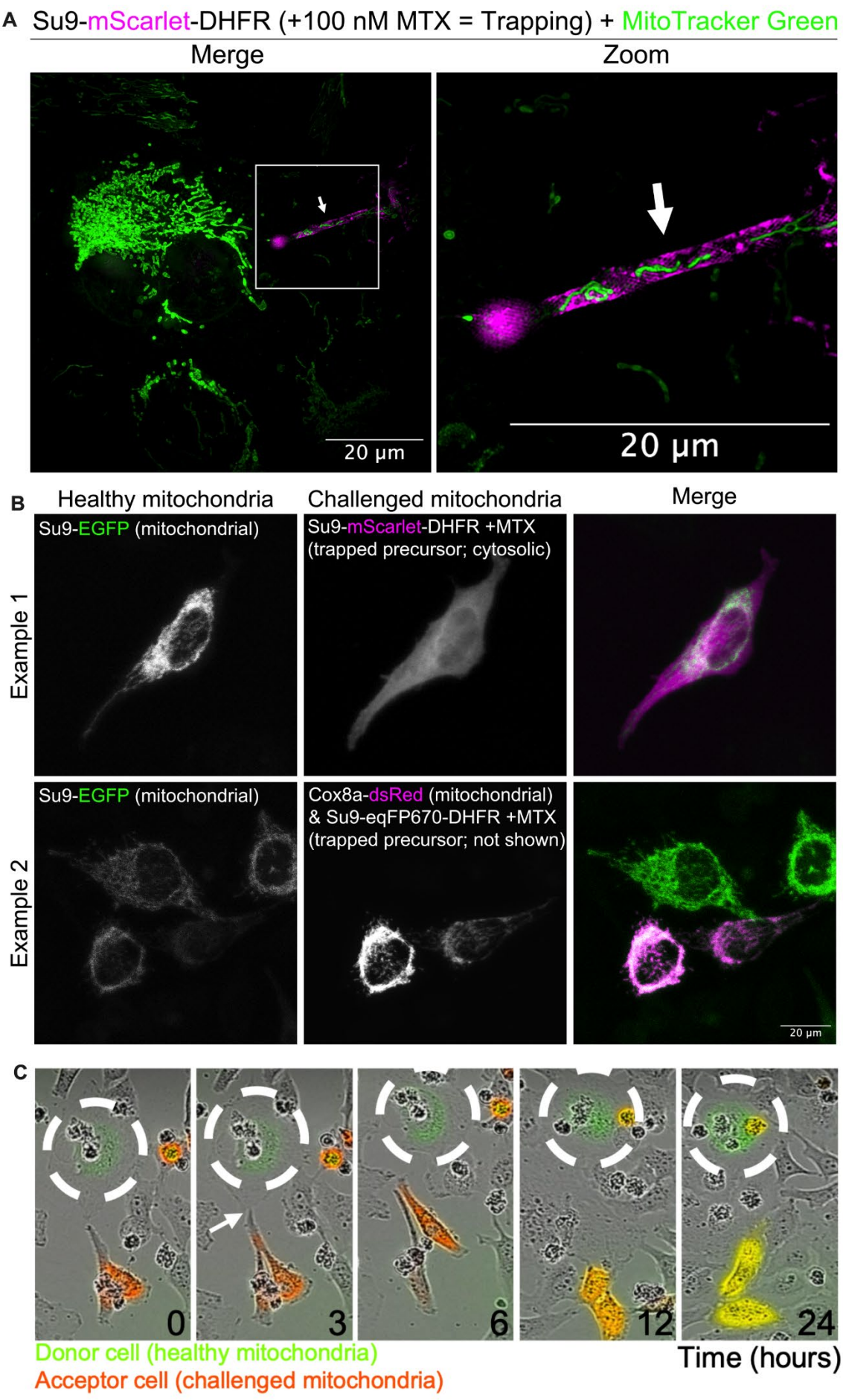
A
Su9-mScarlet-DHFR (+100 nM MTX = Trapping) + MitoTracker Green
Merge
Zoom
20 µm
20 µm
B
Healthy mitochondria
Challenged mitochondria
Merge
Example 1
Su9-EGFP (mitochondrial)
Su9-mScarlet-DHFR +MTX
(trapped precursor; cytosolic)
Example 2
Su9-EGFP (mitochondrial)
Cox8a-dsRed (mitochondrial)
& Su9-eqFP670-DHFR +MTX
(trapped precursor; not shown)
20 µm
C
0
3
6
12
24
Donor cell (healthy mitochondria)
Acceptor cell (challenged mitochondria)
Time (hours)

Figure 7.4: Mitochondria are Transferred *via* TNTs
(A) Representative SR 3D-SIM image showing mitochondria (green) in a TNT formed between a HeLaGAL cell with trapped precursor (Su9-mScarlet-DHFR; magenta), and an untransfected neighbour (green mitochondria, unlabelled cytosol). Cells were transfected with Su9-mScarlet-DHFR and incubated in the presence of 100 nM MTX for 48 hours prior to mitochondrial staining with MitoTracker Green and live imaging by SIM. Arrow highlights TNT and box indicates zoom area. *N=3*.
(B) Representative confocal images from coculture experiments, showing that mitochondria are transferred between healthy and sick cells.
Example 1: one batch of cells was subjected to trapping by expression of Su9-mScarlet-DHFR (magenta = challenged cells) in the presence of 100 nM MTX. Mitochondria of a second batch of cells was stained with Su9-EGFP (healthy mitochondria).
Example 2: one batch was subjected to mito-dsRed expression (magenta) prior to trapping (Su9-eqFP670-DHFR +100nM MTX; not shown). The second batch was exactly as described for example 1. After 48 hours, cells were washed, detached, counted, and mixed at equal ratios, prior to reseeding on coverslips. Cells were co-cultured for a further 48 hours before fixation and visualisation by confocal microscopy. *N=3.*
(C) Representative confocal images from IncuCyte imaging, showing mitochondrial transfer from a healthy to challenged cell. The coculture experiment was repeated exactly as described in (B; example 1), except following mixing of cells, cells were seeded in 24 well plates and placed directly onto the IncuCyte. 9 areas were imaged per well and images were taken every 30 minutes for 48 hours. Snapshots of a representative transfer event are shown. *N=3*.

7.3.3. Inhibiting TNT Formation Blocks Rescue of Import Function

To test whether intercellular mitochondrial transfer *via* TNTs is responsible for rescuing import function in cells subjected to import perturbation, I carried out NanoLuc import assays on cells subjected to precursor trapping in the presence of TNT inhibitors Cytochalasin B, Cytochalasin D, and Nocodazole. If this were the case, inhibition of TNT formation would be expected to correlate with a reduction in import function following chronic precursor trapping, similar to that observed for acute trapping (Figure 4.5).

In the presence of Cytochalasin B, there was no change in import function associated with precursor trapping (Figure 7.5A, amplitude quantified in D). This is consistent with the confocal microscopy data that showed no significant change in TNT formation upon treatment with Cytochalasin B (Figure 7.3). Following treatment of cells with Cytochalasin D, chronic precursor trapping led to a subtle reduction in precursor import of ~16%, however this is not statistically significant (Figure 7.5B and D). The imaging data presented in Figure 7.3 highlighted a similar subtle, yet significant impact of Cytochalasin D on TNT formation.

When cells were treated with Nocodazole, which reduces TNT formation significantly (Figure 7.3), precursor trapping brought about a reduction in import function of ~34% (Figure 7.5C and D). Here, trapping has a similar effect on import to that observed following acute trapping, and a significantly greater impact than chronic trapping in the absence of Nocodazole (Figure 4.5, quantified in Figure 7.5D). Taken together, these data indicate that import viability is at least in part rescued by tubulin/actin dependent mechanisms *i.e.,* TNTs.

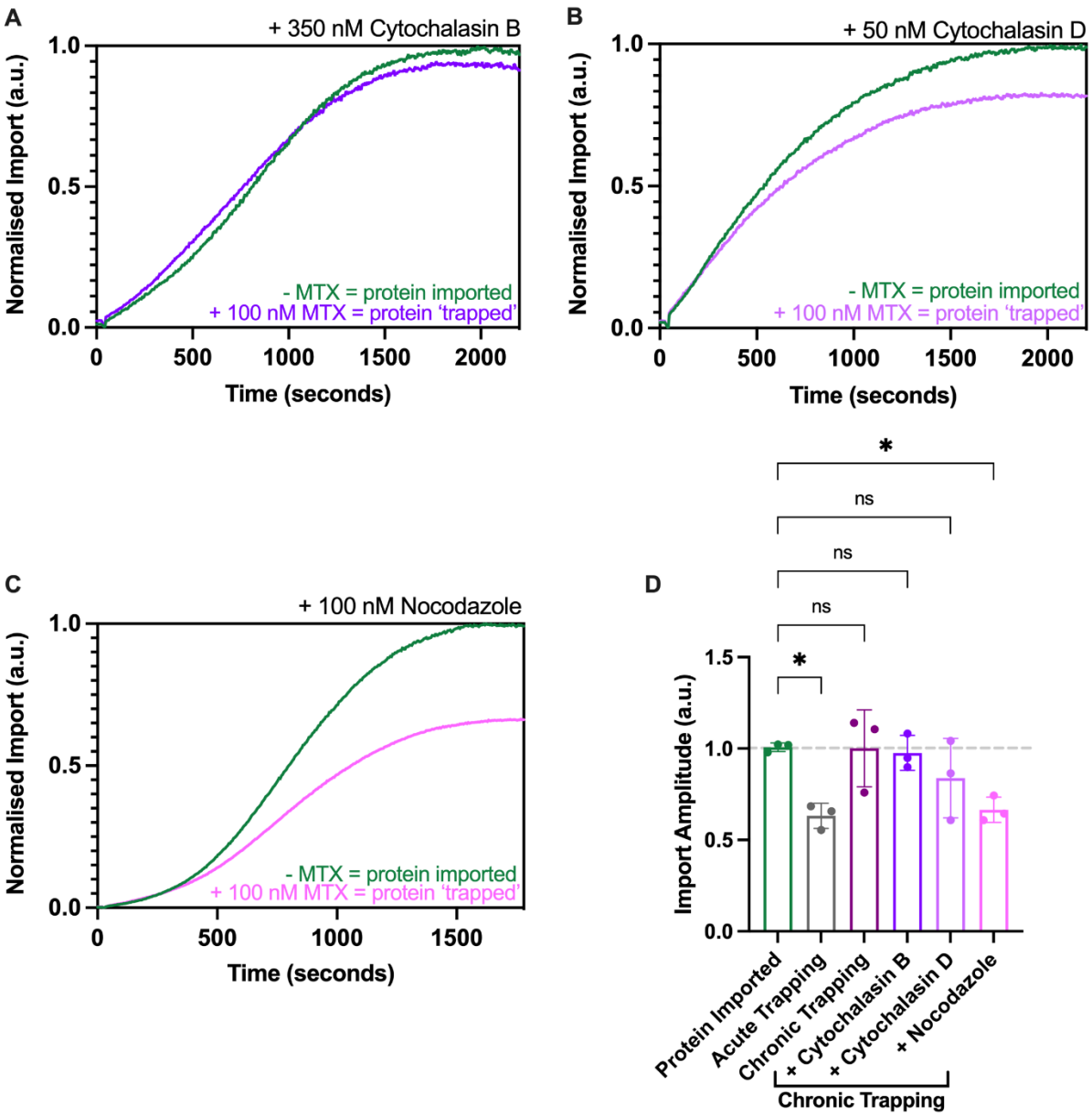

Figure 7.5: Rescue of Import Function is Partially Reversed by Blocking TNT Formation
(A) NanoLuc import trace showing the impact of trapping on import of a precursor protein in HeLaGAL cells treated with Cytochalasin B. Cells were subjected to trapping (+MTX; purple) or not (-MTX; green) and treated with 500 nM Cytochalasin B for 48 hours prior to monitoring the import of Su9-EGFP-6xHis-HiBit by permeabilised cell NanoLuc import assays. *Normalisation was carried out as described in Chapter 3. N=3 biological replicates.*
(B) As in (A) but in the presence of 50 nM Cytochalasin D. *N=3 biological replicates.*
(C) As in (A) but in the presence of 100 nM Nocodazole. *N=3 biological replicates.*
(D) Maximum amplitude of import for traces shown in A-C and Figure 4.5 (acute and chronic trapping in the absence of TNT inhibitors). *Error bars display SD. One-way ANOVA and Tukey's post hoc test were used to determine significance.*

7.3.4. Tau^{P301L} Overexpression Induces TNT Formation

In the previous chapters, the data highlighted a common mechanism of import perturbation for precursor trapping and Tau^{P301L} association with the TOM40 channel. In addition, these insults resulted in similar changes in terms of reduced mitochondrial and neuronal complexity. On this basis, I hypothesised that the normal import function observed in cells overexpressing Tau^{P301L} may also be accounted for by TNT-dependent uptake of healthy mitochondria from neighbouring cells.

To investigate this, I carried out confocal microscopy to examine the morphology of Tau^{P301L} expressing cells, to test whether these cells also produce protrusions. Cells co-expressing mCherry and Myc-GFP, Myc-Tau^{WT}, or Myc-Tau^{P301L} were analysed by confocal microscopy. After 48 hours, 62% of HeLaGAL cells expressing Tau^{P301L} had protrusions, compared to 22% and 18% for HeLaGAL cells expressing Tau^{WT} or GFP, respectively (Figure 7.6A, quantified in B). In HeLaGLU cells, overexpression of Tau^{P301L} had no significant impact on protrusion formation (Figure 7.6A, quantified in B), consistent with what was observed following precursor trapping (Figure 7.1). Expressing a mitochondrial marker (mito-dsRed) in cells subjected to Tau^{P301L} overexpression highlighted that these structures also contain mitochondria (Figure 7.6C).

Next, I examined the composition of these protrusions by staining for actin and tubulin, under normal (NT) conditions as well as in the presence of TNT inhibitors Cytochalasin B, Cytochalasin D, and Nocodazole. The data presented in Figure 7.7 showed that the protrusions contain microtubules and actin, and their formation is reduced by treatment with TNT inhibitors (Figure 7.7A, quantified in B). Like what was shown for trapping induced TNT formation, treatment with Cytochalasin B had no significant impact on TNT formation. Cytochalasin D reduced TNT formation by 44% (from 62% in NT cells to 35% with Cytochalasin D), whilst Nocodazole reduces it by 81% (to 12% of cells; Figure 7.7A, quantified in B). Together, this signifies that Tau^{P301L} expression also induces TNT formation, likely as a rescue mechanism responding to mitochondrial stress.

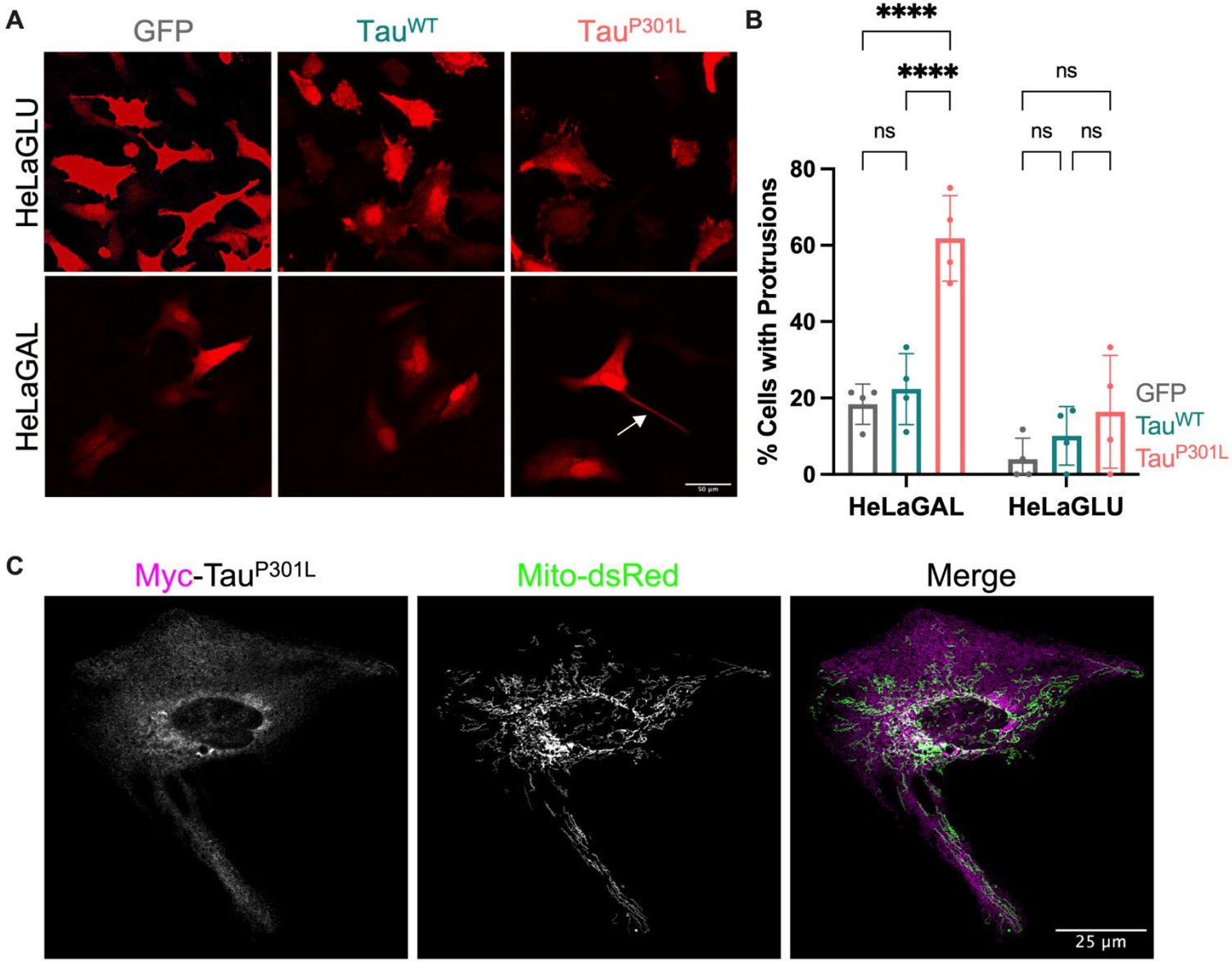
A
GFP
Tau^WT
Tau^P301L
HeLaGLU
HeLaGAL
50 µm
B
****
****
ns
ns
ns
ns
% Cells with Protrusions
80
60
40
20
0
HeLaGAL
HeLaGLU
GFP
Tau^WT
Tau^P301L
C
Myc-Tau^P301L
Mito-dsRed
Merge
25 µm

Figure 7.6: HeLaGAL Cells Expressing Tau^{P301L} Form TNTs that Contain Mitochondria
(A) Representative confocal images showing cell morphology of HeLaGLU or HeLaGAL cells subjected to expression of mCherry (red) as well as GFP, Tau^{WT}, or Tau^{P301L}. TNT is indicated by the arrow. *N=4 biological replicates*.
(B) Quantification of proportion of cells with protrusions. *Error bars show SD. Two-way ANOVA and Tukey's post hoc test were used to determine significance.*
(C) Representative confocal images showing mitochondrial localisation (mito-dsRed; green) in cells overexpressing Myc-Tau^{P301L} (magenta). *N=4 biological replicates*.

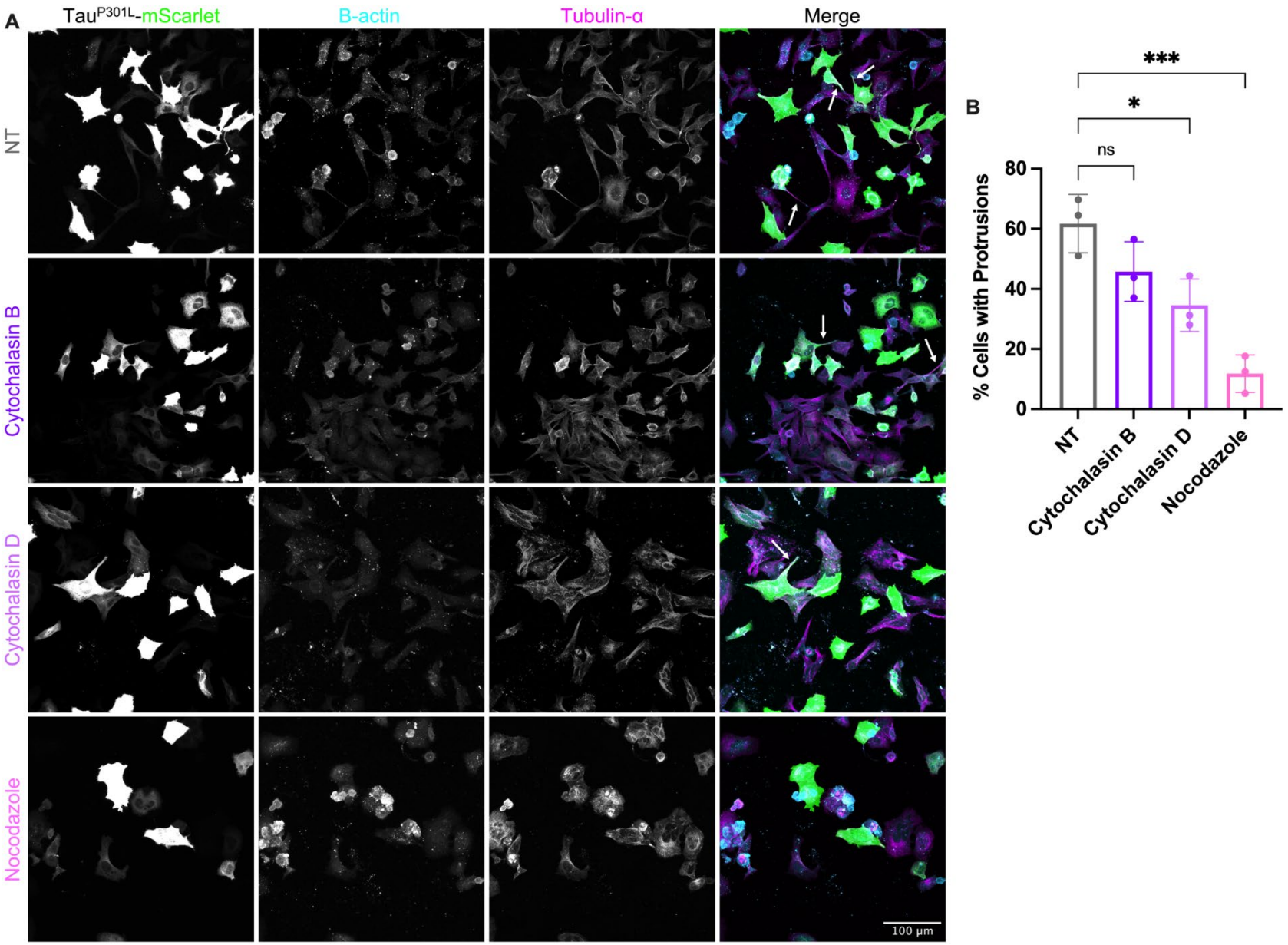
A
Tau^{P301L}-mScarlet
B-actin
Tubulin-α
Merge
NT
Cytochalasin B
Cytochalasin D
Nocodazole
100 µm
B
***
*
ns
% Cells with Protrusions
80
60
40
20
0
NT
Cytochalasin B
Cytochalasin D
Nocodazole

Figure 7.7: Tau^{P301L} Induced TNTs are Dependent on Microtubules and Actin
(A) Representative images of HeLaGAL cells exposed to Tau^{P301L} overexpression in the presence of TNT inhibitors. HeLaGAL cells were subjected to overexpression of Tau^{P301L}-mScarlet (green) and either untreated (NT; DMSO only), or treated with 350 nM Cytochalasin B, 50 nM Cytochalasin D, or 100 nM Nocodazole. Cells were fixed and stained for β-actin (cyan) and tubulin-α (magenta). Arrows in merge highlight TNTs. *N=3 biological replicates.*
(B) Quantification of % cells with protrusions. *Error bars show SD. One-way ANOVA and Tukey's post hoc test were used to determine significance.*

7.3.5. TNTs may Represent a Widespread Response to Import Disruption

The fact that TNT formation was observed following both precursor trapping and Tau^{P301L} association with TOM40 indicated that this may be a widespread cellular response to import perturbation. MitoBloCK-20 (MB20) is a small molecule inhibitor of import [363] that prevents import *via* the presequence pathway by binding to TIM17, a key component of the TIM23 complex [363].

First, I investigated the impacts of both acute and chronic MB20 treatment on mitochondrial protein import, to test whether it mirrored what was previously observed with import perturbation by precursor stalling (Figure 4.5). Whilst NanoLuc import assays showed that acute treatment (10 minutes; red trace) of HeLaGAL cells with MB20 reduced the import of a chasing precursor protein (Su9-EGFP-HiBit) by 61%, chronic treatment (48 hours; orange trace) had no significant effect on import (Figure 7.8A and B). These data suggest that perturbing import by MB20 may activate the same rescue mechanism as that described for precursor trapping, to protect overall mitochondrial import capacity.

Accordingly, I tested whether TNTs form when mitochondrial import is perturbed by chronic treatment with MB20. Treatment of HeLaGAL, but not HeLaGLU, cells with MB20 for 48 hours leads to the TNT-like protrusion formation (Figure 7.8C, quantified in D). Import perturbation with MB20 causes protrusions to form in 55% of HeLaGAL cells, compared to 26% in untreated cells (Figure 7.8C, quantified in D). Characterisation of these protrusions showed that they are composed of microtubules and actin and contain mitochondria (Figure 7.8E). Taken together the data described for precursor trapping and Tau^{P301L}-TOM40 association, these data suggest that mitochondrial transfer *via* TNTs is a widespread recovery mechanism undertaken by cells in response to perturbation of the mitochondrial import machinery.

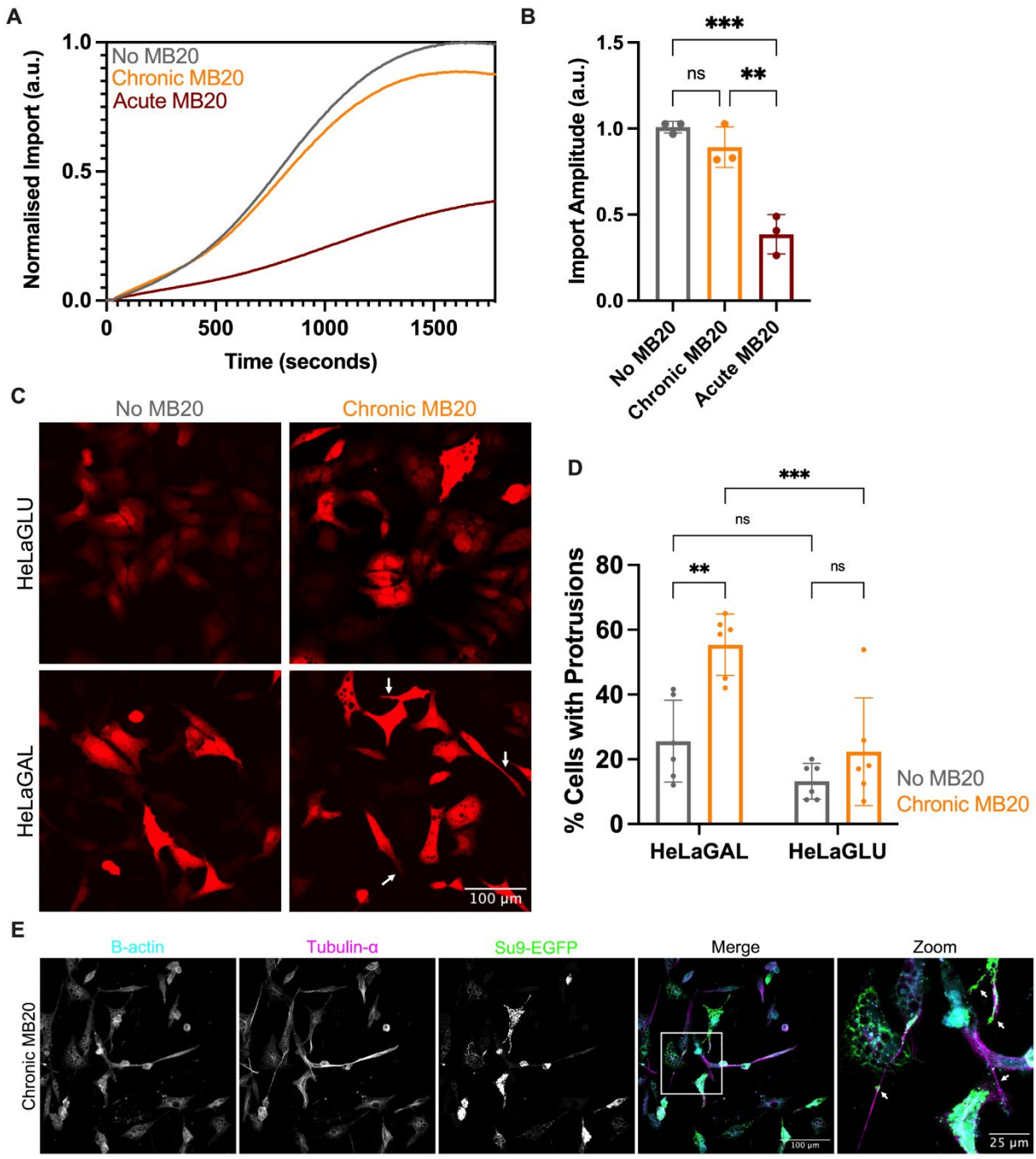

Figure 7.8: MB20 Induced Import Perturbation is Rescued by TNT Formation

(A) NanoLuc import traces showing precursor import in untreated cells (no MB20; grey), cells treated chronically (48 hours; orange) or acutely (10 minutes; red) with MB20. Traces were normalised as in Chapter 3. *N=3 biological replicates.*

(B) Maximum amplitude of import for traces shown in (A). *Error bars show SD. One-way ANOVA and Tukey's post hoc test were used to determine significance.*

(C) Representative images demonstrating morphology (shown by mCherry cytosolic marker; red) of HeLaGLU or HeLaGAL cells treated with 10 µM MB20 for 48 hours, visualised by confocal microscopy. Arrows highlight TNTs. *N=6 biological replicates*.

(D) Quantification of (B). *Error bars show SD. Two-way ANOVA and Tukey's post hoc test were used to determine significance.*

(E) Representative images showing composition of MB20-induced protrusions. Cells expressing Su9-EGFP (mitochondrial marker; green) were subsequently treated for 48 hours with 10 µM MB20. Fixed cells were stained for β-actin (cyan) and tubulin-α (magenta). Box shows zoom area and arrows in zoom highlight TNTs. *N=3 biological replicates*.

7.4. Discussion

The main aim of this chapter was to investigate a possible compensatory mechanism implicated in rescuing cells exposed to mitochondrial import perturbations. The key findings from this chapter are:

- TNTs are formed in response to failed import of a precursor protein.
- TNTs are involved in the intercellular transfer of mitochondria, from cells with normal import function, to cells with reduced import capacity.
- Mitochondrial transfer *via* TNTs is at least partially responsible for the normal import function of cells subjected to chronic trapping.
- TNTs are also formed when import is disturbed by Tau^{P301L} association with the TOM40 pore, or by TIM23 inhibition, representative of a widespread response to import stress.

Overall, the data in this chapter highlights TNT dependent intercellular mitochondrial transfer as a rescue mechanism to restore import function in cells subjected to mitochondrial import perturbation. The proposed mechanism is illustrated schematically in Figure 7.9 and is discussed in detail below.

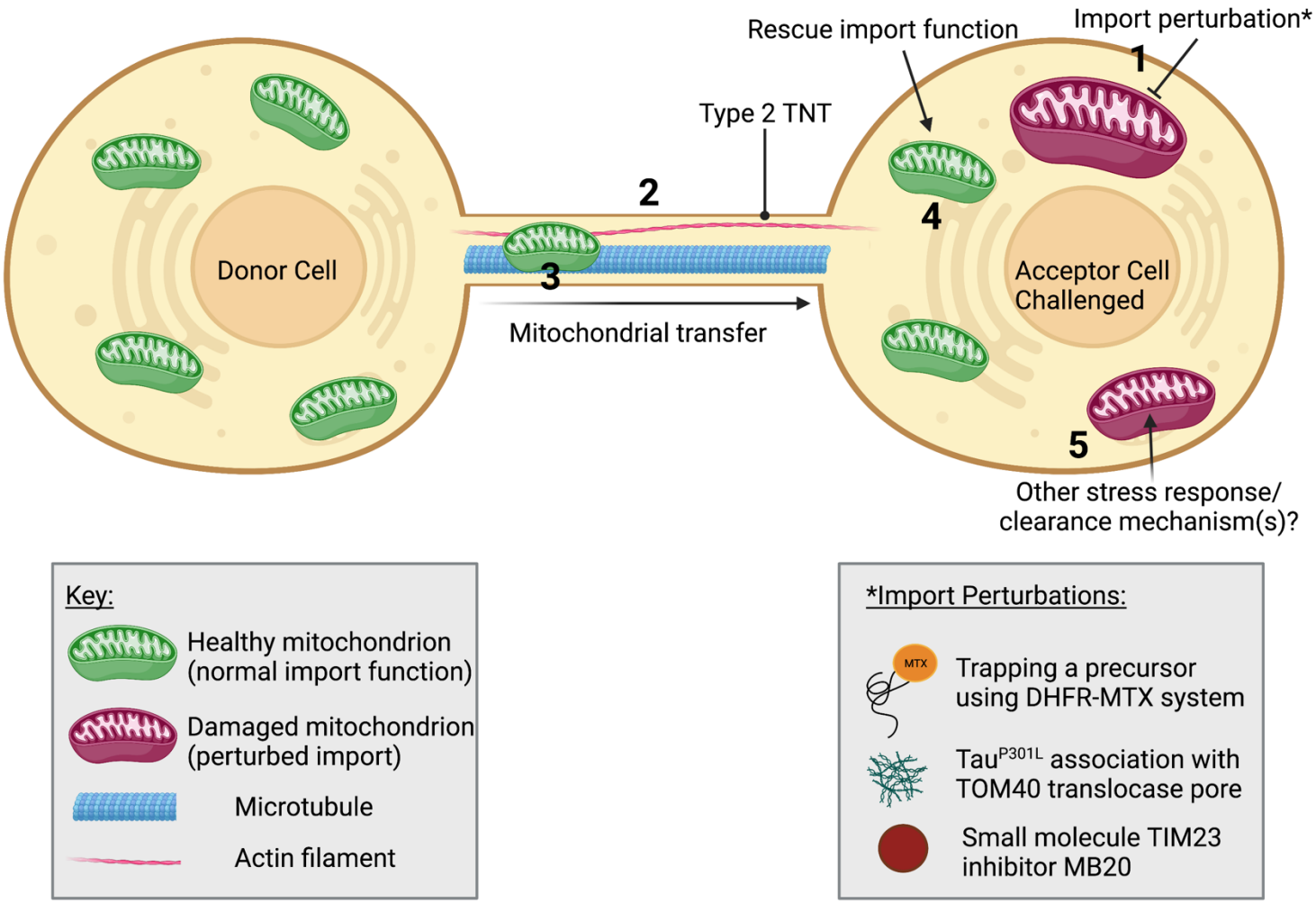

Figure 7.9: Proposed Import Rescue Mechanism by Mitochondrial Transfer *via* TNTs
Cells subjected to import perturbations *(1)* activate the formation of type 2 TNTs *(2)*, composed of microtubules and actin filaments. These TNTs assist in the transfer of healthy mitochondria from neighbouring cells into cells with damaged mitochondria *(3)*. The transfer of healthy mitochondria with normal import function rescues the overall import function of the acceptor cell *(4)*. This rescue effect is probably enhanced by additional, unidentified stress response mechanisms *(5)*.

7.4.1. TNTs as a Compensatory Mechanism to Precursor Trapping

7.4.1.1. Precursor Trapping Induces Type 2 TNT Formation

Throughout the previous chapters, the data had begun to point towards the activation of a compensatory mechanism in cells subjected to import perturbation by precursor trapping. Firstly, there was no change in the import function of cells following chronic precursor trapping, despite a significant reduction with acute trapping. Despite drastic morphological changes, including cristae changes, there was no impediment in respiratory function associated with failed import. Finally, proteomics highlighted several proteins implicated in stress response pathways, as well as in TNT formation, associated with the trapped precursor (Figure 4.11).

Although mitochondrial morphology was drastically altered by precursor trapping (Figure 4.6), cell morphology had not yet been investigated. Examination of cell morphology showed that, following trapping, cells produced long, thin, protrusion like structures, composed of tubulin and actin (Figure 7.1 and Figure 7.2). These structures did not form when HeLa cells were cultured in glucose medium, but only when trapping was induced in galactose cultured HeLa cells. This emphasises the formation of TNTs as an effect specific to mitochondrial dysfunction, as it is well-established that HeLaGAL cells are reliant on their mitochondria, whereas HeLaGLU cells can generate ATP *via* alternative means.

To obtain more structural information on the composition of these protrusions, I carried out cryo-ET (Figure 7.2B). This was a challenging process that required a lot of optimisation and could still benefit greatly from further optimisation to improve data quality. Despite the use of gold grids, growing cells on grids induced high levels of cell death. Cell density also requires optimisation to allow more chance of visualisation of protrusions within the holes. This could be overcome by optimising seeding density, changing the side of blotting, or blotting on both sides, to remove excess cells. Furthermore, protrusions seemed to naturally adhere to the carbon, rather than over the holes, and coating the grids with graphene oxide could also be useful in encouraging protrusions to grow across holes rather than on the carbon grid.

TNT formation and particularly mitochondrial transfer is likely to be a highly transient event and therefore unlikely to be occurring at the time of grid freezing. Correlative light and electron microscopy (CLEM) could be useful in overcoming this, as events could be identified and freezing carried out at the correct time to capture the transfer event. This would also reduce screening time significantly. In addition, CLEM would be useful in confirming the identity of the organelle-like structure observed in Figure 7.2B. A previous study showed similarly transient events captured successfully using CLEM with a fixation step in between light microscopy and

freezing grids [550]. Preliminary data suggested that this would be possible in my setup, however due to time constraints these experiments remain to be completed.

However, from the examples shown in Figure 7.2B, it does seem like there are highly organised structures resembling microtubules (example 1) and that these cells contain membranous cargo (example 2) which may or may not be a mitochondrion. Further processing has the potential to reveal more detail within these structures.

7.4.1.2. Mitochondria Transfer via TNTs

Nonetheless, the data in Figure 7.4 demonstrates that mitochondria are transferred intercellularly *via* these TNTs. The SIM shown in Figure 7.4A shows a TNT protruding from the 'sick' cell (cell subjected to trapping) towards a healthy cell (an untransfected neighbour not subjected to trapping) with mitochondria travelling along it. It is not possible to distinguish directionality here, or even confirm that mitochondria are transferred, since the mitochondria from both cells are labelled with MitoTracker Green. However, this is confirmed in the coculture experiments which show mitochondria transfer to cells with depleted import function (Figure 7.4B and C). This is in line with numerous previous studies which have shown transfer of healthy mitochondria under both physiological and pathological conditions (summarised in [551]). However, this is the first time this has been observed in response to import dysfunction. Whilst there is no evidence for transfer of damaged mitochondria out of the cells subjected to trapping here, previous studies have shown that this transfer can be bidirectional and involve the counter-exchange of healthy and damaged mitochondria (summarised in [551]).

In addition to mitochondrial transfer *via* TNTs, there are other known mechanisms of mitochondrial transfer as a tissue revitalization mechanism that have been studied extensively in health and disease [551]. These mechanisms include mitochondrial transfer *via* MVs [519-524], gap junctions [519, 525, 526], endocytosis [527], tumour microtubules [528], and internalisation [525, 529-532]. It is possible that mitochondrial transfer could also occur *via* these alternative routes here too, however the phenotype observed throughout the data (long, thin protrusions composed of tubulin and actin, containing mitochondria, and connecting neighbouring cells) is consistent with TNTs.

It was necessary to carry out the coculture experiments in multiple ways since each method has its limitations. The data shown in Figure 7.4B could be improved by use of split luciferase technology. This would enhance the clarity of the data since, in the current setup, once mitochondria are transferred and fuse with the mitochondrial network, the fluorescent signal merges and fades (as observed in Figure 7.4). Using a split-luciferase based system would

limit signal to complementation following fusion of the mitochondria, eliminating issues with background or fading signal. This could also be done in a high throughput manner, using a plate reader to measure luminescent signal, allowing many samples/drugs to be screened at once for observation of their impact on mitochondrial transfer. To further improve the data obtained from the IncuCyte experiment (Figure 7.4C), live imaging of the transfer event should be repeated with a higher resolution imaging system (*i.e.,* confocal or SIM) to enable proper visualisation of the mitochondria. This would also allow for labelling of cytosol as well as mitochondria (since the IncuCyte is only a two-colour (red/green) system), allowing for visualisation of the TNT and movement of mitochondria along it. Since the timepoint for transfer has been narrowed down thanks to these long-term imaging experiments, images could be taken at shorter intervals for a shorter overall period (*i.e.,* every 5 minutes for 8 hours, rather than every 30 minutes for 48 hours) to allow better time resolution of the transfer event, without photobleaching the cells. Another limitation is the presence of a high proportion of untransduced cells with unlabelled mitochondria. This could be easily overcome by FACS sorting or the use of stable cell lines expressing mitochondrial markers.

7.4.1.3. Import Recovery is Blocked by Inhibition of TNT Formation

Figure 7.3 shows that the formation of TNTs is reduced when cells are treated with drugs previously shown to inhibit TNT formation. Actin polymerisation inhibitors Cytochalasin B and D both seemed to reduce TNT formation somewhat, though it is only significantly reduced with Cytochalasin D and not with B. Microtubule inhibitor Nocodazole reduced TNT formation to levels observed in cells not subjected to trapping. This is further evidence that the TNTs formed under these conditions are type 2 TNTs, that is, thicker TNTs composed of microtubules [350, 552]. Whilst this is in agreement with some studies that show Nocodazole to reduce TNT formation [546, 547], other studies have shown that, unlike Cytochalasin B and D, Nocodazole has no impact on TNT formation [354, 479]. However, it could be that these studies are observing type 1 TNTs (see Figure 1.9), which are mainly composed of actin filaments and thus do not require microtubules [350, 552]. The effects of these inhibitors on import function in response to trapping, shown in Figure 7.5, are broadly in line with what was observed in Figure 7.3, indicative of a direct correlation between TNT formation and import function rescue. This provides strong evidence that import function is, at least in part, rescued by TNT dependent intercellular mitochondria transfer.

However, this may not be the only mechanism responsible for import rescue. The reduced overall abundance of the trapping protein (Figure 4.4B) as well as enhancement of proteasome-related proteins in association with the trapped precursor (Figure 4.11) suggest that the proteasome is likely involved, and stress response pathways such as the UPR^{am} and

mitoCPR should be investigated. I anticipate this would provide a clearer picture of the interplay between mitochondrial import dysfunction and cell survival.

Though a defined mechanism of TNT formation has not yet been fully established, a recent review provided a summary of all the drugs that have been shown to alter TNT establishment [553]. In addition, a recent study showed how mitochondria are trafficked between cancer and immune cells in a pathological mechanism which can be partially inhibited by treatment with a farnesyltransferase and geranylgeranyl transferase 1 inhibitor, namely, L-778123 [355]. It would be interesting to test how these drugs alter import function, using NanoLuc import assays. Furthermore, it is thought that TNTs require ATP for active transport of cargo [552, 554], and inhibition of mitochondrial ATP production by respiratory chain inhibitors (see Figure 1.4) could confirm whether this is indeed the case in my system.

7.4.2. TNTs as a Rescue Mechanism for Tau^{P301L} Induced Import Dysfunction

In Chapter 5, I described how the accumulation of Tau^{P301L} in the TOM40 channel may be acting in a similar way to stalling with the DHFR precursor and showed that this corresponds to similar changes in mitochondrial and neuronal morphology. Similarly, despite association with TOM40 and reduced translocase abundance, there is no impact on import function or respiratory capacity. This mirrors the cellular changes observed after precursor trapping (Chapter 4) and indicates a common compensatory mechanism. The data (Figure 7.6 and Figure 7.7) highlight that TNTs, which contain mitochondria, are formed in cells overexpressing Tau^{P301L} and are likely to rescue cellular import function in a similar manner to that described for the trapped precursor.

However, it is important to note that Tau is thought to be involved in TNT establishment [360]. Furthermore, TNTs have previously been implicated in the pathological distribution of Tau aggregates as well as other prion-like proteins [360, 361]. Taken together, these studies emphasise that, even without the mitochondrial import defects induced by Tau accumulation, TNTs may form irrespectively, and thus their formation cannot be solely attributed to the import defects associated with Tau^{P301L}.

7.4.3. TNTs as a Widespread Response to Import Dysfunction: MB20

The comparable observations with precursor trapping and Tau led to the broader question: is mitochondrial transfer *via* TNTs a widespread rescue mechanism, activated in response to import disturbance, or is it specific to TOM40 blockage? To address this, I deployed small molecule inhibitor of TIM23, MB20 [363]. Acute MB20 treatment led to a significant reduction in precursor import, while chronic treatment had no effect (Figure 7.8A). This disparity between

the effects of acute *vs.* chronic MB20 treatment on import function was consistent with that observed for precursor trapping (Figure 4.5) and indicative of a similar compensatory mechanism. Imaging experiments showed that cells also form mitochondria-containing TNTs when treated chronically with MB20 (Figure 7.8B-D). Together, this suggests that transfer of mitochondria *via* TNTs is a widespread response mechanism resulting from mitochondrial import stress, at least *via* the presequence pathway (Figure 7.9). In future, it would be interesting to investigate whether cells respond similarly following import dysfunction *via* other pathways. For example subjecting cells to MB6 treatment to block import via the MIA pathway [416], or MitoBloCK-1 (MB1) treatment to block import *via* the carrier (TIM22) pathway [555].

Moreover, it would be interesting to see if TNT-induced mitochondrial transfer occurs in cells with other, more severe mitochondrial defects such as mtDNA depletion. For example, the coculture experiments described in this chapter could be carried out between WT cells and Rho0 cells. Rho0 cells were originally generated by culture in ethidium bromide, and are completely devoid of mtDNA, meaning they are unable to perform electron transport or OXPHOS [556]. These cells are therefore unable to survive in galactose cultures. The success of mitochondrial transfer *via* TNTs could be indicated by fluorescent or luminescent markers, or by an enhancement in viability in galactose culture. It is known that injection of exogenous mitochondria can rescue the phenotype of Rho0 cells [556], so it would be interesting to ascertain whether similar rescue could be obtained by TNT-induced transfer. This would provide more information on the signalling pathways associated with TNT formation and begin to address some outstanding questions. Namely: how is TNT formation activated? Is it a specific response to import defects, or to accompanying dysfunction such as respiratory dysfunction? In this regard, more in depth analysis of the proteomic changes associated with TNT formation would also be beneficial.

7.4.4. Therapeutic Relevance of Mitochondrial Transfer via TNTs

Previous studies have shown mitochondrial transfer or transplantation as a promising therapeutic strategy. For example, a recent study showed how the transfer of exogenous mitochondria can help maintain normal bioenergetic function following spinal cord injury [525]. Additionally, endogenous mitochondrial transfer from astrocytes to neurons *via* MVs and TNTs has been shown to have neuroprotective effects following ischaemic injury [520, 557].

Another recent study described a double rescue strategy in microglia exposed to α-synuclein, whereby TNTs allow cells to pass toxic α-syn fibrils to neighbouring naïve cells for degradation, at the same time as receiving healthy mitochondria from naïve cells [362]. This was shown to reduce the cells' inflammatory response and reactive oxygen species, and in

turn promoted cell survival [362]. In line with the latter, the data here shows how, when subjected to import perturbations, neighbouring cells without such perturbations donate their healthy mitochondria, with fully functional translocation machinery, to the 'sick' cells, enhancing import function, which may be important in promoting cell survival. This impact on cell survival should be tested with viability assays. However, in opposition to what they see with α-syn, here we did not observe the aggregated protein being transferred to neighbouring cells, though this was not tested directly and therefore cannot be ruled out. Nevertheless, this is not necessarily surprising since Tau may well be handled differently to α-syn. Here, Tau appears to be retained in mitochondria and not properly cleared. One possible explanation is that mitochondria are used as 'waste bins' for these protein aggregates, a phenomenon previously characterised as 'Mitochondria as Guardian in Cytosol' [558]. This raises the question of how and when protein aggregates are actively targeted to be internalised by mitochondria, versus when they are mislocalised and result in import defects. In this regard, mitophagy should also be tested.

Considering the revitalising effects of mitochondrial transfer highlighted by previous studies, this mechanism of mitochondrial transfer *via* TNTs as a response to import failure may be promising in terms of neuroprotective outcomes. Particularly so, given its relevance to studies showing how toxic, aggregation prone proteins perturb mitochondrial import and function in neurodegenerative diseases (see Table 1.2). Hypothetically, if mitochondrial transfer *via* TNTs could be induced, could this rescue cells with mitochondrial import defects in disease scenarios? Would this also rescue associated symptoms? Given what was observed in HeLa cells for disease prone Tau^{P301L}, this seems possible. However, a major limitation of this study is that this mechanism was characterised solely in HeLa cells. Thus, to be able to speculate regarding the therapeutic relevance of this system in terms of neurodegenerative disease, the experiments must be repeated in primary cells to ascertain whether this rescue mechanism is conserved. For example, co-culture experiments could be carried out between glia (donors) and neurons subjected to import defects (acceptors).

7.4.5. Summary

Overall, these results highlight how the NanoLuc system can advance understanding of mitochondrial protein translocation and associated mechanisms. The unexpected results obtained led to the finding that cells respond to import perturbations by utilising TNTs to transfer healthy mitochondria from neighbouring cells. This is an intriguing result considering recent advances in the literature surrounding the link between mitochondrial import and neurodegenerative diseases, and the neuroprotective effects of mitochondrial transfer.

Chapter 8. Research Summary & Concluding Remarks

8.1. Summary of Research

Over recent years, remarkable progress has been made towards understanding the processes of mitochondrial protein import. Advances in structural biology have begun to further elucidate the different structural properties of the mitochondrial translocases in high resolution, and this sheds further light on the various processes of mitochondrial import for specific protein classes. Whilst progress has been made, there remain areas of uncertainty regarding the organisation and dynamic action of the translocase complexes. Improved import assay methods, such as the NanoLuc import assay, discussed in detail in Chapter 3 and described previously in yeast mitochondria [108, 364], are also of paramount importance to dissect the mechanism and kinetics of the import process. Hopefully, this revamped in cell assay will allow drug and phenotypic screenings to be performed, facilitating easy identification of new players and modulators as well as small molecules that target this biological pathway.

Mitochondrial dysfunction has long been recognised as a key factor in neurodegenerative diseases. However, mitochondrial protein import is increasingly being highlighted as a key element in this dysfunction, across all levels of neurodegenerative disease models from the simple cell line setup right up to animal models and patient samples [85, 215-230] (Table 1.2). Interestingly, the findings from these studies indicate that defective mitochondrial import is a driving force for the prominent mitochondrial irregularities observed in these diseases. Thus, this represents an important target for further research to address outstanding questions: Are the links between mitochondrial import and disease causative or consequential? What role might such defects play in disease progression? This thesis shows how a novel assay system, and an engineered precursor as a model of failed import, can facilitate exploration of the complex link between mitochondrial protein import and neurodegenerative diseases.

The aims of the work presented in this thesis were:

- To develop an assay system to investigate mitochondrial protein import in live mammalian cells in real time (the NanoLuc system).
- To characterise the impact of failed import on HeLa and neuronal cell health and function by stalling translocation of a bioengineered precursor protein.
- To explore the impact of expressing a naturally occurring aggregation prone protein (Tau^{P301L} variant) on mitochondrial protein import.

Outlined below is a summary of my key findings, with relevance to the rest of the literature and focus on the significance of these findings in relation to health and disease.

8.1.1. The NanoLuc Assay System to Monitor Import in Live Mammalian Cells

Firstly, I developed and characterised an assay system to achieve near real-time monitoring of mitochondrial protein import in live mammalian cells. This was necessary given the considerable limitations of import assays used in the past. The resulting system is a high-resolution system in terms of both sensitivity and time resolution. It has the potential to facilitate detailed kinetic analysis of import events, as has been shown recently in studies from our lab in yeast mitochondria [108, 364]. In addition, it has high-throughput capability, which would facilitate quick and efficient screening of drug libraries or target proteins in terms of their effects on import. This type of analysis could prove instrumental considering the implications of import in neurodegenerative pathogenesis, and the potential for targeting this therapeutically. However, as detailed in Chapter 3, there are still several improvements that could be made to the NanoLuc system:

- Improvement of the intact system by modifications to remove background signal, *e.g.,* incorporation of GST-Dark or a PEST degron to the system.

- Addition of the CUTE technology to the intact system, to facilitate real-time monitoring with kinetic output. This requires further optimisation but will probably be necessary for use in primary neuronal cells.

- Development of a cell line stably expressing mitochondrial LgBit. This would eliminate issues associated with variability of expression, as well as reducing assay time and cell culture costs associated with transfection of cells.

- Alteration of the NanoLuc system for monitoring of import *via* the other major import pathways, namely the TIM22 (carrier) pathway, the MIA pathway, the SAM pathway, and the OXA1 pathway.

8.1.2. Modelling Failed Import via an Engineered Stalled Precursor

The next step was to develop a means of monitoring the direct impact of failed import on cells. This comes following several recent studies that have highlighted links between import function and neurodegeneration ([85, 215-230]; Table 1.2). However, due to the many pathways altered by toxic/aggregating disease prone proteins, it is difficult to accurately define which aspects are attributable to import perturbation caused by the aggregated protein. To this end, I characterised the DHFR-MTX precursor trapping system as a tool to model failed import in mammalian cells. The data in this thesis showed that this system is most useful when used alongside a naturally occurring protein associated with import defects, allowing differentiation between changes caused directly by import failure, and those caused by other factors associated with the disease protein. Using this approach, I described a fission-based change in mitochondrial morphology following import failure, which resembles changes previously observed in disease [559, 560]. This was in line with import changes, observed with acute but not chronic trapping. Furthermore, despite mitochondrial morphological changes, there was no change in the mitochondrial respiratory function. Taken together with clues from the proteomic data, the data suggested a cellular recovery mechanism in response to failed import, which was charactered further in Chapter 7.

8.1.3. Tau^{P301L} and Mitochondrial Import

Beyond investigating the effects of stalling import using a trapped modified precursor, I sought to use the NanoLuc assay system to identify novel associations between aggregation prone proteins and import function. I chose to investigate Tau disease associated variant Tau^{P301L}, since this is a well characterised variant that had not been explored previously in terms of its relation to import [234, 482, 483, 486-488]. Overexpression of Tau^{P301L} in HeLaGAL cells resulted in various changes associated with mitochondrial translocation:

- Increase in Tau^{P301L} localisation to mitochondria.
- Reduction in the abundance of key translocase subunits TIM23 and TOM20.
- Association of Tau^{P301L} with TOM40.

In addition, overexpression of Tau^{P301L} also correlated with alterations in mitochondrial morphology, resembling those observed following DHFR precursor trapping. That is, mitochondria were less branched, suggestive of an increased rate of fission (though fission was not directly tested in Tau expressing cells). Furthermore, as for chronic trapping, Tau^{P301L} had no effect on import efficiency, respiratory function, or membrane potential.

Together, these results propose that Tau^{P301L} is becoming trapped in the TOM40 channel and having a similar subsequent effect on cells to the trapped DHFR protein. These similarities, and in particular the observation of an association between the Tau variant and TOM40, provide a strong and intriguing link between mitochondrial import and Tau. Similar observations have been made previously with regards to other aggregation prone proteins [215, 222, 224], but not with Tau, though various disease associated forms of Tau (N-terminal, caspase cleaved, and phosphorylated) have been shown to associate with mitochondria [217, 218, 248]. This should be investigated further, especially given its direct relevance to tauopathies. Further proposed experiments are discussed in detail in Section 5.4.

8.1.4. The Implications of Import Failure on Primary Neurons

Considering the clear link between import dysfunction and neurodegenerative diseases, highlighted both in this thesis and in previous work [215, 222, 224], I expanded this study to include primary neurons. I carried out parallel experiments to examine the impact of failed import using precursor trapping and Tau mechanisms. This is important in determining which of the neuronal phenotypes associated with Tau^{P301L} overexpression can be attributed to its impact on import.

These experiments revealed various changes in terms of neuronal morphology associated with defective mitochondrial import. Precursor trapping correlated with a reduction in the total number of processes (axons and dendrites), as well as shorter axons and fewer synapses. In cells overexpressing Tau^{P301L}, there was a reduction in the number of processes and synapses, but no significant change to axon length. As mentioned previously, this difference between the impact of trapping and Tau is not necessarily surprising. This is because we are directly perturbing import by blocking import sites when we use the trapping system, whilst the impact of Tau on import in neurons is not known and could be relatively subtle in comparison. Although Tau clearly associates with mitochondria, specifically TOM40, in HeLa cells (Figure 5.3), this has not yet been shown in neurons, and is a vital experiment to carry out in future. In primary neurons, there is a huge amount of work that should be carried out in future to corroborate and obtain further detail on this link, particularly regarding synaptic function. This is discussed in detail in Section 6.4.

8.1.5. Mitochondrial Transfer via TNTs as an Import Rescue Mechanism

Up until this point, the data had begun to establish a strong link between import failure and neurodegeneration. There were, however, perplexing disparities in the data. Firstly, there were marked differences between the import function observed following trapping in a chronic and acute manner. The fact that chronic trapping led to no reduction in import function was surprising given that SIM data showed it aggregated around mitochondrial membranes, suggesting it had not all been cleared. Similarly, Tau^{P301L} associates with TOM40, in line with a reduction in translocase expression, but has no impact on overall import function. In combination, I reasoned that these data pointed towards a compensatory mechanism.

The first indication of TNTs as a rescue mechanism was changes in cell morphology in response to trapping, notably thin protrusions from the plasma membrane. Further investigation showed these protrusions were composed of tubulin and actin and contained mitochondria, consistent with TNTs [344-347, 354]. Moreover, subsequent experiments showed that mitochondria were transferred from healthy to challenged cells *via* the TNTs. This transfer event appeared to be necessary for recovery of normal mitochondrial function following trapping. To investigate whether these TNTs were a widespread response to import dysfunction, I further tested whether they would still form if import were perturbed by Tau^{P301L} overexpression or treatment of cells with small molecule inhibitor MB20. The TNTs still formed and are seemingly responsible for rescuing the import function of cells with a range of import perturbations.

These data regarding TNTs as a rescue mechanism for cells subjected to import defects have potentially far-reaching implications in disease. Recent studies have highlighted how mitochondrial transfer *via* TNTs may be a therapeutic target in disease [354, 362]. Taken together with the growing body of data surrounding the link between import dysfunction and neurodegeneration [85, 215-230], could this represent a potential therapeutic approach in response to import defects in disease? Of course, this study needs to be expanded to investigate its conservation in primary neurons before speculating further about its therapeutic potential in terms of neurodegeneration, however previous studies show that TNTs can be formed between neurons and neighbouring cells such as astrocytes as a neuroprotective rejuvenation mechanism [551], rendering this a promising avenue for further exploration.

8.2. Outstanding Questions

The work presented in this thesis raises several further questions for future studies, some of which are:

- What are the kinetic features of import *via* the presequence pathway in mammalian cells? Do they mirror what has been observed in yeast? How is this altered following chronic/acute import perturbations?

- What other impacts does import dysfunction have on neurons, particularly in terms of function? Can rescuing import function reverse these phenotypes?

- Does Tau^{P301L} associate with TOM40 in neurons?

- Which other stress response pathways are activated in response to failed import? What happens to the damaged mitochondria? Is the blockage eventually cleared or are the damaged mitochondria degraded? Are these pathways defective in disease scenarios and how could they be targeted therapeutically?

- How is the proposed rescue mechanism activated? Is it activated in response to all forms of import perturbation? *I.e.,* perturbation of the TIM22/MIA pathways?

- Is the repair mechanism conserved in neuronal cells? How is the transfer of mitochondria *via* TNTs relevant to translocase blockages and import defects in disease scenarios?

The future experiments detailed in the extensive discussions of each chapter aim to address these broad outstanding questions.

8.3. Final Remarks

Overall, this thesis has explored the complex link between mitochondrial protein import and neurodegenerative disease. The development of a novel system for monitoring import processes with high resolution in live mammalian cells will hopefully be instrumental in furthering knowledge in the field of mitochondrial import research. The work described here shows how the system can assist in identifying changes in import in response to overexpression of Tau^{P301L}, and this study should be expanded in future to include a wide range of disease-related proteins. In addition, I showed the usefulness of modelling failed import using an engineered precursor stalling system. I anticipate that this will be useful in deciphering links between import and disease in future studies. For example, here, this tool was invaluable in the discovery of a cellular response to import perturbations, that is, mitochondrial transfer *via* TNTs. Finally, there is much more work to be done with regards to dissecting the link between mitochondrial protein import and neurodegeneration, and in future I hope to see novel, systematic approaches, such as those demonstrated here, applied to further questions surrounding this link.

Bibliography

1. Needs, H.I., et al., *Interplay between Mitochondrial Protein Import and Respiratory Complexes Assembly in Neuronal Health and Degeneration.* Life-Basel, 2021. **11**(5).
2. Osellame, L.D., T.S. Blacker, and M.R. Duchen, *Cellular and molecular mechanisms of mitochondrial function.* Best Practice & Research Clinical Endocrinology & Metabolism, 2012. **26**(6): p. 711-723.
3. Pfanner, N., B. Warscheid, and N. Wiedemann, *Mitochondrial proteins: from biogenesis to functional networks.* Nature Reviews Molecular Cell Biology, 2019. **20**(5): p. 267-284.
4. Westermann, B., *Mitochondrial fusion and fission in cell life and death.* Nature Reviews Molecular Cell Biology, 2010. **11**(12): p. 872-884.
5. Edwards, R., R. Eaglesfield, and K. Tokatlidis, *The mitochondrial intermembrane space: the most constricted mitochondrial sub-compartment with the largest variety of protein import pathways.* Open Biology, 2021. **11**(3): p. 13.
6. Palade, G.E., *AN ELECTRON MICROSCOPE STUDY OF THE MITOCHONDRIAL STRUCTURE.* Journal of Histochemistry & Cytochemistry, 1953. **1**(4): p. 188-211.
7. Scott, I. and R.J. Youle, *Mitochondrial fission and fusion*, in *Essays in Biochemistry: Mitochondrial Function*, G.C. Brown and M.P. Murphy, Editors. 2010, Portland Press Ltd: London. p. 85-98.
8. Lewis, M.R. and W.H. Lewis, *Mitochondria in tissue culture.* Science, 1914. **39**(1): p. 330-333.
9. Kageyama, Y., Z.Y. Zhang, and H. Sesaki, *Mitochondrial division: molecular machinery and physiological functions.* Current Opinion in Cell Biology, 2011. **23**(4): p. 427-434.
10. Westermann, B., *Bioenergetic role of mitochondrial fusion and fission.* Biochimica Et Biophysica Acta-Bioenergetics, 2012. **1817**(10): p. 1833-1838.
11. Frederick, R.L. and J.M. Shaw, *Moving mitochondria: Establishing distribution of an essential organelle.* Traffic, 2007. **8**(12): p. 1668-1675.
12. Tamura, Y., K. Itoh, and H. Sesaki, *SnapShot: Mitochondrial Dynamics.* Cell, 2011. **145**(7): p. 1.
13. Itoh, K., et al., *Mitochondrial dynamics in neurodegeneration.* Trends in Cell Biology, 2013. **23**(2): p. 64-71.
14. Bleazard, W., et al., *The dynamin-related GTPase Dnm1 regulates mitochondrial fission in yeast.* Nature Cell Biology, 1999. **1**(5): p. 298-304.
15. Labrousse, A.M., et al., *C-elegans dynamin-related protein DRP-1 controls severing of the mitochondrial outer membrane.* Molecular Cell, 1999. **4**(5): p. 815-826.
16. Smirnova, E., et al., *Dynamin-related protein Drp1 is required for mitochondrial division in mammalian cells.* Molecular Biology of the Cell, 2001. **12**(8): p. 2245-2256.
17. Yoon, Y., K.R. Pitts, and M.A. McNiven, *Mammalian dynamin-like protein DLP1 tubulates membranes.* Molecular Biology of the Cell, 2001. **12**(9): p. 2894-2905.
18. Mears, J.A., et al., *Conformational changes in Dnm1 support a contractile mechanism for mitochondrial fission.* Nature Structural & Molecular Biology, 2011. **18**(1).
19. Fukushima, N.H., et al., *The GTPase effector domain sequence of the Dnm1p GTPase regulates self-assembly and controls a rate-limiting step in mitochondrial fission.* Molecular Biology of the Cell, 2001. **12**(9): p. 2756-2766.
20. Friedman, J., et al., *ER tubules mark sites of mitochondrial division.* Molecular Biology of the Cell, 2011. **22**: p. 1.
21. Otera, H., et al., *Mff is an essential factor for mitochondrial recruitment of Drp1 during mitochondrial fission in mammalian cells.* Journal of Cell Biology, 2010. **191**(6): p. 1141-1158.
22. Yoon, Y., et al., *The mitochondrial protein hFis1 regulates mitochondrial fission in mammalian cells through an interaction with the dynamin-like protein DLP1.* Molecular and Cellular Biology, 2003. **23**(15): p. 5409-5420.
23. Palmer, C.S., et al., *MiD49 and MiD51, new components of the mitochondrial fission machinery.* Embo Reports, 2011. **12**(6): p. 565-573.
24. Wilson, T.J., A.M. Slupe, and S. Strack, *Cell signaling and mitochondrial dynamics: Implications for neuronal function and neurodegenerative disease.* Neurobiology of Disease, 2013. **51**: p. 13-26.
25. Chang, C.R. and C. Blackstone, *Dynamic regulation of mitochondrial fission through modification of the dynamin-related protein Drp1.* Mitochondrial Research in Translational Medicine, 2010. **1201**: p. 34-39.
26. Taguchi, N., et al., *Mitotic phosphorylation of dynamin-related GTPase Drp1 participates in mitochondrial fission.* Journal of Biological Chemistry, 2007. **282**(15): p. 11521-11529.

27. Liesa, M., M. Palacin, and A. Zorzano, *Mitochondrial Dynamics in Mammalian Health and Disease.* Physiological Reviews, 2009. **89**(3): p. 799-845.
28. Kashatus, D.F., et al., *RALA and RALBP1 regulate mitochondrial fission at mitosis.* Nature Cell Biology, 2011. **13**(9): p. 1108-1138.
29. Wang, Z.G., et al., *The Mitochondrial Phosphatase PGAM5 Functions at the Convergence Point of Multiple Necrotic Death Pathways.* Cell, 2012. **148**(1-2): p. 228-243.
30. Waterham, H.R., et al., *A lethal defect of mitochondrial and peroxisomal fission.* New England Journal of Medicine, 2007. **356**(17): p. 1736-1741.
31. Wong, E.D., et al., *The dynamin-related GTPase, Mgm1p, is an intermembrane space protein required for maintenance of fusion competent mitochondria.* Journal of Cell Biology, 2000. **151**(2): p. 341-352.
32. Olichon, A., et al., *The human dynamin-related protein OPA1 is anchored to the mitochondrial inner membrane facing the inter-membrane space.* Febs Letters, 2002. **523**(1-3): p. 171-176.
33. Cipolat, S., et al., *OPA1 requires mitofusin 1 to promote mitochondrial fusion.* Proceedings of the National Academy of Sciences of the United States of America, 2004. **101**(45): p. 15927-15932.
34. Song, Z.Y., et al., *Mitofusins and OPA1 Mediate Sequential Steps in Mitochondrial Membrane Fusion.* Molecular Biology of the Cell, 2009. **20**(15): p. 3525-3532.
35. Chen, H.C., et al., *Mitofusins Mfn1 and Mfn2 coordinately regulate mitochondrial fusion and are essential for embryonic development.* Journal of Cell Biology, 2003. **160**(2): p. 189-200.
36. Koshiba, T., et al., *Structural basis of mitochondrial tethering by mitofusin complexes.* Science, 2004. **305**(5685): p. 858-862.
37. Delettre, C., et al., *Mutation spectrum and splicing variants in the OPA1 gene.* Human Genetics, 2001. **109**(6): p. 584-591.
38. McQuibban, G.A., S. Saurya, and M. Freeman, *Mitochondrial membrane remodelling regulated by a conserved rhomboid protease.* Nature, 2003. **423**(6939): p. 537-541.
39. Cipolat, S., et al., *Mitochondrial rhomboid PARL regulates cytochrome c release during apoptosis via OPA1-dependent cristae remodeling.* Cell, 2006. **126**(1): p. 163-175.
40. Griparic, L., T. Kanazawa, and A.M. van der Bliek, *Regulation of the mitochondrial dynamin-like protein Opa1 by proteolytic cleavage.* Journal of Cell Biology, 2007. **178**(5): p. 757-764.
41. Song, Z.Y., et al., *OPA1 processing controls mitochondrial fusion and is regulated by mRNA splicing, membrane potential, and Yme1L.* Journal of Cell Biology, 2007. **178**(5): p. 749-755.
42. Ishihara, N., et al., *Regulation of mitochondrial morphology through proteolytic cleavage of OPA1.* Embo Journal, 2006. **25**(13): p. 2966-2977.
43. Meeusen, S., J.M. McCaffery, and J. Nunnari, *Mitochondrial fusion intermediates revealed in vitro.* Science, 2004. **305**(5691): p. 1747-1752.
44. Zuchner, S. and J.M. Vance, *Mechanisms of Disease: a molecular genetic update on hereditary axonal neuropathies.* Nature Clinical Practice Neurology, 2006. **2**(1): p. 45-53.
45. Skre, H., *GENETIC AND CLINICAL ASPECTS OF CHARCOT-MARIE-TOOTHS DISEASE.* Clinical Genetics, 1974. **6**(2): p. 98-118.
46. Javadov, S., et al., *Mitochondrial respiratory supercomplexes in mammalian cells: structural versus functional role.* Journal of Molecular Medicine-Jmm, 2021. **99**(1): p. 57-73.
47. Mitchell, P., *COUPLING OF PHOSPHORYLATION TO ELECTRON AND HYDROGEN TRANSFER BY A CHEMI-OSMOTIC TYPE OF MECHANISM.* Nature, 1961. **191**(478).
48. Nicholls, D.G. and S.J. Ferguson, *Bioenergetics 4*. 4 ed. 2013: Academic Press, Elsevier. 419.
49. Mitchell, P., *Chemiosmotic coupling in oxidative and photosynthetic phosphorylation.* Biochimica Et Biophysica Acta-Bioenergetics, 2011. **1807**(12): p. 1507-1538.
50. Couvillion, M.T., et al., *Synchronized mitochondrial and cytosolic translation programs.* Nature, 2016. **533**(7604): p. 499-503.
51. Herrmann, J.M., M.W. Woellhaf, and N. Bonnefoy, *Control of protein synthesis in yeast mitochondria: the concept of translational activators.* Biochim Biophys Acta, 2013. **1833**(2): p. 286-294.
52. Ott, M., A. Amunts, and A. Brown, *Organization and Regulation of Mitochondrial Protein Synthesis.* Annu Rev Biochem, 2016. **85**: p. 77-101.
53. Dennerlein, S., C. Wang, and P. Rehling, *Plasticity of Mitochondrial Translation.* Trends Cell Biol, 2017. **27**(10): p. 712-721.
54. Timón-Gómez A, N.E., Abriata LA, Vila AJ, Hosler J, Barrientos A., *Mitochondrial cytochrome c oxidase biogenesis: Recent developments.* Semin Cell Dev Biol. , 2018. **76**: p. 163-178.
55. Gruschke, S., et al., *The Cbp3-Cbp6 complex coordinates cytochrome b synthesis with bc(1) complex assembly in yeast mitochondria.* J Cell Biol, 2012. **199**(1): p. 137-150.

56. Hildenbeutel, M., Hegg EL, Stephan K, Gruschke S, Meunier B, Ott M., *Assembly factors monitor sequential hemylation of cytochrome b to regulate mitochondrial translation.* J Cell Biol. , 2014. **205**(4): p. 511-524.
57. García-Villegas, R., et al., *The Cox1 C-terminal domain is a central regulator of cytochrome c oxidase biogenesis in yeast mitochondria.* J Biol Chem, 2017. **292**(26): p. 10912-10925.
58. Perez-Martinez, X., et al., *Dual functions of Mss51 couple synthesis of Cox1 to assembly of cytochrome c oxidase in Saccharomyces cerevisiae mitochondria.* Mol Biol Cell, 2009. **20**(20): p. 4371-80.
59. Tavares-Carreón, F., et al., *The pentatricopeptide repeats present in Pet309 are necessary for translation but not for stability of the mitochondrial COX1 mRNA in yeast.* J Biol Chem, 2008. **283**(3): p. 1472-9.
60. Zamudio-Ochoa, A., et al., *The Pet309 pentatricopeptide repeat motifs mediate efficient binding to the mitochondrial COX1 transcript in yeast.* RNA Biol, 2014. **11**(7): p. 953-67.
61. Godard, F., et al., *A genetic screen targeted on the FO component of mitochondrial ATP synthase in Saccharomyces cerevisiae.* J Biol Chem, 2011. **286**(20): p. 18181-9.
62. Helfenbein, K.G., et al., *ATP22, a nuclear gene required for expression of the F0 sector of mitochondrial ATPase in Saccharomyces cerevisiae.* J Biol Chem, 2003. **278**(22): p. 19751-6.
63. Rath, S., et al., *MitoCarta3.0: an updated mitochondrial proteome now with sub-organelle localization and pathway annotations.* Nucleic Acids Research, 2021. **49**(D1): p. D1541-D1547.
64. Neupert, W., *Protein import into mitochondria.* Annual Review of Biochemistry, 1997. **66**: p. 863-917.
65. Chacinska, A., et al., *Importing Mitochondrial Proteins: Machineries and Mechanisms.* Cell, 2009. **138**(4): p. 628-644.
66. Tucker, K. and E. Park, *Cryo-EM structure of the mitochondrial protein-import channel TOM complex at near-atomic resolution.* Nature Structural & Molecular Biology, 2019. **26**(12).
67. Sollner, T., et al., *MOM19, AN IMPORT RECEPTOR FOR MITOCHONDRIAL PRECURSOR PROTEINS.* Cell, 1989. **59**(6): p. 1061-1070.
68. Moczko, M., et al., *IDENTIFICATION OF THE MITOCHONDRIAL RECEPTOR COMPLEX IN SACCHAROMYCES-CEREVISIAE.* Febs Letters, 1992. **310**(3): p. 265-268.
69. Hines, V., et al., *PROTEIN IMPORT INTO YEAST MITOCHONDRIA IS ACCELERATED BY THE OUTER-MEMBRANE PROTEIN MAS70.* Embo Journal, 1990. **9**(10): p. 3191-3200.
70. Sollner, T., et al., *A MITOCHONDRIAL IMPORT RECEPTOR FOR THE ADP/ATP CARRIER.* Cell, 1990. **62**(1): p. 107-115.
71. van Wilpe, S., et al., *Tom22 is a multifunctional organizer of the mitochondrial preprotein translocase.* Nature, 1999. **401**(6752): p. 485-489.
72. Lithgow, T., et al., *THE MITOCHONDRIAL OUTER-MEMBRANE PROTEIN MAS22P IS ESSENTIAL FOR PROTEIN IMPORT AND VIABILITY OF YEAST.* Proceedings of the National Academy of Sciences of the United States of America, 1994. **91**(25): p. 11973-11977.
73. Sakaue, H., et al., *Porin Associates with Tom22 to Regulate the Mitochondrial Protein Gate Assembly.* Molecular Cell, 2019. **73**(5).
74. Grevel, A. and T. Becker, *Porins as helpers in mitochondrial protein translocation.* Biological Chemistry, 2020. **401**(6-7): p. 699-708.
75. Harbauer, A.B., et al., *Cell cycle-dependent regulation of mitochondrial preprotein translocase.* Science, 2014. **346**(6213): p. 1109-1113.
76. Kunkele, K.P., et al., *The preprotein translocation channel of the outer membrane of mitochondria.* Cell, 1998. **93**(6): p. 1009-1019.
77. Shiota, T., et al., *Molecular architecture of the active mitochondrial protein gate.* Science, 2015. **349**(6255): p. 1544-1548.
78. Model, K., et al., *Protein translocase of the outer mitochondrial membrane: Role of import receptors in the structural organization of the TOM complex.* Journal of Molecular Biology, 2002. **316**(3): p. 657-666.
79. Model, K., C. Meisinger, and W. Kuhlbrandt, *Cryo-Electron Microscopy Structure of a Yeast Mitochondrial Preprotein Translocase.* Journal of Molecular Biology, 2008. **383**(5): p. 1049-1057.
80. Bausewein, T., et al., *Cryo-EM Structure of the TOM Core Complex from Neurospora crassa.* Cell, 2017. **170**(4).
81. Moczko, M., et al., *The intermembrane space domain of mitochondrial Tom22 functions as a trans binding site for properties with N-terminal targeting sequences.* Molecular and Cellular Biology, 1997. **17**(11): p. 6574-6584.

82. Harner, M., W. Neupert, and M. Deponte, *Lateral release of proteins from the TOM complex into the outer membrane of mitochondria.* Embo Journal, 2011. **30**(16): p. 3232-3241.
83. Sekine, S. and R.J. Youle, *PINK1 import regulation; a fine system to convey mitochondrial stress to the cytosol.* Bmc Biology, 2018. **16**: p. 12.
84. Hasson, S.A., et al., *High-content genome-wide RNAi screens identify regulators of parkin upstream of mitophagy.* Nature, 2013. **504**(7479).
85. Jacoupy, M., et al., *The PINK1 kinase-driven ubiquitin ligase Parkin promotes mitochondrial protein import through the presequence pathway in living cells.* Scientific Reports, 2019. **9**: p. 15.
86. Phu, L., et al., *Dynamic Regulation of Mitochondrial Import by the Ubiquitin System.* Molecular Cell, 2020. **77**(5).
87. Ordureau, A., et al., *Global Landscape and Dynamics of Parkin and USP30-Dependent Ubiquitylomes in iNeurons during Mitophagic Signaling.* Molecular Cell, 2020. **77**(5).
88. Harbauer, A.B., et al., *The Protein Import Machinery of Mitochondria-A Regulatory Hub in Metabolism, Stress, and Disease.* Cell Metabolism, 2014. **19**(3): p. 357-372.
89. Paschen, S.A., et al., *Evolutionary conservation of biogenesis of beta-barrel membrane proteins.* Nature, 2003. **426**(6968): p. 862-866.
90. Kutik, S., et al., *Dissecting membrane insertion of mitochondrial beta-barrel proteins.* Cell, 2008. **132**(6): p. 1011-1024.
91. Becker, T., et al., *Sorting and assembly of mitochondrial outer membrane proteins.* Biochimica Et Biophysica Acta-Bioenergetics, 2008. **1777**(7-8): p. 557-563.
92. Diederichs, K.A., et al., *Structural insight into mitochondrial beta-barrel outer membrane protein biogenesis.* Nature Communications, 2020. **11**(1): p. 13.
93. Imai, K., et al., *Eukaryote-wide sequence analysis of mitochondrial beta-barrel outer membrane proteins.* Bmc Genomics, 2011. **12**: p. 17.
94. Walther, D.M., D. Rapaport, and J. Tommassen, *Biogenesis of beta-barrel membrane proteins in bacteria and eukaryotes: evolutionary conservation and divergence.* Cellular and Molecular Life Sciences, 2009. **66**(17): p. 2789-2804.
95. Wenz, L.S., et al., *Sam37 is crucial for formation of the mitochondrial TOM-SAM supercomplex, thereby promoting beta-barrel biogenesis.* Journal of Cell Biology, 2015. **210**(7): p. 1047-1054.
96. Meisinger, C., et al., *The mitochondrial morphology protein Mdm10 functions in assembly of the preprotein translocase of the outer membrane.* Developmental Cell, 2004. **7**(1): p. 61-71.
97. Doan, K.N., et al., *The Mitochondrial Import Complex MIM Functions as Main Translocase for alpha-Helical Outer Membrane Proteins.* Cell Reports, 2020. **31**(4): p. 15.
98. Becker, T., et al., *The mitochondrial import protein Mim1 promotes biogenesis of multispanning outer membrane proteins.* Journal of Cell Biology, 2011. **194**(3): p. 387-395.
99. Krumpe, K., et al., *Ergosterol content specifies targeting of tail-anchored proteins to mitochondrial outer membranes.* Molecular Biology of the Cell, 2012. **23**(20): p. 3927-3935.
100. Kruger, V., et al., *Identification of new channels by systematic analysis of the mitochondrial outer membrane.* Journal of Cell Biology, 2017. **216**(11): p. 3485-3495.
101. Dimmer, K.S., et al., *A crucial role for Mim2 in the biogenesis of mitochondrial outer membrane proteins.* Journal of Cell Science, 2012. **125**(14): p. 3464-3473.
102. Wenz, L.S., et al., *The presequence pathway is involved in protein sorting to the mitochondrial outer membrane.* Embo Reports, 2014. **15**(6): p. 678-685.
103. Sinzel, M., et al., *Mcp3 is a novel mitochondrial outer membrane protein that follows a unique IMP-dependent biogenesis pathway.* Embo Reports, 2016. **17**(7): p. 965-981.
104. Mokranjac, D. and W. Neupert, *Energetics of protein translocation into mitochondria.* Biochimica Et Biophysica Acta-Bioenergetics, 2008. **1777**(7-8): p. 758-762.
105. Komiya, T., et al., *Binding of mitochondrial precursor proteins to the cytoplasmic domains of the import receptors Tom70 and Tom20 is determined by cytoplasmic chaperones.* Embo Journal, 1997. **16**(14): p. 4267-4275.
106. Yamamoto, H., et al., *Tim50 is a subunit of the TIM23 complex that links protein translocation across the outer and inner mitochondrial membranes.* Cell, 2002. **111**(4): p. 519-528.
107. Komiya, T., et al., *Interaction of mitochondrial targeting signals with acidic receptor domains along the protein import pathway: evidence for the 'acid chain' hypothesis.* Embo Journal, 1998. **17**(14): p. 3886-3898.
108. Ford, H.C., et al., *Towards a molecular mechanism underlying mitochondrial protein import through the TOM and TIM23 complexes.* bioRxiv, 2021: 2021.08.30.458282.

109. Dudek, J., P. Rehling, and M. van der Laan, *Mitochondrial protein import: Common principles and physiological networks.* Biochimica Et Biophysica Acta-Molecular Cell Research, 2013. **1833**(2): p. 274-285.
110. Garcia, M., et al., *Mitochondrial presequence and open reading frame mediate asymmetric localization of messenger RNA.* Embo Reports, 2010. **11**(4): p. 285-291.
111. Margeot, A., et al., *In Saccharomyces cerevisiae, ATP2 mRNA sorting to the vicinity of mitochondria is essential for respiratory function.* Embo Journal, 2002. **21**(24): p. 6893-6904.
112. Corral-Debrinski, M., C. Blugeon, and C. Jacq, *In yeast, the 3' untranslated region or the presequence of ATM1 is required for the exclusive localization of its mRNA to the vicinity of mitochondria.* Mol Cell Biol, 2000. **20**(21): p. 7881-92.
113. George, R., et al., *The nascent polypeptide-associated complex (NAC) promotes interaction of ribosomes with the mitochondrial surface in vivo.* Febs Letters, 2002. **516**(1-3): p. 213-216.
114. MacKenzie, J.A. and R.M. Payne, *Ribosomes specifically bind to mammalian mitochondria via protease-sensitive proteins on the outer membrane.* Journal of Biological Chemistry, 2004. **279**(11): p. 9803-9810.
115. Edwards, R., R. Eaglesfield, and K. Tokatlidis, *The mitochondrial intermembrane space: the most constricted mitochondrial sub-compartment with the largest variety of protein import pathways.* Open Biology, 2021. **11**(3).
116. Peleh, V., E. Cordat, and J.M. Herrmann, *Mia40 is a trans-site receptor that drives protein import into the mitochondrial intermembrane space by hydrophobic substrate binding.* Elife, 2016. **5**: p. 19.
117. Chacinska, A., et al., *Essential role of Mia40 in import and assembly of mitochondrial intermembrane space proteins.* Embo Journal, 2004. **23**(19): p. 3735-3746.
118. Banci, L., et al., *MIA40 is an oxidoreductase that catalyzes oxidative protein folding in mitochondria.* Nature Structural & Molecular Biology, 2009. **16**(2): p. 198-206.
119. Reinhardt, C., et al., *AIF meets the CHCHD4/Mia40-dependent mitochondrial import pathway.* Biochimica Et Biophysica Acta-Molecular Basis of Disease, 2020. **1866**(6): p. 14.
120. Bien, M., et al., *Mitochondrial Disulfide Bond Formation Is Driven by Intersubunit Electron Transfer in Erv1 and Proofread by Glutathione.* Molecular Cell, 2010. **37**(4): p. 516-528.
121. Allen, S., et al., *Erv1 mediates the Mia40-dependent protein import pathway and provides a functional link to the respiratory chain by shuttling electrons to cytochrome c.* Journal of Molecular Biology, 2005. **353**(5): p. 937-944.
122. Backes, S., et al., *Tom70 enhances mitochondrial preprotein import efficiency by binding to internal targeting sequences.* Journal of Cell Biology, 2018. **217**(4): p. 1369-1382.
123. Demishtein-Zohary, K. and A. Azem, *The TIM23 mitochondrial protein import complex: function and dysfunction.* Cell and Tissue Research, 2017. **367**(1): p. 33-41.
124. Maarse, A.C., et al., *IDENTIFICATION OF THE ESSENTIAL YEAST PROTEIN MIM17, AN INTEGRAL MITOCHONDRIAL INNER MEMBRANE-PROTEIN INVOLVED IN PROTEIN IMPORT.* Febs Letters, 1994. **349**(2): p. 215-221.
125. Dekker, P.J.T., et al., *IDENTIFICATION OF MIM23, A PUTATIVE COMPONENT OF THE PROTEIN IMPORT MACHINERY OF THE MITOCHONDRIAL INNER MEMBRANE.* Febs Letters, 1993. **330**(1): p. 66-70.
126. Geissler, A., et al., *The mitochondrial presequence translocase: An essential role of Tim50 in directing preproteins to the import channel.* Cell, 2002. **111**(4): p. 507-518.
127. Gebert, M., et al., *Mgr2 promotes coupling of the mitochondrial presequence translocase to partner complexes.* Journal of Cell Biology, 2012. **197**(5): p. 595-604.
128. Chacinska, A., et al., *Mitochondrial presequence translocase: Switching between TOM tethering and motor recruitment involves Tim21 and Tim17.* Cell, 2005. **120**(6): p. 817-829.
129. Maarse, A.C., et al., *MPI1, AN ESSENTIAL GENE ENCODING A MITOCHONDRIAL-MEMBRANE PROTEIN, IS POSSIBLY INVOLVED IN PROTEIN IMPORT INTO YEAST MITOCHONDRIA.* Embo Journal, 1992. **11**(10): p. 3619-3628.
130. Kang, P.J., et al., *REQUIREMENT FOR HSP70 IN THE MITOCHONDRIAL MATRIX FOR TRANSLOCATION AND FOLDING OF PRECURSOR PROTEINS.* Nature, 1990. **348**(6297): p. 137-143.
131. Frazier, A.E., et al., *Pam16 has an essential role in the mitochondrial protein import motor.* Nature Structural & Molecular Biology, 2004. **11**(3): p. 226-233.
132. Truscott, K.N., et al., *A J-protein is an essential subunit of the presequence translocase-associated protein import motor of mitochondria.* Journal of Cell Biology, 2003. **163**(4): p. 707-713.

133. van der Laan, M., et al., *Pam17 is required for architecture and translocation activity of the mitochondrial protein import motor.* Molecular and Cellular Biology, 2005. **25**(17): p. 7449-7458.
134. Laloraya, S., B.D. Gambill, and E.A. Craig, *A ROLE FOR A EUKARYOTIC GRPE-RELATED PROTEIN, MGE1P, IN PROTEIN TRANSLOCATION.* Proceedings of the National Academy of Sciences of the United States of America, 1994. **91**(14): p. 6481-6485.
135. Tamura, Y., et al., *Tim23-Tim50 pair coordinates functions of translocators and motor proteins in mitochondrial protein import.* Journal of Cell Biology, 2009. **184**(1): p. 129-141.
136. Schwartz, M.P. and A. Matouschek, *The dimensions of the protein import channels in the outer and inner mitochondrial membranes.* Proceedings of the National Academy of Sciences of the United States of America, 1999. **96**(23): p. 13086-13090.
137. Truscott, K.N., et al., *A presequence- and voltage-sensitive channel of the mitochondrial preprotein translocase formed by Tim23.* Nature Structural Biology, 2001. **8**(12): p. 1074-1082.
138. Martinez-Caballero, S., et al., *Tim17p regulates the twin pore structure and voltage gating of the mitochondrial protein import complex TIM23.* Journal of Biological Chemistry, 2007. **282**(6): p. 3584-3593.
139. Chacinska, A., et al., *Mitochondrial translocation contact sites: separation of dynamic and stabilizing elements in formation of a TOM-TIM-preprotein supercomplex.* Embo Journal, 2003. **22**(20): p. 5370-5381.
140. Waegemann, K., et al., *Cooperation of TOM and TIM23 Complexes during Trans location of Proteins into Mitochondria.* Journal of Molecular Biology, 2015. **427**(5): p. 1075-1084.
141. Shiota, T., et al., *In vivo protein-interaction mapping of a mitochondrial translocator protein Tom22 at work.* Proceedings of the National Academy of Sciences of the United States of America, 2011. **108**(37): p. 15179-15183.
142. Niemi, N.M., et al., *Pptc7 is an essential phosphatase for promoting mammalian mitochondrial metabolism and biogenesis.* Nature Communications, 2019. **10**: p. 14.
143. Marom, M., et al., *Direct Interaction of Mitochondrial Targeting Presequences with Purified Components of the TIM23 Protein Complex.* Journal of Biological Chemistry, 2011. **286**(51): p. 43809-43815.
144. Ting, S.Y., et al., *Dual interaction of scaffold protein Tim44 of mitochondrial import motor with channel-forming translocase subunit Tim23.* Elife, 2017. **6**: p. 22.
145. Neupert, W. and M. Brunner, *The protein import motor of mitochondria.* Nature Reviews Molecular Cell Biology, 2002. **3**(8): p. 555-565.
146. Gruhler, A., et al., *N-terminal hydrophobic sorting signals of preproteins confer mitochondrial hsp70 independence for import into mitochondria.* Journal of Biological Chemistry, 1997. **272**(28): p. 17410-17415.
147. van der Laan, M., et al., *A role for Tim21 in membrane-potential-dependent preprotein sorting in mitochondria.* Current Biology, 2006. **16**(22): p. 2271-2276.
148. Albrecht, R., et al., *The Tim21 binding domain connects the preprotein translocases of both mitochondrial membranes.* Embo Reports, 2006. **7**(12): p. 1233-1238.
149. Mokranjac, D., et al., *Role of Tim21 in mitochondrial translocation contact sites.* Journal of Biological Chemistry, 2005. **280**(25): p. 23437-23440.
150. Ieva, R., et al., *Mgr2 Functions as Lateral Gatekeeper for Preprotein Sorting in the Mitochondrial Inner Membrane.* Molecular Cell, 2014. **56**(5): p. 641-652.
151. Endres, M., W. Neupert, and M. Brunner, *Transport of the ADP ATP carrier of mitochondria from the TOM complex to the TIM22.54 complex.* Embo Journal, 1999. **18**(12): p. 3214-3221.
152. Curran, S.P., et al., *The Tim9p-Tim10p complex binds to the transmembrane domains of the ADP/ATP carrier.* Embo Journal, 2002. **21**(5): p. 942-953.
153. Rehling, P., et al., *Protein insertion into the mitochondrial inner membrane by a twin-pore translocase.* Science, 2003. **299**(5613): p. 1747-1751.
154. Brix, J., et al., *Distribution of binding sequences for the mitochondrial import receptors Tom20, Tom22, and Tom70 in a presequence-carrying preprotein and a non-cleavable preprotein.* Journal of Biological Chemistry, 1999. **274**(23): p. 16522-16530.
155. Curran, S.P., et al., *The role of the Tim8p-Tim13p complex in a conserved import pathway for mitochondrial polytopic inner membrane proteins.* Journal of Cell Biology, 2002. **158**(6): p. 1017-1027.
156. Qi, L.B., et al., *Cryo-EM structure of the human mitochondrial translocase TIM22 complex.* Cell Research, 2021. **31**(3): p. 369-372.
157. Zhang, Y.T., et al., *Structure of the mitochondrial TIM22 complex from yeast.* Cell Research, 2021. **31**(3): p. 366-368.

158. Callegari, S., et al., *TIM29 is a subunit of the human carrier translocase required for protein transport.* Febs Letters, 2016. **590**(23): p. 4147-4158.
159. Kang, Y.L., et al., *Tim29 is a novel subunit of the human TIM22 translocase and is involved in complex assembly and stability.* Elife, 2016. **5**: p. 22.
160. Vukotic, M., et al., *Acylglycerol Kinase Mutated in Sengers Syndrome Is a Subunit of the TIM22 Protein Translocase in Mitochondria.* Molecular Cell, 2017. **67**(3).
161. Kang, Y.L., et al., *Sengers Syndrome-Associated Mitochondrial Acylglycerol Kinase Is a Subunit of the Human TIM22 Protein Import Complex.* Molecular Cell, 2017. **67**(3).
162. Wiedemann, N. and N. Pfanner, *Mitochondrial Machineries for Protein Import and Assembly*, in *Annual Review of Biochemistry, Vol 86*, R.D. Kornberg, Editor. 2017, Annual Reviews: Palo Alto. p. 685-714.
163. Rehling, P., K. Brandner, and N. Pfanner, *Mitochondrial import and the twin-pore translocase.* Nature Reviews Molecular Cell Biology, 2004. **5**(7): p. 519-530.
164. Wu, Y.K. and B.D. Sha, *Crystal structure of yeast mitochondrial outer membrane translocon member Tom70p.* Nature Structural & Molecular Biology, 2006. **13**(7): p. 589-593.
165. Young, J.C., N.J. Hoogenraad, and F.U. Hartl, *Molecular chaperones Hsp90 and Hsp70 deliver preproteins to the mitochondrial import receptor Tom70.* Cell, 2003. **112**(1): p. 41-50.
166. Bhangoo, M.K., et al., *Multiple 40-kDa heat-shock protein chaperones function in Tom70-dependent mitochondrial import.* Molecular Biology of the Cell, 2007. **18**(9): p. 3414-3428.
167. Backes, S., et al., *The mitochondrial surface receptor Tom70 protects the cytosol against mitoprotein-induced stress.* bioRxiv, 2020. 2020.09.14.296194.
168. Wiedemann, N., N. Pfanner, and M.T. Ryan, *The three modules of ADP/ATP carrier cooperate in receptor recruitment and translocation into mitochondria.* Embo Journal, 2001. **20**(5): p. 951-960.
169. Ellenrieder, L., et al., *Dual Role of Mitochondrial Porin in Metabolite Transport across the Outer Membrane and Protein Transfer to the Inner Membrane.* Molecular Cell, 2019. **73**(5).
170. Callegari, S., et al., *A MICOS-TIM22 Association Promotes Carrier Import into Human Mitochondria.* Journal of Molecular Biology, 2019. **431**(15): p. 2835-2851.
171. Rampelt, H., et al., *The mitochondrial carrier pathway transports non-canonical substrates with an odd number of transmembrane segments.* Bmc Biology, 2020. **18**(1): p. 14.
172. Jackson, T.D., et al., *The TIM22 complex mediates the import of Sideroflexins and is required for efficient mitochondrial one-carbon metabolism.* Molecular Biology of the Cell. **0**(0): p. mbc.E20-06-0390.
173. Luirink, J., T. Samuelsson, and J.W. de Gier, *YidC/Oxa1p/Alb3: evolutionarily conserved mediators of membrane protein assembly.* Febs Letters, 2001. **501**(1): p. 1-5.
174. Bonnefoy, N., et al., *OXA1, A SACCHAROMYCES-CEREVISIAE NUCLEAR GENE WHOSE SEQUENCE IS CONSERVED FROM PROKARYOTES TO EUKARYOTES CONTROLS CYTOCHROME-OXIDASE BIOGENESIS.* Journal of Molecular Biology, 1994. **239**(2): p. 201-212.
175. Herrmann, J.M., W. Neupert, and R.A. Stuart, *Insertion into the mitochondrial inner membrane of a polytopic protein, the nuclear-encoded Oxa1p.* Embo Journal, 1997. **16**(9): p. 2217-2226.
176. Nargang, F.E., et al., *The oxal protein forms a homooligomeric complex and is an essential part of the mitochondrial export translocase in Neurospora crassa.* Journal of Biological Chemistry, 2002. **277**(15): p. 12846-12853.
177. Stiburek, L., et al., *Knockdown of human Oxa1l impairs the biogenesis of F1Fo-ATP synthase and NADH : Ubiquinone oxidoreductase.* Journal of Molecular Biology, 2007. **374**(2): p. 506-516.
178. Haque, M.E., et al., *Properties of the C-terminal Tail of Human Mitochondrial Inner Membrane Protein Oxa1L and Its Interactions with Mammalian Mitochondrial Ribosomes.* Journal of Biological Chemistry, 2010. **285**(36): p. 28353-28362.
179. Itoh, Y., et al., *Mechanism of membrane-tethered mitochondrial protein synthesis.* Science, 2021. **371**(6531).
180. Stuart, R.A., *Insertion of proteins into the inner membrane of mitochondria: the role of the Oxa1 complex.* Biochimica Et Biophysica Acta-Molecular Cell Research, 2002. **1592**(1): p. 79-87.
181. Bohnert, M., et al., *Cooperation of Stop-Transfer and Conservative Sorting Mechanisms in Mitochondrial Protein Transport.* Current Biology, 2010. **20**(13): p. 1227-1232.
182. Anghel, S.A., et al., *Identification of Oxa1 Homologs Operating in the Eukaryotic Endoplasmic Reticulum.* Cell Reports, 2017. **21**(13): p. 3708-3716.
183. Pleiner, T., et al., *Structural basis for membrane insertion by the human ER membrane protein complex.* Science, 2020. **369**(6502).

184. Bai, L., et al., *Structure of the ER membrane complex, a transmembrane-domain insertase.* Nature, 2020. **584**(7821).
185. Chitwood, P.J., et al., *EMC Is Required to Initiate Accurate Membrane Protein Topogenesis.* Cell, 2018. **175**(6).
186. Rojo, E.E., R.A. Stuart, and W. Neupert, *CONSERVATIVE SORTING OF F-0-ATPASE SUBUNIT-9 - EXPORT FROM MATRIX REQUIRES DELTA-PH ACROSS INNER MEMBRANE AND MATRIX ATP.* Embo Journal, 1995. **14**(14): p. 3445-3451.
187. Hell, K., W. Neupert, and R.A. Stuart, *Oxa1p acts as a general membrane insertion machinery for proteins encoded by mitochondrial DNA.* Embo Journal, 2001. **20**(6): p. 1281-1288.
188. Herrmann, J.M. and N. Bonnefoy, *Protein export across the inner membrane of mitochondria - The nature of translocated domains determines the dependence on the Oxa1 translocase.* Journal of Biological Chemistry, 2004. **279**(4): p. 2507-2512.
189. MacKenzie, J.A. and R.M. Payne, *Mitochondrial protein import and human health and disease.* Biochimica Et Biophysica Acta-Molecular Basis of Disease, 2007. **1772**(5): p. 509-523.
190. Briston, T. and A.R. Hicks, *Mitochondrial dysfunction and neurodegenerative proteinopathies: mechanisms and prospects for therapeutic intervention.* Biochemical Society Transactions, 2018. **46**: p. 829-842.
191. Jackson, T.D., C.S. Palmer, and D. Stojanovski, *Mitochondrial diseases caused by dysfunctional mitochondrial protein import.* Biochemical Society Transactions, 2018. **46**: p. 1225-1238.
192. Gerstner, W., et al., *Neuronal Dynamics*, in *From single neurons to networks and models of cognition and beyond*. 2014.
193. Spaulding, E.L. and R.W. Burgess, *Accumulating Evidence for Axonal Translation in Neuronal Homeostasis.* Frontiers in Neuroscience, 2017. **11**: p. 7.
194. Sleigh, J.N., et al., *Axonal transport and neurological disease.* Nature Reviews Neurology, 2019. **15**(12): p. 691-703.
195. Meriney, S.D. and E.E. Fanselow, *Synaptic Transmission*. 2019, Academic Press, Elsevier. p. 1-516.
196. Watts, M.E., R. Pocock, and C. Claudianos, *Brain Energy and Oxygen Metabolism: Emerging Role in Normal Function and Disease.* Frontiers in Molecular Neuroscience, 2018. **11**: p. 13.
197. Morris, R.L. and P.J. Hollenbeck, *THE REGULATION OF BIDIRECTIONAL MITOCHONDRIAL TRANSPORT IS COORDINATED WITH AXONAL OUTGROWTH.* Journal of Cell Science, 1993. **104**: p. 917-927.
198. Ruthel, G. and P.J. Hollenbeck, *Response of mitochondrial traffic to axon determination and differential branch growth.* Journal of Neuroscience, 2003. **23**(24): p. 8618-8624.
199. Przedborski, S., M. Vila, and V. Jackson-Lewis, *Neurodegeneration: What is it and where are we?* Journal of Clinical Investigation, 2003. **111**(1): p. 3-10.
200. Dugger, B.N. and D.W. Dickson, *Pathology of Neurodegenerative Diseases.* Cold Spring Harbor Perspectives in Biology, 2017. **9**(7): p. 22.
201. Jellinger, K.A., *Basic mechanisms of neurodegeneration: a critical update.* Journal of Cellular and Molecular Medicine, 2010. **14**(3): p. 457-487.
202. Perl, D.P. and W.W. Pendlebury, *NEUROPATHOLOGY OF DEMENTIA.* Neurologic Clinics, 1986. **4**(2): p. 355-368.
203. Coleman, M.P. and V.H. Perry, *Axon pathology in neurological disease: a neglected therapeutic target.* Trends in Neurosciences, 2002. **25**(10): p. 532-537.
204. Raff, M.C., A.V. Whitmore, and J.T. Finn, *Neuroscience - Axonal self-destruction and neurodegeneration.* Science, 2002. **296**(5569): p. 868-871.
205. Kweon, J.H., S. Kim, and S.B. Lee, *The cellular basis of dendrite pathology in neurodegenerative diseases.* Bmb Reports, 2017. **50**(1): p. 5-11.
206. Jaworski, T., et al., *Dendritic Degeneration, Neurovascular Defects, and Inflammation Precede Neuronal Loss in a Mouse Model for Tau-Mediated Neurodegeneration.* American Journal of Pathology, 2011. **179**(4): p. 2001-2015.
207. Colom-Cadena, M., et al., *The clinical promise of biomarkers of synapse damage or loss in Alzheimer's disease.* Alzheimers Research & Therapy, 2020. **12**(1): p. 12.
208. Wishart, T.M., S.H. Parson, and T.H. Gillingwater, *Synaptic vulnerability in neurodegenerative disease.* Journal of Neuropathology and Experimental Neurology, 2006. **65**(8): p. 733-739.
209. Gillingwater, T.H. and T.M. Wishart, *Mechanisms underlying synaptic vulnerability and degeneration in neurodegenerative disease.* Neuropathology and Applied Neurobiology, 2013. **39**(4): p. 320-334.

210. Kumar, V., et al., *Protein aggregation and neurodegenerative diseases: From theory to therapy.* European Journal of Medicinal Chemistry, 2016. **124**: p. 1105-1120.
211. Wu, Y.B., M.Q. Chen, and J.L. Jiang, *Mitochondrial dysfunction in neurodegenerative diseases and drug targets via apoptotic signaling.* Mitochondrion, 2019. **49**: p. 35-45.
212. Wang, Y., et al., *Mitochondrial dysfunction in neurodegenerative diseases and the potential countermeasure.* Cns Neuroscience & Therapeutics, 2019. **25**(7): p. 816-824.
213. Franco-Iborra, S., M. Vila, and C. Perier, *Mitochondrial Quality Control in Neurodegenerative Diseases: Focus on Parkinson's Disease and Huntington's Disease.* Frontiers in Neuroscience, 2018. **12**: p. 25.
214. Amor, S. and M.N. Woodroofe, *Innate and adaptive immune responses in neurodegeneration and repair.* Immunology, 2014. **141**(3): p. 287-291.
215. Devi, L., et al., *Accumulation of amyloid precursor protein in the mitochondrial import channels of human Alzheimer's disease brain is associated with mitochondrial dysfunction.* Journal of Neuroscience, 2006. **26**(35): p. 9057-9068.
216. Sirk, D., et al., *Chronic exposure to sub-lethal beta-amyloid (A beta) inhibits the import of nuclear-encoded proteins to mitochondria in differentiated PC12 cells*.* Journal of Neurochemistry, 2007. **103**(5): p. 1989-2003.
217. Hu, Y., et al., *Tau accumulation impairs mitophagy via increasing mitochondrial membrane potential and reducing mitochondrial Parkin.* Oncotarget, 2016. **7**(14): p. 17356-17368.
218. Cieri, D., et al., *Tau localises within mitochondrial sub-compartments and its caspase cleavage affects ER-mitochondria interactions and cellular Ca2+ handling.* Biochimica Et Biophysica Acta-Molecular Basis of Disease, 2018. **1864**(10): p. 3247-3256.
219. Parihar, M.S., et al., *Mitochondrial association of alpha-synuclein causes oxidative stress.* Cellular and Molecular Life Sciences, 2008. **65**(7-8): p. 1272-1284.
220. Devi, L., et al., *Mitochondrial import and accumulation of alpha-synuclein impair complex I in human dopaminergic neuronal cultures and Parkinson disease brain.* Journal of Biological Chemistry, 2008. **283**(14): p. 9089-9100.
221. Smith, W.W., et al., *Endoplasmic reticulum stress and mitochondrial cell death pathways mediate A53T mutant alpha-synuclein-induced toxicity.* Human Molecular Genetics, 2005. **14**(24): p. 3801-3811.
222. Di Maio, R., et al., *alpha-Synuclein binds to TOM20 and inhibits mitochondrial protein import in Parkinson's disease.* Science Translational Medicine, 2016. **8**(342): p. 14.
223. Bender, A., et al., *TOM40 Mediates Mitochondrial Dysfunction Induced by alpha-Synuclein Accumulation in Parkinson's Disease.* Plos One, 2013. **8**(4): p. 11.
224. Yano, H., et al., *Inhibition of mitochondrial protein import by mutant huntingtin.* Nature Neuroscience, 2014. **17**(6): p. 822-831.
225. Napoli, E., et al., *Defective mitochondrial disulfide relay system, altered mitochondrial morphology and function in Huntingtons disease.* Human Molecular Genetics, 2013. **22**(5): p. 989-1004.
226. Vijayvergiya, C., et al., *Mutant superoxide dismutase 1 forms aggregates in the brain mitochondrial matrix of amyotrophic lateral sclerosis mice.* Journal of Neuroscience, 2005. **25**(10): p. 2463-2470.
227. Pasinelli, P., et al., *Amyotrophic lateral sclerosis-associated SOD1 mutant proteins bind and aggregate with Bcl-2 in spinal cord mitochondria.* Neuron, 2004. **43**(1): p. 19-30.
228. Fischer, L.R., et al., *SOD1 targeted to the mitochondrial intermembrane space prevents motor neuropathy in the Sod1 knockout mouse.* Brain, 2011. **134**: p. 196-209.
229. Li, Q.A., et al., *ALS-linked mutant superoxide dismutase 1 (SOD1) alters mitochondrial protein composition and decreases protein import.* Proceedings of the National Academy of Sciences of the United States of America, 2010. **107**(49): p. 21146-21151.
230. Bannwarth, S., et al., *A mitochondrial origin for frontotemporal dementia and amyotrophic lateral sclerosis through CHCHD10 involvement.* Brain, 2014. **137**: p. 2329-2345.
231. Zheng, H. and E.H. Koo, *Biology and pathophysiology of the amyloid precursor protein.* Molecular Neurodegeneration, 2011. **6**: p. 16.
232. Shui, G., *5.44 - Development of In Vitro Neural Models for Drug Discovery and Toxicity Screening*, in *Comprehensive Biotechnology (Second Edition)*, M. Moo-Young, Editor. 2011, Academic Press: Burlington. p. 565-572.
233. Tapia-Rojas, C., et al., *It's all about tau.* Progress in Neurobiology, 2019. **175**: p. 54-76.
234. Szabo, L., A. Eckert, and A. Grimm, *Insights into Disease-Associated Tau Impact on Mitochondria.* International Journal of Molecular Sciences, 2020. **21**(17): p. 27.

235. Witman, G.B., et al., *TUBULIN REQUIRES TAU FOR GROWTH ONTO MICROTUBULE INITIATING SITES.* Proceedings of the National Academy of Sciences of the United States of America, 1976. **73**(11): p. 4070-4074.
236. Binder, L.I., A. Frankfurter, and L.I. Rebhun, *THE DISTRIBUTION OF TAU IN THE MAMMALIAN CENTRAL NERVOUS-SYSTEM.* Journal of Cell Biology, 1985. **101**(4): p. 1371-1378.
237. Black, M.M., et al., *Tau is enriched on dynamic microtubules in the distal region of growing axons.* Journal of Neuroscience, 1996. **16**(11): p. 3601-3619.
238. Chaudhary, A.R., et al., *Tau directs intracellular trafficking by regulating the forces exerted by kinesin and dynein teams.* Traffic, 2018. **19**(2): p. 111-121.
239. Dixit, R., et al., *Differential regulation of dynein and kinesin motor proteins by tau.* Science, 2008. **319**(5866): p. 1086-1089.
240. Mandelkow, E.M., et al., *MARK/PAR1 kinase is a regulator of microtubuledependent transport in axons.* Journal of Cell Biology, 2004. **167**(1): p. 99-110.
241. Ebneth, A., et al., *Overexpression of tau protein inhibits kinesin-dependent trafficking of vesicles, mitochondria, and endoplasmic reticulum: Implications for Alzheimer's disease.* Journal of Cell Biology, 1998. **143**(3): p. 777-794.
242. Stamer, K., et al., *Tau blocks traffic of organelles, neurofilaments, and APP vesicles in neurons and enhances oxidative stress.* Journal of Cell Biology, 2002. **156**(6): p. 1051-1063.
243. Barbier, P., et al., *Role of Tau as a Microtubule-Associated Protein: Structural and Functional Aspects.* Frontiers in Aging Neuroscience, 2019. **11**: p. 14.
244. Guo, T., W. Noble, and D.P. Hanger, *Roles of tau protein in health and disease.* Acta Neuropathologica, 2017. **133**(5): p. 665-704.
245. Avila, J., et al., *Role of tau protein in both physiological and pathological conditions.* Physiological Reviews, 2004. **84**(2): p. 361-384.
246. Li, X.C., et al., *Human wild-type full-length tau accumulation disrupts mitochondrial dynamics and the functions via increasing mitofusins.* Scientific Reports, 2016. **6**: p. 10.
247. Lasagna-Reeves, C.A., et al., *Tau oligomers impair memory and induce synaptic and mitochondrial dysfunction in wild-type mice.* Molecular Neurodegeneration, 2011. **6**: p. 14.
248. Tang, Z., et al., *mTor mediates tau localization and secretion: Implication for Alzheimer's disease.* Biochimica Et Biophysica Acta-Molecular Cell Research, 2015. **1853**(7): p. 1646-1657.
249. Mann, V.M., et al., *COMPLEX-I, IRON, AND FERRITIN IN PARKINSONS-DISEASE SUBSTANTIA-NIGRA.* Annals of Neurology, 1994. **36**(6): p. 876-881.
250. Bindoff, L.A., et al., *RESPIRATORY-CHAIN ABNORMALITIES IN SKELETAL-MUSCLE FROM PATIENTS WITH PARKINSONS-DISEASE.* Journal of the Neurological Sciences, 1991. **104**(2): p. 203-208.
251. Schapira, A.H.V., *Mitochondria in the aetiology and pathogenesis of Parkinson's disease.* Parkinsonism & Related Disorders, 1999. **5**(4): p. 139-143.
252. Macdonald, R., et al., *Mitochondrial abnormalities in Parkinson's disease and Alzheimer's disease: can mitochondria be targeted therapeutically?* Biochemical Society Transactions, 2018. **46**: p. 891-909.
253. Iwai, A., et al., *THE PRECURSOR PROTEIN OF NON-A-BETA COMPONENT OF ALZHEIMERS-DISEASE AMYLOID IS A PRESYNAPTIC PROTEIN OF THE CENTRAL-NERVOUS-SYSTEM.* Neuron, 1995. **14**(2): p. 467-475.
254. Spillantini, M.G., et al., *alpha-synuclein in Lewy bodies.* Nature, 1997. **388**(6645): p. 839-840.
255. Clayton, D.F. and J.M. George, *The synucleins: a family of proteins involved in synaptic function, plasticity, neurodegeneration and disease.* Trends in Neurosciences, 1998. **21**(6): p. 249-254.
256. Jakes, R., M.G. Spillantini, and M. Goedert, *IDENTIFICATION OF 2 DISTINCT SYNUCLEINS FROM HUMAN BRAIN.* Febs Letters, 1994. **345**(1): p. 27-32.
257. Masliah, E., et al., *Dopaminergic loss and inclusion body formation in alpha-synuclein mice: Implications for neurodegenerative disorders.* Science, 2000. **287**(5456): p. 1265-1269.
258. Banerjee, R., et al., *Mitochondrial dysfunction in the limelight of Parkinson's disease pathogenesis.* Biochimica Et Biophysica Acta-Molecular Basis of Disease, 2009. **1792**(7): p. 651-663.
259. Martin, L.J., et al., *Parkinson's disease alpha-synuclein transgenic mice develop neuronal mitochondrial degeneration and cell death.* Journal of Neuroscience, 2006. **26**(1): p. 41-50.
260. Song, D.D., et al., *Enhanced substantia nigra mitochondrial pathology in human alpha-synuclein transgenic mice after treatment with MPTP.* Experimental Neurology, 2004. **186**(2): p. 158-172.

261. Li, W.W., et al., *Localization of alpha-synuclein to mitochondria within midbrain of mice.* Neuroreport, 2007. **18**(15): p. 1543-1546.
262. Parihar, M.S., et al., *Alpha-synuclein overexpression and aggregation exacerbates impairment of mitochondrial functions by augmenting oxidative stress in human neuroblastoma cells.* International Journal of Biochemistry & Cell Biology, 2009. **41**(10): p. 2015-2024.
263. Tanner, C.M., et al., *Rotenone, Paraquat, and Parkinson's Disease.* Environmental Health Perspectives, 2011. **119**(6): p. 866-872.
264. Pickrell, A.M. and R.J. Youle, *The Roles of PINK1, Parkin, and Mitochondrial Fidelity in Parkinson's Disease.* Neuron, 2015. **85**(2): p. 257-273.
265. Kazlauskaite, A., et al., *Parkin is activated by PINK1-dependent phosphorylation of ubiquitin at Ser(65).* Biochemical Journal, 2014. **460**: p. 127-139.
266. Kondapalli, C., et al., *PINK1 is activated by mitochondrial membrane potential depolarization and stimulates Parkin E3 ligase activity by phosphorylating Serine 65.* Open Biology, 2012. **2**: p. 17.
267. Lee, Y., et al., *PINK1 Primes Parkin-Mediated Ubiquitination of PARIS in Dopaminergic Neuronal Survival.* Cell Reports, 2017. **18**(4): p. 918-932.
268. Bertolin, G., et al., *Parkin maintains mitochondrial levels of the protective Parkinson's disease-related enzyme 17-beta hydroxysteroid dehydrogenase type 10.* Cell Death and Differentiation, 2015. **22**(10): p. 1563-1576.
269. Gehrke, S., et al., *PINK1 and Parkin Control Localized Translation of Respiratory Chain Component mRNAs on Mitochondria Outer Membrane.* Cell Metabolism, 2015. **21**(1): p. 95-108.
270. Macdonald, M.E., et al., *A NOVEL GENE CONTAINING A TRINUCLEOTIDE REPEAT THAT IS EXPANDED AND UNSTABLE ON HUNTINGTONS-DISEASE CHROMOSOMES.* Cell, 1993. **72**(6): p. 971-983.
271. Li, H., et al., *Amino-terminal fragments of mutant huntingtin show selective accumulation in striatal neurons and synaptic toxicity.* Nature Genetics, 2000. **25**(4): p. 385-389.
272. DiFiglia, M., et al., *Aggregation of huntingtin in neuronal intranuclear inclusions and dystrophic neurites in brain.* Science, 1997. **277**(5334): p. 1990-1993.
273. Orr, A.L., et al., *N-terminal mutant huntingtin associates with mitochondria and impairs mitochondrial trafficking.* Journal of Neuroscience, 2008. **28**(11): p. 2783-2792.
274. Yu, Z.X., et al., *Mutant huntingtin causes context-dependent neurodegeneration in mice with Huntington's disease.* Journal of Neuroscience, 2003. **23**(6): p. 2193-2202.
275. Bae, B.I., et al., *p53 mediates cellular dysfunction and behavioral abnormalities in Huntington's disease.* Neuron, 2005. **47**(1): p. 29-41.
276. Benchoua, A., et al., *Involvement of mitochondrial complex II defects in neuronal death produced by N-terminus fragment of mutated Huntingtin.* Molecular Biology of the Cell, 2006. **17**(4): p. 1652-1663.
277. Brennan, W.A., E.D. Bird, and J.R. Aprille, *REGIONAL MITOCHONDRIAL RESPIRATORY ACTIVITY IN HUNTINGTONS-DISEASE BRAIN.* Journal of Neurochemistry, 1985. **44**(6): p. 1948-1950.
278. Damiano, M., et al., *Neural mitochondrial Ca2+ capacity impairment precedes the onset of motor symptoms in G93A Cu/Zn-superoxide dismutase mutant mice.* Journal of Neurochemistry, 2006. **96**(5): p. 1349-1361.
279. Kim, J., et al., *Mitochondrial loss, dysfunction and altered dynamics in Huntington's disease.* Human Molecular Genetics, 2010. **19**(20): p. 3919-3935.
280. Lisowsky, T., *ERV1 IS INVOLVED IN THE CELL-DIVISION CYCLE AND THE MAINTENANCE OF MITOCHONDRIAL GENOMES IN SACCHAROMYCES-CEREVISIAE.* Current Genetics, 1994. **26**(1): p. 15-20.
281. Becher, D., et al., *A mutant for the yeast scERV1 gene displays a new defect in mitochondrial morphology and distribution.* Yeast, 1999. **15**(12): p. 1171-1181.
282. Di Fonzo, A., et al., *The Mitochondrial Disulfide Relay System Protein GFER Is Mutated in Autosomal-Recessive Myopathy with Cataract and Combined Respiratory-Chain Deficiency.* American Journal of Human Genetics, 2009. **84**(5): p. 594-604.
283. Browne, S.E., et al., *Oxidative damage and metabolic dysfunction in Huntington's disease: Selective vulnerability of the basal ganglia.* Annals of Neurology, 1997. **41**(5): p. 646-653.
284. Gu, M., et al., *Mitochondrial defect in Huntington's disease on caudate nucleus.* Annals of Neurology, 1996. **39**(3): p. 385-389.
285. Browne, S.E. and M.F. Beal, *The energetics of Huntington's disease.* Neurochemical Research, 2004. **29**(3): p. 531-546.

286. Valentine, J.S., P.A. Doucette, and S.Z. Potter, *Copper-zinc superoxide dismutase and amyotrophic lateral sclerosis*, in *Annual Review of Biochemistry*. 2005, Annual Reviews: Palo Alto. p. 563-593.
287. Carri, M.T. and M. Cozzolino, *SOD1 and mitochondria in ALS: a dangerous liaison.* Journal of Bioenergetics and Biomembranes, 2011. **43**(6): p. 593-599.
288. Cozzolino, M., et al., *Mitochondrial dynamism and the pathogenesis of Amyotrophic Lateral Sclerosis.* Frontiers in Cellular Neuroscience, 2015. **9**: p. 5.
289. Crugnola, V., et al., *Mitochondrial Respiratory Chain Dysfunction in Muscle From Patients With Amyotrophic Lateral Sclerosis.* Archives of Neurology, 2010. **67**(7): p. 849-854.
290. Corti, S., et al., *Amyotrophic lateral sclerosis linked to a novel SOD1 mutation with muscle mitochondrial dysfunction.* Journal of the Neurological Sciences, 2009. **276**(1-2): p. 170-174.
291. Schon, E.A. and S. Przedborski, *Mitochondria: The Next (Neurode)Generation.* Neuron, 2011. **70**(6): p. 1033-1053.
292. Sturtz, L.A., et al., *A fraction of yeast Cu,Zn-superoxide dismutase and its metallochaperone, CCS, localize to the intermembrane space of mitochondria - A physiological role for SOD1 in guarding against mitochondrial oxidative damage.* Journal of Biological Chemistry, 2001. **276**(41): p. 38084-38089.
293. Okado-Matsumoto, A. and I. Fridovich, *Subcellular distribution of superoxide dismutases (SOD) in rat liver - Cu,Zn-SOD in mitochondria.* Journal of Biological Chemistry, 2001. **276**(42): p. 38388-38393.
294. Murphy, M.P., *How mitochondria produce reactive oxygen species.* Biochemical Journal, 2009. **417**: p. 1-13.
295. Hervias, I., M.F. Beal, and G. Manfredi, *Mitochondrial dysfunction and amyotrophic lateral sclerosis.* Muscle & Nerve, 2006. **33**(5): p. 598-608.
296. Lehmer, C., et al., *A novel CHCHD10 mutation implicates a Mia40-dependent mitochondrial import deficit in ALS.* Embo Molecular Medicine, 2018. **10**(6): p. 14.
297. Wang, T., et al., *C9orf72 regulates energy homeostasis by stabilizing mitochondrial complex I assembly.* Cell Metabolism, 2021. **33**(3): p. 531-546.
298. Baker, M.J., C.S. Palmer, and D. Stojanovski, *Mitochondrial protein quality control in health and disease.* British Journal of Pharmacology, 2014. **171**(8): p. 1870-1889.
299. Zhao, Q., et al., *A mitochondrial specific stress response in mammalian cells.* Embo Journal, 2002. **21**(17): p. 4411-4419.
300. Samluk, L., P. Chroscicki, and A. Chacinska, *Mitochondrial protein import stress and signaling.* Current Opinion in Physiology, 2018. **3**: p. 41-48.
301. Haynes, C.M., et al., *The Matrix Peptide Exporter HAF-1 Signals a Mitochondrial UPR by Activating the Transcription Factor ZC376.7 in C. elegans.* Molecular Cell, 2010. **37**(4): p. 529-540.
302. Haynes, C.M. and D. Ron, *The mitochondrial UPR - protecting organelle protein homeostasis.* Journal of Cell Science, 2010. **123**(22): p. 3849-3855.
303. Nargund, A.M., et al., *Mitochondrial Import Efficiency of ATFS-1 Regulates Mitochondrial UPR Activation.* Science, 2012. **337**(6094): p. 587-590.
304. Quiros, P.M., A. Mottis, and J. Auwerx, *Mitonuclear communication in homeostasis and stress.* Nature Reviews Molecular Cell Biology, 2016. **17**(4): p. 213-226.
305. D'Amico, D., V. Sorrentino, and J. Auwerx, *Cytosolic Proteostasis Networks of the Nlitochondrial Stress Response.* Trends in Biochemical Sciences, 2017. **42**(9): p. 712-725.
306. Aldridge, J.E., T. Horibe, and N.J. Hoogenraad, *Discovery of Genes Activated by the Mitochondrial Unfolded Protein Response (mtUPR) and Cognate Promoter Elements.* Plos One, 2007. **2**(9): p. 8.
307. Nargund, A.M., et al., *Mitochondrial and Nuclear Accumulation of the Transcription Factor ATFS-1 Promotes OXPHOS Recovery during the UPRmt.* Molecular Cell, 2015. **58**(1): p. 123-133.
308. Rolland, S.G., et al., *Compromised Mitochondrial Protein Import Acts as a Signal for UPRmt.* Cell Reports, 2019. **28**(7): p. 1659.
309. Fiorese, C.J., et al., *The Transcription Factor ATF5 Mediates a Mammalian Mitochondrial UPR.* Current Biology, 2016. **26**(15): p. 2037-2043.
310. Kuhl, I., et al., *Transcriptomic and proteomic landscape of mitochondrial dysfunction reveals secondary coenzyme Q deficiency in mammals.* Elife, 2017. **6**: p. 33.
311. Quiros, P.M., et al., *Multi-omics analysis identifies ATF4 as a key regulator of the mitochondrial stress response in mammals.* Journal of Cell Biology, 2017. **216**(7): p. 2027-2045.

312. Labbadia, J., et al., *Mitochondrial Stress Restores the Heat Shock Response and Prevents Proteostasis Collapse during Aging.* Cell Reports, 2017. **21**(6): p. 1481-1494.
313. Cooper, J.F., et al., *Activation of the mitochondrial unfolded protein response promotes longevity and dopamine neuron survival in Parkinson's disease models.* Scientific Reports, 2017. **7**: p. 16.
314. Martinez, B.A., et al., *Dysregulation of the Mitochondrial Unfolded Protein Response Induces Non-Apoptotic Dopaminergic Neurodegeneration in C-elegans Models of Parkinson's Disease.* Journal of Neuroscience, 2017. **37**(46): p. 11085-11100.
315. St Martin, J.L., et al., *Dopaminergic neuron loss and up-regulation of chaperone protein mRNA induced by targeted over-expression of alpha-synuclein in mouse substantia nigra.* Journal of Neurochemistry, 2007. **100**(6): p. 1449-1457.
316. Gorman, A.M., et al., *Hsp27 inhibits 6-hydroxydopamine-induced cytochrome c release and apoptosis in PC12 cells.* Biochemical and Biophysical Research Communications, 2005. **327**(3): p. 801-810.
317. Klucken, J., et al., *Hsp70 reduces alpha-synuclein aggregation and toxicity.* Journal of Biological Chemistry, 2004. **279**(24): p. 25497-25502.
318. Riar, A.K., et al., *Sex specific activation of the ER alpha axis of the mitochondrial UPR (UPRmt) in the G93A-SOD1 mouse model of familial ALS.* Human Molecular Genetics, 2017. **26**(7): p. 1318-1327.
319. Pharaoh, G., et al., *Metabolic and Stress Response Changes Precede Disease Onset in the Spinal Cord of Mutant SOD1 ALS Mice.* Frontiers in Neuroscience, 2019. **13**: p. 19.
320. Shen, Y., et al., *Activation of Mitochondrial Unfolded Protein Response in SHSY5Y Expressing APP Cells and APP/PS1 Mice.* Frontiers in Cellular Neuroscience, 2020. **13**: p. 12.
321. Beck, J.S., E.J. Mufson, and S.E. Counts, *Evidence for Mitochondrial UPR Gene Activation in Familial and Sporadic Alzheimer's Disease.* Current Alzheimer Research, 2016. **13**(6): p. 610-614.
322. Regitz, C., et al., *Resveratrol reduces amyloid-beta (A beta(1-42))-induced paralysis through targeting proteostasis in an Alzheimer model of Caenorhabditis elegans.* European Journal of Nutrition, 2016. **55**(2): p. 741-747.
323. Poveda-Huertes, D., et al., *An Early mtUPR: Redistribution of the Nuclear Transcription Factor Rox1 to Mitochondria Protects against Intramitochondrial Proteotoxic Aggregates.* Molecular Cell, 2020. **77**(1): p. 180.
324. Wrobel, L., et al., *Mistargeted mitochondrial proteins activate a proteostatic response in the cytosol.* Nature, 2015. **524**(7566): p. 485.
325. Papa, L. and D. Germain, *Estrogen receptor mediates a distinct mitochondrial unfolded protein response.* Journal of Cell Science, 2011. **124**(9): p. 1396-1402.
326. Wasilewski, M., K. Chojnacka, and A. Chacinska, *Protein trafficking at the crossroads to mitochondria.* Biochimica Et Biophysica Acta-Molecular Cell Research, 2017. **1864**(1): p. 125-137.
327. Callegari, S. and S. Dennerlein, *Sensing the Stress: A Role for the UPRmt and UPRam in the Quality Control of Mitochondria.* Frontiers in Cell and Developmental Biology, 2018. **6**: p. 10.
328. Hegde, A.N. and S.C. Upadhya, *Role of ubiquitin-proteasome-mediated proteolysis in nervous system disease.* Biochimica Et Biophysica Acta-Gene Regulatory Mechanisms, 2011. **1809**(2): p. 128-140.
329. Dennissen, F.J.A., N. Kholod, and F.W. van Leeuwen, *The ubiquitin proteasome system in neurodegenerative diseases: Culprit, accomplice or victim?* Progress in Neurobiology, 2012. **96**(2): p. 190-207.
330. Ciechanover, A. and Y.T. Kwon, *Degradation of misfolded proteins in neurodegenerative diseases: therapeutic targets and strategies.* Experimental and Molecular Medicine, 2015. **47**: p. 16.
331. Tai, H.C., et al., *The Synaptic Accumulation of Hyperphosphorylated Tau Oligomers in Alzheimer Disease Is Associated With Dysfunction of the Ubiquitin-Proteasome System.* American Journal of Pathology, 2012. **181**(4): p. 1426-1435.
332. Wang, X.W. and X.J. Chen, *A cytosolic network suppressing mitochondria-mediated proteostatic stress and cell death.* Nature, 2015. **524**(7566): p. 481.
333. Gerbasi, V.R. and A.J. Link, *The myotonic dystrophy type 2 protein ZNF9 is part of an ITAF complex that promotes cap-independent translation.* Molecular & Cellular Proteomics, 2007. **6**(6): p. 1049-1058.
334. Matsuo, Y., et al., *Coupled GTPase and remodelling ATPase activities form a checkpoint for ribosome export.* Nature, 2014. **505**(7481): p. 112.

335. Pakos-Zebrucka, K., et al., *The integrated stress response.* Embo Reports, 2016. **17**(10): p. 1374-1395.
336. Elden, A.C., et al., *Ataxin-2 intermediate-length polyglutamine expansions are associated with increased risk for ALS.* Nature, 2010. **466**(7310): p. 1069-77.
337. Chartier-Harlin, M.C., et al., *Translation Initiator EIF4G1 Mutations in Familial Parkinson Disease.* American Journal of Human Genetics, 2011. **89**(3): p. 398-406.
338. Coyne, L.P. and X.J. Chen, *mPOS is a novel mitochondrial trigger of cell death - implications for neurodegeneration.* Febs Letters, 2018. **592**(5): p. 759-775.
339. Weidberg, H. and A. Amon, *MitoCPR-A surveillance pathway that protects mitochondria in response to protein import stress.* Science, 2018. **360**(6385): p. 10.
340. Tang, M.Z., et al., *MitoCPR: a novel protective mechanism in response to mitochondrial protein import stress.* Acta Biochimica Et Biophysica Sinica, 2018. **50**(10): p. 1072-1074.
341. Martensson, C.U., et al., *Mitochondrial protein translocation-associated degradation.* Nature, 2019. **569**(7758): p. 679.
342. Neuber, O., et al., *Ubx2 links the Cdc48 complex to ER-associated protein degradation.* Nature Cell Biology, 2005. **7**(10): p. 993.
343. Schuberth, C. and A. Buchberger, *Membrane-bound Ubx2 recruits Cdc48 to ubiquitin ligases and their substrates to ensure efficient ER-associated protein degradation.* Nature Cell Biology, 2005. **7**(10): p. 999.
344. Rustom, A., et al., *Nanotubular highways for intercellular organelle transport.* Science, 2004. **303**(5660): p. 1007-1010.
345. Gurke, S., J.F.V. Barroso, and H.H. Gerdes, *The art of cellular communication: tunneling nanotubes bridge the divide.* Histochemistry and Cell Biology, 2008. **129**(5): p. 539-550.
346. Gerdes, H.H., N.V. Bukoreshtliev, and J.F.V. Barroso, *Tunneling nanotubes: A new route for the exchange of components between animal cells.* Febs Letters, 2007. **581**(11): p. 2194-2201.
347. Drab, M., et al., *Inception Mechanisms of Tunneling Nanotubes.* Cells, 2019. **8**(6): p. 17.
348. Jackson, M.V., et al., *Mitochondrial Transfer via Tunneling Nanotubes is an Important Mechanism by Which Mesenchymal Stem Cells Enhance Macrophage Phagocytosis in the In Vitro and In Vivo Models of ARDS.* Stem Cells, 2016. **34**(8): p. 2210-2223.
349. Chinnery, H.R. and K.E. Keller, *Tunneling Nanotubes and the Eye: Intercellular Communication and Implications for Ocular Health and Disease.* Biomed Research International, 2020. **2020**: p. 15.
350. Dupont, M., et al., *Tunneling nanotubes: intimate Communication between Myeloid Cells.* Frontiers in Immunology, 2018. **9**: p. 6.
351. Souriant, S., et al., *Tuberculosis Exacerbates HIV-1 Infection through IL-10/STAT3-Dependent Tunneling Nanotube Formation in Macrophages.* Cell Reports, 2019. **26**(13): p. 3586.
352. Eugenin, E.A., P.J. Gaskill, and J.W. Berman, *Tunneling nanotubes (TNT) are induced by HIV-infection of macrophages: A potential mechanism for intercellular HIV trafficking.* Cellular Immunology, 2009. **254**(2): p. 142-148.
353. Wang, Y., et al., *Tunneling-nanotube development in astrocytes depends on p53 activation.* Cell Death and Differentiation, 2011. **18**(4): p. 732-742.
354. Wang, X. and H.H. Gerdes, *Transfer of mitochondria via tunneling nanotubes rescues apoptotic PC12 cells.* Cell Death and Differentiation, 2015. **22**(7): p. 1181-1191.
355. Saha, T., et al., *Intercellular nanotubes mediate mitochondrial trafficking between cancer and immune cells.* Nature Nanotechnology: p. 14.
356. Gousset, K., et al., *Prions hijack tunnelling nanotubes for intercellular spread.* Nature Cell Biology, 2009. **11**(3): p. 328.
357. Costanzo, M., et al., *Transfer of polyglutamine aggregates in neuronal cells occurs in tunneling nanotubes.* Journal of Cell Science, 2013. **126**(16): p. 3678-3685.
358. Ding, X.B., et al., *Exposure to ALS-FTD-CSF generates TDP-43 aggregates in glioblastoma cells through exosomes and TNTs-like structure.* Oncotarget, 2015. **6**(27): p. 24178-24191.
359. Aguzzit, A. and A.K.K. Lakkaraju, *Cell Biology of Prions and Prionoids: A Status Report.* Trends in Cell Biology, 2016. **26**(1): p. 40-51.
360. Tardivel, M., et al., *Tunneling nanotube (TNT)-mediated neuron-to neuron transfer of pathological Tau protein assemblies.* Acta Neuropathologica Communications, 2016. **4**.
361. Abounit, S., et al., *Tunneling nanotubes: A possible highway in the spreading of tau and other prion-like proteins in neurodegenerative diseases.* Prion, 2016. **10**(5): p. 344-351.
362. Scheiblich, H., et al., *Microglia jointly degrade fibrillar alpha-synuclein cargo by distribution through tunneling nanotubes.* Cell, 2021. **184**(20): p. 5089.

363. Cheung, T.M.J., *A small molecule dissociates the PAM motor from the TIM23 channel*, in *Biochemistry and Molecular Biology*. 2017, University of California Los Angeles. p. 123.
364. Pereira, G.C., et al., *A High-Resolution Luminescent Assay for Rapid and Continuous Monitoring of Protein Translocation across Biological Membranes.* Journal of Molecular Biology, 2019. **431**(8): p. 1689-1699.
365. Kacprzyk-Stokowiec, A., et al., *Crucial Role of Perfringolysin O D1 Domain in Orchestrating Structural Transitions Leading to Membrane-perforating Pores A HYDROGEN-DEUTERIUM EXCHANGE STUDY.* Journal of Biological Chemistry, 2014. **289**(41): p. 28738-28752.
366. Dixon, A.S., et al., *Activation of bioluminescence by structural complementation*. 2017, Promega Corporation: USA.
367. Dixon, A.S., et al., *NanoLuc Complementation Reporter Optimized for Accurate Measurement of Protein Interactions in Cells.* Acs Chemical Biology, 2016. **11**(2): p. 400-408.
368. Martin, S. and J.M. Henley, *Activity-dependent endocytic sorting of kainate receptors to recycling or degradation pathways.* Embo Journal, 2004. **23**(24): p. 4749-4759.
369. Vichai, V. and K. Kirtikara, *Sulforhodamine B colorimetric assay for cytotoxicity screening.* Nature Protocols, 2006. **1**(3): p. 1112-1116.
370. Heintzmann, R. and T. Huser, *Super-Resolution Structured Illumination Microscopy.* Chemical Reviews, 2017. **117**(23): p. 13890-13908.
371. Wegel, E., et al., *Imaging cellular structures in super-resolution with SIM, STED and Localisation Microscopy: A practical comparison.* Scientific Reports, 2016. **6**: p. 13.
372. Gustafsson, M.G.L., *Surpassing the lateral resolution limit by a factor of two using structured illumination microscopy.* Journal of Microscopy, 2000. **198**: p. 82-87.
373. Gustafsson, M.G.L., et al., *Three-dimensional resolution doubling in wide-field fluorescence microscopy by structured illumination.* Biophysical Journal, 2008. **94**(12): p. 4957-4970.
374. Rueden, C.T., et al., *ImageJ2: ImageJ for the next generation of scientific image data.* Bmc Bioinformatics, 2017. **18**: p. 26.
375. Schindelin, J., et al., *Fiji: an open-source platform for biological-image analysis.* Nature Methods, 2012. **9**(7): p. 676-682.
376. Cross, S. *miaanalysis/mia: Version 0.21.0*. 2021 [cited 2022 18th January].
377. Seager, R.A., *Investigating the role of SUMOylation of Mitochondrial Fission Factor in Mitochondrial Dynamics*. 2020, University of Bristol. p. 289.
378. Creed, S. and M. McKenzie, *Measurement of Mitochondrial Membrane Potential with the Fluorescent Dye Tetramethylrhodamine Methyl Ester (TMRM)*, in *Cancer Metabolism: Methods and Protocols*, M. Haznadar, Editor. 2019, Springer New York: New York, NY. p. 69-76.
379. Doerr, A., *Cryo-electron tomography.* Nature Methods, 2017. **14**(1): p. 34-34.
380. Abraham, O., et al., *Control of protein trafficking by reversible masking of transport signals.* Molecular Biology of the Cell, 2016. **27**(8): p. 1310-1319.
381. Zhang, L. and J.E. Elias, *Relative Protein Quantification Using Tandem Mass Tag Mass Spectrometry*, in *Proteomics: Methods and Protocols*, L. Comai, J.E. Katz, and P. Mallick, Editors. 2017, Springer New York: New York, NY. p. 185-198.
382. Miyata, N., et al., *Pharmacologic rescue of an enzyme-trafficking defect in primary hyperoxaluria 1.* Proceedings of the National Academy of Sciences of the United States of America, 2014. **111**(40): p. 14406-14411.
383. Miyata, N., et al., *Adaptation of a Genetic Screen Reveals an Inhibitor for Mitochondrial Protein Import Component Tim44.* Journal of Biological Chemistry, 2017. **292**(13): p. 5429-5442.
384. Smoyer, C.J., et al., *Analysis of membrane proteins localizing to the inner nuclear envelope in living cells.* Journal of Cell Biology, 2016. **215**(4): p. 575-590.
385. Wehrman, T.S., et al., *Enzymatic detection of protein translocation.* Nature Methods, 2005. **2**(7): p. 521-527.
386. Krayl, M., et al., *Fluorescence-mediated analysis of mitochondrial preprotein import in vitro.* Analytical Biochemistry, 2006. **355**(1): p. 81-89.
387. Hall, M.P., et al., *Engineered Luciferase Reporter from a Deep Sea Shrimp Utilizing a Novel Imidazopyrazinone Substrate.* Acs Chemical Biology, 2012. **7**(11): p. 1848-1857.
388. England, C.G., E.B. Ehlerding, and W.B. Cai, *NanoLuc: A Small Luciferase Is Brightening Up the Field of Bioluminescence.* Bioconjugate Chemistry, 2016. **27**(5): p. 1175-1187.
389. Liu, Z.Q., et al., *Systematic comparison of 2A peptides for cloning multi-genes in a polycistronic vector.* Scientific Reports, 2017. **7**: p. 9.
390. Daniels, R.W., et al., *Expression of Multiple Transgenes from a Single Construct Using Viral 2A Peptides in Drosophila.* Plos One, 2014. **9**(6): p. 10.
391. Shcherbo, D., et al., *Near-infrared fluorescent proteins.* Nature Methods, 2010. **7**(10): p. 827.

392. Westermann, B. and W. Neupert, *Mitochondria-targeted green fluorescent proteins: convenient tools for the study of organelle biogenesis in Saccharomyces cerevisiae.* Yeast, 2000. **16**(15): p. 1421-1427.
393. Huttemann, M., T.R. Schmidt, and L.I. Grossman, *A third isoform of cytochrome c oxidase subunit VIII is present in mammals.* Gene, 2003. **312**: p. 95-102.
394. Verechshagina, N., et al., *Future of human mitochondrial DNA editing technologies.* Mitochondrial DNA Part A, 2019. **30**(2): p. 214-221.
395. Aguer, C., et al., *Galactose Enhances Oxidative Metabolism and Reveals Mitochondrial Dysfunction in Human Primary Muscle Cells.* Plos One, 2011. **6**(12): p. 11.
396. Hartl, F.U., et al., *MITOCHONDRIAL PROTEIN IMPORT.* Biochimica Et Biophysica Acta, 1989. **988**(1): p. 1-45.
397. Perry, S.W., et al., *Mitochondrial membrane potential probes and the proton gradient: a practical usage guide.* Biotechniques, 2011. **50**(2): p. 98.
398. Boncompain, G., et al., *Synchronization of secretory protein traffic in populations of cells.* Nature Methods, 2012. **9**(5): p. 493.
399. Wilson, D.S., A.D. Keefe, and J.W. Szostak, *The use of mRNA display to select high-affinity protein-binding peptides.* Proceedings of the National Academy of Sciences of the United States of America, 2001. **98**(7): p. 3750-3755.
400. Pelletier, J. and N. Sonenberg, *INTERNAL INITIATION OF TRANSLATION OF EUKARYOTIC MESSENGER-RNA DIRECTED BY A SEQUENCE DERIVED FROM POLIOVIRUS RNA.* Nature, 1988. **334**(6180): p. 320-325.
401. Jang, S.K., et al., *A SEGMENT OF THE 5′ NONTRANSLATED REGION OF ENCEPHALOMYOCARDITIS VIRUS-RNA DIRECTS INTERNAL ENTRY OF RIBOSOMES DURING INVITRO TRANSLATION.* Journal of Virology, 1988. **62**(8): p. 2636-2643.
402. Shaimardanova, A.A., et al., *Production and Application of Multicistronic Constructs for Various Human Disease Therapies.* Pharmaceutics, 2019. **11**(11): p. 16.
403. Atamna, H., et al., *Biotin deficiency inhibits heme synthesis and impairs mitochondria in human lung fibroblasts.* Journal of Nutrition, 2007. **137**(1): p. 25-30.
404. Shpilka, T., et al., *UPRmt scales mitochondrial network expansion with protein synthesis via mitochondrial import in Caenorhabditis elegans.* Nature Communications, 2021. **12**(1): p. 11.
405. Burak, E., et al., *Evolving Dual Targeting of a Prokaryotic Protein in Yeast.* Molecular Biology and Evolution, 2013. **30**(7): p. 1563-1573.
406. Balleza, E., J.M. Kim, and P. Cluzel, *Systematic characterization of maturation time of fluorescent proteins in living cells.* Nature Methods, 2018. **15**(1): p. 47.
407. Prasad, P.D., et al., *Cloning and functional expression of a cDNA encoding a mammalian sodium-dependent vitamin transporter mediating the uptake of pantothenate, biotin, and lipoate.* Journal of Biological Chemistry, 1998. **273**(13): p. 7501-7506.
408. Rossjohn, J., et al., *Structures of perfringolysin O suggest a pathway for activation of cholesterol-dependent cytolysins.* Journal of Molecular Biology, 2007. **367**(5): p. 1227-1236.
409. Ramachandran, R., et al., *Structural insights into the membrane-anchoring mechanism of a cholesterol-dependent cytolysin.* Nature Structural Biology, 2002. **9**(11): p. 823-827.
410. Martin, J., K. Mahlke, and N. Pfanner, *ROLE OF AN ENERGIZED INNER MEMBRANE IN MITOCHONDRIAL PROTEIN IMPORT - DELTA-PSI DRIVES THE MOVEMENT OF PRESEQUENCES.* Journal of Biological Chemistry, 1991. **266**(27): p. 18051-18057.
411. Wachter, C., G. Schatz, and B.S. Glick, *PROTEIN IMPORT INTO MITOCHONDRIA - THE REQUIREMENT FOR EXTERNAL ATF IS PRECURSOR-SPECIFIC WHEREAS INTRAMITOCHONDRIAL ATP IS UNIVERSALLY NEEDED FOR TRANSLOCATION INTO THE MATRIX.* Molecular Biology of the Cell, 1994. **5**(4): p. 465-474.
412. Geissler, A., et al., *Membrane potential-driven protein import into mitochondria - The sorting sequence cytochrome b(2) modulates the Delta psi-dependence of translocation of the matrix-targeting sequence.* Molecular Biology of the Cell, 2000. **11**(11): p. 3977-3991.
413. Wisen, S., et al., *Binding of a Small Molecule at a Protein-Protein Interface Regulates the Chaperone Activity of Hsp70-Hsp40.* Acs Chemical Biology, 2010. **5**(6): p. 611-622.
414. Williamson, D.S., et al., *Novel Adenosine-Derived Inhibitors of 70 kDa Heat Shock Protein, Discovered Through Structure-Based Design.* Journal of Medicinal Chemistry, 2009. **52**(6): p. 1510-1513.
415. ModicaNapolitano, J.S., et al., *Selective damage to carcinoma mitochondria by the rhodacyanine MKT-077.* Cancer Research, 1996. **56**(3): p. 544-550.
416. Dabir, D.V., et al., *A Small Molecule Inhibitor of Redox-Regulated Protein Translocation into Mitochondria.* Developmental Cell, 2013. **25**(1): p. 81-92.

417. Ohmuro-Matsuyama, Y. and H. Ueda, *Protein-Protein Interaction Assays Using Split-NanoLuc*, in *Bioluminescence - Analytical Applications and Basic Biology*, H. Suzuki, Editor. 2019.
418. Rechsteiner, M. and S.W. Rogers, *PEST sequences and regulation by proteolysis.* Trends in Biochemical Sciences, 1996. **21**(7): p. 267-271.
419. Li, X.Q., et al., *Generation of destabilized green fluorescent protein transcription reporter.* Journal of Biological Chemistry, 1998. **273**(52): p. 34970-34975.
420. Molinari, P., I. Casella, and T. Costa, *Functional complementation of high-efficiency resonance energy transfer: a new tool for the study of protein binding interactions in living cells.* Biochemical Journal, 2008. **409**: p. 251-261.
421. Guardia, C.M., et al., *Reversible association with motor proteins (RAMP): A streptavidin-based method to manipulate organelle positioning.* Plos Biology, 2019. **17**(5): p. 27.
422. Evans, A.J., et al., *Assembly, Secretory Pathway Trafficking, and Surface Delivery of Kainate Receptors Is Regulated by Neuronal Activity.* Cell Reports, 2017. **19**(12): p. 2613-2626.
423. Farías, G.G., D.J. Britt, and J.S. Bonifacino, *Imaging the Polarized Sorting of Proteins from the Golgi Complex in Live Neurons*, in *The Golgi Complex: Methods and Protocols*, W.J. Brown, Editor. 2016, Springer New York: New York, NY. p. 13-30.
424. Su, A.I., et al., *A gene atlas of the mouse and human protein-encoding transcriptomes.* Proceedings of the National Academy of Sciences of the United States of America, 2004. **101**(16): p. 6062-6067.
425. Su, A.I., et al., *Large-scale analysis of the human and mouse transcriptomes.* Proceedings of the National Academy of Sciences of the United States of America, 2002. **99**(7): p. 4465-4470.
426. Wu, C.L., I. MacLeod, and A.I. Su, *BioGPS and MyGene.info: organizing online, gene-centric information.* Nucleic Acids Research, 2013. **41**(D1): p. D561-D565.
427. Dowbaj, A.M., et al., *An optogenetic method for interrogating YAP1 and TAZ nuclear-cytoplasmic shuttling.* Journal of Cell Science, 2021. **134**(13): p. 20.
428. Stornaiuolo, M., et al., *KDEL and KKXX retrieval signals appended to the same reporter protein determine different trafficking between endoplasmic reticulum, intermediate compartment, and Golgi complex.* Molecular Biology of the Cell, 2003. **14**(3): p. 889-902.
429. Allen, W.J., et al., *Refined measurement of SecA-driven protein secretion reveals that translocation is indirectly coupled to ATP turnover.* Proceedings of the National Academy of Sciences of the United States of America, 2020. **117**(50): p. 31808-31816.
430. Allen, W.J., et al., *A 'proton ratchet' for coupling the membrane potential to protein transport.* bioRxiv, 2019: p. 592543.
431. Combs, B., et al., *Frontotemporal Lobar Dementia Mutant Tau Impairs Axonal Transport through a Protein Phosphatase 1 gamma-Dependent Mechanism.* Journal of Neuroscience, 2021. **41**(45): p. 9431-9451.
432. Tuck, B.J., et al., *Tau assemblies enter the cytosol in a cholesterol sensitive process essential to seeded aggregation.* BioRxiv, 2021.
433. Lan, J., et al., *Structure of the SARS-CoV-2 spike receptor-binding domain bound to the ACE2 receptor.* Nature, 2020. **581**(7807): p. 215.
434. Lim, J. and Z.Y. Yue, *Neuronal Aggregates: Formation, Clearance, and Spreading.* Developmental Cell, 2015. **32**(4): p. 491-501.
435. Morimoto, R.I. and P. Cold Spring Harbor Lab, *The Heat Shock Response: Systems Biology of Proteotoxic Stress in Aging and Disease.* Metabolism and Disease, 2011. **76**: p. 91-99.
436. Sweeney, P., et al., *Protein misfolding in neurodegenerative diseases: implications and strategies.* Translational Neurodegeneration, 2017. **6**: p. 13.
437. Matouschek, A., et al., *Active unfolding of precursor proteins during mitochondrial protein import.* Embo Journal, 1997. **16**(22): p. 6727-6736.
438. Schendzielorz, A.B., et al., *Two distinct membrane potential-dependent steps drive mitochondrial matrix protein translocation.* Journal of Cell Biology, 2017. **216**(1): p. 83-92.
439. Eilers, M. and G. Schatz, *BINDING OF A SPECIFIC LIGAND INHIBITS IMPORT OF A PURIFIED PRECURSOR PROTEIN INTO MITOCHONDRIA.* Nature, 1986. **322**(6076): p. 228-232.
440. Harsman, A., et al., *The non-canonical mitochondrial inner membrane presequence translocase of trypanosomatids contains two essential rhomboid-like proteins.* Nature Communications, 2016. **7**: p. 12.
441. Heintzmann, R. and C. Cremer. *Laterally modulated excitation microscopy: Improvement of resolution by using a diffraction grating*. in *Conference on Optical Biopsies and Microscopic Techniques III*. 1998. Stockholm, Sweden: Spie-Int Soc Optical Engineering.

442. Komis, G., et al., *Superresolution live imaging of plant cells using structured illumination microscopy.* Nature Protocols, 2015. **10**(8): p. 1248-1263.
443. Sesaki, H. and R.E. Jensen, *Division versus fusion: Dnm1p and Fzo1p antagonistically regulate mitochondrial shape.* Journal of Cell Biology, 1999. **147**(4): p. 699-706.
444. Gilkerson, R.W., et al., *Mitochondrial DNA depletion causes morphological changes in the mitochondrial reticulum of cultured human cells.* Febs Letters, 2000. **474**(1): p. 1-4.
445. Legros, F., et al., *Mitochondrial fusion in human cells is efficient, requires the inner membrane potential, and is mediated by mitofusins.* Molecular Biology of the Cell, 2002. **13**(12): p. 4343-4354.
446. Gottlieb, R.A. and D. Bernstein, *Mitochondrial remodeling: Rearranging, recycling, and reprogramming.* Cell Calcium, 2016. **60**(2): p. 88-101.
447. Cogliati, S., J.A. Enriquez, and L. Scorrano, *Mitochondrial Cristae: Where Beauty Meets Functionality.* Trends in Biochemical Sciences, 2016. **41**(3): p. 261-273.
448. Kotani, T., et al., *Human G-proteins, ObgH1 and Mtg1, associate with the large mitochondrial ribosome subunit and are involved in translation and assembly of respiratory complexes.* Nucleic Acids Research, 2013. **41**(6): p. 3713-3722.
449. Tsuboi, M., et al., *EF-G2mt Is an Exclusive Recycling Factor in Mammalian Mitochondrial Protein Synthesis.* Molecular Cell, 2009. **35**(4): p. 502-510.
450. Ohsakaya, S., et al., *Knockdown of DAPIT (Diabetes-associated Protein in Insulin-sensitive Tissue) Results in Loss of ATP Synthase in Mitochondria.* Journal of Biological Chemistry, 2011. **286**(23): p. 20292-20296.
451. Barca, E., et al., *USMG5 Ashkenazi Jewish founder mutation impairs mitochondrial complex V dimerization and ATP synthesis.* Human Molecular Genetics, 2018. **27**(19): p. 3305-3312.
452. Balsa, E., et al., *NDUFA4 Is a Subunit of Complex IV of the Mammalian Electron Transport Chain.* Cell Metabolism, 2012. **16**(3): p. 378-386.
453. Lagresle-Peyrou, C., et al., *Human adenylate kinase 2 deficiency causes a profound hematopoietic defect associated with sensorineural deafness.* Nature Genetics, 2009. **41**(1): p. 106-111.
454. Sanchez, E., et al., *LYRM7/MZM1L is a UQCRFS1 chaperone involved in the last steps of mitochondrial Complex III assembly in human cells.* Biochimica Et Biophysica Acta-Bioenergetics, 2013. **1827**(3): p. 285-293.
455. Santel, A. and M.T. Fuller, *Control of mitochondrial morphology by a human mitofusin.* Journal of Cell Science, 2001. **114**(5): p. 867-874.
456. Jobling, R.K., et al., *PMPCA mutations cause abnormal mitochondrial protein processing in patients with non-progressive cerebellar ataxia.* Brain, 2015. **138**: p. 1505-1517.
457. Vogtle, F.N., et al., *Mutations in PMPCB Encoding the Catalytic Subunit of the Mitochondrial Presequence Protease Cause Neurodegeneration in Early Childhood.* American Journal of Human Genetics, 2018. **102**(4): p. 557-573.
458. Yamaguchi, F., et al., *S100 Proteins Modulate Protein Phosphatase 5 Function A LINK BETWEEN CA(2+) SIGNAL TRANSDUCTION AND PROTEIN DEPHOSPHORYLATION.* Journal of Biological Chemistry, 2012. **287**(17): p. 13787-13798.
459. Vargas, J.Y., et al., *The Wnt/Ca2+ pathway is involved in interneuronal communication mediated by tunneling nanotubes.* Embo Journal, 2019. **38**(23): p. 21.
460. Owens, R.J. and F.E. Baralle, *MAPPING THE COLLAGEN-BINDING SITE OF HUMAN FIBRONECTIN BY EXPRESSION IN ESCHERICHIA-COLI.* Embo Journal, 1986. **5**(11): p. 2825-2830.
461. Osteikoetxea-Molnar, A., et al., *The growth determinants and transport properties of tunneling nanotube networks between B lymphocytes.* Cellular and Molecular Life Sciences, 2016. **73**(23): p. 4531-4545.
462. Kitazawa, H., et al., *Ser787 in the proline-rich region of human MAP4 is a critical phosphorylation site that reduces its activity to promote tubulin polymerization.* Cell Structure and Function, 2000. **25**(1): p. 33-39.
463. Burbelo, P.D., et al., *MSE55, a Cdc42 effector protein, induces long cellular extensions in fibroblasts.* Proceedings of the National Academy of Sciences of the United States of America, 1999. **96**(16): p. 9083-9088.
464. Miriyala, S., et al., *Novel role of 4-hydroxy-2-nonenal in AIFm2-mediated mitochondrial stress signaling.* Free Radical Biology and Medicine, 2016. **91**: p. 68-80.
465. Clements, C.M., et al., *DJ-1, a cancer- and Parkinson's disease-associated protein, stabilizes the antioxidant transcriptional master regulator Nrf2.* Proceedings of the National Academy of Sciences of the United States of America, 2006. **103**(41): p. 15091-15096.

466. Xiong, H., et al., *Parkin, PINK1, and DJ-1 form a ubiquitin E3 ligase complex promoting unfolded protein degradation.* Journal of Clinical Investigation, 2009. **119**(3): p. 650-660.
467. Zou, W.G. and D.E. Zhang, *The interferon-inducible ubiquitin-protein isopeptide ligase (E3) EFP also functions as an ISG15 E3 ligase.* Journal of Biological Chemistry, 2006. **281**(7): p. 3989-3994.
468. Yano, M., et al., *20S proteasorne prevents aggregation of heat-denatured proteins without PA700 regulatory subcomplex like a molecular chaperone.* Biomacromolecules, 2004. **5**(4): p. 1465-1469.
469. Matsumura, Y., J. Sakai, and W.R. Skach, *Endoplasmic Reticulum Protein Quality Control Is Determined by Cooperative Interactions between Hsp/c70 Protein and the CHIP E3 Ligase.* Journal of Biological Chemistry, 2013. **288**(43): p. 31069-31079.
470. Chacinska, A., et al., *Distinct Forms of Mitochondrial TOM-TIM Supercomplexes Define Signal-Dependent States of Preprotein Sorting.* Molecular and Cellular Biology, 2010. **30**(1): p. 307-318.
471. Exner, N., et al., *Loss-of-function of human PINK1 results in mitochondrial pathology and can be rescued by parkin.* Journal of Neuroscience, 2007. **27**(45): p. 12413-12418.
472. Van Laar, V.S., S.B. Berman, and T.G. Hastings, *Mic60/mitofilin overexpression alters mitochondrial dynamics and attenuates vulnerability of dopaminergic cells to dopamine and rotenone.* Neurobiology of Disease, 2016. **91**: p. 247-261.
473. Baloyannis, S.J., *Mitochondrial alterations in Alzheimer's disease.* Journal of Alzheimers Disease, 2006. **9**(2): p. 119-126.
474. Shoffner, J.M., et al., *MITOCHONDRIAL-DNA VARIANTS OBSERVED IN ALZHEIMER-DISEASE AND PARKINSON DISEASE PATIENTS.* Genomics, 1993. **17**(1): p. 171-184.
475. Knapp-Wilson, A., et al., *Maintenance of complex I and its supercomplexes by NDUF-11 is essential for mitochondrial structure, function and health.* Journal of Cell Science, 2021. **134**(13): p. 17.
476. Harner, M., et al., *The mitochondrial contact site complex, a determinant of mitochondrial architecture.* Embo Journal, 2011. **30**(21): p. 4356-4370.
477. Tang, J.X., et al., *Mitochondrial OXPHOS Biogenesis: Co-Regulation of Protein Synthesis, Import, and Assembly Pathways.* International Journal of Molecular Sciences, 2020. **21**(11): p. 32.
478. Priesnitz, C. and T. Becker, *Pathways to balance mitochondrial translation and protein import.* Genes & Development, 2018. **32**(19-20): p. 1285-1296.
479. Hanna, S.J., et al., *The Role of Rho-GTPases and actin polymerization during Macrophage Tunneling Nanotube Biogenesis.* Scientific Reports, 2017. **7**: p. 16.
480. Zhang, S.L., M.G. Kazanietz, and M. Cooke, *Rho GTPases and the emerging role of tunneling nanotubes in physiology and disease.* American Journal of Physiology-Cell Physiology, 2020. **319**(5): p. C877-C884.
481. Ross, R.A., B.A. Spengler, and J.L. Biedler, *COORDINATE MORPHOLOGICAL AND BIOCHEMICAL INTERCONVERSION OF HUMAN NEURO-BLASTOMA CELLS.* Journal of the National Cancer Institute, 1983. **71**(4): p. 741-749.
482. Poorkaj, P., et al., *Frequency of tau gene mutations in familial and sporadic cases of non-Alzheimer dementia.* Archives of Neurology, 2001. **58**(3): p. 383-387.
483. Goedert, M. and R. Jakes, *Mutations causing neurodegenerative tauopathies.* Biochimica Et Biophysica Acta-Molecular Basis of Disease, 2005. **1739**(2-3): p. 240-250.
484. Mandelkow, E., et al., *Structural principles of tau and the paired helical filaments of Alzheimer's disease.* Brain Pathology, 2007. **17**(1): p. 83-90.
485. Goedert, M., *The ordered assembly of tau is the gain-of-toxic function that causes human tauopathies.* Alzheimers & Dementia, 2016. **12**(10): p. 1040-1050.
486. DeTure, M., et al., *tau assembly in inducible transfectants expressing wild-type or FTDP-17 tau.* American Journal of Pathology, 2002. **161**(5): p. 1711-1722.
487. Kent, B.A., et al., *Longitudinal evaluation of Tau-P301L transgenic mice reveals no cognitive impairments at 17months of age.* Brain and Behavior, 2018. **8**(1): p. 12.
488. Lewis, J., et al., *Neurofibrillary tangles, amyotrophy and progressive motor disturbance in mice expressing mutant (P301L) tau protein.* Nature Genetics, 2000. **25**(4): p. 402-405.
489. Alberici, A., et al., *Frontotemporal dementia: impact of P301L tau mutation on a healthy carrier.* Journal of Neurology Neurosurgery and Psychiatry, 2004. **75**(11): p. 1607-1610.
490. Bardai, F.H., et al., *Lrrk promotes tau neurotoxicity through dysregulation of actin and mitochondrial dynamics.* Plos Biology, 2018. **16**(12): p. 28.

491. Perez, M.J., et al., *Caspase-Cleaved Tau Impairs Mitochondrial Dynamics in Alzheimer's Disease.* Molecular Neurobiology, 2018. **55**(2): p. 1004-1018.
492. Cupo, R.R. and J. Shorter, *Skd3 (human ClpB) is a potent mitochondrial protein disaggregase that is inactivated by 3-methylglutaconic aciduria-linked mutations.* Elife, 2020. **9**: p. 37.
493. Beal, M.F., *Mitochondrial dysfunction in neurodegenerative diseases.* Biochimica Et Biophysica Acta-Bioenergetics, 1998. **1366**(1-2): p. 211-223.
494. Penney, J., W.T. Ralvenius, and L.H. Tsai, *Modeling Alzheimer's disease with iPSC-derived brain cells.* Molecular Psychiatry, 2020. **25**(1): p. 148-167.
495. Hammond, T.R., S.E. Marsh, and B. Stevens, *Immune Signaling in Neurodegeneration.* Immunity, 2019. **50**(4): p. 955-974.
496. Grabrucker, A., et al., *Synaptogenesis of hippocampal neurons in primary cell culture.* Cell and Tissue Research, 2009. **338**(3): p. 333-341.
497. LaBarbera, K.M., et al., *Modeling the mature CNS: A predictive screening platform for neurodegenerative disease drug discovery.* Journal of Neuroscience Methods, 2021. **358**: p. 9.
498. Grubb, M.S. and J. Burrone, *Building and maintaining the axon initial segment.* Current Opinion in Neurobiology, 2010. **20**(4): p. 481-488.
499. Broadhead, M.J., et al., *PSD95 nanoclusters are postsynaptic building blocks in hippocampus circuits.* Scientific Reports, 2016. **6**: p. 14.
500. Chen, X.B., et al., *PSD-95 Is Required to Sustain the Molecular Organization of the Postsynaptic Density.* Journal of Neuroscience, 2011. **31**(17): p. 6329-6338.
501. Wiedenmann, B. and W.W. Franke, *IDENTIFICATION AND LOCALIZATION OF SYNAPTOPHYSIN, AN INTEGRAL MEMBRANE GLYCOPROTEIN OF MR 38,000 CHARACTERISTIC OF PRESYNAPTIC VESICLES.* Cell, 1985. **41**(3): p. 1017-1028.
502. Tretter, V., et al., *Gephyrin, the enigmatic organizer at GABAergic synapses.* Frontiers in Cellular Neuroscience, 2012. **6**: p. 16.
503. Lopez-Domenech, G., et al., *Loss of Dendritic Complexity Precedes Neurodegeneration in a Mouse Model with Disrupted Mitochondrial Distribution in Mature Dendrites.* Cell Reports, 2016. **17**(2): p. 317-327.
504. Luebke, J.I., et al., *Dendritic vulnerability in neurodegenerative disease: insights from analyses of cortical pyramidal neurons in transgenic mouse models.* Brain Structure & Function, 2010. **214**(2-3): p. 181-199.
505. Hilliard, M.A., *Axonal degeneration and regeneration: a mechanistic tug-of-war.* Journal of Neurochemistry, 2009. **108**(1): p. 23-32.
506. Traynelis, S.F., et al., *Glutamate Receptor Ion Channels: Structure, Regulation, and Function.* Pharmacological Reviews, 2010. **62**(3): p. 405-496.
507. Kuzniewska, B., et al., *Mitochondrial protein biogenesis in the synapse is supported by local translation.* Embo Reports, 2020. **21**(8): p. 15.
508. Cai, Q. and P. Tammineni, *Mitochondrial Aspects of Synaptic Dysfunction in Alzheimer's Disease.* Journal of Alzheimers Disease, 2017. **57**(4): p. 1087-1103.
509. Graham, L.C., et al., *Proteomic profiling of neuronal mitochondria reveals modulators of synaptic architecture.* Molecular Neurodegeneration, 2017. **12**: p. 16.
510. Baranov, S.V., et al., *Two hit mitochondrial-driven model of synapse loss in neurodegeneration.* Neurobiology of Disease, 2021. **158**: p. 10.
511. Mandal, A. and C.M. Drerup, *Axonal Transport and Mitochondrial Function in Neurons.* Frontiers in Cellular Neuroscience, 2019. **13**: p. 11.
512. Rangaraju, V., M. Lauterbach, and E.M. Schuman, *Spatially Stable Mitochondrial Compartments Fuel Local Translation during Plasticity.* Cell, 2019. **176**(1-2): p. 73.
513. Maglioni, S. and N. Ventura, *C. elegans as a model organism for human mitochondrial associated disorders.* Mitochondrion, 2016. **30**: p. 117-125.
514. Tsang, W.Y. and B.D. Lemire, *The role of mitochondria in the life of the nematode, Caenorhabditis elegans.* Biochimica Et Biophysica Acta-Molecular Basis of Disease, 2003. **1638**(2): p. 91-105.
515. Kirstein-Miles, J. and R.I. Morimoto, *Caenorhabditis Elegans as a Model System to Study Intercompartmental Proteostasis: Interrelation of Mitochondrial Function, Longevity, and Neurodegenerative Diseases.* Developmental Dynamics, 2010. **239**(5): p. 1529-1538.
516. Bolus, H., et al., *Modeling Neurodegenerative Disorders in Drosophila melanogaster.* International Journal of Molecular Sciences, 2020. **21**(9): p. 28.
517. Guo, M., *Drosophila as a Model to Study Mitochondrial Dysfunction in Parkinson's Disease.* Cold Spring Harbor Perspectives in Medicine, 2012. **2**(11): p. 17.

518. Sen, A. and R.T. Cox, *Fly Models of Human Diseases: Drosophila as a Model for Understanding Human Mitochondrial Mutations and Disease*, in *Fly Models of Human Diseases*, L. Pick, Editor. 2017, Elsevier Academic Press Inc: San Diego. p. 1-27.
519. Sinclair, K.A., et al., *Characterization of intercellular communication and mitochondrial donation by mesenchymal stromal cells derived from the human lung.* Stem Cell Research & Therapy, 2016. **7**: p. 10.
520. Hayakawa, K., et al., *Transfer of mitochondria from astrocytes to neurons after stroke.* Nature, 2016. **535**(7613): p. 551.
521. Islam, M.N., et al., *Mitochondrial transfer from bone-marrow-derived stromal cells to pulmonary alveoli protects against acute lung injury.* Nature Medicine, 2012. **18**(5): p. 759.
522. Morrison, T.J., et al., *Mesenchymal Stromal Cells Modulate Macrophages in Clinically Relevant Lung Injury Models by Extracellular Vesicle Mitochondrial Transfer.* American Journal of Respiratory and Critical Care Medicine, 2017. **196**(10): p. 1275-1286.
523. Davis, C.H.O., et al., *Transcellular degradation of axonal mitochondria.* Proceedings of the National Academy of Sciences of the United States of America, 2014. **111**(26): p. 9633-9638.
524. Phinney, D.G., et al., *Mesenchymal stem cells use extracellular vesicles to outsource mitophagy and shuttle microRNAs.* Nature Communications, 2015. **6**: p. 15.
525. Gollihue, J.L., et al., *Effects of Mitochondrial Transplantation on Bioenergetics, Cellular Incorporation, and Functional Recovery after Spinal Cord Injury.* Journal of Neurotrauma, 2018. **35**(15): p. 1800-1818.
526. Plotnikov, E.Y., et al., *Cytoplasm and organelle transfer between mesenchymal multipotent stromal cells and renal tubular cells in co-culture.* Experimental Cell Research, 2010. **316**(15): p. 2447-2455.
527. Moschoi, R., et al., *Protective mitochondrial transfer from bone marrow stromal cells to acute myeloid leukemic cells during chemotherapy.* Blood, 2016. **128**(2): p. 253-264.
528. Osswald, M., et al., *Brain tumour cells interconnect to a functional and resistant network.* Nature, 2015. **528**(7580): p. 93.
529. Hayakawa, K., et al., *Protective Effects of Endothelial Progenitor Cell-Derived Extracellular Mitochondria in Brain Endothelium.* Stem Cells, 2018. **36**(9): p. 1404-1410.
530. Masuzawa, A., et al., *Transplantation of autologously derived mitochondria protects the heart from ischemia-reperfusion injury.* American Journal of Physiology-Heart and Circulatory Physiology, 2013. **304**(7): p. H966-H982.
531. Caicedo, A., et al., *MitoCeption as a new tool to assess the effects of mesenchymal stem/stromal cell mitochondria on cancer cell metabolism and function.* Scientific Reports, 2015. **5**: p. 10.
532. Court, A.C., et al., *Mitochondrial transfer from MSCs to T cells induces Treg differentiation and restricts inflammatory response.* Embo Reports, 2020. **21**(2): p. 17.
533. Sowinski, S., et al., *Membrane nanotubes physically connect T cells over long distances presenting a novel route for HIV-1 transmission.* Nature Cell Biology, 2008. **10**(2): p. 211-219.
534. Etienne-Manneville, S., *Microtubules in Cell Migration*, in *Annual Review of Cell and Developmental Biology, Vol 29*, R. Schekman, Editor. 2013, Annual Reviews: Palo Alto. p. 471-499.
535. Parsons, J.T., A.R. Horwitz, and M.A. Schwartz, *Cell adhesion: integrating cytoskeletal dynamics and cellular tension.* Nature Reviews Molecular Cell Biology, 2010. **11**(9): p. 633-643.
536. Woodham, E.F. and L.M. Machesky, *Polarised cell migration: intrinsic and extrinsic drivers.* Current Opinion in Cell Biology, 2014. **30**: p. 25-32.
537. Zheng, J.Q., J.J. Wan, and M.M. Poo, *Essential role of filopodia in chemotropic turning of nerve growth cone induced by a glutamate gradient.* Journal of Neuroscience, 1996. **16**(3): p. 1140-1149.
538. Burnette, D.T., et al., *Filopodial actin bundles are not necessary for microtubule advance into the peripheral domain of Aplysia neuronal growth cones.* Nature Cell Biology, 2007. **9**(12): p. 1360.
539. Bukoreshtliev, N.V., et al., *Selective block of tunneling nanotube (TNT) formation inhibits intercellular organelle transfer between PC12 cells.* Febs Letters, 2009. **583**(9): p. 1481-1488.
540. Gurke, S., et al., *Tunneling nanotube (TNT)-like structures facilitate a constitutive, actomyosin-dependent exchange of endocytic organelles between normal rat kidney cells.* Experimental Cell Research, 2008. **314**(20): p. 3669-3683.

541. Vallabhaneni, K.C., H. Haller, and I. Dumler, *Vascular Smooth Muscle Cells Initiate Proliferation of Mesenchymal Stem Cells by Mitochondrial Transfer via Tunneling Nanotubes.* Stem Cells and Development, 2012. **21**(17): p. 3104-3113.
542. Bittins, M. and X. Wang, *TNT-Induced Phagocytosis: Tunneling Nanotubes Mediate the Transfer of Pro-Phagocytic Signals From Apoptotic to Viable Cells.* Journal of Cellular Physiology, 2017. **232**(9): p. 2271-2279.
543. Hoebeke, J., G. Vannijen, and M. Debrabander, *INTERACTION OF ONCODAZOLE (R 17934), NEW ANTI-TUMORAL DRUG, WITH RAT-BRAIN TUBULIN.* Biochemical and Biophysical Research Communications, 1976. **69**(2): p. 319-324.
544. Friedman, P.A. and E.G. Platzer, *INTERACTION OF ANTHELMINTIC BENZIMIDAZOLES AND BENZIMIDAZOLE DERIVATIVES WITH BOVINE BRAIN TUBULIN.* Biochimica Et Biophysica Acta, 1978. **544**(3): p. 605-614.
545. Debrabander, M.J., et al., *EFFECTS OF METHYL 5-(2-THIENYLCARBONYL)-1H-BENZIMIDAZOL-2-YL CARBAMATE, (R-17934-NSC-238159), A NEW SYNTHETIC ANTITUMORAL DRUG INTERFERING WITH MICROTUBULES, ON MAMMALIAN-CELLS CULTURED INVITRO.* Cancer Research, 1976. **36**(3): p. 905-916.
546. Kumar, A., et al., *Influenza virus exploits tunneling nanotubes for cell-to-cell spread.* Scientific Reports, 2017. **7**: p. 14.
547. Luchetti, F., et al., *Fas Signalling Promotes Intercellular Communication in T Cells.* Plos One, 2012. **7**(4): p. 12.
548. Trendowski, M., *Exploiting the cytoskeletal filaments of neoplastic cells to potentiate a novel therapeutic approach.* Biochimica Et Biophysica Acta-Reviews on Cancer, 2014. **1846**(2): p. 599-616.
549. Van Goietsenoven, G., et al., *In Vitro Growth Inhibitory Effects of Cytochalasins and Derivatives in Cancer Cells.* Planta Medica, 2011. **77**(7): p. 711-717.
550. Mageswaran, S.K., et al., *A cryo-electron tomography workflow reveals protrusion-mediated shedding on injured plasma membrane.* Science Advances, 2021. **7**(13): p. 15.
551. Liu, D.L., et al., *Intercellular mitochondrial transfer as a means of tissue revitalization.* Signal Transduction and Targeted Therapy, 2021. **6**(1): p. 18.
552. Sisakhtnezhad, S. and L. Khosravi, *Emerging physiological and pathological implications of tunneling nanotubes formation between cells.* European Journal of Cell Biology, 2015. **94**(10): p. 429-443.
553. Mittal, R., et al., *Cell communication by tunneling nanotubes: Implications in disease and therapeutic applications.* Journal of Cellular Physiology, 2019. **234**(2): p. 1130-1146.
554. Domhan, S., et al., *Intercellular Communication by Exchange of Cytoplasmic Material via Tunneling Nano-Tube Like Structures in Primary Human Renal Epithelial Cells.* Plos One, 2011. **6**(6): p. 8.
555. Hasson, S.A., et al., *Substrate specificity of the TIM22 mitochondrial import pathway revealed with small molecule inhibitor of protein translocation.* Proceedings of the National Academy of Sciences of the United States of America, 2010. **107**(21): p. 9578-9583.
556. King, M.P. and G. Attardi, *HUMAN-CELLS LACKING MTDNA - REPOPULATION WITH EXOGENOUS MITOCHONDRIA BY COMPLEMENTATION.* Science, 1989. **246**(4929): p. 500-503.
557. Babenko, V.A., et al., *Improving the Post-Stroke Therapeutic Potency of Mesenchymal Multipotent Stromal Cells by Cocultivation With Cortical Neurons: The Role of Crosstalk Between Cells.* Stem Cells Translational Medicine, 2015. **4**(9): p. 1011-1020.
558. Ruan, L.H., et al., *Cytosolic proteostasis through importing of misfolded proteins into mitochondria.* Nature, 2017. **543**(7645): p. 443.
559. Archer, S.L., *Mitochondrial Dynamics - Mitochondrial Fission and Fusion in Human Diseases.* New England Journal of Medicine, 2013. **369**(23): p. 2236-2251.
560. Liu, Y.J., et al., *Mitochondrial fission and fusion: A dynamic role in aging and potential target for age-related disease.* Mechanisms of Ageing and Development, 2020. **186**: p. 13.
561. Guo, C., et al., *SENP3-mediated deSUMOylation of dynamin-related protein 1 promotes cell death following ischaemia.* Embo Journal, 2013. **32**(11): p. 1514-1528.

Appendix 1: Constructs and Cloning Methods

Construct	Vector	Cloning Method	Protein Sequence
Su9-EGFP-HiBit	pLVX	HiBit tag added to Su9-EGFP by PCR	MASTRVLASRLASRMAASAKVARPAVRVAQVSKRTIQTGSPLQTLKRTQMTSIVNATTRQAFQKR AYSSGSIATMVSKGEELFTGVVPILVELDGDVNGHKFSVSGEGEGDATYGKLTLKFICTTGKLPVP WPTLVTTLTYGVQCFSRYPDHMKQHDFFKSAMPEGYVQERTIFFKDDGNYKTRAEVKFEGDTLV NRIELKGIDFKEDGNILGHKLEYNYNSHNVYIMADKQKNGIKVNFKIRHNIEDGSVQLADHYQQNT PIGDGPVLLPDNHYLSTQSALSKDPNEKRDHMVLLEFVTAAGITLGMDELYKSGGSGGGSVSGW RLFKKIS*
Su9-EGFP-DHFR-HiBit	pLVX	SLIM from Su9-EGFP-HiBit and DHFR gene string (purchased from Eurofins Genomics).	MASTRVLASRLASRMAASAKVARPAVRVAQVSKRTIQTGSPLQTLKRTQMTSIVNATTRQAFQKR AYSSGSIATMVSKGEELFTGVVPILVELDGDVNGHKFSVSGEGEGDATYGKLTLKFICTTGKLPVP WPTLVTTLTYGVQCFSRYPDHMKQHDFFKSAMPEGYVQERTIFFKDDGNYKTRAEVKFEGDTLV NRIELKGIDFKEDGNILGHKLEYNYNSHNVYIMADKQKNGIKVNFKIRHNIEDGSVQLADHYQQNT PIGDGPVLLPDNHYLSTQSALSKDPNEKRDHMVLLEFVTAAGITLGMDELYKSGGSVRPLNCIVAV SQNMGIGKNGDLPWPPLRNEFKYFQRMTTTSSVEGKQNLVIMGRKTWFSIPEKNRPLKDRINIVL SRELKEPPRGAHFLAKSLDDALRLIEQPELASKVDMVWIVGGSSVYQEAMNQPGHLRLFVTRIMQ EFESDTFFPEIDLGKYKLLPEYPGVLSEVQEEKGIKYKFEVYEKKDGGGSVSGWRLFKKIS*
Su9-mScarlet-DHFR	pLVX	Gene synthesised by Eurofins Genomics and subcloned into pLVX by restriction digest.	MASTRVLASRLASRMAASAKVARPAVRVAQVSKRTIQTGSPLQTLKRTQMTSIVNATTRQAFQKR AYSAIAMVSKGEAVIKEFMRFKVHMEGSMNGHEFEIEGEGEGRPYEGTQTAKLKVTKGGPLPFS WDILSPQFMYGSRAFTKHPADIPDYYKQSFPEGFKWERVMNFEDGGAVTVTQDTSLEDGTLIYK VKLRGTNFPPDGPVMQKKTMGWEASTERLYPEDGVLKGDIKMALRLKDGGRYLADFKTTYKAKK PVQMPGAYNVDRKLDITSHNEDYTVVEQYERSEGRHSTGGMDELYKSTVRPLNCIVAVSQNMGI GKNGDLPWPPLRNEFKYFQRMTTTSSVEGKQNLVIMGRKTWFSIPEKNRPLKDRINIVLSRELKE PPRGAHFLAKSLDDALRLIEQPELASKVDMVWIVGGSSVYQEAMNQPGHLRLFVTRIMQEFESDT FFPEIDLGKYKLLPEYPGVLSEVQEEKGIKYKFEVYEKKD*
Su9-eqFP670-DHFR-HiBit	pXLG3	Gibson assembly (from Su9-EGFP-DHFR-HiBit and eqFP670-P2A-LgBit).	MASTRVLASRLASRMAASAKVARPAVRVAQVSKRTIQTGSPLQTLKRTQMTSIVNATTRQAFQKR AYSSGSIATMGEDSELISENMHTKLYMEGTVNGHHFKCTSEGEGKPYEGTQTCKIKVVEGGPLPF AFDILATSFMYGSKTFINHTQGIPDFFKQSFPEGFTWERITTYEDGGVLTATQDTSLQNGCLIYNVK INGVNFPSNGPVMQKKTLGWEANTEMLYPADSGLRGHNQMALKLVGGGYLHCSLKTTYRSKKP AKNLKMPGFYFVDRKLERIKEADKETYVEQHEMAVARYCDLPSKLGHSSGGSVRPLNCIVAVSQ NMGIGKNGDLPWPPLRNEFKYFQRMTTTSSVEGKQNLVIMGRKTWFSIPEKNRPLKDRINIVLSR ELKEPPRGAHFLAKSLDDALRLIEQPELASKVDMVWIVGGSSVYQEAMNQPGHLRLFVTRIMQEF ESDTFFPEIDLGKYKLLPEYPGVLSEVQEEKGIKYKFEVYEKKDGGGSVSGWRLFKKIS*

EGFP-DHFR-HiBit	pLVX	Su9 removed from Su9-EGFP-DHFR-HiBit by PCR.	MVSKGEELFTGVVPILVELDGDVNGHKFSVSGEGEGDATYGKLTLKFICTTGKLPVPWPTLVTTLT YGVQCFSRYPDHMKQHDFFKSAMPEGYVQERTIFFKDDGNYKTRAEVKFEGDTLVNRIELKGIDF KEDGNILGHKLEYNYNSHNVYIMADKQKNGIKVNFKIRHNIEDGSVQLADHYQQNTPIGDGPVLLP DNHYLSTQSALSKDPNEKRDHMVLLEFVTAAGITLGMDELYKSGGSVRPLNCIVAVSQNMGIGKN GDLPWPPLRNEFKYFQRMTTTSSVEGKQNLVIMGRKTWFSIPEKNRPLKDRINIVLSRELKEPPR GAHFLAKSLDDALRLIEQPELASKVDMVWIVGGSSVYQEAMNQPGHLRLFVTRIMQEFESDTFFP EIDLGKYKLLPEYPGVLSEVQEEKGIKYKFEVYEKKDGGGSVSGWRLFKKIS*
	pXLG3	Subcloned from pLVX—EGFP-DHFR-HiBit by restriction digest.	
mScarlet-DHFR	pLVX	Su9 removed from Su9-EGFP-DHFR-HiBit by PCR.	MVSKGEAVIKEFMRFKVHMEGSMNGHEFEIEGEGEGRPYEGTQTAKLKVTKGGPLPFSWDILSP QFMYGSRAFTKHPADIPDYYKQSFPEGFKWERVMNFEDGGAVTVTQDTSLEDGTLIYKVKLRGT NFPPDGPVMQKKTMGWEASTERLYPEDGVLKGDIKMALRLKDGGRYLADFKTTYKAKKPVQMP GAYNVDRKLDITSHNEDYTVVEQYERSEGRHSTGGMDELYKSTVRPLNCIVAVSQNMGIGKNGD LPWPPLRNEFKYFQRMTTTSSVEGKQNLVIMGRKTWFSIPEKNRPLKDRINIVLSRELKEPPRGAH FLAKSLDDALRLIEQPELASKVDMVWIVGGSSVYQEAMNQPGHLRLFVTRIMQEFESDTFFPEIDL GKYKLLPEYPGVLSEVQEEKGIKYKFEVYEKKD*
EGFP	pXLG3	EGFP from Su9-EGFP cloned into pXLG3 vector by PCR.	MVSKGEELFTGVVPILVELDGDVNGHKFSVSGEGEGDATYGKLTLKFICTTGKLPVPWPTLVTTLT YGVQCFSRYPDHMKQHDFFKSAMPEGYVQERTIFFKDDGNYKTRAEVKFEGDTLVNRIELKGIDF KEDGNILGHKLEYNYNSHNVYIMADKQKNGIKVNFKIRHNIEDGSVQLADHYQQNTPIGDGPVLLP DNHYLSTQSALSKDPNEKRDHMVLLEFVTAAGITLGMDELYK*
mCherry	pFIV	Gift from Henley lab.	MVSKGEEDNMAIIKEFMRFKVHMEGSVNGHEFEIEGEGEGRPYEGTQTAKLKVTKGGPLPFAWD ILSPQFMYGSKAYVKHPADIPDYLKLSFPEGFKWERVMNFEDGGVVTVTQDSSLQDGEFIYKVKL RGTNFPSDGPVMQKKTMGWEASSERMYPEDGALKGEIKQRLKLKDGGHYDAEVKTTYKAKKPV QLPGAYNVNIKLDITSHNEDYTIVEQYERAEGRHSTGGMDELYK*
Su9-EGFP	pXLG3	Addgene (Plasmid #23214).	MASTRVLASRLASRMAASAKVARPAVRVAQVSKRTIQTGSPLQTLKRTQMTSIVNATTRQAFQKR AYSSGSIATMVSKGEELFTGVVPILVELDGDVNGHKFSVSGEGEGDATYGKLTLKFICTTGKLPVP WPTLVTTLTYGVQCFSRYPDHMKQHDFFKSAMPEGYVQERTIFFKDDGNYKTRAEVKFEGDTLV NRIELKGIDFKEDGNILGHKLEYNYNSHNVYIMADKQKNGIKVNFKIRHNIEDGSVQLADHYQQNT PIGDGPVLLPDNHYLSTQSALSKDPNEKRDHMVLLEFVTAAGITLGMDELYK*
Mito-dsRed (dsRed2-Cox8A)	pLVX-CMV	Gift from Henley lab (originally purchased from Clonetech, [561]).	MSVLTPLLLRGLTGSARRLPVPRAKIHSLPPEGKLRILQSTVPRARDPPVATMVRSSKNVIKEFMR FKVRMEGTVNGHEFEIEGEGEGRPYEGHNTVKLKVTKGGPLPFAWDILSPQFQYGSKVYVKHPA DIPDYKKLSFPEGFKWERVMNFEDGGVVTVTQDSSLQDGCFIYKVKFIGVNFPSDGPVMQKKTM GWEASTERLYPRDGVLKGEIHKALKLKDGGHYLVEFKSIYMAKKPVQLPGYYYVDSKLDITSHNE DYTIVEQYERTEGRHHLFL*
eqFP670-(P2A)-	pLVX-EF1α	Gene synthesised by Eurofins Genomics and	MGEDSELISENMHTKLYMEGTVNGHHFKCTSEGEGKPYEGTQTCKIKVVEGGPLPFAFDILATSF MYGSKTFINHTQGIPDFFKQSFPEGFTWERITTYEDGGVLTATQDTSLQNGCLIYNVKINGVNFPS

Cox8a-LgBit		subcloned into pLVX by restriction digest.	NGPVMQKKTLGWEANTEMLYPADSGLRGHNQMALKLVGGGYLHCSLKTTYRSKKPAKNLKMPG FYFVDRKLERIKEADKETYVEQHEMAVARYCDLPSKLGHS* (GSGATNFSLLKQAGDVEENPGP) *and* MSVLTPLLLRGLTGSARRLPVPRAKVFTLEDFVGDWEQTAAYNLDQVLEQGGVSSLLQNLAVSV TPIQRIVRSGENALKIDIHVIIPYEGLSADQMAQIEEVFKVVYPVDDHHFKVILPYGTLVIDGVTPNML NYFGRPYEGIAVFDGKKITVTGTLWNGNKIIDERLITPDGSMLFRVTINS*
Streptavidin-IRES-Su9-SBP-EGFP-HiBit	pEX	Gibson assembly from Su9-EGFP-HiBit and Streptavidin (gifted from Henley lab)	MDPSKDSKAQVSAAEAGITGTWYNQLGSTFIVTAGADGALTGTYESAVGNAESRYVLTGRYDSA PATDGSGTALGWTVAWKNNYRNAHSATTWSGQYVGGAEARINTQWLLTSGTTEANAWKSTLV GHDTFTKVKPSAASIDAAKKAGVNNGNPLDAVQQLGP* *and* MASTRVLASRLASRMAASAKVARPAVRVAQVSKRTIQTGSPLQTLKRTQMTSIVNATTRQAFQKR AYSDEKTTGWRGGHVVEGLAGELEQLRARLEHHPQGQREPSGSIATMVSKGEELFTGVVPILVE LDGDVNGHKFSVSGEGEGDATYGKLTLKFICTTGKLPVPWPTLVTTLTYGVQCFSRYPDHMKQH DFFKSAMPEGYVQERTIFFKDDGNYKTRAEVKFEGDTLVNRIELKGIDFKEDGNILGHKLEYNYNS HNVYIMADKQKNGIKVNFKIRHNIEDGSVQLADHYQQNTPIGDGPVLLPDNHYLSTQSALSKDPNE KRDHMVLLEFVTAAGITLGMDELYKSGGSGGGSVSGWRLFKKIS*
Streptavidin-IRES-Cox8a-SBP-EGFP-HiBit		Substituted Su9 with Cox8a from Streptavidin-IRES-Su9-SBP-EGFP-HiBit by PCR	MDPSKDSKAQVSAAEAGITGTWYNQLGSTFIVTAGADGALTGTYESAVGNAESRYVLTGRYDSA PATDGSGTALGWTVAWKNNYRNAHSATTWSGQYVGGAEARINTQWLLTSGTTEANAWKSTLV GHDTFTKVKPSAASIDAAKKAGVNNGNPLDAVQQLGP* *and* MSVLTPLLLRGLTGSARRLPVPRAKDEKTTGWRGGHVVEGLAGELEQLRARLEHHPQGQREPS GSIATMVSKGEELFTGVVPILVELDGDVNGHKFSVSGEGEGDATYGKLTLKFICTTGKLPVPWPTL VTTLTYGVQCFSRYPDHMKQHDFFKSAMPEGYVQERTIFFKDDGNYKTRAEVKFEGDTLVNRIEL KGIDFKEDGNILGHKLEYNYNSHNVYIMADKQKNGIKVNFKIRHNIEDGSVQLADHYQQNTPIGDG PVLLPDNHYLSTQSALSKDPNEKRDHMVLLEFVTAAGITLGMDELYKSGGSGGGSVSGWRLFKKI S*
Streptavidin	pLVX-CMV	PCR from Streptavidin-IRES-Su9-SBP-EGFP-HiBit	MDPSKDSKAQVSAAEAGITGTWYNQLGSTFIVTAGADGALTGTYESAVGNAESRYVLTGRYDSA PATDGSGTALGWTVAWKNNYRNAHSATTWSGQYVGGAEARINTQWLLTSGTTEANAWKSTLV GHDTFTKVKPSAASIDAAKKAGVNNGNPLDAVQQLGP*
SLC5A6	pLVX-CMV	Addgene (Plasmid # 132194)	MSVGVSTSAPLSPTSGTSVGMSTFSIMDYVVFVLLLVLSLAIGLYHACRGWGRHTVGELLMADRK MGCLPVALSLLATFQSAVAILGVPSEIYRFGTQYWFLGCCYFLGLLIPAHIFIPVFYRLHLTSAYEYL ELRFNKTVRVCGTVTFIFQMVIYMGVVLYAPSLALNAVTGFDLWLSVLALGIVCTVYTALGGLKAVI WTDVFQTLVMFLGQLAVIIVGSAKVGGLGRVWAVASQHGRISGFELDPDPFVRHTFWTLAFGGV FMMLSLYGVNQAQVQRYLSSRTEKAAVLSCYAVFPFQQVSLCVGCLIGLVMFAYYQEYPMSIQQ

			AQAAPDQFVLYFVMDLLKGLPGLPGLFIACLFSGSLSTISSAFNSLATVTMEDLIRPWFPEFSEARA IMLSRGLAFGYGLLCLGMAYISSQMGPVLQAAISIFGMVGGPLLGLFCLGMFFPCANPPGAVVGLL AGLVMAFWIGIGSIVTSMGSSMPPSPSNGSSFSLPTNLTVATVTTLMPLTTFSKPTGLQRFYSLSY LWYSAHNSTTVIVVGLIVSLLTGRMRGRSLNPATIYPVLPKLLSLLPLSCQKRLHCRSYGQDHLDT GLFPEKPRNGVLGDSRDKEAMALDGTAYQGSSSTCILQETSL*
Myc-Tau^{WT}	pXLG3	Gift from Henley lab (Tau^{WT} originally purchased from Addgene, plasmid #46904 and subcloned into pXLG3-PX—Myc by restriction digest).	MEQKLISEEDLGTAEPRQEFEVMEDHAGTYGLGDRKDQGGYTMHQDQEGDTDAGLKAEEAGIG DTPSLEDEAAGHVTQARMVSKSKDGTGSDDKKAKGADGKTKIATPRGAAPPGQKGQANATRIPA KTPPAPKTPPSSGEPPKSGDRSGYSSPGSPGTPGSRSRTPSLPTPPTREPKKVAVVRTPPKSPS SAKSRLQTAPVPMPDLKNVKSKIGSTENLKHQPGGGKVQIINKKLDLSNVQSKCGSKDNIKHV**P**G GGSVQIVYKPVDLSKVTSKCGSLGNIHHKPGGGQVEVKSEKLDFKDRVQSKIGSLDNITHVPGGG NKKIETHKLTFRENAKAKTDHGAEIVYKSPVVSGDTSPRHLSNVSSTGSIDMVDSPQLATLADEVS ASLAKQGL*
Myc-Tau^{P301L}		Gift from Henley lab (Tau^{P301L} originally purchased from Addgene (plasmid #46908) and subcloned into pXLG3-PX—Myc by restriction digest).	MEQKLISEEDLGTAEPRQEFEVMEDHAGTYGLGDRKDQGGYTMHQDQEGDTDAGLKAEEAGIG DTPSLEDEAAGHVTQARMVSKSKDGTGSDDKKAKGADGKTKIATPRGAAPPGQKGQANATRIPA KTPPAPKTPPSSGEPPKSGDRSGYSSPGSPGTPGSRSRTPSLPTPPTREPKKVAVVRTPPKSPS SAKSRLQTAPVPMPDLKNVKSKIGSTENLKHQPGGGKVQIINKKLDLSNVQSKCGSKDNIKHV**L**G GGSVQIVYKPVDLSKVTSKCGSLGNIHHKPGGGQVEVKSEKLDFKDRVQSKIGSLDNITHVPGGG NKKIETHKLTFRENAKAKTDHGAEIVYKSPVVSGDTSPRHLSNVSSTGSIDMVDSPQLATLADEVS ASLAKQGL*
Myc-EGFP		Gibson assembly (to add Myc tag to EGFP).	MEQKLISEEDLVSKGEELFTGVVPILVELDGDVNGHKFSVSGEGEGDATYGKLTLKFICTTGKLPV PWPTLVTTLTYGVQCFSRYPDHMKQHDFFKSAMPEGYVQERTIFFKDDGNYKTRAEVKFEGDTL VNRIELKGIDFKEDGNILGHKLEYNYNSHNVYIMADKQKNGIKVNFKIRHNIEDGSVQLADHYQQN TPIGDGPVLLPDNHYLSTQSALSKDPNEKRDHMVLLEFVTAAGITLGMDELYKGGSGWP*
Tau^{WT}-mScarlet	pLVX	Gibson assembly (from Myc-Tau^{WT} and mScarlet-DHFR).	MGTAEPRQEFEVMEDHAGTYGLGDRKDQGGYTMHQDQEGDTDAGLKAEEAGIGDTPSLEDEA AGHVTQARMVSKSKDGTGSDDKKAKGADGKTKIATPRGAAPPGQKGQANATRIPAKTPPAPKTP PSSGEPPKSGDRSGYSSPGSPGTPGSRSRTPSLPTPPTREPKKVAVVRTPPKSPSSAKSRLQTA PVPMPDLKNVKSKIGSTENLKHQPGGGKVQIINKKLDLSNVQSKCGSKDNIKHV**P**GGGSVQIVYK PVDLSKVTSKCGSLGNIHHKPGGGQVEVKSEKLDFKDRVQSKIGSLDNITHVPGGGNKKIETHKL TFRENAKAKTDHGAEIVYKSPVVSGDTSPRHLSNVSSTGSIDMVDSPQLATLADEVSASLAKQGL GSGVSKGEAVIKEFMRFKVHMEGSMNGHEFEIEGEGEGRPYEGTQTAKLKVTKGGPLPFSWDIL SPQFMYGSRAFTKHPADIPDYYKQSFPEGFKWERVMNFEDGGAVTVTQDTSLEDGTLIYKVKLR GTNFPPDGPVMQKKTMGWEASTERLYPEDGVLKGDIKMALRLKDGGRYLADFKTTYKAKKPVQ MPGAYNVDRKLDITSHNEDYTVVEQYERSEGRHSTGGMDELYK*

Tau^{P301L}-mScarlet		Gibson assembly (from Myc-Tau^{P301L} and mScarlet-DHFR).	MGTAEPRQEFEVMEDHAGTYGLGDRKDQGGYTMHQDQEGDTDAGLKAEEAGIGDTPSLEDEA AGHVTQARMVSKSKDGTGSDDKKAKGADGKTKIATPRGAAPPGQKGQANATRIPAKTPPAPKTP PSSGEPPKSGDRSGYSSPGSPGTPGSRSRTPSLPTPPTREPKKVAVVRTPPKSPSSAKSRLQTA PVPMPDLKNVKSKIGSTENLKHQPGGGKVQIINKKLDLSNVQSKCGSKDNIKHV**L**GGGSVQIVYK PVDLSKVTSKCGSLGNIHHKPGGGQVEVKSEKLDFKDRVQSKIGSLDNITHVPGGGNKKIETHKL TFRENAKAKTDHGAEIVYKSPVVSGDTSPRHLSNVSSTGSIDMVDSPQLATLADEVSASLAKQGL GSGVSKGEAVIKEFMRFKVHMEGSMNGHEFEIEGEGEGRPYEGTQTAKLKVTKGGPLPFSWDIL SPQFMYGSRAFTKHPADIPDYYKQSFPEGFKWERVMNFEDGGAVTVTQDTSLEDGTLIYKVKLR GTNFPPDGPVMQKKTMGWEASTERLYPEDGVLKGDIKMALRLKDGGRYLADFKTTYKAKKPVQ MPGAYNVDRKLDITSHNEDYTVVEQYERSEGRHSTGGMDELYK*
mScarlet		DHFR removed from mScarlet-DHFR by PCR.	MVSKGEAVIKEFMRFKVHMEGSMNGHEFEIEGEGEGRPYEGTQTAKLKVTKGGPLPFSWDILSP QFMYGSRAFTKHPADIPDYYKQSFPEGFKWERVMNFEDGGAVTVTQDTSLEDGTLIYKVKLRGT NFPPDGPVMQKKTMGWEASTERLYPEDGVLKGDIKMALRLKDGGRYLADFKTTYKAKKPVQMP GAYNVDRKLDITSHNEDYTVVEQYERSEGRHSTGGMDELYK*
Su9-EGFP-6xHis-HiBit	pBad	Gene synthesised by Eurofins Genomics, subcloned into pBad by restriction digest.	MASTRVLASRLASRMAASAKVARPAVRVAQVSKRTIQTGSPLQTLKRTQMTSIVNATTRQAFQKR AYSELVSKGEELFTGVVPILVELDGDVNGHKFSVSGEGEGDATYGKLTLKFICTTGKLPVPWPTLV TTLTYGVQCFSRYPDHMKQHDFFKSAMPEGYVQERTIFFKDDGNYKTRAEVKFEGDTLVNRIELK GIDFKEDGNILGHKLEYNYNSHNVYIMADKQKNGIKVNFKIRHNIEDGSVQLADHYQQNTPIGDGP VLLPDNHYLSTQSALSKDPNEKRDHMVLLEFVTAAGITLGMDELYKGTHHHHHHGSGVSGWRLF KKIS*
His-SUMO—Su9-ACP1-D-ACP1-D-DHFR-Myc	pE-SUMO pro	Gibson assembly (by Holly Ford [108]).	MGHHHHHHGSLQDSEVNQEAKPEVKPEVKPETHINLKVSDGSSEIFFKIKKTTPLRRLMEAFAKR QGKEMDSLRFLYDGIRIQADQAPEDLDMEDNDIIEAHREQIGGMASTRVLASRLASQMAASAKVA RPAVRVAQVSKRTIQTGSPLQTLKRTQMTSIVNATTRQAFQKRAYSSSANLSKDQVSQRVIDVIKA FDKNSPNIANKQISSDTQFHKDLGLDSLDTVELLVAIEEEFDIEIPDKVADELRSVGETVDYIASNPD ANGSGVSWGLRKFKISGSGSANLSKDQVSQRVIDVIKAFDKNSPNIANKQISSDTQFHKDLGLDSL DTVELLVAIEEEFDIEIPDKVADELRSVGETVDYIASNPDANGSGVSWGLRKFKISVRPLNSIVAVS QNMGIGKNGDLPWPPLRNEFKYFQRMTTTSSVEGKQNLVIMGRKTWFSIPEKNRPLKDRINIVLS RELKEPPRGAHFLAKSLDDALRLIEQPELASKVDMVWIVGGSSVYQEAMNQPGHLRLFVTRIMQE FESDTFFPEIDLGKYKLLPEYPGVLSEVQEEKGIKYKFEVYEKKDFEAYVEQKLISEEDLNSAVC*
GST-Dark	pGEX	Fusion of GST and DarkBiT peptide (by Goncalo Pereira [364]).	MSPILGYWKIKGLVQPTRLLLEYLEEKYEEHLYERDEGDKWRNKKFELGLEFPNLPYYIDGDVKLT QSMAIIRYIADKHNMLGGCPKERAEISMLEGAVLDIRYGVSRIAYSKDFETLKVDFLSKLPEMLKMF EDRLCHKTYLNGDHVTHPDFMLYDALDVVLYMDPMCLDAFPKLVCFKKRIEAIPQIDKYLKSSKYI AWPLQGWQATFGGGDHPPKSDPGVSGWALFKKIS*

GST-rPFO	pGEX	rPFO was synthesised as a gene string by Life Technologies, and subcloned into pGEX—GST-TEV vector by SLIM.	MSPILGYWKIKGLVQPTRLLLEYLEEKYEEHLYERDEGDKWRNKKFELGLEFPNLPYYIDGDVKLT QSMAIIRYIADKHNMLGGCPKERAEISMLEGAVLDIRYGVSRIAYSKDFETLKVDFLSKLPEMLKMF EDRLCHKTYLNGDHVTHPDFMLYDALDVVLYMDPMCLDAFPKLVCFKKRIEAIPQIDKYLKSSKYI AWPLQGWQATFGGGDHPPKSENLYFQGKDITDKNQSIDSGISSLSYNRNEVLASNGDKIESFVPK EGKKTGNKFIVVERQKRSLTTSPVDISIIDSVNDRTYPGALQLADKAFVENRPTILMVKRKPININIDL PGLKGENSIKVDDPTYGKVSGAIDELVSKWNEKYSSTHTLPARTQYSESMVYSKSQISSALNVNA KVLENSLGVDFNAVANNEKKVMILAYKQIFYTVSADLPKNPSDLFDDSVTFNDLKQKGVSNEAPPL MVSNVAYGRTIYVKLETTSSSKDVQAAFKALIKNTDIKNSQQYKDIYENSSFTAVVLGGDAQEHNK VVTKDFDEIRKVIKDNATFSTKNPAYPISYTSVFLKDNSVAAVHNKTDYIETTSTEYSKGKINLDHSG AYVAQFEVAWDEVSYDKEGNEVLTHKTWDGNYQDKTAHYSTVIPLEANARNIRIKAREATGLAW EWWRDVISEYDVPLTNNINVSIWGTTLYPGSSITYN*

Appendix 2: Image Analysis Macros

Google Drive link to automated image analysis files: ***Image Analysis Files***

The files in the above folder are labelled as follows:

Preprocess.ijm is the file used for mitochondrial pre-processing (z stack, thresholding, segmentation, creation of skeleton) prior to running other analysis scripts to analyse mitochondrial morphology.

MiNA_210.ijm is the file used for analysis of mitochondrial morphology. This allows measurement of mitochondrial network morphology including branching and junctions.

2020-05-06 Mitochondria classifier.model is the script used for mitochondrial classification, which allowed circularity analysis.

2021-10-05 TMRM analysis.mia is the file used for quantification of TMRM intensity to determine the mitochondrial membrane potential.

2021-12-06 Mitos and protein aggregation.mia is the file used for analysis of the proportion of mitochondria with aggregated protein surrounding them.

All the image analysis scripts and files were developed and provided by Dr Stephen Cross of the Wolfson Bioimaging Facility who developed the scripts based on my analysis needs. They are all runnable by loading into FiJi. The .mia files need to be run through the MIA package (details in methods), whilst the others can be run directly in the FiJi script editor. Further details are provided in Chapter 2: Materials & Methods.

Appendix 3: Proteomic Data

All significant hits ($p<0.05$) from the proteomic enrichment analysis carried out in Chapter 4 are listed below. These proteins were enhanced in association with the mitochondrial portion of the trapped precursor protein. The fold change indicates the level of enrichment compared to the imported precursor, whilst the p value represents the significance of this enhancement. This is processed data from 3 biological replicates. Bioinformatic analysis was carried out by Dr Phil Lewis (Proteomics Facility, University of Bristol).

Table S1: Significantly Enhanced Proteins Associated with the Trapped Precursor

Gene	Protein	Log FC	T-Test
ADAR	Double-stranded RNA-specific adenosine deaminase (DRADA) (EC 3.5.4.37) (136 kDa double-stranded RNA-binding protein) (p136) (Interferon-inducible protein 4) (IFI-4) (K88DSRBP)	0.44	3.84E-05
PPP2R2A	Serine/threonine-protein phosphatase 2A 55 kDa regulatory subunit B alpha isoform (PP2A subunit B isoform B55-alpha) (PP2A subunit B isoform PR55-alpha) (PP2A subunit B isoform R2-alpha) (PP2A subunit B isoform alpha)	0.23	1.35E-04
MTG1	Mitochondrial ribosome-associated GTPase 1 (GTP-binding protein 7) (Mitochondrial GTPase 1)	0.62	4.31E-04
PLOD2	Procollagen-lysine,2-oxoglutarate 5-dioxygenase 2 (EC 1.14.11.4) (Lysyl hydroxylase 2) (LH2)	0.79	5.34E-04
RPRD1A	Regulation of nuclear pre-mRNA domain-containing protein 1A (Cyclin-dependent kinase inhibitor 2B-related protein) (p15INK4B-related protein)	0.66	5.62E-04
MYOF	Myoferlin (Fer-1-like protein 3)	0.53	7.52E-04
SMCHD1	Structural maintenance of chromosomes flexible hinge domain-containing protein 1 (SMC hinge domain-containing protein 1) (EC 3.6.1.-)	0.57	9.86E-04
TARDBP	TAR DNA-binding protein 43 (TDP-43)	0.58	1.04E-03
PDK1	[Pyruvate dehydrogenase (acetyl-transferring)] kinase isozyme 1, mitochondrial (EC 2.7.11.2) (Pyruvate dehydrogenase kinase isoform 1) (PDH kinase 1)	0.74	1.15E-03
FMR1	Synaptic functional regulator FMR1 (Fragile X mental retardation protein 1) (FMRP) (Protein FMR-1)	0.40	1.17E-03
ACOT8	Acyl-coenzyme A thioesterase 8 (Acyl-CoA thioesterase 8) (EC 3.1.2.1) (EC 3.1.2.11) (EC 3.1.2.2) (EC 3.1.2.3) (EC 3.1.2.5) (Choloyl-coenzyme A thioesterase) (EC 3.1.2.27) (HIV-Nef-associated acyl-CoA thioesterase) (Peroxisomal acyl-CoA thioesterase 2) (PTE-2) (Peroxisomal acyl-coenzyme A thioester hydrolase 1) (PTE-1) (Peroxisomal long-chain acyl-CoA thioesterase 1) (Thioesterase II) (hACTE-III) (hACTEIII) (hTE)	0.55	1.24E-03
S100A2	Protein S100-A2 (CAN19) (Protein S-100L) (S100 calcium-binding protein A2)	0.84	1.25E-03
CFL1	Cofilin-1 (18 kDa phosphoprotein) (p18) (Cofilin, non-muscle isoform)	0.56	1.46E-03

	cDNA FLJ55806, highly similar to Golgi phosphoprotein 3	0.76	1.74E-03
TRIM25	E3 ubiquitin/ISG15 ligase TRIM25 (EC 6.3.2.n3) (Estrogen-responsive finger protein) (RING finger protein 147) (RING-type E3 ubiquitin transferase) (EC 2.3.2.27) (RING-type E3 ubiquitin transferase TRIM25) (Tripartite motif-containing protein 25) (Ubiquitin/ISG15-conjugating enzyme TRIM25) (Zinc finger protein 147)	0.36	2.05E-03
GSTM3	Glutathione S-transferase Mu 3 (EC 2.5.1.18) (GST class-mu 3) (GSTM3-3) (hGSTM3-3)	0.61	2.22E-03
RPL11	60S ribosomal protein L11 (CLL-associated antigen KW-12) (Large ribosomal subunit protein uL5)	0.28	2.78E-03
RCN2	Reticulocalbin-2 (Calcium-binding protein ERC-55) (E6-binding protein) (E6BP)	0.26	3.25E-03
RPL30	60S ribosomal protein L30 (Large ribosomal subunit protein eL30)	0.46	3.37E-03
PDP1	[Pyruvate dehydrogenase [acetyl-transferring]]-phosphatase 1, mitochondrial (PDP 1) (EC 3.1.3.43) (Protein phosphatase 2C) (Pyruvate dehydrogenase phosphatase catalytic subunit 1) (PDPC 1)	0.71	3.55E-03
ALDH3A2	Aldehyde dehydrogenase family 3 member A2 (EC 1.2.1.3) (EC 1.2.1.94) (Aldehyde dehydrogenase 10) (Fatty aldehyde dehydrogenase) (Microsomal aldehyde dehydrogenase)	0.50	3.65E-03
VPS26C	Vacuolar protein sorting-associated protein 26C (Down syndrome critical region protein 3) (Down syndrome critical region protein A)	0.39	3.91E-03
PARK7	Parkinson disease protein 7 (Maillard deglycase) (Oncogene DJ1) (Parkinsonism-associated deglycase) (Protein DJ-1) (DJ-1) (Protein/nucleic acid deglycase DJ-1) (EC 3.1.2.-) (EC 3.5.1.-) (EC 3.5.1.124)	0.58	3.93E-03
LYRM7	Complex III assembly factor LYRM7 (LYR motif-containing protein 7)	0.66	3.94E-03
GFM2	Ribosome-releasing factor 2, mitochondrial (RRF2mt) (Elongation factor G 2, mitochondrial) (EF-G2mt) (mEF-G 2) (Elongation factor G2) (hEFG2)	0.39	4.00E-03
FARS2	Phenylalanine--tRNA ligase, mitochondrial (EC 6.1.1.20) (Phenylalanyl-tRNA synthetase) (PheRS)	0.60	4.11E-03
TBC1D24	TBC1 domain family member 24	0.78	4.13E-03
SH3GL1	Endophilin-A2 (EEN fusion partner of MLL) (Endophilin-2) (Extra eleven-nineteen leukemia fusion gene protein) (EEN) (SH3 domain protein 2B) (SH3 domain-containing GRB2-like protein 1)	0.68	4.27E-03
RECQL	ATP-dependent DNA helicase Q1 (EC 3.6.4.12) (DNA helicase, RecQ-like type 1) (RecQ1) (DNA-dependent ATPase Q1) (RecQ protein-like 1)	0.45	4.47E-03
C1QBP	Complement component 1 Q subcomponent-binding protein, mitochondrial (ASF/SF2-associated protein p32) (Glycoprotein gC1qBP) (C1qBP) (Hyaluronan-binding protein 1) (Mitochondrial matrix protein p32) (gC1q-R protein) (p33) (SF2AP32)	0.35	4.72E-03
CLCC1	Chloride channel CLIC-like protein 1 (Mid-1-related chloride channel protein 1)	1.03	4.99E-03
BUB3	Mitotic checkpoint protein BUB3	0.34	5.11E-03
DDX5	Probable ATP-dependent RNA helicase DDX5 (EC 3.6.4.13) (DEAD box protein 5) (RNA helicase p68)	0.40	5.22E-03

LANCL1	Glutathione S-transferase LANCL1 (EC 2.5.1.18) (40 kDa erythrocyte membrane protein) (p40) (LanC-like protein 1)	0.64	5.47E-03
LAMP1	Lysosome-associated membrane glycoprotein 1 (LAMP-1) (Lysosome-associated membrane protein 1) (CD107 antigen-like family member A) (CD antigen CD107a)	0.57	5.52E-03
HNRNPA3	Heterogeneous nuclear ribonucleoprotein A3 (hnRNP A3)	0.84	5.55E-03
EEF1A1	Elongation factor 1-alpha 1 (EF-1-alpha-1) (Elongation factor Tu) (EF-Tu) (Eukaryotic elongation factor 1 A-1) (eEF1A-1) (Leukocyte receptor cluster member 7)	0.17	5.58E-03
SRPRB	Signal recognition particle receptor subunit beta (SR-beta) (Protein APMCF1)	0.50	5.65E-03
DDX3X	ATP-dependent RNA helicase DDX3X (EC 3.6.4.13) (CAP-Rf) (DEAD box protein 3, X-chromosomal) (DEAD box, X isoform) (DBX) (Helicase-like protein 2) (HLP2)	0.31	5.73E-03
DSC3	Desmocollin-3 (Cadherin family member 3) (Desmocollin-4) (HT-CP)	0.58	6.02E-03
AUP1	Lipid droplet regulating VLDL assembly factor AUP1 (Ancient ubiquitous protein 1)	0.56	6.12E-03
PSMB5	Proteasome subunit beta type-5 (EC 3.4.25.1) (Macropain epsilon chain) (Multicatalytic endopeptidase complex epsilon chain) (Proteasome chain 6) (Proteasome epsilon chain) (Proteasome subunit MB1) (Proteasome subunit X)	0.69	6.21E-03
	Dynamin-like 120 kDa protein, mitochondrial (EC 3.6.5.5)	0.69	6.97E-03
GNA14	Guanine nucleotide-binding protein subunit alpha-14 (G alpha-14) (G-protein subunit alpha-14)	0.51	7.33E-03
RPN1	Dolichyl-diphosphooligosaccharide--protein glycosyltransferase subunit 1 (Dolichyl-diphosphooligosaccharide--protein glycosyltransferase 67 kDa subunit) (Ribophorin I) (RPN-I) (Ribophorin-1)	0.61	7.36E-03
PMPCA	Mitochondrial-processing peptidase subunit alpha (Alpha-MPP) (Inactive zinc metalloprotease alpha) (P-55)	0.47	7.76E-03
	cDNA FLJ90170 fis, clone MAMMA1000370, highly similar to Ig alpha-1 chain C region	0.79	7.79E-03
CALU	Calumenin (Crocalbin) (IEF SSP 9302)	0.55	8.11E-03
LANCL2	LanC-like protein 2 (Testis-specific adriamycin sensitivity protein)	0.69	8.12E-03
RAB5C	Ras-related protein Rab-5C (EC 3.6.5.2) (L1880) (RAB5L)	0.96	8.49E-03
PPOX	Protoporphyrinogen oxidase (PPO) (EC 1.3.3.4)	0.46	8.71E-03
RTCB	RNA-splicing ligase RtcB homolog (EC 6.5.1.8) (3'-phosphate/5'-hydroxy nucleic acid ligase)	0.30	8.94E-03
LYPLA1	Acyl-protein thioesterase 1 (APT-1) (hAPT1) (EC 3.1.2.-) (Lysophospholipase 1) (Lysophospholipase I) (LPL-I) (LysoPLA I) (Palmitoyl-protein hydrolase) (EC 3.1.2.22)	0.58	8.99E-03
CSNK1D	Casein kinase I isoform delta (CKI-delta) (CKId) (EC 2.7.11.1) (Tau-protein kinase CSNK1D) (EC 2.7.11.26)	0.64	9.24E-03

B4GALT1	Beta-1,4-galactosyltransferase 1 (Beta-1,4-GalTase 1) (Beta4Gal-T1) (b4Gal-T1) (EC 2.4.1.-) (Beta-N-acetylglucosaminyl-glycolipid beta-1,4-galactosyltransferase) (Beta-N-acetylglucosaminylglycopeptide beta-1,4-galactosyltransferase) (EC 2.4.1.38) (Lactose synthase A protein) (EC 2.4.1.22) (N-acetyllactosamine synthase) (EC 2.4.1.90) (Nal synthase) (Neolactotriaosylceramide beta-1,4-galactosyltransferase) (EC 2.4.1.275) (UDP-Gal:beta-GlcNAc beta-1,4-galactosyltransferase 1) (UDP-galactose:beta-N-acetylglucosamine beta-1,4-galactosyltransferase 1) [Cleaved into: Processed beta-1,4-galactosyltransferase 1]	0.88	9.26E-03
HNRNPK	Heterogeneous nuclear ribonucleoprotein K (hnRNP K) (Transformation up-regulated nuclear protein) (TUNP)	0.65	9.51E-03
RAB34	Ras-related protein Rab-34 (Ras-related protein Rab-39) (Ras-related protein Rah)	0.41	9.58E-03
LYPLAL1	Lysophospholipase-like protein 1 (EC 3.1.2.22)	0.69	9.60E-03
FN1	Fibronectin (FN) (Cold-insoluble globulin) (CIG) [Cleaved into: Anastellin; Ugl-Y1; Ugl-Y2; Ugl-Y3]	1.12	9.72E-03
NSF	Vesicle-fusing ATPase (EC 3.6.4.6) (N-ethylmaleimide-sensitive fusion protein) (NEM-sensitive fusion protein) (Vesicular-fusion protein NSF)	0.72	9.97E-03
DNAJC7	DnaJ homolog subfamily C member 7 (Tetratricopeptide repeat protein 2) (TPR repeat protein 2)	0.65	9.98E-03
RNPC3	RNA-binding region-containing protein 3 (RNA-binding motif protein 40) (RNA-binding protein 40) (U11/U12 small nuclear ribonucleoprotein 65 kDa protein) (U11/U12 snRNP 65 kDa protein) (U11/U12-65K)	0.56	1.00E-02
ACAA1	3-ketoacyl-CoA thiolase, peroxisomal (EC 2.3.1.16) (Acetyl-CoA C-myristoyltransferase) (EC 2.3.1.155) (Acetyl-CoA acyltransferase) (EC 2.3.1.9) (Beta-ketothiolase) (Peroxisomal 3-oxoacyl-CoA thiolase)	0.78	1.05E-02
AK2	Adenylate kinase 2, mitochondrial (AK 2) (EC 2.7.4.3) (ATP-AMP transphosphorylase 2) (ATP: AMP phosphotransferase) (Adenylate monophosphate kinase) [Cleaved into: Adenylate kinase 2, mitochondrial, N-terminally processed]	0.73	1.08E-02
ILVBL	2-hydroxyacyl-CoA lyase 2 (EC 4.1.2.-) (Acetolactate synthase-like protein) (IlvB-like protein)	0.69	1.08E-02
IMPA2	Inositol monophosphatase 2 (IMP 2) (IMPase 2) (EC 3.1.3.25) (Inositol-1(or 4)-monophosphatase 2) (Myo-inositol monophosphatase A2)	0.41	1.09E-02
GALNT2	Polypeptide N-acetylgalactosaminyltransferase 2 (EC 2.4.1.41) (Polypeptide GalNAc transferase 2) (GalNAc-T2) (pp-GaNTase 2) (Protein-UDP acetylgalactosaminyltransferase 2) (UDP-GalNAc: polypeptide N-acetylgalactosaminyltransferase 2) [Cleaved into: Polypeptide N-acetylgalactosaminyltransferase 2 soluble form]	0.74	1.10E-02
MAGT1	Magnesium transporter protein 1 (MagT1) (Dolichyl-diphosphooligosaccharide--protein glycosyltransferase subunit MAGT1) (Oligosaccharyl transferase subunit MAGT1) (Implantation-associated protein) (IAP)	0.70	1.11E-02
TK2	Thymidine kinase 2, mitochondrial (EC 2.7.1.21) (2'-deoxyuridine kinase TK2) (EC 2.7.1.74) (Deoxycytidine kinase TK2) (EC 2.7.1.-) (Mt-TK)	0.75	1.16E-02
MRPS6	28S ribosomal protein S6, mitochondrial (MRP-S6) (S6mt) (Mitochondrial small ribosomal subunit protein bS6m)	0.78	1.16E-02
ACTA2	Actin, aortic smooth muscle (Alpha-actin-2) (Cell growth-inhibiting gene 46 protein) [Cleaved into: Actin, aortic smooth muscle, intermediate form]	-0.08	1.19E-02

PRORP	Mitochondrial ribonuclease P catalytic subunit (EC 3.1.26.5) (Mitochondrial ribonuclease P protein 3) (Mitochondrial RNase P protein 3) (Protein only RNase P catalytic subunit)	0.65	1.22E-02
KIF2C	Kinesin-like protein KIF2C (Kinesin-like protein 6) (Mitotic centromere-associated kinesin) (MCAK)	0.47	1.23E-02
SPART	Spartin (Spastic paraplegia 20 protein) (Trans-activated by hepatitis C virus core protein 1)	0.35	1.23E-02
PHLDA3	Pleckstrin homology-like domain family A member 3 (TDAG51/Ipl homolog 1)	0.63	1.24E-02
ATP2B4	Plasma membrane calcium-transporting ATPase 4 (PMCA4) (EC 7.2.2.10) (Matrix-remodeling-associated protein 1) (Plasma membrane calcium ATPase isoform 4) (Plasma membrane calcium pump isoform 4)	0.60	1.25E-02
STARD7	StAR-related lipid transfer protein 7, mitochondrial (Gestational trophoblastic tumor protein 1) (START domain-containing protein 7) (StARD7)	0.86	1.27E-02
	cDNA FLJ58476, highly similar to Poly(rC)-binding protein 2	0.29	1.30E-02
HACL1	2-hydroxyacyl-CoA lyase 1 (EC 4.1.2.63) (2-hydroxyphytanoyl-CoA lyase) (2-HPCL) (Phytanoyl-CoA 2-hydroxylase 2)	0.84	1.30E-02
SSR4	Translocon-associated protein subunit delta (TRAP-delta) (Signal sequence receptor subunit delta) (SSR-delta)	0.84	1.34E-02
INPP5K	Inositol polyphosphate 5-phosphatase K (EC 3.1.3.56) (Phosphatidylinositol-3,4,5-trisphosphate 5-phosphatase) (EC 3.1.3.86) (Phosphatidylinositol-4,5-bisphosphate 5-phosphatase) (EC 3.1.3.36) (Skeletal muscle and kidney-enriched inositol phosphatase)	0.24	1.34E-02
PTBP1	Polypyrimidine tract-binding protein 1 (PTB) (57 kDa RNA-binding protein PPTB-1) (Heterogeneous nuclear ribonucleoprotein I) (hnRNP I)	0.48	1.43E-02
TRIO	Triple functional domain protein (EC 2.7.11.1) (PTPRF-interacting protein)	0.65	1.44E-02
ARG1	Arginase-1 (EC 3.5.3.1) (Liver-type arginase) (Type I arginase)	0.69	1.45E-02
HNRNPL	Heterogeneous nuclear ribonucleoprotein L (hnRNP L)	0.67	1.45E-02
GNPAT	Dihydroxyacetone phosphate acyltransferase (DAP-AT) (DHAP-AT) (EC 2.3.1.42) (Acyl-CoA: dihydroxyacetonephosphateacyl transferase) (Glycerone-phosphate O-acyltransferase)	0.47	1.46E-02
DDX47	Probable ATP-dependent RNA helicase DDX47 (EC 3.6.4.13) (DEAD box protein 47)	0.53	1.48E-02
ACTN4	Alpha-actinin-4 (non-muscle alpha-actinin 4)	0.35	1.49E-02
MYL12B	Myosin regulatory light chain 12B (MLC-2A) (MLC-2) (Myosin regulatory light chain 2-B, smooth muscle isoform) (Myosin regulatory light chain 20 kDa) (MLC20) (Myosin regulatory light chain MRLC2) (SHUJUN-1)	0.23	1.49E-02
FECH	Ferrochelatase, mitochondrial (EC 4.99.1.1) (Heme synthase) (Protoheme ferro-lyase)	0.67	1.51E-02
TPD52L2	Tumor protein D54 (hD54) (Tumor protein D52-like 2)	0.61	1.55E-02
HTATIP2	Oxidoreductase HTATIP2 (EC 1.1.1.-) (30 kDa HIV-1 TAT-interacting protein) (HIV-1 TAT-interactive protein 2)	0.57	1.56E-02

DHRS7B	Dehydrogenase/reductase SDR family member 7B (EC 1.1.-.-) (Short-chain dehydrogenase/reductase family 32C member 1) (Protein SDR32C1)	0.43	1.57E-02
AIFM2	Ferroptosis suppressor protein 1 (FSP1) (EC 1.6.5.-) (Apoptosis-inducing factor homologous mitochondrion-associated inducer of death) (AMID) (p53-responsive gene 3 protein)	1.12	1.61E-02
PCBP1	Poly(rC)-binding protein 1 (Alpha-CP1) (Heterogeneous nuclear ribonucleoprotein E1) (hnRNP E1) (Nucleic acid-binding protein SUB2.3)	0.37	1.62E-02
TFB2M	Dimethyladenosine transferase 2, mitochondrial (EC 2.1.1.-) (Hepatitis C virus NS5A-transactivated protein 5) (HCV NS5A-transactivated protein 5) (Mitochondrial 12S rRNA dimethylase 2) (Mitochondrial transcription factor B2) (h-mtTFB) (h-mtTFB2) (hTFB2M) (mtTFB2) (S-adenosylmethionine-6-N', N'-adenosyl(rRNA) dimethyltransferase 2)	0.62	1.63E-02
KDELR1	ER lumen protein-retaining receptor 1 (KDEL endoplasmic reticulum protein retention receptor 1) (KDEL receptor 1) (Putative MAPK-activating protein PM23)	0.54	1.65E-02
NUDT16L1	Tudor-interacting repair regulator protein (NUDT16-like protein 1) (Protein syndesmos)	0.61	1.65E-02
DDOST	Dolichyl-diphosphooligosaccharide--protein glycosyltransferase 48 kDa subunit (DDOST 48 kDa subunit) (Oligosaccharyl transferase 48 kDa subunit)	0.51	1.74E-02
ACOT13	Acyl-coenzyme A thioesterase 13 (Acyl-CoA thioesterase 13) (EC 3.1.2.-) (Hotdog-fold thioesterase superfamily member 2) (Palmitoyl-CoA hydrolase) (EC 3.1.2.2) (Thioesterase superfamily member 2) (THEM2) [Cleaved into: Acyl-coenzyme A thioesterase 13, N-terminally processed]	0.66	1.74E-02
YIPF5	Protein YIPF5 (Five-pass transmembrane protein localizing in the Golgi apparatus and the endoplasmic reticulum 5) (Smooth muscle cell-associated protein 5) (SMAP-5) (YIP1 family member 5) (YPT-interacting protein 1 A)	0.47	1.75E-02
COMT	Catechol O-methyltransferase (EC 2.1.1.6)	0.59	1.78E-02
ACO2	Aconitate hydratase, mitochondrial (Aconitase) (EC 4.2.1.3) (Citrate hydro-lyase)	0.60	1.78E-02
MCM5	DNA replication licensing factor MCM5 (EC 3.6.4.12) (CDC46 homolog) (P1-CDC46)	0.86	1.84E-02
RAB18	Ras-related protein Rab-18	0.75	1.86E-02
CPOX	Oxygen-dependent coproporphyrinogen-III oxidase, mitochondrial (COX) (Coprogen oxidase) (Coproporphyrinogenase) (EC 1.3.3.3)	0.85	1.91E-02
DECR2	Peroxisomal 2,4-dienoyl-CoA reductase [(3E)-enoyl-CoA-producing] (pDCR) (EC 1.3.1.124) (2,4-dienoyl-CoA reductase 2) (Short chain dehydrogenase/reductase family 17C member 1)	0.65	1.92E-02
RRM1	Ribonucleoside-diphosphate reductase large subunit (EC 1.17.4.1) (Ribonucleoside-diphosphate reductase subunit M1) (Ribonucleotide reductase large subunit)	0.70	1.94E-02
AZGP1	Zinc-alpha-2-glycoprotein (Zn-alpha-2-GP) (Zn-alpha-2-glycoprotein)	0.82	1.96E-02
PTRH1	Probable peptidyl-tRNA hydrolase (PTH) (EC 3.1.1.29)	0.62	1.98E-02

CAPZA1	F-actin-capping protein subunit alpha-1 (CapZ alpha-1)	0.24	1.98E-02
LMF2	Lipase maturation factor 2 (Transmembrane protein 112B) (Transmembrane protein 153)	0.84	1.99E-02
SPTBN1	Spectrin beta chain, non-erythrocytic 1 (Beta-II spectrin) (Fodrin beta chain) (Spectrin, non-erythroid beta chain 1)	0.76	2.07E-02
GNB2	Guanine nucleotide-binding protein G(I)/G(S)/G(T) subunit beta-2 (G protein subunit beta-2) (Transducin beta chain 2)	0.49	2.13E-02
KHDRBS1	KH domain-containing, RNA-binding, signal transduction-associated protein 1 (GAP-associated tyrosine phosphoprotein p62) (Src-associated in mitosis 68 kDa protein) (Sam68) (p21 Ras GTPase-activating protein-associated p62) (p68)	0.57	2.16E-02
RARS2	Probable arginine--tRNA ligase, mitochondrial (EC 6.1.1.19) (Arginyl-tRNA synthetase) (ArgRS)	0.51	2.17E-02
HNRNPUL2	Heterogeneous nuclear ribonucleoprotein U-like protein 2 (Scaffold-attachment factor A2) (SAF-A2)	0.62	2.18E-02
DGUOK	Deoxyguanosine kinase, mitochondrial (EC 2.7.1.113) (Deoxyadenosine kinase, mitochondrial) (EC 2.7.1.76)	0.56	2.19E-02
PRKDC	DNA-dependent protein kinase catalytic subunit (DNA-PK catalytic subunit) (DNA-PKcs) (EC 2.7.11.1) (DNPK1) (p460)	0.53	2.20E-02
VAPA	Vesicle-associated membrane protein-associated protein A (VAMP-A) (VAMP-associated protein A) (VAP-A) (33 kDa VAMP-associated protein) (VAP-33)	0.34	2.23E-02
FUBP3	Far upstream element-binding protein 3 (FUSE-binding protein 3)	0.46	2.28E-02
MCM3	DNA replication licensing factor MCM3 (EC 3.6.4.12) (DNA polymerase alpha holoenzyme-associated protein P1) (P1-MCM3) (RLF subunit beta) (p102)	1.07	2.28E-02
RBM14	RNA-binding protein 14 (Paraspeckle protein 2) (PSP2) (RNA-binding motif protein 14) (RRM-containing coactivator activator/modulator) (Synaptotagmin-interacting protein) (SYT-interacting protein)	1.23	2.29E-02
SLC27A4	Long-chain fatty acid transport protein 4 (FATP-4) (Fatty acid transport protein 4) (Arachidonate--CoA ligase) (EC 6.2.1.15) (Long-chain-fatty-acid--CoA ligase) (Solute carrier family 27 member 4) (Very long-chain acyl-CoA synthetase 4) (ACSVL4) (EC 6.2.1.-)	0.52	2.30E-02
EIF5B	Eukaryotic translation initiation factor 5B (eIF-5B) (EC 3.6.5.3) (Translation initiation factor IF-2)	0.77	2.35E-02
PDHA1	Pyruvate dehydrogenase E1 component subunit alpha, somatic form, mitochondrial (EC 1.2.4.1) (PDHE1-A type I)	0.64	2.36E-02
HSPA8	Heat shock cognate 71 kDa protein (Fragment)	0.51	2.36E-02
RCC1	Regulator of chromosome condensation (Cell cycle regulatory protein) (Chromosome condensation protein 1)	0.65	2.37E-02
ECI2	Enoyl-CoA delta isomerase 2 (EC 5.3.3.8) (DRS-1) (Delta(3), delta(2)-enoyl-CoA isomerase) (D3, D2-enoyl-CoA isomerase) (Diazepam-binding inhibitor-related protein 1) (DBI-related protein 1) (Dodecenoyl-CoA isomerase) (Hepatocellular carcinoma-associated antigen 88) (Peroxisomal 3,2-trans-enoyl-CoA isomerase) (pECI) (Renal carcinoma antigen NY-REN-1)	0.57	2.39E-02

	Monocarboxylate transporter 1 (Solute carrier family 16 member 1)	0.47	2.42E-02
MMAB	Corrinoid adenosyltransferase (EC 2.5.1.17) (Cob(II)alamin adenosyltransferase) (Cob(II)yrinic acid a, c-diamide adenosyltransferase) (Cobinamide/cobalamin adenosyltransferase) (Methylmalonic aciduria type B protein)	0.75	2.43E-02
NDUFA4	Cytochrome c oxidase subunit NDUFA4 (Complex I-MLRQ) (CI-MLRQ) (NADH-ubiquinone oxidoreductase MLRQ subunit)	0.82	2.44E-02
PRDX3	Thioredoxin-dependent peroxide reductase, mitochondrial (EC 1.11.1.24) (Antioxidant protein 1) (AOP-1) (HBC189) (Peroxiredoxin III) (Prx-III) (Peroxiredoxin-3) (Protein MER5 homolog) (Thioredoxin-dependent peroxiredoxin 3)	0.77	2.46E-02
RTN3	Reticulon-3 (Homolog of ASY protein) (HAP) (Neuroendocrine-specific protein-like 2) (NSP-like protein 2) (Neuroendocrine-specific protein-like II) (NSP-like protein II) (NSPLII)	0.67	2.49E-02
PMPCB	Mitochondrial-processing peptidase subunit beta (EC 3.4.24.64) (Beta-MPP) (P-52)	0.66	2.51E-02
ATP6V1E1	V-type proton ATPase subunit E 1 (V-ATPase subunit E 1) (V-ATPase 31 kDa subunit) (p31) (Vacuolar proton pump subunit E 1)	0.52	2.51E-02
GSDMA	Gasdermin-A (Gasdermin-1) [Cleaved into: Gasdermin-A, N-terminal (GSDMA-NT); Gasdermin-A, C-terminal (GSDMA-CT)]	0.56	2.54E-02
VMP1	Vacuole membrane protein 1 (Transmembrane protein 49)	0.56	2.54E-02
MTPAP	Poly(A) RNA polymerase, mitochondrial (PAP) (EC 2.7.7.19) (PAP-associated domain-containing protein 1) (Polynucleotide adenylyltransferase) (Terminal uridylyltransferase 1) (TUTase 1) (mtPAP)	0.55	2.55E-02
PCMT1	Protein-L-isoaspartate(D-aspartate) O-methyltransferase (PIMT) (EC 2.1.1.77) (L-isoaspartyl protein carboxyl methyltransferase) (Protein L-isoaspartyl/D-aspartyl methyltransferase) (Protein-beta-aspartate methyltransferase)	0.50	2.56E-02
MAP4	Microtubule-associated protein 4 (MAP-4)	0.42	2.57E-02
CDC42EP1	Cdc42 effector protein 1 (Binder of Rho GTPases 5) (Serum protein MSE55)	0.50	2.62E-02
DPM1	Dolichol-phosphate mannosyltransferase subunit 1 (EC 2.4.1.83) (Dolichol-phosphate mannose synthase subunit 1) (DPM synthase subunit 1) (Dolichyl-phosphate beta-D-mannosyltransferase subunit 1) (Mannose-P-dolichol synthase subunit 1) (MPD synthase subunit 1)	0.60	2.62E-02
CAMK2D	Calcium/calmodulin-dependent protein kinase type II subunit delta (CaM kinase II subunit delta) (CaMK-II subunit delta) (EC 2.7.11.17)	0.68	2.64E-02
PTPRE	Receptor-type tyrosine-protein phosphatase epsilon (Protein-tyrosine phosphatase epsilon) (R-PTP-epsilon) (EC 3.1.3.48)	0.95	2.65E-02
	IG c828_heavy_IGHV3-21_IGHD7-27_IGHJ3 (Fragment)	0.83	2.65E-02
CDK2	Cyclin-dependent kinase 2 (EC 2.7.11.22) (Cell division protein kinase 2) (p33 protein kinase)	0.77	2.65E-02

	AEG2C7 (Fragment)	0.80	2.66E-02
APMAP	Adipocyte plasma membrane-associated protein (Protein BSCv)	0.59	2.68E-02
AGPS	Alkyldihydroxyacetonephosphate synthase, peroxisomal (Alkyl-DHAP synthase) (EC 2.5.1.26) (Aging-associated gene 5 protein) (Alkylglycerone-phosphate synthase)	0.46	2.69E-02
RAN	GTP-binding nuclear protein Ran (Androgen receptor-associated protein 24) (GTPase Ran) (Ras-like protein TC4) (Ras-related nuclear protein)	0.41	2.70E-02
ATP5MK	ATP synthase membrane subunit K, mitochondrial (ATP synthase membrane subunit DAPIT, mitochondrial) (Diabetes-associated protein in insulin-sensitive tissues) (HCV F-transactivated protein 2) (Up-regulated during skeletal muscle growth protein 5)	0.87	2.71E-02
NCKAP1	Nck-associated protein 1 (NAP 1) (Membrane-associated protein HEM-2) (p125Nap1)	0.28	2.71E-02
DNAJA1	DnaJ homolog subfamily A member 1 (DnaJ protein homolog 2) (HSDJ) (Heat shock 40 kDa protein 4) (Heat shock protein J2) (HSJ-2) (Human DnaJ protein 2) (hDj-2)	0.63	2.72E-02
HARS2	Histidine--tRNA ligase, mitochondrial (EC 6.1.1.21) (Histidine--tRNA ligase-like) (Histidyl-tRNA synthetase) (HisRS)	0.53	2.74E-02
TXN	Thioredoxin (Trx) (ATL-derived factor) (ADF) (Surface-associated sulphydryl protein) (SASP) (allergen Hom s Trx)	0.56	2.78E-02
HM13	Minor histocompatibility antigen H13 (EC 3.4.23.-) (Intramembrane protease 1) (IMP-1) (IMPAS-1) (hIMP1) (Presenilin-like protein 3) (Signal peptide peptidase)	0.47	2.79E-02
PSIP1	PC4 and SFRS1-interacting protein (CLL-associated antigen KW-7) (Dense fine speckles 70 kDa protein) (DFS 70) (Lens epithelium-derived growth factor) (Transcriptional coactivator p75/p52)	0.83	2.80E-02
SEPTIN6	Septin-6	0.92	2.84E-02
ACOT9	Acyl-coenzyme A thioesterase 9, mitochondrial (Acyl-CoA thioesterase 9) (EC 3.1.2.-) (Acyl-CoA thioester hydrolase 9)	0.58	2.85E-02
SDHA	Succinate dehydrogenase [ubiquinone] flavoprotein subunit, mitochondrial (EC 1.3.5.1) (Flavoprotein subunit of complex II) (Fp)	0.61	2.88E-02
MYADM	Myeloid-associated differentiation marker (Protein SB135)	0.56	2.89E-02
NTPCR	Cancer-related nucleoside-triphosphatase (NTPase) (EC 3.6.1.15) (Nucleoside triphosphate phosphohydrolase)	0.48	2.89E-02
IDH3B	Isocitrate dehydrogenase [NAD] subunit beta, mitochondrial (Isocitric dehydrogenase subunit beta) (NAD(+)-specific ICDH subunit beta)	0.72	2.89E-02
COPA	Coatomer subunit alpha (Alpha-coat protein) (Alpha-COP) (HEP-COP) (HEPCOP) [Cleaved into: Xenin (Xenopsin-related peptide); Proxenin]	0.64	2.92E-02
SEC63	Translocation protein SEC63 homolog	0.42	2.96E-02
RPN2	Dolichyl-diphosphooligosaccharide--protein glycosyltransferase subunit 2 (Dolichyl-diphosphooligosaccharide--protein glycosyltransferase 63 kDa subunit) (RIBIIR) (Ribophorin II) (RPN-II) (Ribophorin-2)	0.57	2.97E-02

PDIA4	Protein disulfide-isomerase A4 (EC 5.3.4.1) (Endoplasmic reticulum resident protein 70) (ER protein 70) (ERp70) (Endoplasmic reticulum resident protein 72) (ER protein 72) (ERp-72) (ERp72)	0.54	2.99E-02
TSG101	Tumor susceptibility gene 101 protein (ESCRT-I complex subunit TSG101)	0.31	2.99E-02
	cDNA FLJ41538 fis, clone BRTHA2018129	0.63	3.01E-02
PRDX1	Peroxiredoxin-1 (EC 1.11.1.24) (Natural killer cell-enhancing factor A) (NKEF-A) (Proliferation-associated gene protein) (PAG) (Thioredoxin peroxidase 2) (Thioredoxin-dependent peroxide reductase 2) (Thioredoxin-dependent peroxiredoxin 1)	0.38	3.01E-02
DAD1	Dolichyl-diphosphooligosaccharide--protein glycosyltransferase subunit DAD1 (Oligosaccharyl transferase subunit DAD1) (Defender against cell death 1) (DAD-1)	0.65	3.02E-02
YWHAG	14-3-3 protein gamma (Protein kinase C inhibitor protein 1) (KCIP-1) [Cleaved into: 14-3-3 protein gamma, N-terminally processed]	0.35	3.02E-02
SLC2A1	Solute carrier family 2, facilitated glucose transporter member 1 (Glucose transporter type 1, erythrocyte/brain) (GLUT-1) (HepG2 glucose transporter)	0.45	3.11E-02
HMGCL	3-hydroxy-3-methylglutarate-CoA lyase (EC 4.1.3.4) (Hydroxymethylglutaryl-CoA lyase, mitochondrial)	0.49	3.13E-02
EZR	Ezrin (Cytovillin) (Villin-2) (p81)	0.23	3.16E-02
ATP1A1	Sodium/potassium-transporting ATPase subunit alpha-1 (Na(+)/K(+) ATPase alpha-1 subunit) (EC 7.2.2.13) (Sodium pump subunit alpha-1)	0.45	3.16E-02
KIF4A	Chromosome-associated kinesin KIF4A (Chromokinesin-A)	0.69	3.20E-02
SFPQ	Splicing factor, proline- and glutamine-rich (100 kDa DNA-pairing protein) (hPOMp100) (DNA-binding p52/p100 complex, 100 kDa subunit) (Polypyrimidine tract-binding protein-associated-splicing factor) (PSF) (PTB-associated-splicing factor)	0.52	3.23E-02
	F-actin-capping protein subunit beta	0.36	3.28E-02
STX5	Syntaxin-5	0.57	3.29E-02
PPA2	Inorganic pyrophosphatase 2, mitochondrial (EC 3.6.1.1) (Pyrophosphatase SID6-306) (Pyrophosphate phospho-hydrolase 2) (PPase 2)	0.64	3.30E-02
EEF1D	Elongation factor 1-delta (EF-1-delta) (Antigen NY-CO-4)	0.29	3.32E-02
PTGES3	Prostaglandin E synthase 3 (EC 5.3.99.3) (Cytosolic prostaglandin E2 synthase) (cPGES) (Hsp90 co-chaperone) (Progesterone receptor complex p23) (Telomerase-binding protein p23)	0.46	3.32E-02
MAT2A	S-adenosylmethionine synthase isoform type-2 (AdoMet synthase 2) (EC 2.5.1.6) (Methionine adenosyltransferase 2) (MAT 2) (Methionine adenosyltransferase II) (MAT-II)	0.32	3.34E-02
MCAT	Malonyl-CoA-acyl carrier protein transacylase, mitochondrial (MCT) (EC 2.3.1.39) (Mitochondrial malonyl CoA: ACP acyltransferase) (Mitochondrial malonyltransferase) ([Acyl-carrier-protein] malonyltransferase)	0.61	3.35E-02

TBL2	Transducin beta-like protein 2 (WS beta-transducin repeats protein) (WS-betaTRP) (Williams-Beuren syndrome chromosomal region 13 protein)	0.69	3.42E-02
SRPRA	Signal recognition particle receptor subunit alpha (SR-alpha) (Docking protein alpha) (DP-alpha)	0.60	3.45E-02
CNP	2',3'-cyclic-nucleotide 3'-phosphodiesterase (CNP) (CNPase) (EC 3.1.4.37)	0.60	3.47E-02
SNRPA1	U2 small nuclear ribonucleoprotein A' (U2 snRNP A')	0.65	3.47E-02
HNRNPDL	Heterogeneous nuclear ribonucleoprotein D-like (hnRNP D-like) (hnRNP DL) (AU-rich element RNA-binding factor) (JKT41-binding protein) (Protein laAUF1)	0.60	3.47E-02
ACSL3	Fatty acid CoA ligase Acsl3 (Arachidonate--CoA ligase) (EC 6.2.1.15) (Long-chain acyl-CoA synthetase 3) (LACS 3) (Long-chain-fatty-acid--CoA ligase 3) (EC 6.2.1.3) (Medium-chain acyl-CoA ligase Acsl3) (EC 6.2.1.2)	0.55	3.48E-02
YWHAQ	14-3-3 protein theta (14-3-3 protein T-cell) (14-3-3 protein tau) (Protein HS1)	0.51	3.48E-02
ISOC2	Isochorismatase domain-containing protein 2	0.70	3.49E-02
CTNND1	Catenin delta-1 (Cadherin-associated Src substrate) (CAS) (p120 catenin) (p120(ctn)) (p120(cas))	0.53	3.49E-02
SYNCRIP	Heterogeneous nuclear ribonucleoprotein Q (hnRNP Q) (Glycine- and tyrosine-rich RNA-binding protein) (GRY-RBP) (NS1-associated protein 1) (Synaptotagmin-binding, cytoplasmic RNA-interacting protein)	0.45	3.50E-02
MRPL15	39S ribosomal protein L15, mitochondrial (L15mt) (MRP-L15) (Mitochondrial large ribosomal subunit protein uL15m)	0.46	3.51E-02
TARS2	Threonine--tRNA ligase, mitochondrial (EC 6.1.1.3) (Threonyl-tRNA synthetase) (ThrRS) (Threonyl-tRNA synthetase-like 1)	0.64	3.53E-02
SPTAN1	Spectrin alpha chain, non-erythrocytic 1 (Alpha-II spectrin) (Fodrin alpha chain) (Spectrin, non-erythroid alpha subunit)	0.68	3.55E-02
HSD17B10	3-hydroxyacyl-CoA dehydrogenase type-2 (EC 1.1.1.35) (17-beta-estradiol 17-dehydrogenase) (EC 1.1.1.62) (2-methyl-3-hydroxybutyryl-CoA dehydrogenase) (MHBD) (3-alpha-(17-beta)-hydroxysteroid dehydrogenase (NAD(+))) (EC 1.1.1.239) (3-hydroxy-2-methylbutyryl-CoA dehydrogenase) (EC 1.1.1.178) (3-hydroxyacyl-CoA dehydrogenase type II) (3alpha(or 20beta)-hydroxysteroid dehydrogenase) (EC 1.1.1.53) (7-alpha-hydroxysteroid dehydrogenase) (EC 1.1.1.159) (Endoplasmic reticulum-associated amyloid beta-peptide-binding protein) (Mitochondrial ribonuclease P protein 2) (Mitochondrial RNase P protein 2) (Short chain dehydrogenase/reductase family 5C member 1) (Short-chain type dehydrogenase/reductase XH98G2) (Type II HADH)	0.48	3.60E-02
FASTKD1	FAST kinase domain-containing protein 1, mitochondrial	0.38	3.62E-02
EPHX1	Epoxide hydrolase 1 (EC 3.3.2.9) (Epoxide hydratase) (Microsomal epoxide hydrolase) (mEH)	0.70	3.70E-02
CALD1	Caldesmon (CDM)	0.51	3.71E-02
MMUT	Methylmalonyl-CoA mutase, mitochondrial (MCM) (EC 5.4.99.2) (Methylmalonyl-CoA isomerase)	0.48	3.79E-02

ATP2B1	Plasma membrane calcium-transporting ATPase 1 (EC 7.2.2.10) (Plasma membrane calcium ATPase isoform 1) (PMCA1) (Plasma membrane calcium pump isoform 1)	0.49	3.81E-02
WDR74	WD repeat-containing protein 74 (NOP seven-associated protein 1)	0.85	3.82E-02
LPCAT2	Lysophosphatidylcholine acyltransferase 2 (LPC acyltransferase 2) (LPCAT-2) (LysoPC acyltransferase 2) (EC 2.3.1.23) (1-acylglycerol-3-phosphate O-acyltransferase 11) (1-AGP acyltransferase 11) (1-AGPAT 11) (EC 2.3.1.51) (1-acylglycerophosphocholine O-acyltransferase) (1-alkenylglycerophosphocholine O-acyltransferase) (EC 2.3.1.25) (1-alkylglycerophosphocholine O-acetyltransferase) (EC 2.3.1.67) (Acetyl-CoA:lyso-platelet-activating factor acetyltransferase) (Acetyl-CoA:lyso-PAF acetyltransferase) (Lyso-PAF acetyltransferase) (LysoPAFAT) (Acyltransferase-like 1) (Lysophosphatidic acid acyltransferase alpha) (LPAAT-alpha)	0.38	3.84E-02
	IG c1122_heavy_IGHV3-7_IGHD3-3_IGHJ4 (IG c1192_heavy_IGHV3-7_IGHD3-3_IGHJ4) (IG c695_heavy_IGHV3-7_IGHD3-3_IGHJ4) (Fragment)	0.72	3.86E-02
PDIA6	Protein disulfide-isomerase A6 (EC 5.3.4.1) (Endoplasmic reticulum protein 5) (ER protein 5) (ERp5) (Protein disulfide isomerase P5) (Thioredoxin domain-containing protein 7)	0.57	3.89E-02
DSG2	Desmoglein-2 (Cadherin family member 5) (HDGC)	0.40	3.90E-02
RPS19	40S ribosomal protein S19 (Small ribosomal subunit protein eS19)	0.23	3.92E-02
NFIB	Nuclear factor 1 B-type (NF1-B) (Nuclear factor 1/B) (CCAAT-box-binding transcription factor) (CTF) (Nuclear factor I/B) (NF-I/B) (NFI-B) (TGGCA-binding protein)	0.43	3.93E-02
POLR1G	DNA-directed RNA polymerase I subunit RPA34 (A34.5) (Antisense to ERCC-1 protein) (ASE-1) (CD3-epsilon-associated protein) (CD3E-associated protein) (DNA-directed RNA polymerase I subunit G) (RNA polymerase I-associated factor PAF49)	0.65	3.93E-02
PLS3	Plastin-3 (T-plastin)	0.21	3.94E-02
PPIA	Peptidyl-prolyl cis-trans isomerase A (PPIase A) (EC 5.2.1.8) (Cyclophilin A) (Cyclosporin A-binding protein) (Rotamase A) [Cleaved into: Peptidyl-prolyl cis-trans isomerase A, N-terminally processed]	0.44	3.96E-02
LGALS1	Galectin-1 (Gal-1) (14 kDa laminin-binding protein) (HLBP14) (14 kDa lectin) (Beta-galactoside-binding lectin L-14-I) (Galaptin) (HBL) (HPL) (Lactose-binding lectin 1) (Lectin galactoside-binding soluble 1) (Putative MAPK-activating protein PM12) (S-Lac lectin 1)	0.64	3.97E-02
STT3A	Dolichyl-diphosphooligosaccharide--protein glycosyltransferase subunit STT3A (Oligosaccharyl transferase subunit STT3A) (STT3-A) (EC 2.4.99.18) (B5) (Integral membrane protein 1) (Transmembrane protein TMC)	0.45	3.98E-02
CORO1C	Coronin-1C (Coronin-3) (hCRNN4)	0.46	3.98E-02
CTSZ	Cathepsin Z (EC 3.4.18.1) (Cathepsin P) (Cathepsin X)	0.81	4.02E-02
PHGDH	D-3-phosphoglycerate dehydrogenase (3-PGDH) (EC 1.1.1.95) (2-oxoglutarate reductase) (EC 1.1.1.399) (Malate dehydrogenase) (EC 1.1.1.37)	0.27	4.09E-02
ACOX3	Peroxisomal acyl-coenzyme A oxidase 3 (EC 1.3.3.6) (Branched-chain acyl-CoA oxidase) (BRCACox) (Pristanoyl-CoA oxidase)	0.57	4.17E-02

FLNA	Filamin-A (FLN-A) (Actin-binding protein 280) (ABP-280) (Alpha-filamin) (Endothelial actin-binding protein) (Filamin-1) (non-muscle filamin)	0.49	4.17E-02
RPS26	40S ribosomal protein S26 (Small ribosomal subunit protein eS26)	0.37	4.21E-02
RMC1	Regulator of MON1-CCZ1 complex (Colon cancer-associated protein Mic1) (Mic-1) (WD repeat-containing protein 98)	0.54	4.24E-02
FLNB	Filamin-B (FLN-B) (ABP-278) (ABP-280 homolog) (Actin-binding-like protein) (Beta-filamin) (Filamin homolog 1) (Fh1) (Filamin-3) (Thyroid autoantigen) (Truncated actin-binding protein) (Truncated ABP)	0.36	4.27E-02
SLFN5	Schlafen family member 5	0.29	4.28E-02
ATAD1	Outer mitochondrial transmembrane helix translocase (EC 7.4.2.-) (ATPase family AAA domain-containing protein 1) (hATAD1) (Thorase)	0.76	4.28E-02
HSD17B12	Very-long-chain 3-oxoacyl-CoA reductase (EC 1.1.1.330) (17-beta-hydroxysteroid dehydrogenase 12) (17-beta-HSD 12) (3-ketoacyl-CoA reductase) (KAR) (Estradiol 17-beta-dehydrogenase 12) (EC 1.1.1.62) (Short chain dehydrogenase/reductase family 12C member 1)	0.44	4.28E-02
MFN2	Mitofusin-2 (EC 3.6.5.-) (Transmembrane GTPase MFN2)	0.85	4.33E-02
EEF1B2	Elongation factor 1-beta (EF-1-beta)	0.52	4.35E-02
MRPS16	28S ribosomal protein S16, mitochondrial (MRP-S16) (S16mt) (Mitochondrial small ribosomal subunit protein bS16m)	0.47	4.35E-02
NFATC1	Nuclear factor of activated T-cells, cytoplasmic 1 (NF-ATc1) (NFATc1) (NFAT transcription complex cytosolic component) (NF-ATc) (NFATc)	0.85	4.35E-02
DYNLL1	Dynein light chain 1, cytoplasmic (8 kDa dynein light chain) (DLC8) (Dynein light chain LC8-type 1) (Protein inhibitor of neuronal nitric oxide synthase) (PIN)	0.85	4.39E-02
	IGH c241_heavy__IGHV3-15_IGHD3-10_IGHJ4 (Fragment)	1.13	4.40E-02
NR1H4	Bile acid receptor (Farnesoid X-activated receptor) (Farnesol receptor HRR-1) (Nuclear receptor subfamily 1 group H member 4) (Retinoid X receptor-interacting protein 14) (RXR-interacting protein 14)	0.86	4.41E-02
DDX1	ATP-dependent RNA helicase DDX1 (EC 3.6.4.13) (DEAD box protein 1) (DEAD box protein retinoblastoma) (DBP-RB)	0.32	4.46E-02
SRP9	Signal recognition particle 9 kDa protein (SRP9)	0.87	4.48E-02
ATP2A2	Sarcoplasmic/endoplasmic reticulum calcium ATPase 2 (SERCA2) (SR Ca(2+)-ATPase 2) (EC 7.2.2.10) (Calcium pump 2) (Calcium-transporting ATPase sarcoplasmic reticulum type, slow twitch skeletal muscle isoform) (Endoplasmic reticulum class 1/2 Ca(2+) ATPase)	0.40	4.52E-02
MRPL16	39S ribosomal protein L16, mitochondrial (L16mt) (MRP-L16) (Mitochondrial large ribosomal subunit protein uL16m)	0.65	4.56E-02

KANK2	KN motif and ankyrin repeat domain-containing protein 2 (Ankyrin repeat domain-containing protein 25) (Matrix-remodeling-associated protein 3) (SRC-1-interacting protein) (SIP) (SRC-interacting protein) (SRC1-interacting protein)	0.58	4.56E-02
PLD3	5'-3' exonuclease PLD3 (EC 3.1.16.1) (Choline phosphatase 3) (HindIII K4L homolog) (Hu-K4) (Phosphatidylcholine-hydrolyzing phospholipase D3) (Phospholipase D3) (PLD 3)	0.69	4.58E-02
NADK2	NAD kinase 2, mitochondrial (EC 2.7.1.23) (Mitochondrial NAD kinase) (NAD kinase domain-containing protein 1, mitochondrial)	0.55	4.63E-02
EFNB2	Ephrin-B2 (EPH-related receptor tyrosine kinase ligand 5) (LERK-5) (HTK ligand) (HTK-L)	0.87	4.64E-02
RPLP1	60S acidic ribosomal protein P1 (Large ribosomal subunit protein P1)	0.20	4.67E-02
TIMM44	Mitochondrial import inner membrane translocase subunit TIM44	0.60	4.70E-02
CORO2A	Coronin-2A (IR10) (WD repeat-containing protein 2)	0.57	4.71E-02
	cDNA FLJ26613 fis, clone MPB05565, highly similar to Serine/threonine protein phosphatase 2A, 55 kDa regulatory subunit B, alpha isoform	0.49	4.71E-02
EIF2S3	Eukaryotic translation initiation factor 2 subunit 3 (EC 3.6.5.3) (Eukaryotic translation initiation factor 2 subunit gamma X) (eIF-2-gamma X) (eIF-2gX)	0.35	4.74E-02
HNRNPH1	Heterogeneous nuclear ribonucleoprotein H (hnRNP H) [Cleaved into: Heterogeneous nuclear ribonucleoprotein H, N-terminally processed]	0.45	4.76E-02
PTBP3	Polypyrimidine tract-binding protein 3 (Regulator of differentiation 1) (Rod1)	0.47	4.79E-02
UFM1	Ubiquitin-fold modifier 1	0.83	4.80E-02
ITPR1	Inositol 1,4,5-trisphosphate receptor type 1 (IP3 receptor isoform 1) (IP3R 1) (InsP3R1) (Type 1 inositol 1,4,5-trisphosphate receptor) (Type 1 InsP3 receptor)	0.63	4.82E-02
PITRM1	Presequence protease, mitochondrial (hPreP) (EC 3.4.24.-) (Pitrilysin metalloproteinase 1) (Metalloprotease 1) (hMP1)	0.52	4.85E-02
CD9	CD9 antigen (5H9 antigen) (Cell growth-inhibiting gene 2 protein) (Leukocyte antigen MIC3) (Motility-related protein) (MRP-1) (Tetraspanin-29) (Tspan-29) (p24) (CD antigen CD9)	0.66	4.89E-02
KIFC1	Kinesin-like protein KIFC1 (Kinesin-like protein 2) (Kinesin-related protein HSET)	0.70	4.90E-02
LGALS3BP	Galectin-3-binding protein (Basement membrane autoantigen p105) (Lectin galactoside-binding soluble 3-binding protein) (Mac-2-binding protein) (MAC2BP) (Mac-2 BP) (Tumor-associated antigen 90K)	1.11	4.90E-02
HNRNPA2B1	Heterogeneous nuclear ribonucleoproteins A2/B1 (hnRNP A2/B1)	0.68	4.92E-02
IGHV3OR16-13	Immunoglobulin heavy variable 3/OR16-13 (non-functional) (Fragment)	0.88	4.93E-02

The significantly enhanced proteins associated with the trapped precursor were further analysed for their relevance to cellular pathways, using the PANTHER classification system tool. This is represented in graphic and tabular form below.

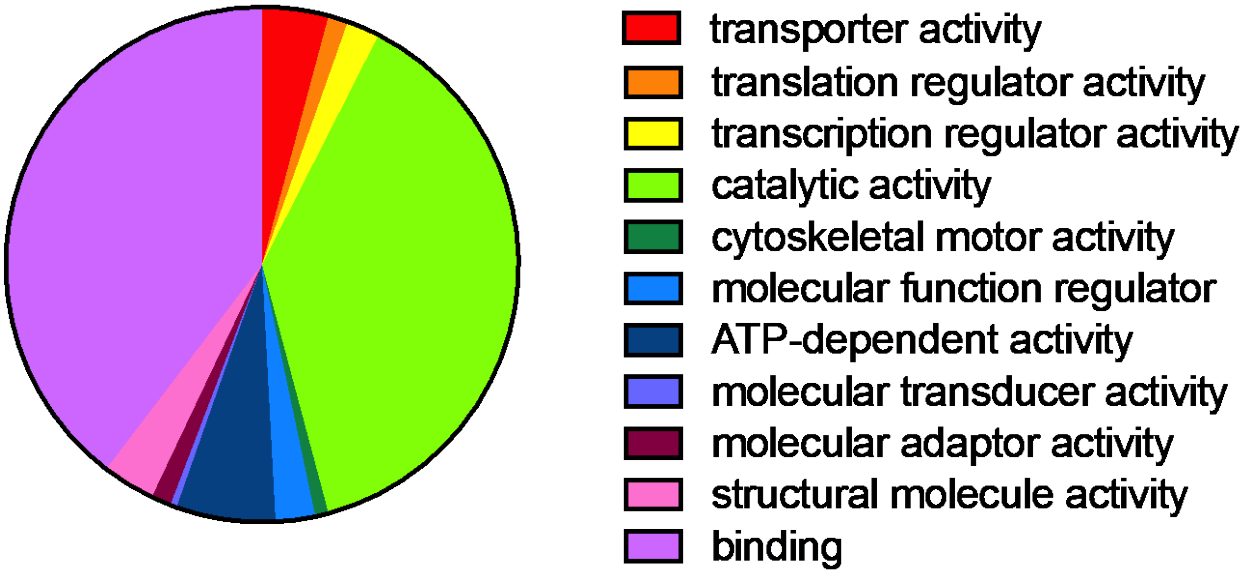

Figure S1: Representation of Possible Cellular Pathways Associated with Precursor Trapping

Table S2: Details of Possible Cellular Pathways Associated with Precursor Trapping

Function	Number of proteins	Proportion of Total (%)
Transporter Activity	10	4.2
Translation Regulator Activity	3	1.3
Transcription Regulator Activity	5	2.1
Catalytic Activity	92	38.3
Cytoskeletal Motor Activity	2	0.8
Molecular Function Regulator	6	2.5
ATP-Dependent Activity	15	6.3
Molecular Transducer Activity	1	0.4
Molecular Adaptor Activity	3	1.3
Structural Molecule Activity	8	3.3
Binding	95	39.6